# Syncytiotrophoblast Extracellular Vesicles: Their role in Gestational Diabetes Mellitus




Neva Kandžija

St Peter's College

&

Nuffield Department of Women's & Reproductive Health

Supervisors: Prof Manu Vatish, Dr Wei Zhang, and Dr Kevin Coward

This thesis is submitted in partial fulfilment of the requirements for the degree of Doctor of Philosophy, Trinity Term, 2020

# Declaration

This thesis is submitted to the University of Oxford, in partial fulfilment of the requirements for the degree of Doctor of Philosophy.

This thesis is entirely my own work, and except where otherwise stated, describes my own research.

# Acknowledgments

Like my friend Sofia says, ‘in science, no journey is undertaken alone’. I feel beyond lucky that I shared my journey with some truly wonderful people.

To Prof. Manu Vatish, my supervisor: Manu, to put it simply, you’re one of a kind – it is a privilege and pleasure to be part of your group. Thank you for keeping your door open always, and for providing an immeasurable amount of support, wisdom and guidance as we’ve navigated this project together. Thank you, too, for your seemingly endless good humour – it has made this project much easier having a supervisor who can always cheer me up!

To Dr Wei Zhang: Wei, words are not enough for you. Your support has extended far beyond the lab (all the way to the allotments and further still). I will be forever grateful for all the help you’ve given me, both as a colleague and mentor, and as my friend. Thank you for being my family away from my family!

To Dr Kevin Coward, thank you for your assistance and guidance, and for always being available when I needed a push in the right direction.

To Prof. Chris Redman, it has been such a privilege to learn from you, and to know you. Your passion for science is contagious and I shall carry it with me for the rest of my life. You’ve inspired my work from the beginning, and I can’t see that changing as I move through my career. Thank you for your endless generosity, interest, and support for my work.

Thank you to Dr Helen Sheldon for providing me with exosomes isolated from sources other than the placenta, Dr Karl Morten for generously sharing C2C12 cells and Dr Roman Fischer for mass spectrometry measurements. Thank you, too, to Veronica Sanchez-Gonzalez for the ExoView analysis, and Zhu Liang and Toluwalase Awoyemi for chats about proteomics analysis.

To all the amazing members of Team Manu past and present – Tolu, Will, Kirsten, Manjot, Qing, Alexandra, Dani, Sina, Jenny, Rannya, Gavin, Alice, Prasanna, Shuhan, Maryam, Emily.

You're all wonderful scientists and people, and it was such a joy to work with you. This thesis would never have been finished without your technical support in the lab. You are the best team I could have wished for. Special thanks must be reserved for Carolina (you were the best lab mate one could have); my wonderful and inspirationally brilliant friend, Vuyane; and Sofia – thank you for the endless support and friendship you provided throughout this journey.

Special thanks to our research midwives Fenella Roseman and Linda Holden for recruiting the patients for us and making our work possible.

To my loveliest office mates Michelle, Janet, Kavita, Helena, Thomas and Taha. A little bit of chocolate (and a lot of laughter) has made this process bearable, even on the difficult days.

To my dear Oxford friends: Ana, Ana, Teresa, Magda, Lucia, Georgie and Filip. People make places, and my Oxford has been, and will always be, a wonderful place.

To my friends back home: Nuša, Ija, Maja, Goran, Darka, Teuta, Maja, Sara, Martina, Majna and Darija – miles do nothing to us. I never question our friendship, but neither do I take it for granted. Knowing you're there when I need you, no matter how far away 'there' may be, is worth the world to me. Thank you for that stability and for more love and support than a person could ever expect.

To Max, thank you for everything we share. Thank you for walking with me and providing me with unfailing support. Volim te!

Finally, but most of all, to my family – this would not have been achieved without you, my biggest cheerleaders and greatest support. Thank you for showing me what unconditional love is. Volim vas! With a very special thanks to my brother Matko for all his technical support throughout the writing process – I am so grateful that *AnyDesk* allowed you to access my computer while an ocean away and save me numerous times. You are so loved!

# Abstract

Gestational diabetes mellitus (GDM) is the most common metabolic complication of pregnancy. It affects more than 17 million women each year and causes adverse consequences for both mother and baby. Previous research has observed that the placenta plays an important role in the pathogenesis of GDM, since delivery of the placenta results in the immediate reversal of diabetic symptoms. The aim of this thesis is to investigate the nature of the placenta's role in GDM, building on the knowledge that the organ releases extracellular vesicles (EVs) into the maternal circulation from six weeks gestation until delivery. EVs carry a variety of ligands, including both proteins and RNA species, between the cells. As such, they have an important role in cell-cell communication in both physiological and pathophysiological conditions, and may provide novel biomarkers of disease. We hypothesized that placental EVs might carry factors impacting insulin availability, a hallmark of pregnancy altered during the establishment of GDM. We identified two novel biomarkers (dipeptidyl peptidase 4 (DPPIV) and insulin receptor (IR)) on placental EVs. DPPIV is a glycoprotein that rapidly degrades incretin hormones, which are known to increase insulin secretion, and thus regulate glucose homeostasis. DPPIV inhibitors are established as therapeutic agents for type 2 diabetes mellitus, and we confirmed that they can be used to inhibit placental DPPIV-EV activity. IR is a key regulator of glucose uptake by skeletal muscles and adipose cells. We showed that placental IR-EVs can act as decoy receptors capable of neutralising maternal insulin. We demonstrated that GDM patients exhibited significantly higher levels of circulating placental DPPIV-EVs and IR-EVs. The final aim of this project was to characterise the protein cargo of placental EVs from GDM pregnancy using mass spectrometry. We identified 56 proteins as differentially expressed between GDM and normal pregnancy. In conclusion, this DPhil project shows that STB-EVs carry biologically active molecules that have the potential to regulate maternal insulin levels in GDM and could represent biologically plausible biomarkers for the disease.

# Table of Content

**DECLARATION** ..... **2**

**ACKNOWLEDGMENTS** ..... **3**

**ABSTRACT** ..... **5**

**TABLE OF CONTENT** ..... **7**

**LIST OF FIGURES** ..... **13**

**LIST OF TABLES** ..... **16**

**1. INTRODUCTION** ..... **17**

1.1. CHANGES IN GLUCOSE METABOLISM DURING NORMAL PREGNANCY ..... 18
1.2. GESTATIONAL DIABETES MELLITUS ..... 19
*1.2.1. Definition and prevalence* ..... *19*
*1.2.2. Diagnostic criteria* ..... *19*
*1.2.3. Symptoms and complications* ..... *21*
*1.2.4. Treatment of GDM* ..... *21*
*1.2.5. Pathophysiology of GDM* ..... *22*
1.3. PLACENTAL EXTRACELLULAR VESICLES ..... 24
*1.3.1. Extracellular vesicles* ..... *24*
*1.3.2. Placenta* ..... *32*
*1.3.3. Syncytiotrophoblast extracellular vesicles* ..... *34*
*1.3.4. STB-EVs in GDM Pregnancy* ..... *40*
1.4. AIMS ..... 43

**2. MATERIAL AND METHODS** ..... **44**

2. 1. PATIENTS AND SAMPLES ..... 45
2.2. IMMUNOHISTOCHEMISTRY ..... 45
2.3. ISOLATION AND CHARACTERISATION OF STB-EVS ..... 46
2.4. BCA PROTEIN ASSAY ..... 48
2.5. NANOPARTICLE TRACKING ANALYSIS ..... 48
2.6. IMMUNOBLOTTING ..... 51
2.7. MAGNETIC BEAD DEPLETION ..... 53
2.8. CO-EXPRESSION OF IR & PLAP ON SMALL STB-EVS USING EXOVIEW ANALYSIS ..... 55
2.9. FLOW CYTOMETRY ANALYSIS ..... 57
2.10. DPPIV ENZYME ACTIVITY ASSAY ..... 61
2.11. PLASMA INSULIN DEPLETION BY STB-EVS ..... 61
2.12. GLUCOSE UPTAKE ASSAY ..... 62
2.13. MASS SPECTROMETRY ..... 62
2.14. STATISTICS ..... 64

**3. STB-EVS EXPRESS ACTIVE DIPEPTIDYL PEPTIDASE IV (DPPIV); CIRCULATING LEVELS ARE INCREASED IN GDM** ..... **65**

3.1. INTRODUCTION ..... 66
3.2. RESULTS ..... 70
*3.2.1. Characterisation of STB-EVs* ..... *70*
*3.2.2. DPPIV is present in normal STB-EVs* ..... *75*
*3.2.3. DPPIV is co-expressed with PLAP on STB-EVs* ..... *76*

*3.2.4. DPPIV present in STB-EVs displays enzymatic activity* ..... *82*
*3.2.5. DPPIV expressing STB-EVs in the maternal circulation* ..... *86*
*3.2.6. DPPIV activity is increased in STB-EVs of GDM pregnancies* ..... *89*
*3.2.7. STB-EV bound DPPIV expression is increased in GDM peripheral plasma* ..... *92*
3.3. DISCUSSION ..... 93
3.4. SUMMARY ..... 97

**4. STB-EVS EXPRESS FUNCTIONAL INSULIN RECEPTOR (IR) CAPABLE OF BINDING INSULIN; CIRCULATING LEVELS ARE INCREASED IN GDM ..... 98**

4.1. INTRODUCTION ..... 99
4.2. RESULTS ..... 104
*4.2.1. IR is present on STB-EVs* ..... *104*
*4.2.2. IR is co-expressed with PLAP on STB-EVs* ..... *105*
*4.2.3. IR expressed on EVs in unique to placental vesicles* ..... *112*
*4.2.4. IR expressed on STB-EVs binds insulin* ..... *114*
*4.2.5. STB-EV reduced cellular glucose uptake* ..... *114*
*4.2.6. IR expressing STB-EVs in the maternal circulation* ..... *116*
*4.2.7. Circulating STB-EV bound IR in normal and GDM pregnancies* ..... *119*
*4.2.8. Postnatal reduction of STB-EVs* ..... *121*
4.3. DISCUSSION ..... 123
4.4. SUMMARY ..... 128

**5. CHARACTERISATION OF THE PROTEIN CARGO OF STB-EVS FROM NORMAL AND GDM PREGNANCY USING MASS SPECTROMETRY ..... 129**

5.1. INTRODUCTION ..... 130
5.2. RESULTS ..... 136
*5.2.1. Patient characteristics* ..... *136*
*5.2.2. Proteomic characterisation of STB-EVs from GDM and normal pregnancy* ..... *137*
*5.2.3. Differentially expressed proteins between MEDIUM/LARGE and SMALL STB-EVs* ..... *141*
*5.2.4. Differentially expressed proteins in STB-EVs from GDM and NORMAL pregnancy* ..... *153*
5.3. DISCUSSION ..... 165
5.4. SUMMARY ..... 169

**6. THESIS SUMMARY AND FUTURE WORK ..... 170**

**BIBLIOGRAPHY ..... 175**

**LIST OF PUBLICATIONS ..... 200**

# Abbreviations

| | |
|---|---|
| ACPP | Acid phosphatase |
| ADP | Adenosine diphosphatase |
| AFP | Alpha-fetoprotein |
| Akt | Protein kinase B |
| ALIX | ALG-2-interacting protein X |
| ANO10 | Anoctamin 10 |
| APC | Allophycocyanin |
| ApoA1 | Apolipoprotein A-I |
| ARH-3 | ADP-ribosyl-acceptor hydrolase |
| AS160 | Akt substrate of 160 kDa |
| ATP | Adenosine triphosphate |
| BANF1 | Barrier to autointegration factor 1 |
| BCA | Bicinchoninic acid |
| BioM | BODIPY FL N-(2-aminoethyl)-maleimide |
| BMI | Body mass index |
| BSA | Bovine albumin serum |
| CAMK2β | Calcium/calmodulin-dependent protein kinase type II subunit beta |
| cAMP | Cyclic adenosine monophosphate |
| CARHSP1 | Calcium-regulated heat-stable protein 1 |
| CD | Cluster of differentiation |
| cGMP | Cyclic guanosine monophosphate |
| CRH | Corticotropin-releasing hormone |
| CRYZL1 | Quinone oxidoreductase-like protein 1 |
| CYC1 | Cytochrome c1 |
| DAB | 3,3’-diaminobenzidine |
| DM | Diabetes mellitus |
| DMEM | Dulbecco's modified Eagle's medium |
| DMSO | Dimethyl sulfoxid |
| DPPIV | Dipeptidyl peptidase 4 |
| ECL | Enhanced chemiluminescence |
| EDTA | Ethylenediaminetetraacetic acid |
| EIF3M | Eukaryotic translation initiation factor 3 |

| | |
|---|---|
| ELISA | Enzyme-linked immunosorbent assay |
| EM | Electron microscopy |
| EV | Extracellular vesicles |
| FABP | Fatty acid binding protein 3 |
| FACS | Fluorescence-activated cell sorting |
| Fc | Fragment crystallizable |
| FCS | Foetal calf serum |
| FDR | False discovery rate |
| FITC | Fluorescein isothiocyanate |
| FLT-1 | Vascular endothelial growth factor receptor 1 precursor |
| FMO | Fluorescence minus one |
| FSC | Forward scatter |
| GDM | Gestational diabetes mellitus |
| GBP1 | Guanylate binding protein 1 |
| GIP | Gastric inhibitory polypeptide |
| GLP-1 | Glucagon-like peptide-1 |
| GLUT | Glucose transporters |
| GPI | Glycosylphosphatidylinositol |
| GSK-3β | Glycogen synthase kinase 3 beta |
| GSV | GLUT4 storage vesicles |
| GTP | Guanosine-5'-triphosphate |
| HAPO | Hyperglycaemia and Adverse Pregnancy Outcomes |
| HAPO-FUS | Hyperglycaemia and Adverse Pregnancy Outcomes Follow-up Study |
| HepG2 | Human hepatocellular liver carcinoma cell line |
| HLA | Human leukocyte antigen |
| HRP | Horseradish peroxidase |
| HTRF | Homogeneous time resolved fluorescence |
| HUVEC | Human umbilical endothelial vein cells |
| IADPSG | International Association of Diabetes in Pregnancy Study Groups |
| IGF | Insulin-like growth factor |
| IgG | Immunoglobulin G |
| IL | Interleukin |
| IR | Insulin receptor |
| IRS | Insulin receptor substrate |

| | |
|---|---|
| ISEV | International Society of Extracellular Vesicles |
| ITIH2 | Inter-alpha-trypsin inhibitor heavy chain 2 |
| MMP | Matric metallopeptidase |
| microRNA | Micro ribonucleic acid |
| mRNA | Messenger ribonucleic acid |
| MVB | Multivesicular bodies |
| NADP | Nicotinamide adenine dinucleotide phosphatase |
| NK | Natural killer cells |
| NTA | Nanoparticle Tracking Analysis |
| NICE | National Institute of Clinical Excellence |
| OGTT | Oral glucose tolerance test |
| OTUB1 | Ubiquitin thioesterase |
| PAPP-A | Pappalysin 1 |
| PAR | Poly (ADP ribose) |
| PB | Peripheral vein blood |
| PBMC | Peripheral blood mononuclear cells |
| PBS | Phosphate buffered saline |
| PBS-T | Phosphate buffered saline-Tween |
| PDK1 | 3-phosphoinositide-dependent protein kinase-1 |
| PE-CY5 | Phycoerythrin cyanine 5 |
| PE-CY7 | Phycoerythrin cyanine 7 |
| PE | Phycoerythin |
| PE | Preeclampsia |
| PFP | Platelet-free plasma |
| PIP3 | Phosphatidylinositol (3,4,5)-trisphosphate |
| PKB | Protein kinase B |
| PLAP | Placental alkaline phosphates |
| PLGF | Placental growth factor |
| PPP | Platelet-poor plasma |
| PSG3 | Pregnancy specific beta-1-glycoprotein 3 |
| PVDF | Polyvinylidene difluoride |
| PTGES3 | Prostaglandin E synthase 3 |
| PZP | Pregnancy zone protein |
| RAL-GAP | Ral GTPase-activating protein |

| | |
|---|---|
| RANBP1 | RAN binding protein 1 |
| RBC | Red blood cells |
| REA | Recombinant engineered antibodies |
| PI3K | Phosphoinositide 3-kinases |
| RI | Refractive index |
| RIPA | Radioimmunoprecipitation assay buffer |
| RNA | Ribonucleic acid |
| rRNA | Ribosomal ribonucleic acid |
| RT | Room temperature |
| SCC | Side scatter |
| SD | Standard deviation |
| sDPPIV | Soluble dipeptidyl peptidase IV |
| SDS | Sodium dodecyl sulphate |
| SEM | Standard error mean |
| sFlt | Soluble fms-like tyrosine kinase-1 |
| SPTA | Spectrin alpha, erythrocytic |
| STB | Syncytiotrophoblast |
| STB-EV | Syncytiotrophoblast extracellular vesicles |
| Sw71 | Immortalized human trophoblast cells |
| TBS | Tris-buffered saline |
| TBS-T | Tris-buffered saline-Tween |
| TDI | Target Discovery Institute |
| TEM | Transmission electron microscopy |
| TNF-α | Tumour necrosis factor-alpha |
| TRAIL | TNF-related apoptosis-induced ligand |
| TREML2 | Trem-like transcript 2 protein |
| Tris | Tris(hydroxymethyl)aminomethane |
| T1DM | Type 1 diabetes mellitus |
| T2DM | Type 2 diabetes mellitus |
| UV | Uterine vein blood |
| VEGF | Vascular endothelial growth factor |

# List of figures

**Chapter1**

*Figure 1. Number of publications in the EV field over the last five years.*.....25
*Figure 2. Schematic representation of different mode of biogenesis of three main subgroups of EVs.*.....26
*Figure 3. Overview of EVs' mode of biogenesis, composition and biomarkers.*.....28
*Figure 4. Schematic presentation of term human placenta, which consists of two circulations: maternal and foetal.*.....33
*Figure 5. STB-EVs are released from syncytiotrophoblast layer into maternal circulation.*...35
*Figure 6. Schematic illustration of dual perfusion of a single placental lobe.*.....37

**Chapter 2**

*Figure 7. A schematic representation of the STB-EV isolation process from maternal perfusate after ex vivo placenta perfusion.*.....47
*Figure 8. Nanoparticle Tracking Analysis (NTA).*.....50
*Figure 9. Schematic illustration of the immunoprecipitation protocol using magnetic Dynabeads*.....55
*Figure 10. Schematic representation of ExoView technology.*.....57
*Figure 11. Protocol for flow cytometry analysis of platelet-poor plasma (PPP) sample.*.....59

**Chapter 3**

*Figure 12. Schematic representation of DPPIV role in glycaemic control.*.....68
*Figure 13. Characterisation of MEDIUM/LARGE STB-EVs and SMALL STB-EVs by TEM and NTA.*.....71
*Figure 14. Characterisation of normal pregnancy derived MEDIUM/LARGE STB-EVs and small extracellular vesicles SMALL STB-EVs by western blotting.*.....72
*Figure 15. Specificity of PLAP antibody confirmed by western blotting using SMALL EVs from different sources.*.....73
*Figure 16. Characterisation of normal pregnancy derived MEDIUM/LARGE STB-EVs and small extracellular vesicles SMALL STB-EVs by western blotting.*.....74
*Figure 17. Placental tissue express DPPIV.*.....75
*Figure 18. Representative Western blot of DPPIV protein expression in whole placental lysates, MEDIUM/LARGE STB-EVs and SMALL STB-EVs isolated from control term placentae.*.....76

*Figure 19. Representative image of flow cytometry analysis of MEDIUM/LARGE STB-EV derived from placental perfusion.* ..... *77*
*Figure 20. DPPIV and PLAP co-expression in MEDIUM/LARGE STB-EVs.* ..... *79*
*Figure 21. DPPIV and PLAP co-expression in SMALL STB-EVs* ..... *81*
*Figure 22. DPPIV in MEDIUM/LARGE STB-EVs and SMALL STB-EVs is enzymatically functional.* ..... *83*
*Figure 23. STB-EV-bound DPPIV can degrade active GLP-1* ..... *85*
*Figure 24. PLAP expressing STB-EVs are present in the circulation and are higher in the uterine vein* ..... *86*
*Figure 25. DPPIV expressing STB-EVs are present in the circulation and are placentally derived* ..... *87*
*Figure 26. Representative flow cytometry analysis of platelet-poor plasma (PPP) from peripheral and uterine vein.* ..... *88*
*Figure 27. DPPIV activity is increased in STB-EVs of GDM pregnancies.* ..... *91*
*Figure 28. Placenta-derived DPPIV expression is increased in GDM peripheral plasma.* ..... *92*

**Chapter 4**

*Figure 29. Schematic representation of insulin stimulated glucose transport across a cell membrane* ..... *101*
*Figure 30. IR is expressed on placental tissue.* ..... *104*
*Figure 31. IR and PLAP expression on placental tissue and STB-EVs.* ..... *105*
*Figure 32. ExoView images of MEDIUM/LARGE STB-EVs showing co-expression of IR and PLAP.* ..... *107*
*Figure 33. Flow cytometry analysis of PLAP and IR co-expression on MEDIUM/LARGE STB-EVs.* ..... *108*
*Figure 34. ExoView analysis of PLAP and IR co-expression on SMALL STB-EVs.* ..... *111*
*Figure 35. Magnetic beads immunodepletion analysis of IR and PLAP co-expression on SMALL EVs.* ..... *111*
*Figure 36. Western blot analysis of IR expression on SMALL EVs from different sources.* ..... *113*
*Figure 37. STB-EV mediated depletion of insulin from plasma.* ..... *114*
*Figure 38. Pilot experiment showing C2C12 glucose uptake in the presence of STB-EVs.* ..... *115*
*Figure 39. PLAP-bound STB-EVs are present in the circulation of pregnant women and are higher in the uterine vein.* ..... *117*

*Figure 40. PLAP/IR are present in the circulation of pregnant women and are higher in the uterine vein.....118*
*Figure 41. Representative flow cytometry analysis of platelet-poor plasma (PPP) from peripheral and uterine vein.....119*
*Figure 42. Placenta-derived IR expression is increased in GDM peripheral plasma. .....121*
*Figure 43. Postnatal reduction of STB-EVs. .....122*

**Chapter 5**

*Figure 44. Summary of various functions ascribed to STB-EV's cargo.....132*
*Figure 45. Histograms of normalised protein abundance for all samples. .....138*
*Figure 46. Hierarchical clustering of MEDIUM/LARGE and SMALL STB-EVs from GDM and normal pregnancy. .....139*
*Figure 47. Multi-scatter plot of MEDIUM/LARGE and SMALL STB-EVs isolated from GDM and normal pregnancies with the corresponding Pearson correlation factor (R). .....140*
*Figure 48. Principal component analysis (PCA) for all samples. .....141*
*Figure 49. Comparison of protein profile between MEDIUM/LARGE and SMALL STB-EVs. .....143*
*Figure 50. Manhattan plot of functional enrichment analysis of differently expressed proteins between MEDIUM/LARGE and SMALL STB-EVs in GDM pregnancy.....145*
*Figure 51. Manhattan plot of functional enrichment analysis of differently expressed proteins between MEDIUM/LARGE and SMALL STB-EVs in normal pregnancy. .....148*
*Figure 52. GO enrich terms summarised by REVIGO. .....152*
*Figure 53. Comparison of MEDIUM/LARGE STB-EV protein profile between GDM and normal pregnancy. .....154*
*Figure 54. Comparison of SMALL STB-EV protein profiles between GDM and normal pregnancy.....155*
*Figure 55. Manhattan plot of Functional enrichment analysis of differently expressed proteins in GDM MEDIUM/LARGE STB-EVs. .....161*
*Figure 56. Summary of GO enriched terms between MEDIUM/LARGE STB-EVS from GDM and normal pregnancy. .....164*

# List of tables

**Chapter 1**

*Table 1. Key methods used to detect single extracellular vesicles .....30*

**Chapter 2**

*Table 2. Composition of western blotting reagents. .....52*

*Table 3. Antibodies used in western blotting analysis. .....53*

*Table 4. Antibodies used for flow cytometry. .....60*

**Chapter 3**

*Table 5. Percentage of DPPIV expression on MEDIUM/LARGE STB-EV assessed by flow cytometry. .....78*

*Table 6. Patient characteristics. .....90*

**Chapter 4**

*Table 7. Percentage of IR expression on MEDIUM/LARGE STB-EV assessed by flow cytometry. .....107*

*Table 8. Patient characteristics. .....120*

**Chapter 5**

*Table 9. Patient characteristics. .....136*

*Table 10. Functional enrichment analysis of differentially expressed proteins between MEDIUM/LARGE and SMALL STB-EVs in GDM. .....146*

*Table 11. Functional enrichment analysis of differentially expressed proteins between MEDIUM/LARGE and SMALL STB-EVs in normal pregnancy. .....149*

*Table 12. Differentially expressed proteins between MEDIUM/LARGE STB-EVs from GDM and normal pregnancy. .....156*

*Table 13. Functional enrichment analysis of differentially expressed proteins between GDM and normal pregnancy from MEDIUM/LARGE STB-EVs. .....162*

# 1. Introduction

## 1.1. Changes in glucose metabolism during normal pregnancy

In order to support foetal growth, pregnancy induces many changes in maternal metabolism. Maternal metabolism during gestation can be divided approximately into two phases. Firstly, early pregnancy is described as an anabolic state in which the mother's body prepares for the demands to come. This phase is important because the energy requirements of the feto-placental unit in the third trimester cannot be met only by increased energy uptake, and therefore, hugely depend on fat stored during early gestation (Armistead *et al.*, 2020). Mid to late pregnancy, on the other hand, is described as a catabolic state. It is in this phase that most foetal growth occurs and it is characterised by the lipolysis and mobilisation of fat storage, accumulated earlier in pregnancy (Lain and Catalano, 2007; Armistead *et al.*, 2020). While lipids are the main source for maternal energy, glucose is the dominant energy fuel for foetal development, thus, many of the metabolic alterations in pregnancy relate to glucose metabolism in particular. During normal gestation, foetal glucose requirements surge at around 26 weeks of pregnancy, which in turn causes basal endogenous glucose production to rise, increasing by 30% by term. To further increase the availability of glucose for the feto-placental unit, pregnancy is also characterised by increased insulin resistance (or decreased insulin sensitivity). More specifically, maternal peripheral insulin sensitivity decreases by 50% at term. As a result, insulin secretion by the maternal pancreatic cells is increased up to three-fold by term to compensate for the reduced insulin sensitivity and maintain euglycaemia (Lain and Catalano, 2007).

## 1.2. Gestational Diabetes Mellitus

### 1.2.1. Definition and prevalence

Gestational Diabetes Mellitus (GDM) is the most common metabolic complication of pregnancy, but as of yet, there is no universal diagnostic criteria or definition for GDM globally accepted. In 2010, the International Association of Diabetes in Pregnancy Study Groups (IADPSG) proposed a new definition of GDM, excluding women with undiagnosed pre-pregnancy diabetes (Metzger, 2010). According to IADPSG these patients are classified as "over diabetes". In our hospital (John Radcliffe Hospital, Oxford University Hospitals), however, GDM is defined as glucose intolerance resulting in hyperglycaemia with an onset or first recognition during pregnancy.

Cases of GDM are rising, with instances of the disease increase by between 10-100% across several race and ethnicity populations over the last three decades (Ferrara, 2007). In 2015, approximately 17.8 million births were affected by GDM worldwide (Ogurtsova *et al.*, 2017), with this trend linked directly to elevated risk factors in women of reproductive age (Chu *et al.*, 2007). Risk factors for the development of GDM include having a high body-mass index, higher maternal age, ethnicity (the highest GDM prevalence was observed in the Middle East and some North African countries, reaching up to 15.2%, while Europe has the lowest case rate at 6.1% (McIntyre *et al.*, 2019)), family history of diabetes, previous GDM diagnosis or previous macrosomic pregnancy (Di Cianni *et al.*, 2003; Ben-Haroush, Yogev and Hod, 2004). Additionally, GDM prevalence will vary significantly among different populations due to different diagnostic criteria and screening strategies (Zhu and Zhang, 2016).

### 1.2.2. Diagnostic criteria

In the United Kingdom, GDM is diagnosed using an oral glucose tolerance test (OGTT) at between 24 and 26 weeks of pregnancy. An OGTT is advised if the woman has presented

previously with GDM, has a body mass index above 30 kg/m$^2$, the weight of a previous child was over 4.5 kg at term, has a first-degree relative with diabetes, or if she is not of Caucasian origin. If one or more of these risk factors are present, blood glucose levels are measured after overnight fasting, and following 75 g of glucose administration. Glucose levels are measured after one and two hours of glucose uptake. According to the National Institute of Clinical Excellence (NICE) 2015 guidelines, a woman is diagnosed with GDM if she showed either a fasting plasma glucose level of ≥ 5.6 mmol/L and/or a glucose level ≥ 7.8 mmol/L at two hours after glucose uptake (*NICE Guidelines. Diabetes in Pregnancy: Management from Preconception to the Postnatal Period*, 2015). Currently, there is a debate as to whether to update the NICE guidelines as they have a higher cut-off value for fasting glucose than the internationally recommended threshold (5.1 mmol/L). Additionally, there is an ongoing discussion on the OGTT's screening approach as well as the efficacy of OGTT as a diagnostic test for GDM in general.

There are two key problems in the diagnosis of GDM. Firstly, the OGTT is not reliable at diagnosing GDM after 28 weeks, meaning serial serum glucose measurement is used. Secondly, the sensitivity of the OGTT at 28 weeks gestation is 76%, meaning 24% of women with GDM are incorrectly diagnosed as "normal" (Donovan *et al.*, 2013). There is a clinical need for a diagnostic test for GDM after 28 weeks gestation. Clinicians need a better test to correctly identify all women with GDM, allowing close antenatal monitoring to mitigate the disease's complications.

The HAPO Study Cooperative Research Group project, *Hyperglycemia and Adverse Pregnancy Outcomes* (HAPO) Study, investigated the correlation between mild hyperglycaemia in gestation and adverse outcomes for both mother and foetus in 25,505 pregnant women at 15 different centres in nine countries. (Metzger *et al.*, 2008). The study showed there is no natural inflection point that will associate glucose levels and pregnancy

outcome, and it is therefore challenging to set the diagnostic threshold for OGTT, again confirming the need for novel diagnostic methods.

### 1.2.3. Symptoms and complications

GDM causes short- and long-term complications for both mother and foetus. Maternal short-term risks include caesarean section, post-partum haemorrhage and/or preeclampsia. The foetus is at increased risk of macrosomia, birth trauma and a number of metabolic imbalances including hypoglycaemia, increasing the risk of neonatal unit admission (Casey *et al.*, 1997; Jensen *et al.*, 2003; Landon *et al.*, 2011). In the longer term, women with GDM are at elevated risk for developing impaired glucose tolerance and type 2 diabetes mellitus (T2DM) later in life. It is reported that women who suffered from GDM are seven times more likely to develop T2DM in the future (Bellamy *et al.*, 2009). Children of women with GDM also have increased lifetime risks of obesity and are more likely to have impaired glucose tolerance and diabetes in childhood and early adulthood (Catalano *et al.*, 2003; American Diabetes Association, 2004). GDM represents a significant burden for healthcare systems around the world and new strategies for its diagnosis and treatment are urgently needed.

### 1.2.4. Treatment of GDM

The *Hyperglycemia and Adverse Pregnancy Outcome Follow-up Study (HAPO FUS)* was published in 2019, investigating the long-term impact of GDM in untreated pregnant women. The authors identified a group of women not considered to have GDM in the initial HAPO study, but whose index pregnancies were later classified as GDM affected using new IADPSG/WHO criteria. The analysis included 4,160 children age 10 to 14 and confirmed that untreated GDM has long-term health impacts (i.e. obesity, impaired glucose tolerance later in life) for children whose mothers developed untreated GDM in the index pregnancy (Lowe *et*

*al.*, 2019). Furthermore, these trends have been shown to be independent of mother's and offspring's BMI and family history of diabetes (Scholtens *et al.*, 2019). Therefore, to prevent and lessen GDM-associated complications, it is crucial that the blood glucose concentrations of those impacted by the disease are well managed and controlled. In the UK, according to NICE guidelines, the first line of GDM management is a change in diet and physical activity. If the patient does not respond to lifestyle changes after two weeks, an oral antidiabetic is prescribed. Metformin acts through the inhibition of hepatic glucose production and is considered the present gold standard for the treatment of T2DM. However, an average of one-third of women with GDM who use metformin to achieve glycaemic control, will experience treatment failure (Balsells *et al.*, 2015). When the blood glucose concentration is higher than 5.6 mmol/L, insulin is introduced to the therapy (*NICE Guidelines. Diabetes in Pregnancy: Management from Preconception to the Postnatal Period*, 2015). Subcutaneous insulin injections have low patient compliance; therefore, there is continuous need for new treatment options. In women who cannot tolerate metformin and do not accept insulin therapy, or it is not possible to achieve target glucose values with metformin, glibenclamide can be prescribed. However, meta-analysis comparison on safety and efficacy of metformin, insulin, and glibenclamide showed that glibenclamide is inferior to both insulin and metformin (Balsells *et al.*, 2015).

### 1.2.5. Pathophysiology of GDM

As mentioned above, normal pregnancy is characterised by a progressive decrease in maternal insulin sensitivity, which facilitates glucose and lipid bioavailability for the foetus (Buchanan and Xiang, 2005; Barbour *et al.*, 2007). Despite this, women are able to maintain euglycaemia due to commensurate increases in pancreatic islet β cell production of insulin (Catalano *et al.*, 1991). This is reinforced by the fact that type 1 diabetic women (whose β cell do not produce

functional insulin) see their insulin requirements increase as pregnancy progresses (Fuglsang *et al.*, 2003). As such, hyperinsulinemia with euglycemia is observed in normal pregnant women. GDM, on the other hand, is characterised by an exacerbation of this physiological insulin resistance state associated with an insufficient insulin secretion, ultimately resulting in hyperglycaemia (Catalano *et al.*, 1999). The placenta is known to be central to inducing the insulin resistance seen in this condition, and delivering the placenta rapidly improves GDM in the short term, with simultaneous decreases in the requirements for insulin and/or metformin and reduction of glucose levels to normal (Homko *et al.*, 2001).

While the exact molecular mechanism of GDM remains unknown, all the evidence so far suggest that it is a complex process. In some women who developed GDM, increased insulin resistance has been observed before conception (Catalano *et al.*, 1999). It has also been reported that the autophosphorylation of insulin receptor substrate (IRS1) is lower in pregnancies complicated with GDM because of the lower expression of IRS1 protein (Friedman *et al.*, 1999). Decreased phosphorylated IRS1 leads to a lower transfer of glucose transporter type 4 (GLUT4) to cell membranes resulting in lower cellular glucose uptake. Additionally, they reported that in GDM there is also a decreased ability for insulin receptor β-subunit to undergo tyrosine phosphorylation, again, resulting in a lower translocation of GLUT4 vesicles to the cell membrane.

For a long time, it was believed that placental hormones were responsible for insulin resistance during gestation. To date, the investigation of placentally derived circulating hormones and cytokines has shown little correlation with insulin sensitivity other than an inverse correlation with tumour necrosis factor (TNFα) (Kirwan *et al.*, 2002). TNFα is a pro-inflammatory cytokine that has been associated with insulin resistance, and which is highly expressed in the adipose tissue of obese animals and humans. It has also been reported that TNFα can downregulate insulin receptor signalling *in vitro* in numerous cell types (Hotamisligil *et al.*,

1994, 1996). Anti-TNFα therapy for the treatment of insulin resistance and diabetes in humans has been unsuccessful (Ofei *et al.*, 1996), suggesting that more complex mechanisms are involved in regulation of insulin sensitivity.

## 1.3. Placental extracellular vesicles

### 1.3.1. Extracellular vesicles

In the last two decades, a growing body of literature has recognised the role of extracellular vesicles (EVs) in both physiological and pathological processes in our bodies. EVs are cell-derived vesicles that carry a large variety of proteins, nucleic acids and lipids as means of intercellular communication. EVs can transfer their cargo to a recipient cell causing a biological response. EVs can also cause an effect on the surface of another cell without the cargo being transferred. For these reasons, the importance of EVs as therapeutic targets, drug carriers as well as new diagnostic biomarkers, has been studied in relation to several diseases (e.g. cancer, neurodegenerative diseases, infectious diseases etc.) (Lo Cicero, Stahl and Raposo, 2015).

The first report of EVs was in 1946 by Chargaff and West (Chargaff and West, 1946). This was followed by Peter Wolf's discovery of platelet-dust in 1967. He observed that the subcellular material, collected after ultracentrifugation of platelet-free plasma samples, had coagulant properties, was rich in phospholipids and originated from platelets (Wolf, 1967). The name "platelet-dust" used to describe this component of plasma was later replaced by the term microvesicles. The discovery of EVs containing and transferring RNA in 2007 heightened the need for its further study. In their landmark study, Valadi *et al*. showed that human mast cells were able to produce new mouse proteins when exposed to exosomal RNA derived from mouse mast cells, confirming that functional mRNA and microRNA can be transferred through exosomes (Valadi *et al.*, 2007).

In 2019, more than 2500 papers were published in the field of extracellular vesicles emphasising the prevalence of the conviction that EVs are mediators of intercellular communication (**Figure *1***). Accordingly, more effort has been put into the definition and characterisation of EVs.

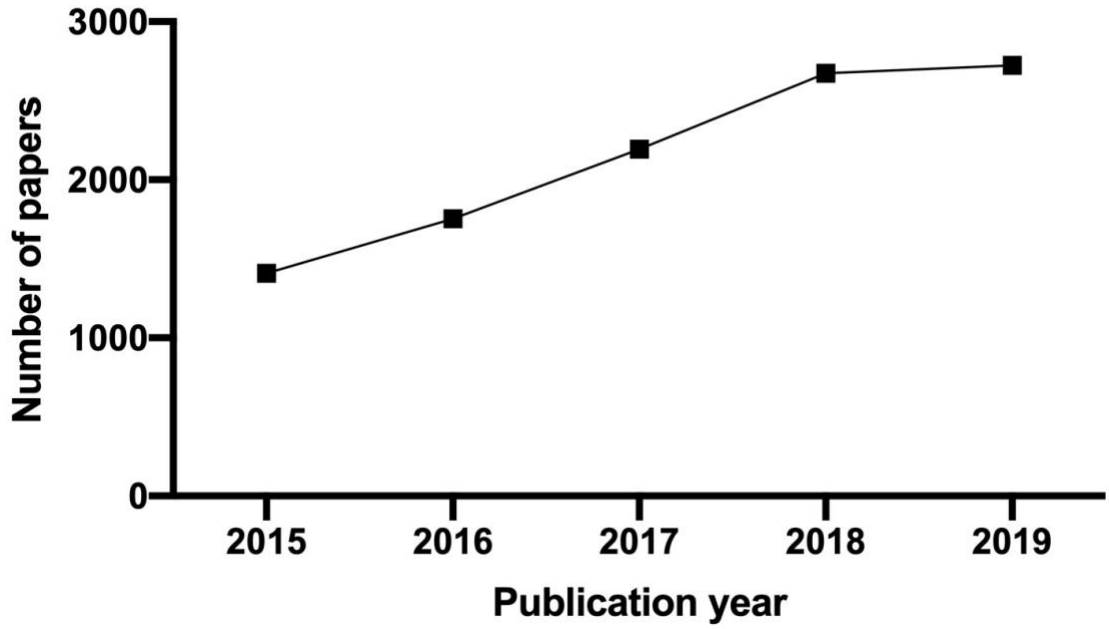



**Figure 1. Number of publications in the EV field over the last five years.**

An advanced search was performed using Solo Search Oxford Libraries Online database. For each year of publication, the search term was as follows: "exosomes" OR "extracellular vesicles" OR "EV(s)" OR "microvesicles". Filters applied were: "Peer-reviewed" and "Article".

EVs are highly heterogeneous, and as such, they can be divided into different subtypes. EVs are divided into three main groups according to their biogenesis: exosomes, microvesicles and apoptotic bodies (**Figure *2***). Exosomes are produced within the endosomal network when the inward budding of early endosome occurs and forms an intraluminal vesicle (ILV). ILVs are then accumulated within larger multivesicular bodies (MVBs). Upon the fusion of MVBs with the cell membrane, MVBs release their cargo (now called exosomes) into the extracellular space. Exosomes can be characterised by the presence of Alix, HSP70, and tetraspanins (CD63, CD9, CD81) on their surface (even though used as exosomal markers, these proteins can be

found on other EVs subtypes as well) (Baietti *et al.*, 2012; Raposo and Stoorvogel, 2013; Yáñez-Mó *et al.*, 2015).

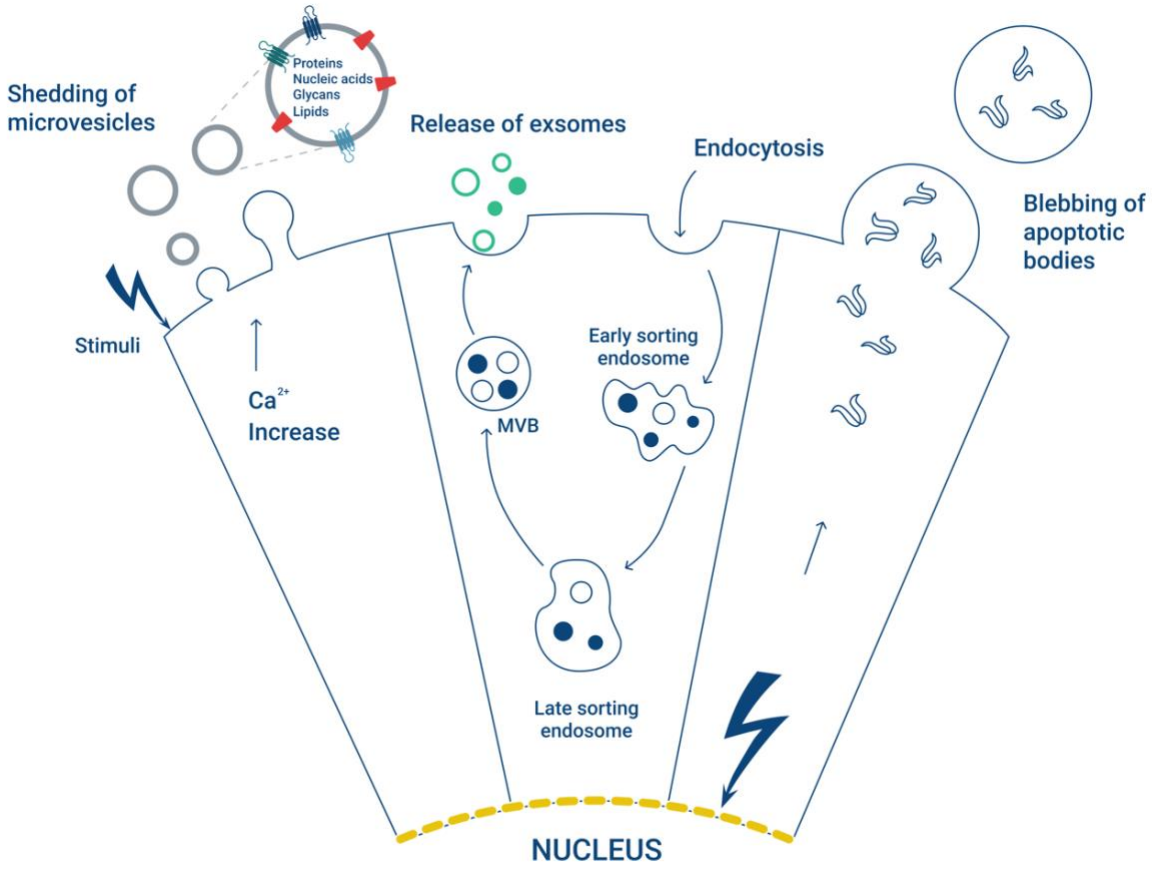



**Figure 2. Schematic representation of different mode of biogenesis of three main subgroups of EVs.**

Microvesicles are formed by budding of the cell membrane in a response to a stimulus. Exosomes are constitutively released by a multivesicular endosome while apoptotic bodies are secreted during programmed cell death in part mediated by actin-myosin membrane blebbing.

Microvesicles are formed by the budding of the cell membrane. The exact mechanism is unclear, but evidence suggests that an increase in intracellular calcium, which activates calcium-sensitive protease calpain (Yano *et al.*, 1993), plays a significant role in the process. Activation of calpain leads to the fragmentation of the cytoskeleton as well as the loosening of the cell membrane, which now forms a growing bud that will eventually detach from the

membrane into the extracellular environment (Cocucci, Racchetti and Meldolesi, 2009). Recently, Jeppesen *et al.* identified Annexin 1 as a marker of microvesicles (Jeppesen *et al.*, 2019).

Apoptotic bodies are released from cells undergoing apoptosis (programmed cell death) and their biomarkers include Annexin V, thrombospondin, and C3b (György *et al.*, 2011; Revenfeld *et al.*, 2014). During apoptosis, the dying cell condenses and fragments into apoptotic bodies, which carry its nuclear content. Once released, apoptotic bodies are phagocytosed and degraded by other cells (i.e. macrophages) (Kerr, Wyllie and Currie, 1972). Later, however, Holmgren *et al.* showed that Epstein-Barr virus DNA can be delivered to a phagocytotic cell through apoptotic bodies demonstrating that apoptotic bodies, like other EVs, are capable of transferring nucleic acids upon phagocytosis (Holmgren *et al.*, 1999).

The challenge of separating different EV subtypes is yet to be fully overcome and has led to many discussions about the correct nomenclature. For years, microvesicles were considered as larger particles (200 – 1000 nm), and exosomes were described as smaller vesicles (50 - 200 nm). However, the debate about EVs' nomenclature has gained fresh prominence with evidence that populations of microvesicles overlap with exosomes in size, and therefore, it is not possible to separate them based on their physical characteristics as was thought previously (Gould and Raposo, 2013). As a result, the International Society of Extracellular Vesicles has recently urged authors to use terms such as "small EVs" and "medium/large EVs" if the EVs' physical characteristics have been used to separate them (Théry *et al.*, 2018).

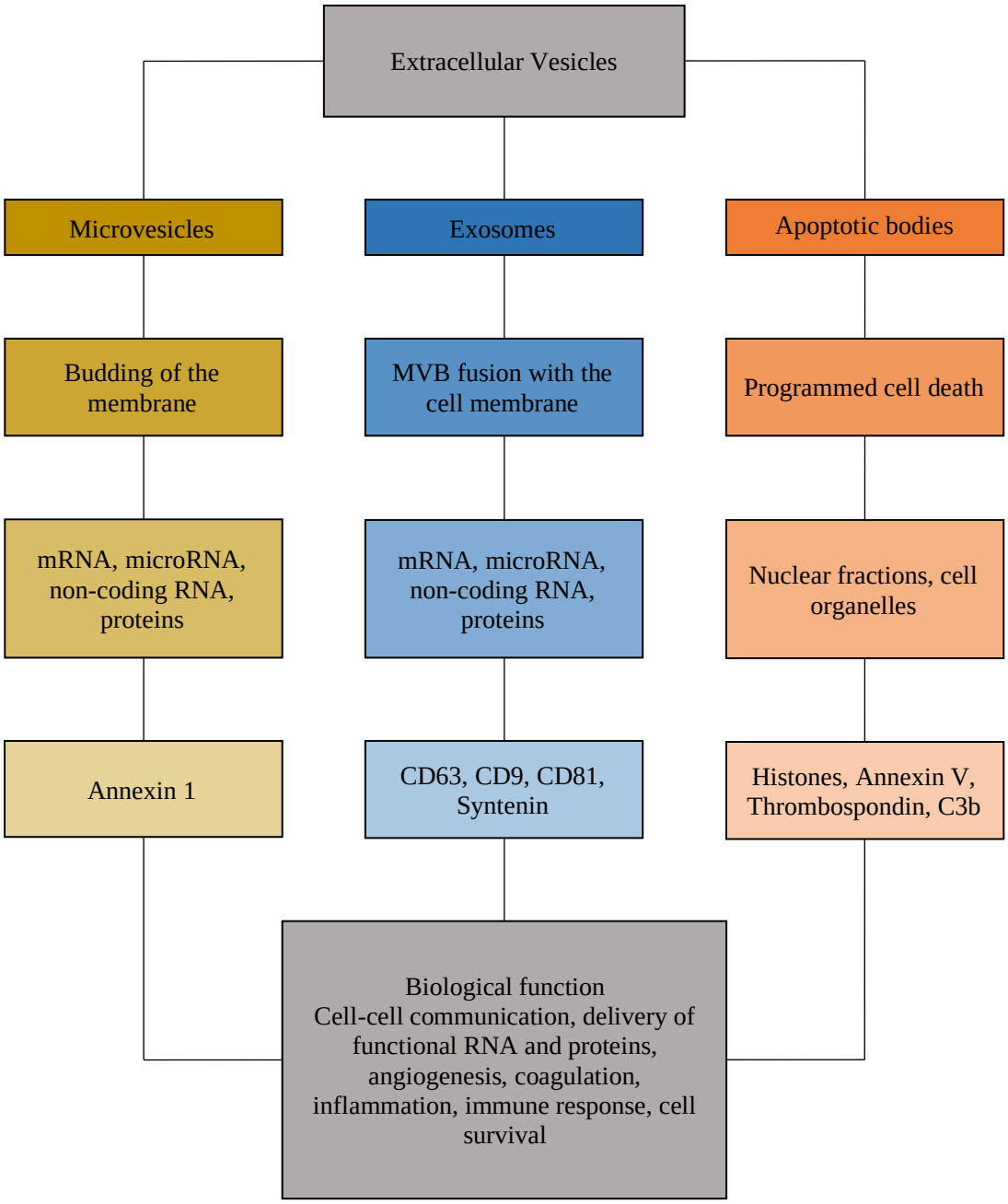



**Figure 3. Overview of EVs' mode of biogenesis, composition and biomarkers.**

EVs are a heterogeneous population, with three main subtypes, defined according to their biogenesis: microvesicles, exosomes and apoptotic bodies.

Currently, several different EV isolation methods are available. Most widely used are differential centrifugation, density gradient centrifugation, size exclusion chromatography, ultrafiltration, immune-capture and precipitation. Each have their own limitations and advantages. After the isolation and separation of EVs, and before any subsequent experiment,

it is crucial to characterise and evaluate the purity of the obtained material, as other secreted particles such as lipoproteins can be co-isolated with EVs (Xu *et al.*, 2016). In 2018, the International Society of Extracellular Vesicles (ISEV) published an updated description of the minimal requirements for EVs work (Théry *et al.*, 2018).

The characterisation of EVs should be done using several different approaches to assess their physical and biochemical characteristics (**Table *1*** discusses key methods to analyse EVs). Physical characterisation of EVs is challenging due to their size and low refractive index (RI). It has been demonstrated that both polystyrene and silica beads, commonly used for the calibration of the optical methods used to measure EV's size, have higher RI than EVs, and therefore, can overestimate their size (Valkonen *et al.*, 2017). Currently, size measurements can be achieved by transmission electron microscopy (gold standard), nanoparticle tracking analysis, standard flow cytometry for larger EVs, resistive pulse sensing, cryo-EM, etc (Xu *et al.*, 2016).

EVs should also be assessed for their biochemical properties. This is accomplished by evaluating the expression of specific EV biomarkers. According to ISEV guidelines, markers are divided into five categories: transmembrane or GPI-anchored proteins; cytosolic proteins; major components of non-EV co-isolated structures; transmembrane, lipid-bound and soluble proteins associated to other intracellular compartments; and secreted proteins recovered with EVs. Groups one and two serve to analyse the existence of EVs in the sample. Group three aims to evaluate the purity of the sample, while group four should be assessed if the authors claim specificity of their research to a certain EV subtype. Proteins of group five include luminal or secreted proteins that can be associated with EVs through binding to the receptors on their surface. Proteins are the most commonly used markers of EVs, but phospholipids can be used as an additional method to confirm EVs presence too (i.e. detection of

phosphatidylserine through the binding of fluorescently-labelled PS protein) (Théry *et al.*, 2018).

**Table 1. Key methods used to detect single extracellular vesicles**

| Technique | Measurement principle | Advantages | Limitations | Size | Concentration | Targeting surface marker |
|---|---|---|---|---|---|---|
| **Nanoparticle tracking analysis** | Records the Brownian motion of the particles in the solution | Can be used for both monodisperse and polydisperse samples | Underestimates larger vesicles (>500 nm) | Yes | Yes | Yes (in fluorescent mode) |
| **Electron microscopy** | Utilizes electrons to create an image | Gold standard for size and shape of EVs | Time consuming, specific expertise | Yes | No | Yes |
| **Flow cytometry** | Detects light scattering and fluorescent signal that is generated when a particle is illuminated by a laser | Detection of multiple surface markers simultaneously | Suitable for larger particles, swarm effect | No | Yes/No | Yes |
| **Resistive pulse sensing** | Measures the difference in the conductance when a particle is passing through a sensing pore | Limited reliance on instrument settings | Not suitable for the detection of all particles >70 nm | Yes | Yes | No |

To date, EVs have been isolated from various cell types and biological fluids (i.e. blood, urine, saliva, amniotic fluid, breast milk, seminal fluid, etc.) and several different cellular functions have been ascribed to them (Yáñez-Mó *et al.*, 2015). It has been shown EVs play a role in angiogenesis, coagulation, inflammation and immune response, intercellular communication and cell survival (Yuana, Sturk and Nieuwland, 2013). EV function relies not only on their

surface markers, but on their cargo as well. For example, the role of EVs in angiogenesis has been scrutinised over the last couple of years. Studies showed that microvesicles derived from endothelial cells carry metalloproteinase proteins MMP-2 and MMP-9 that have proangiogenic properties (Taraboletti *et al.*, 2002). Similar function has been observed by platelet microvesicles – though through a different mechanism of action. These microvesicles contain vascular endothelial grow factor (and other grow factors) that stimulate angiogenesis by the activation of phosphoinositide 3-kinases (PI3-kinase) (Brill *et al.*, 2005). Lymphocytes derived microvesicles have anti-angiogenic properties due to their ability to increase the production of reactive oxygen species and reduce the production of nitric oxide (NO) (Yang *et al.*, 2008; Yuana, Sturk and Nieuwland, 2013). Some of the work done in cancer research showed that EVs released from stromal cells can induce breast cancer cell growth through the activation of antiviral and NOTCH3 pathway (Boelens *et al.*, 2014), while EVs from breast cancer cells contain miR-122 that inhibits glucose-uptake by non-cancer cells in pre-metastatic niches (Fong *et al.*, 2015). All these studies confirm that EV function depends on their content, which reflects the type and physiological or pathological state of their cellular origin, and that the packing of their cargo is a controlled process.

A number of papers have been published discussing the cargo of EVs, and databases that categorise and describe the composition (lipids, proteins, RNA) of EVs from different sources are available (Vesiclepedia, http://microvesicles.org/ (Kalra *et al.*, 2012); the exRNA Atlas, https://exrna-atlas.org (Subramanian *et al.*, 2015)). The uptake of EV by recipient cells consist of three major processes: targeting, entry, and delivery of the cargo. Targeting of the recipient cell can either be specific through the recognition of EVs' surface components (proteins, sugars, lipids) by the recipient cell, or unspecific through pinocytosis. Once EVs are internalised, their cargo is released through endosomal escape. Another possibility is that they are re-cycled and released again or degraded by the lysosomes. However, most studies have

focused on the content of the cargo rather than the final stage of EV internalisation. Further research is needed to gain better understanding of this process (Mathieu *et al.*, 2019).

### 1.3.2. Placenta

The placenta is a fascinating organ. During its temporary existence, it acts as many organs (liver, kidney, lung, gut etc.) in one in order to shelter the growth of the foetus. The placenta's development starts with blastocyst invasion of the endometrium at day six or seven post-conception (Myren *et al.*, 2007), and therefore, genetically it belongs to the foetus. The placenta is the interface of foetal and maternal interactions. Its main role is to transfer nutrients and oxygen from the mother to the foetus, and to remove waste from the foetus. It is also responsible for hormone and protein production that will mediate maternal physiological adaptation during pregnancy. In order to secure these transfers, the placenta has a complex structure (Burton and Fowden, 2015; Griffiths and Campbell, 2015).

The human placenta is a discoid organ that consists of a chorionic plate (attached to the foetus through the umbilical cord) and a basal plate (adjoined to the maternal endometrium). Between these plates there is a cavity, filled with maternal blood, called intervillous space (**Figure *4***).

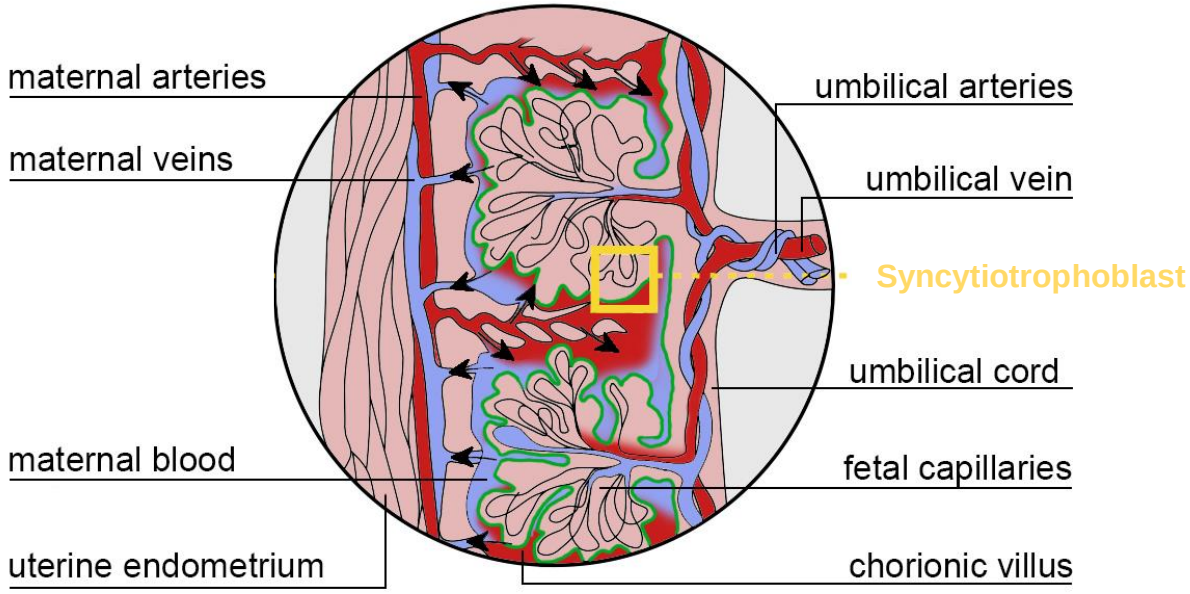



**Figure 4. Schematic presentation of term human placenta, which consists of two circulations: maternal and foetal.**

Oxygenated blood arrives from the maternal circulation into the intervillous space. Deoxygenated foetal blood comes through umbilical arteries to chorionic villi capillaries for the exchange of nutrients and gases. The interface of these circulations is the syncytiotrophoblast, the outer layer of chorionic villi trees.

The foetal side of the placenta consists of chorionic villi trees. 'The trunk' of this villus tree is attached to the chorionic plate, while the "branches" are projected into the intervillous space. Chorionic villi contain foetal vessels with their terminal brunches being highly vascularised with foetal capillaries. It is on the outer layer of these terminal villi that the majority of foetal-maternal exchange occurs (Burton, Fowden and Thornburg, 2016). The outer layer is called the sycytiotrophoblast layer (STB) – a multinucleated epithelium with no intercellular cleft and an area of 12-14 $m^2$ that separates maternal and foetal circulation. The STB has no proliferative features but instead is formed and continuously replenished by the fusion of underlying cytotrophoblast cells (Simpson, Mayhew and Barnes, 1992). A unique characteristic of the STB is that it does not express major histocompatibility region antigens HLA-A and HLA-B,

which are normally expressed by nucleated cells, and thus prevents the rejection of the organ by maternal natural killer (NK) and T cells (Burton and Fowden, 2015). Furthermore, due to its strategic position, the STB has an important paracrine function during pregnancy. The STB layer releases soluble factors such as placental hormones, growth factors and extracellular vesicles into maternal blood, aiding the development of the foetus.

### 1.3.3. Syncytiotrophoblast extracellular vesicles

It is now well established that the syncytiotrophoblast monolayer covering the placental chorionic villi releases syncytiotrophoblast extracellular vesicles (STB-EVs) into the maternal circulation during pregnancy (**Figure *5***) (Knight *et al.*, 1998; Pantham, Askelund and Chamley, 2011; Sarker *et al.*, 2014). In line with new ISEV guidelines, in this thesis the syncytiotrophoblast-derived vesicles (STB-EVs) are classified as "small EV" (SMALL STB-EV; <200nm) and "medium/large EVs" (MEDIUM/LARGE STB-EV; >200nm) as the two subtypes of vesicles have been obtained according to their size (Théry *et al.*, 2018).

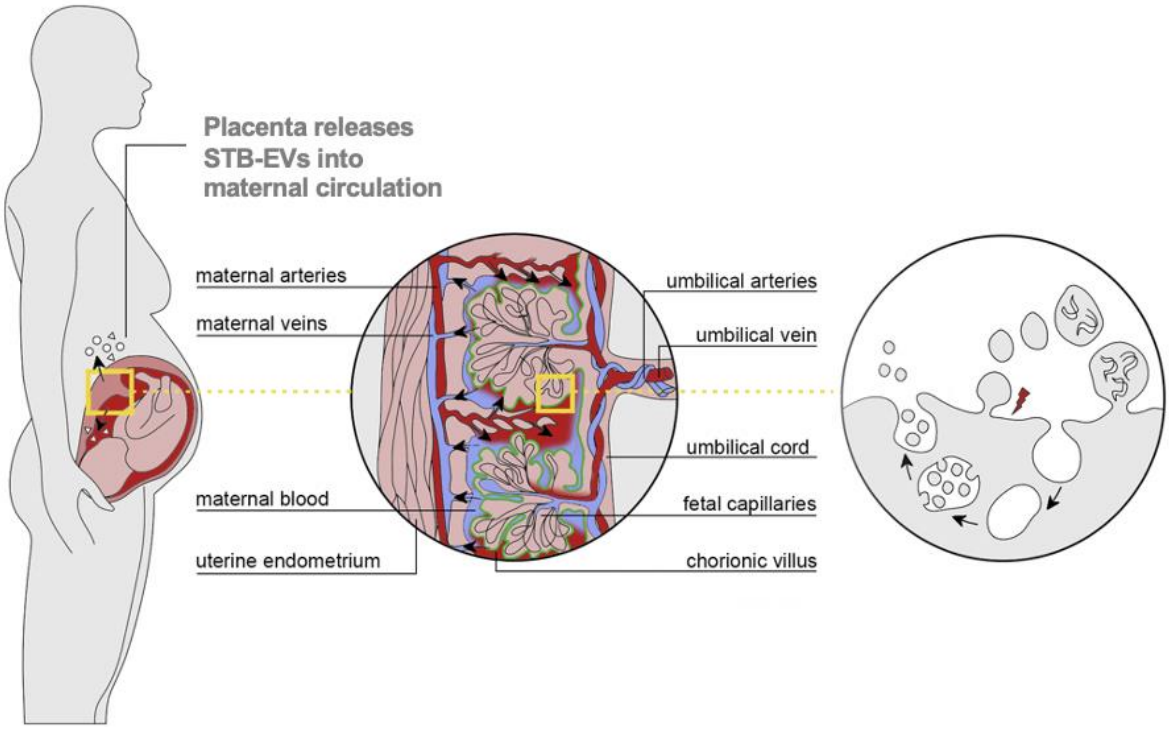



**Figure 5. STB-EVs are released from syncytiotrophoblast layer into maternal circulation.**

It has been reported that STB-EVs can be detected in the maternal blood as early as six weeks of gestation (Sarker *et al.*, 2014), which is before the establishment of the maternal blood flow in the intervillous space (though the mechanism remains unclear). The secretion of placental EVs increases as pregnancy progresses and rapidly decreases immediately after delivery (Reddy *et al.*, 2008). The placental origin of these EVs is determined by the expression of the placental alkaline phosphate (PLAP) present in these EVs (Cockell *et al.*, 1997; Germain *et al.*, 2007; Luo *et al.*, 2009) and the ratio of quantity of these EVs between uterine and peripheral vein blood (Knight *et al.*, 1998). *Ex vivo* STB-EVs can be obtained using mechanical disruption, cultured placental explants and dual lobe placenta perfusion (Burton *et al.*, 2014).

Producing STB-EVs through mechanical disruption, as the name suggests, involves physical agitation of STB in order to stimulate vesiculation. The vesicles collected with this method have been reported to have higher lipid content that can increase their ability to inhibit

endothelial cell proliferation. Therefore, less disruptive methods (i.e. placental explants and placental prefusion) are preferred techniques for obtaining more physiologically representative STB-EVs. Placental explants STB-EVs are generated by culturing placental tissue and isolating EV from the culture medium (Gupta, Holzgreve and Hahn, 2008; Tannetta *et al.*, 2013; Tong, Abrahams and Chamley, 2018).

In this thesis, *ex vivo* dual perfusion of a single placental lobe was used to collect the STB-EVs. The technique tries to preserve the phycological state of a single cotyledon by maintaining the circulation on both foetal and maternal side of placenta once the placenta is delivered. As a non-invasive technique that causes no harm to mother and baby, it has been widely used to study different placental functions including drug transport and metabolism, release of steroids hormones, cytokines as well as STB-EVs. The principal advantage of this technique is that the structural integrity of the placenta is preserved, while the main disadvantage of the method is the lack of standardization in the experimental set up among different laboratories (Hutson *et al.*, 2011; Burton *et al.*, 2014). A schematic diagram of the perfusion system is shown in **Figure *6***. Firstly, a well-defined and preserved cotyledon is identified. A vein-artery pair on the foetal side is cannulated before the placenta has been placed into a water bath chamber (37°C). The perfusion of the maternal side (facing up in the chamber) is initiated with gentle insertion of an "octopus" (six blunt-tipped needles) in the decidual plate. The foetal and maternal circulations are maintained by roller pumps. As oxygenated maternal perfusate is recirculating through the same lobe, after three hours the medium will be saturated with STB-EVs. In order to validate cotyledon's integrity throughout perfusion, foetal vein outflow is monitored every 20 minutes (Myllynen *et al.*, 2010; Dragovic *et al.*, 2015). The success rate of this technique is reported to be 30-75%, with the most common reasons for failure being leakage or tears in placental tissue (Burton *et al.*, 2014).

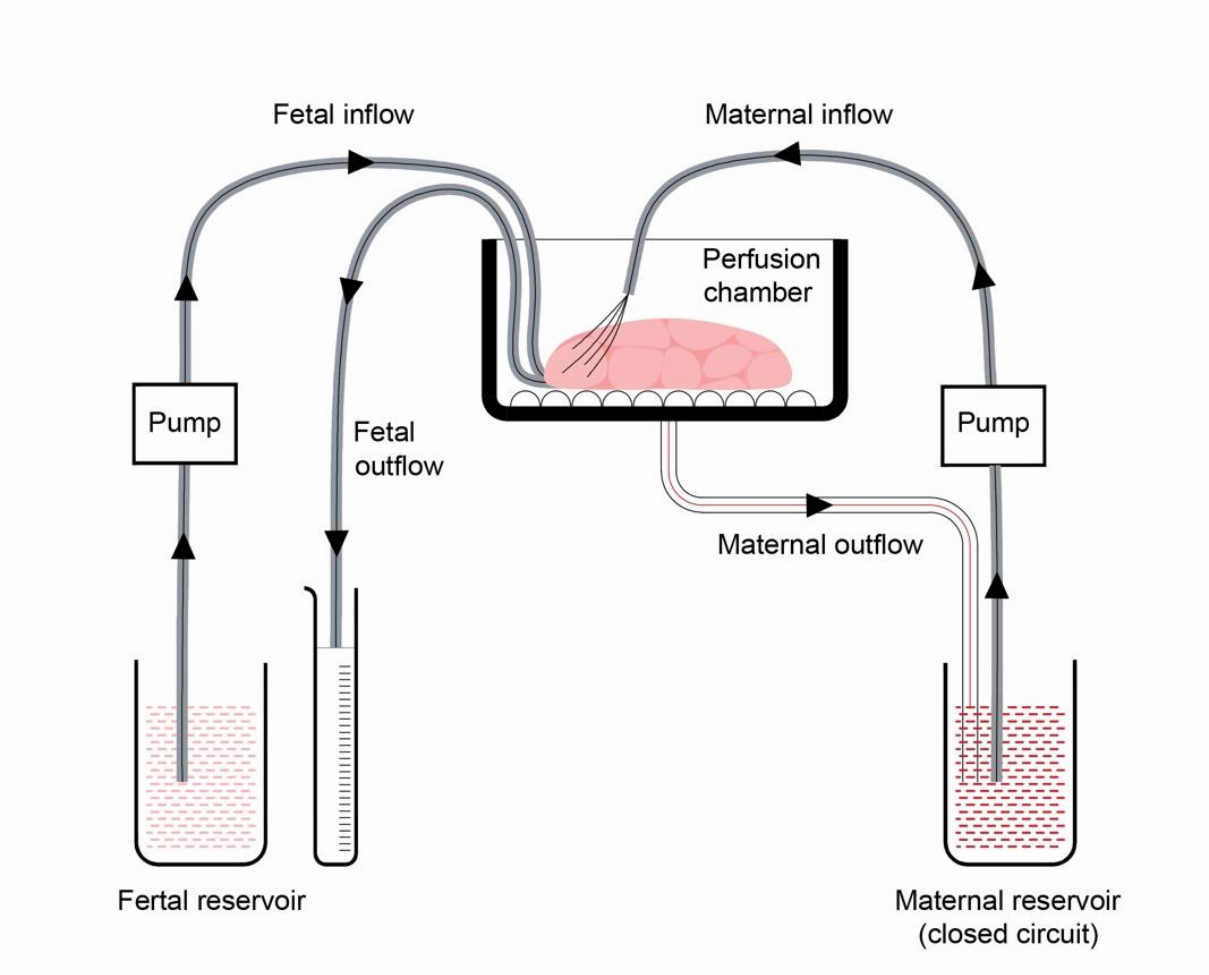



**Figure 6. Schematic illustration of dual perfusion of a single placental lobe.**

To date, several studies have investigated the cargo of extracellular vesicles in pregnancy using mass spectrometry. However, most of these studies did not analyse placental vesicles exclusively, instead performing the proteomic characterisation of total plasma EVs. Atay *et al.* studied exosomes isolated from trophoblast Swan-71 cells and identified 232 unique proteins (Atay, Gercel-Taylor, Kesimer, *et al.*, 2011). Identified proteins were involved in the cell adhesion, membrane transport and fusion. On the other hand, Burkova *et al*. reported a significantly lower number of proteins identified in placental EVs, suggesting that some of the published results might be overestimated. Another explanation for their data might also be the use of an extensive purification protocol used prior to mass spectrometry analysis. In order to further purify the preparation, the authors used affinity chromatography against CD81

immobilised antibodies. However, it is still to be proven if all the placental exosomes express CD81 (Burkova *et al.*, 2018). The first report of RNA within STB-EVs was confirmed in 2004 by Gupta *et al.* who found corticotropin-releasing hormone (CRH) mRNA in STB-EVs from a villous explant culture, mechanical dissection and placental perfusion. In 2007, the interest in the functionality of STB-EV nucleic acid cargo was furthered by the discovery of microRNAs in them (Luo *et al.*, 2009). The cargo of placental EVs will be discussed in more details later in this thesis (Chapter 5).

As mentioned above, the secretion of placental EVs into the maternal circulation increases as pregnancy progresses (Germain *et al.*, 2007), positively correlating with insulin resistance during pregnancy. As such, STB-EVs might represent a mechanism for potential crosstalk between the placenta and maternal metabolism. The characterisation of STB-EVs biological function(s) has been under increasing scrutiny, and that they may play a role in placental-related disorders has been suggested. Levels of STB-EVs in maternal blood are elevated in pre-eclampsia compared to healthy pregnancies, as discussed below. This strongly supports the concept that STB-EVs are not simple microvillus fragments, but 'vehicles' with considerable biological activity that can interact with maternal cells, with most reports describing their interactions with endothelial and immune cells.

#### 1.3.3.1. Effect of STB-EVs on endothelial cells

Extensive research in the past two decades showed that syncytiotrophoblast extracellular vesicles interact with endothelial cells causing an antiangiogenic and hypertensive effect. In 1993, Smárason *et al.* showed that syncytiotrophoblast microvilli from normal and preeclamptic pregnancies suppressed endothelial cells proliferation *in vitro* to similar extent (Smárason *et al.*, 1993). The same authors later showed that the plasma from preeclamptic patients presented higher inhibitory activity compared to gestationally matched control. This

can be due to the increased release of syncytiotrophoblast microvesicles into the circulation of preeclamptic women, as reported in several studies. According to Knight *et al.*, there is a 40% increase in release of STB-EVs in pre-eclampsia in comparison to healthy pregnancy (Knight *et al.*, 1998). Other reports confirmed that STB-EVs can be internalised by endothelial cells and inhibit their growth *in vitro* (Shomer *et al.*, 2013). Additionally, a study performed by Tong *et al.* showed that placental vesicles, when administrated *in vivo*, interact rapidly with endothelial cells, with 60% of interactions happening within 30 min after the injection, supporting STB-EV's potential role in maternal cardiovascular adaptations during pregnancy (Tong *et al.*, 2017).

Tannetta *et al.* reported that STB-EV-bound Flt-1 and endoglin might contribute to the perturbation of the maternal vascular endothelium. Furthermore, they demonstrated that both factors can bind their respective ligands resulting in the reduction of human umbilical vein endothelial cells (HUVEC) monolayer disruption (Tannetta *et al.*, 2013). The effect of placental microvesicles on HUVEC gene expression was also studied, but no significant difference was found between treated and non-treated cells.

In addition to damaging endothelial cells directly, STB-EVs can produce an excessive inflammatory response through the activation of neutrophils. Von Dadelszen *et al.* reported that supernatants from human umbilical endothelial cells that were treated with STB-EVs, have the ability to secondarily activate neutrophils (von Dadelszen, Hurst and Redman, 1999).

In contrast to the aforementioned research, O'Brien *et al.* (O'Brien, Baczyk and Kingdom, 2017) reported recently that the disruption of endothelial cells is due to soluble factors released from placentae rather than placental exosomes. The group used ultracentrifugation to separate the two fractions and showed significant angiogenesis suppression when the endothelial cells were treated with soluble factors in comparison to the treatment with placental exosomes.

#### 1.3.3.2. Effect of STB-EVs on immune cells

Previous research has established that STB-EVs can interact with immune cells such as peripheral blood mononuclear cells (PBMCs), natural killer cells (NK cells), monocytes/macrophages, T cells, and neutrophils. It has been suggested that STB-EV support complex alteration in the maternal immune system to help secure the growth of the foetus. It has been shown that STB-EVs have immunosuppressive properties on natural killer cells and T-cells suggesting that placental EVs might help prevent foetal rejection by the maternal immune system (Thibault *et al.*, 1991; Pap *et al.*, 2008). Additionally, STB-EVs can mediate the immune privilege of the foetus through the activation of PBMCs apoptosis. Death messengers, Fas Ligand (FasL) and TNF-related apoptosis-induced ligand (TRAIL), expressed by STB-EVs, are able to trigger Jurkat T cell and stimulate PBMC apoptosis (Stenqvist *et al.*, 2013). Normal pregnancy is also an inflammatory state due to the controlled activation of the maternal innate immune system, and it possibly represents a physiological compensation for suppressed T and NK cell mediated immune responses (Tannetta, Masliukaite, *et al.*, 2017). For example, STB-EVs have a pro-inflammatory effect through the stimulation of monocyte migration as well as their production of pro-inflammatory cytokines such as interleukin (IL)-1 β, IL-6, Serpin-E1 and TNF-α (Atay, Gercel-Taylor, Suttles, *et al.*, 2011).

### 1.3.4. STB-EVs in GDM Pregnancy

In contrast to preeclampsia, little attention has been paid to EVs' role in GDM. As in preeclampsia, the mechanism by which GDM occurs is not fully understood, but clearly involves the placenta since delivery rapidly attenuates insulin resistance. Recently, Salomon *et al*. reported an increased concentration of placenta-derived exosomes in GDM pregnancies' maternal plasma during gestation, with a two-fold greater increase in the first trimester of pregnancy. This finding supports the potential of placental vesicles as a diagnostic tool for

GDM. However, while both total and placenta-derived concentrations of exosomes were higher in GDM when compared to normal pregnancy, the ratio of placenta-derived exosomes to total plasma exosomes was lower in GDM than in normal pregnancy at early, mid and late gestation. The authors did not provide evidence to explain this finding but suggested this might be due to increase in release of exosomes from non-placental sources or/and changes in the release of placenta-derived exosomes. As GDM is a proinflammatory condition, the same study investigated the release of proinflammatory cytokines from endothelial cells treated with placental exosomes and showed a 3.3-fold increase in cytokine production from the cells treated with exosomes isolated from GDM pregnancies (Salomon *et al.*, 2016).

The same group also reported that first trimester trophoblast cells release more exosomes under high glucose treatment (although this model would be more reflective of the Type 2 Diabetic environment rather than the GDM). Furthermore, human umbilical endothelial cells treated with those exosomes showed increased production of proinflammatory cytokines under high glucose. However, in this *in vitro* study supraphysiological glucose levels (25mM) were used, and therefore, the question remains if the same effect would have be observed *in vivo* (Rice *et al.*, 2015).

Another study further established these observations – again, showing that placental exosomes (measured by ELISA with immobilised CD63 and PLAP antibodies) are increased significantly in GDM plasma samples in comparison to control at corresponding gestational age throughout pregnancy. In the same study, endothelial cells were treated with exosomes isolated from plasma samples of women with GDM and demonstrated increased secretion of inflammatory cytokines confirming the association between inflammation and GDM placental exosomes (Liu *et al.*, 2018).

It is known that women with higher BMI are more likely to develop GDM. In 2017, Elfeky *et al.* reported a positive correlation between maternal BMI and exosomal concentration. Using

Nanoparticle Tracking Analysis they observed that both total and placental exosomes counts are increased with higher maternal BMI. In the first trimester, around 12% of circulating exosomes were placental in origin, while in the third trimester the number was significantly increased reaching ~20% (Elfeky *et al.*, 2017).

Most recently, two reports investigating the cargo of extracellular vesicles obtained from GDM have been published – both discussed later in this thesis. Taken together, these studies highlight the need for further investigation of the role of placentally derived extracellular vesicles in GDM.

## 1.4. Aims

In summary, GDM is the most common metabolic disorder in pregnancy and a significant predictor of long-term T2DM in affected mothers. Although the cause of GDM is not fully understood, it has been shown to involve the placenta since the organ's delivery leads to a rapid improvement in insulin sensitivity. The placenta releases extracellular vesicles (STB-EVs) into the maternal circulation, carrying proteins and nucleic acids. This DPhil seeks to study the role of STB-EVs in orchestrating pathophysiology of GDM with the following aims:

1. To investigate the expression and activity of dipeptidyl peptidase IV (DPPIV) on STB-EVs in normal and GDM pregnancies.

2. To study the expression of insulin receptor (IR) on STB-EVs, and their role as decoy receptors capable of neutralising maternal insulin.

3. To systematically and comprehensively characterise the proteomic cargo of normal and GDM STB-EVs using mass spectrometry. Our goal is to identify differences at the proteomic level and potentially identify novel disease-causing or disease-reporting targets.

# 2. Material and methods

## 2. 1. Patients and samples

This project was approved by the Central Oxfordshire Research Ethics Committee C (REFS 07/H0607/74 & 07/H0606/148). All participants gave written informed consent and all were pregnant women scheduled for elective Caesarean section. In order to diagnose GDM, oral glucose tests (OGTT) were performed at 26-28 weeks of gestation. Cut-off values established by guidelines from the Oxford University Hospital for GDM diagnosis were either a fasting plasma glucose level ≥ 5.1 mmol/L and/or a glucose level ≥10.1 mmol/L at one hour and/or ≥ 8.5 mmol/L at two hours after a 75 g oral glucose load. Exclusion criteria for this study led to the omission of women with multiple pregnancies, as well as patients with pre-pregnancy diabetes, cardiovascular disease or pre-eclampsia. Women without abnormal OGTT results formed a control group.

Here, we collected either blood or placentae from participants. Placentae were perfused within 10-15 min of collection following the protocol described below. Blood samples were collected in citrated plasma tubes (BD Vacutainer, UK). Peripheral blood samples were taken from the left antecubital fossa, while uterine vein blood samples were taken at Caesarean section prior to delivery of the foetus. Samples were centrifuged at 1,500 x g for 15 min to separate cells from supernatant. The resulting platelet-poor plasma was immediately used for flow cytometry analysis or stored at -80°C until used on ExoView platform (NanoView Biosciences, US).

Additionally, placental lysates were obtained with HEPES buffer and a protease inhibitor cocktail (Sigma Aldrich, UK), and subjected to a BCA protein assay (Sigma Aldrich, UK), before storage at -20°C until analysis.

## 2.2. Immunohistochemistry

Fixed placental tissues (4% v/v formaldehyde) were embedded in paraffin blocks and cut into 10 μm thick sections. Placental sections were deparaffinised in Histoclear (Sigma Aldrich,

UK), and rehydrated in graded ethanol. Slides were then heated in 10 mM sodium citrate (pH 6, 10 min) and cooled down at RT. Endogenous peroxidase activity was blocked with 3% $H_2O_2$ in PBS to prevent high background staining. Slides were rinsed with water prior to blocking for non-specific antibody binding using 10% foetal calf serum (FCS) (Sigma Aldrich, UK) in PBS-T (PBS with Tween-20) (Sigma Aldrich, UK) at RT for 1 h. For the primary antibody staining, sections were incubated overnight at 4°C with 1% FCS and the antibody of interest (0.5 µg/mL anti-CD26 (Abcam, Cambridge, UK) or 1:10 anti-IR (Atlas Antibodies, Sweden)) or non-immune mouse IgG1 (negative control) (Biolegend, UK) in PBS-T. The following morning, sections were washed in PBS and incubated with an appropriate IgG secondary antibody in a humidifying chamber at room temperature for 1 h. Slides were washed with 0.01% PBS-T before being stained with DAB (Vector Laboratories, US). All slides were washed in 0.01% PBS-T and in distilled water before nuclei were counter-stained with Hematoxylin (Thermo Fisher, UK) for 10 min. The slides were then dehydrated in graded ethanol and Histoclear. Finally, slides were mounted in Depex mounting medium (Sigma Aldrich, UK) and examined using a Leica DMIRE 2 microscope. Hamamatsu Orca digital camera and HCI software were used to take images.

## 2.3. Isolation and characterisation of STB-EVs

The placental dual lobe perfusion system was performed as previously published (Dragovic *et al.*, 2015). Placentae were perfused for 3 h and the maternal side perfusate was collected. The perfusate was immediately centrifuged twice at 1,500 x g for 10 min at 4°C to remove erythrocytes and large cellular debris (Beckman Coulter Avanti J-20XP centrifuge and Beckman Coulter JS-5.3 swing out rotor). Sequential centrifugations were performed to separate STB-EVs according to their size. The supernatant was collected and spun at 10,000 x g (Beckman L80 ultracentrifuge and Sorvall TST28.39 swing out rotor) for 35 min at 4°C,

before the pellet was re-suspended in sterile PBS to obtain MEDIUM/LARGE STB-EVs (100 nm - 1 μm in diameter). The remaining supernatant was filtered through a 0.2 μm Stericup filter (Millipore, Watford, UK) and spun at 150,000 x g for 125 minutes at 4°C (Beckman L80 ultracentrifuge and Sorvall TST28.39 swing out rotor) to pellet smaller size exosomes (SMALL STB-EVs) (50 μm – 250 μm) (**Figure *7***). SMALL STB-EVs were resuspended in sterile PBS. Bicinchoninic Acid (BCA) protein assay kit (Thermo Scientific Pierce, UK) was used to measure protein concentration of both MEDIUM/LARGE STB-EVs and SMALL STB-EVs (as described below). Particle size was characterized with Nanoparticle Tracking Analysis (Nanosight NS500, Malvern Instruments, Malvern, UK). To confirm STB origin, both EV types were assessed for PLAP (placental alkaline phosphatase; a marker of STB) expression. Additionally, SMALL STB-EVs were analysed for the expression of exosomal markers (syntenin, Alix and CD9). Resin embedded transmission electron microscopy (TEM) analyses were done by Prof David Ferguson, Radcliffe Department of Medicine, University of Oxford.

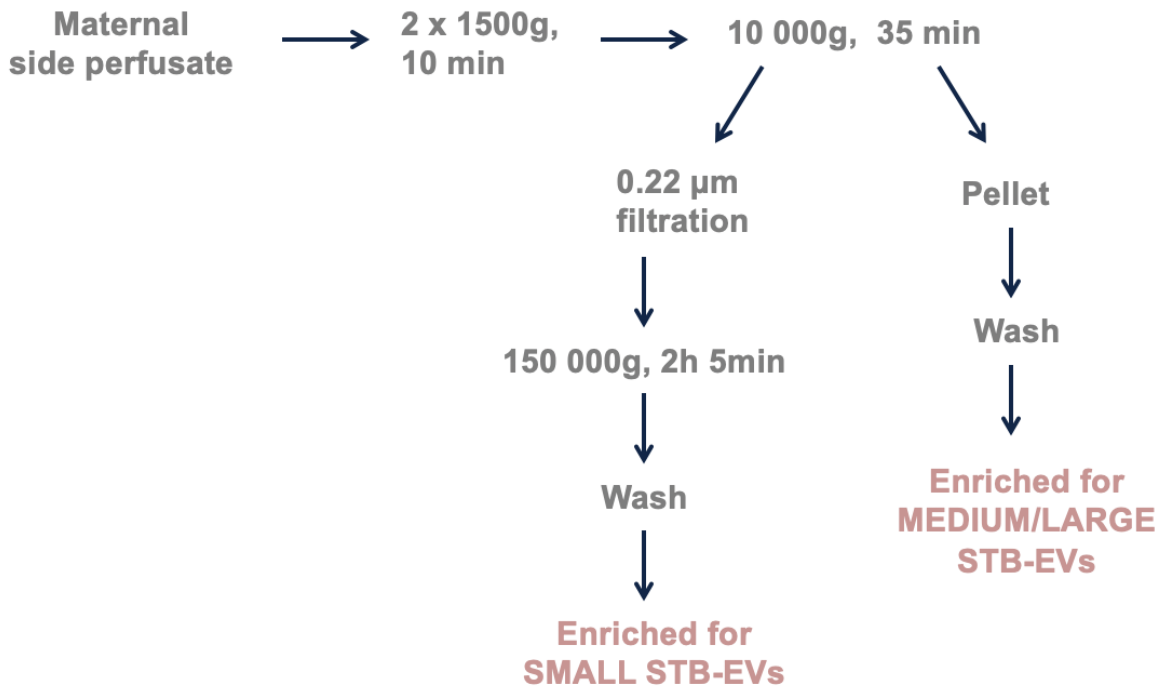



**Figure 7. A schematic representation of the STB-EV isolation process from maternal perfusate after ex vivo placenta perfusion.**

## 2.4. BCA protein assay

Protein concentration in placental lysates, MEDIUM/LARGE STB-EVs and SMALL STB-EVs, was assessed using the bicinchoninic acid (BCA) protein assay kit (Thermo Scientific Pierce, UK). In an alkaline medium, proteins reduce $Cu^{+2}$ into $Cu^{+1}$ (the biuret reaction). $Cu^{+1}$ then reacts with bicinchoninic acid giving a purple-coloured reaction product.

Bovine serum albumin (BSA) stock solution (2 mg/mL) was diluted in filtered PBS to prepare protein standards with following the concentrations: 2, 1, 0.5, 0.25, 0.125 and 0.0625 mg/mL. If the protein concentration was above the standards' regression line, samples were diluted in filtered PBS accordingly. 12.5 µL of standards and samples in replicates were loaded to a 96-well plate, followed by 100 µL of BCA working reagent (50 parts of BCA Reagent A mixed with 1 part of BCA Reagent B). The plate was covered in foil and put on the shaker briefly before 30 minutes incubation at 37°C. Absorbance was measured at 562 nm using a FluoStar OPTIMA (BMG Labtech, Aylesbury, UK) plate reader.

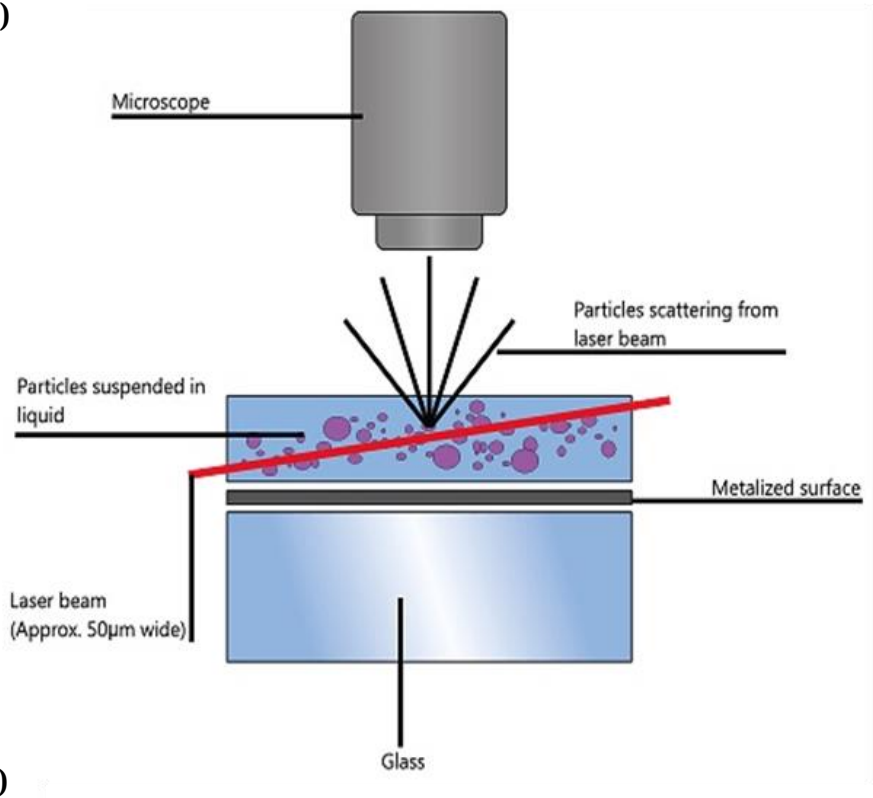
## 2.5. Nanoparticle Tracking Analysis

The size and concentration of STB-EVs were measured using a NanoSight NS500 (Malvern Instruments, Malvern, UK) as previously described (Dragovic *et al.*, 2015). The sample is first distributed into a glass prism before a finely focused laser beam passes through the sample and illuminates particles. Illuminated vesicles are visualised using a conventional optical microscope with an incorporated charged-couple device camera. The camera collects light scatter from all the particles in the view field of the sample chamber (**Figure *8A***). Recorded videos are analysed by Nanoparticle Tracking Analysis (NTA) software, developed to first identify the particles in the solution before tracking the Brownian movement of each. The software uses the two-dimensional Stokes-Einstein equation (Filipe, Hawe and Jiskoot, 2010)

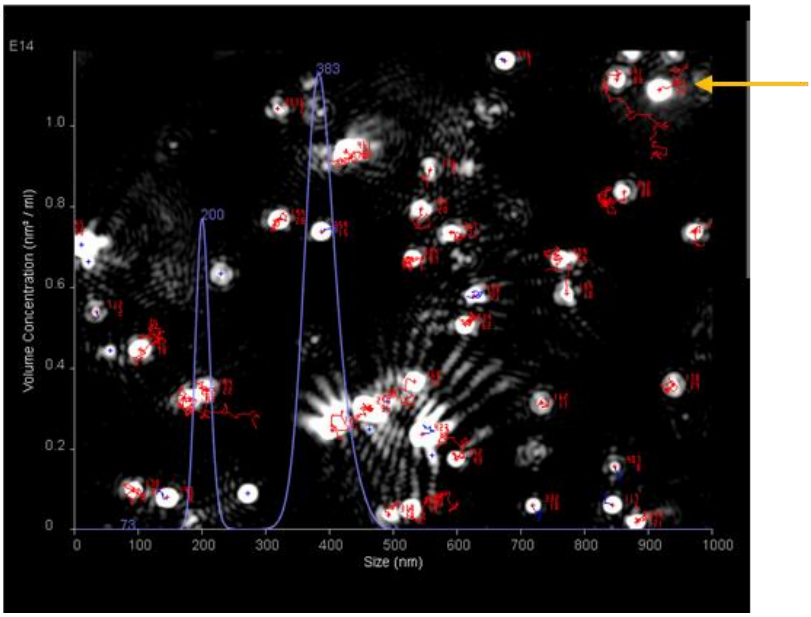
to calculate particles' size and concentration by the velocity of their movement (***Figure 8B***). Our NTA machine was equipped with a sCMOS camera and software version 2.3, Build 0033 (Malvern Instruments, UK). At the beginning of the day, the instrument was calibrated using silica 100 nm microspheres (Polysciences, UK).

The calibration protocol starts with flushing the system slowly with filtered PBS, accompanied by a few rapid flushes to remove any air bubbles that might be stuck in the sample chamber. Next, chamber's correct stage position is checked. The video camera is kept at Level 12. Silica beads (100 nm size) were diluted in filtered PBS to achieve a 1:50,000 dilution before passing them through the NTA system using a 1mL syringe device. The camera focus was set up using the beads, and the script 'PRIME, DELAY 5, CAPTURE 30; REPEAT4' was loaded for recording five 30 seconds long videos with 15 frames per second. The data summary includes particle number, mean size and mode. NTA calibration is considered accomplished if silica beads particle number is close to $5x10^8$ particles/mL and mode size is close to 100 nm.

**A)**




**B)**




**Individual particle's movement is tracked under the Brownian motion**

**Figure 8. Nanoparticle Tracking Analysis (NTA).**

Finely focused laser beam passes through the sample and illuminates particles. Particles scatter the light that is collected using a conventional optical microscope with an incorporated charged-couple device camera. **(A)** NTA software analyses recorded videos to identify the particles and to track their Brownian movement. The software uses the two-dimensional Stokes-Einstein equation to calculate the size (nm) and number of particles (particle/mL) by the velocity of their movement. **(B)** Image taken from Malvern Panalytical Website (www.malvernpanalytical.com).

## 2.6. Immunoblotting

30 µg/well of placental lysates, MEDIUM/LARGE STB-EVs and SMALL STB-EVs were denatured at 95°C in Laemmli Sample Buffer and β-mercaptoethanol (Bio-Rad, UK) and separated on Mini-Protean TGX NuPAGE gel cassettes (Bio-Rad, UK) for 1 h at 150 V. Proteins were transferred onto an immuno-blot polyvinylidene difluoride membrane (Bio-Rad Laboratories, UK) in a Novex Semi-Dry Blotter (Life Technologies, UK) for 45 min at 25 V. Membranes were blocked for 1 h at RT in 5% (w/v) Blotto (Alpha Diagnostic, UK) in TBS-T (Tris-buffered saline solution with 0.1% Tween-20) and incubated with the primary antibody of interest (**Table *3***) overnight at 4°C. Membranes were washed 3 times in TBS-T and incubated with HRP-conjugated secondary antibodies in Blotto/0.1% TBS-T for 1 h at RT (Life Technologies, UK). After washing the membranes with TBS-T, antigen-antibody complexes were visualised by chemiluminescence using an ECL kit (ECL Western Blotting substrate, Thermo Scientific, UK).

SMALL EVs isolated from HUVEC, MDA-MB-231, and EAHY923 cells were a gift from Dr Helen Sheldon. Ms Teresa Vilanova Perez provided SMALL EV from HEK293T cells, and Prof Qing Cao MEDIUM/LARGE and SMALL EVs from platelets.

**Table 2. Composition of western blotting reagents.**

| Buffers | Composition |
|---|---|
| **Laemmli 4X reducing buffer pH 6.8** | 90% 4 x Laemmli buffer<br>10% 2-beta-mercaptoethanol |
| **Anode buffer 1 pH 10.4** | 300 mM Tris base<br>20% methanol<br>dH2O to 1 L |
| **Anode buffer 2 pH 10.4** | 25mM Tris base<br>20% methanol<br>dH2O to 1 L |
| **Cathode buffer pH 9.4** | 25mM Tris base<br>40nM 6-aminocaproic acid<br>20% methanol<br>dH2O to 1 L |
| **TBS X10 pH 8.0** | 87.6 g NaCl<br>12.1 g Tris base<br>700 mL dH2O<br>pH 8.0 adjusted by HCl |
| **TBS-T pH 8.0** | 100 mL TBS X10<br>0.1% Tween-20<br>900 mL dH2O |

**Table 3. Antibodies used in western blotting analysis.**

| Antibodies | Concentration/Dilution | Antigen | Manufacturer |
|---|---|---|---|
| **Anti-CD26** | 1 µg/mL | DPPIV | R&D |
| **Anti-CD220** | 1 µg/mL | IR | R&D |
| **Anti-PLAP (NDOG2)** | 0.6 µg/mL | PLAP | In-house antibody |
| **Anti-Alix** | 1:1000 | Alix | Cell Signalling |
| **Anti-Syntenin** | 1:1000 | Syntenin | Abcam |
| **Anti-CD9** | 1:200 | CD9 | Santa Cruz |
| **β-actin** | 1:5000 | β-actin | Abcam |
| **APO1A** | 1 µg/mL | APO1A | Abcam |
| **Anti-CYC1** | 1:1000 | Cytochrome C1 | Cell Signalling |
| **Monoclonal anti-mouse/rabbit immunoglobulin HRP** | 1:2000 | Mouse/rabbit immunoglobulins | Cell Signalling |
| **Polyclonal anti-goat immunoglobulin HRP** | 1:4000 | Goat immunoglobulins | Dako |

## 2.7. Magnetic Bead Depletion

Dynabeads M-280 Sheep Anti-Mouse IgG (Life Technologies, UK) were conjugated to anti-DPPIV (anti-CD26) antibody (Biolegend, UK) or anti-PLAP antibody according to the manufacturer's instructions. Dynabeads coated with anti-IgG1 antibody (Biolegend, USA) or anti-IgG2a antibody (Dako, UK) were used as controls. Briefly, Dynabeads (50 µL) were

washed in $Ca^{2+}$ and $Mg^{2+}$free PBS supplemented with 0.1% BSA and 2 mM EDTA at pH 7.4, pelleted with a magnet, and resuspended in the same buffer. The beads were incubated with 6 µg of either anti-PLAP, anti-DPPIV, anti-IgG1 or anti-IgG2a antibody on a rotating plate overnight, at 4°C. The beads were aggregated using a magnet and supernatants were discarded. MEDIUM/LARGE STB-EVs or SMALL STB-EVs (25 µg for both) were incubated with 10 µL of anti-human Fc receptor blocking reagent for 10 min at 4°C prior to incubation with the beads overnight at 4°C for depletion. Bound and unbound STB-EVs were separated using a magnetic separator (Dynal, Norway). Pellets containing bound antigen-positive STB-EVs were immunoblotted (**Figure *9***). Supernatants (antigen-negative STB-EVs) were analysed by NTA to calculate the percentage of STB-EVs bound to the beads as follows:

% DPPIV or PLAP= ([Total]-[DPPIV or PLAP negative])/([Total])*100

The experimental approach used to investigate IR/PLAP co-expression on SMALL STB-EVs only differed from that outlined above in that the magnetic beads were coated with IR antibody (BD Biosciences, USA).

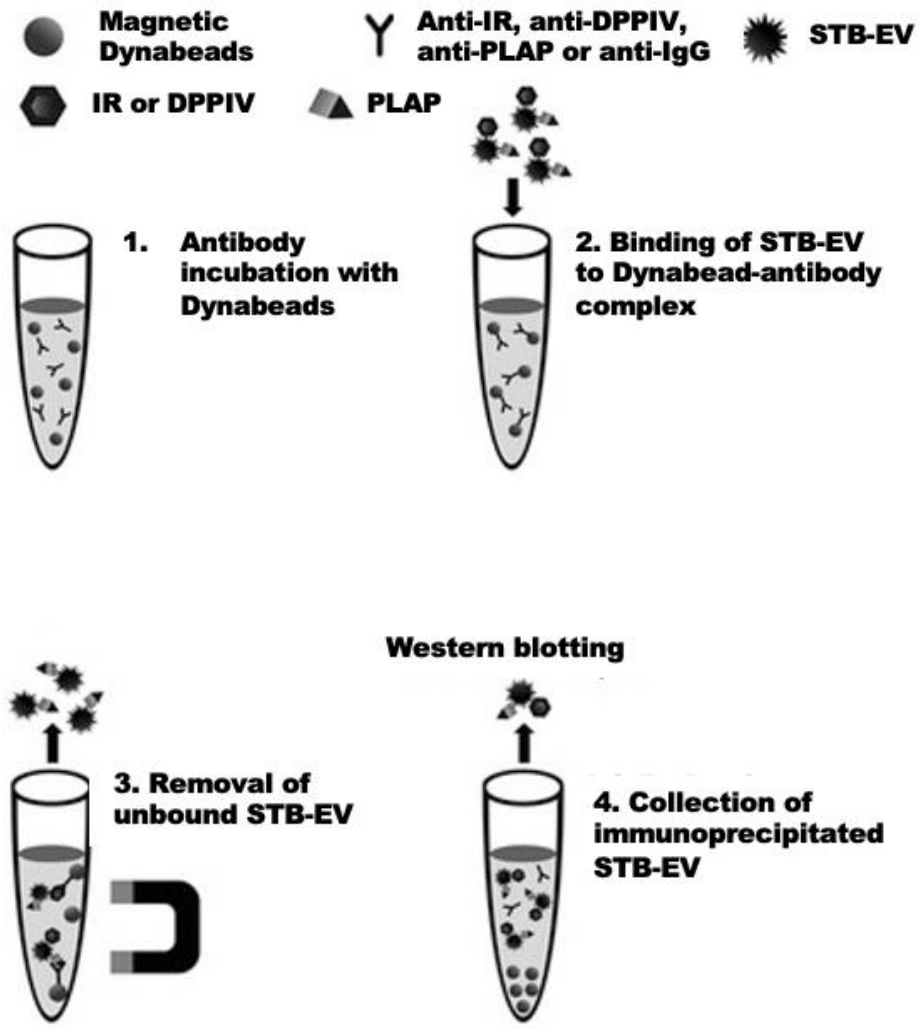



**Figure 9. Schematic illustration of the immunoprecipitation protocol using magnetic Dynabeads.**

First, magnetic beads are coated with the antibody of interest (DPPIV, IR, PLAP or IgG). The STB-EVs are then incubated with a magnetic bead-antibody complex. The unbound STB-EVs are washed away, and those attached to the magnetic bead-antibody complex are collected for subsequent western blot analysis. Adapted from Gill *et al.* (Gill *et al.*, 2019).

## 2.8. Co-expression of IR & PLAP on SMALL STB-EVs using ExoView analysis

ExoView analysis of STB-EVs from placenta perfusion

The ExoView platform from NanoView Biosciences can detect co-expression of different proteins on a single particle (**Figure *10***). An ExoView custom kit (Nanoview Biosciences, Cat.

No. EV-CUST-2) was generated with minor modifications using anti-CD81, anti-PLAP and isotype control antibodies. STB-EVs obtained by placenta perfusion were diluted 1:20 (SMALL STB-EVs) or 1:75 (MEDIUM/LARGE STB-EVs) to avoid oversaturation of the chip, allowing for better visual co-localization. Diluted samples were individually incubated on the custom chips, placed in a sealed 24-well plate for 16 h at RT. The chips were then washed three times in Solution A for 3 min each on an orbital shaker, and subsequently incubated with a cocktail of fluorescently labelled antibodies: anti-IR-Alexa 647 and anti-PLAP-Alexa 555. Antibody incubation was allowed for 1 h at RT with mild shaking. The chips were then washed three times in Solution A for 3 min each on an orbital shaker, then twice in Solution B before being rinsed once in deionised water. After drying, chip imaging was done using the ExoView R100 reader (software nScan v2.8.7.3 for MEDIUM/LARGE STB-EVs and 2.4.3 for SMALL STB-EVs) with enabled fluorescence acquisition. The data were then analysed using NanoViewer v2.8.8. Background fluorescence and non-specific binding were determined based on the isotype control. The scale bar on each image was set to 5µm. All images are sized equally to maintain aspect ratio.

ExoView plasma analysis

Peripheral blood samples were taken from the left antecubital fossa, initially at Caesarean section, and then again, 24 hours after delivery from the same patient (n=5). Platelet poor-plasma was obtained with centrifugation at 1,500 x g for 15 min at RT to separate cells from supernatant. 150 µL of platelet poor-plasma was purified using IZON 70 nm columns (Izon Science, New Zeland). Samples were then concentrated down to 100 µL using ultrafiltration. Subsequent analysis has been performed as described above.

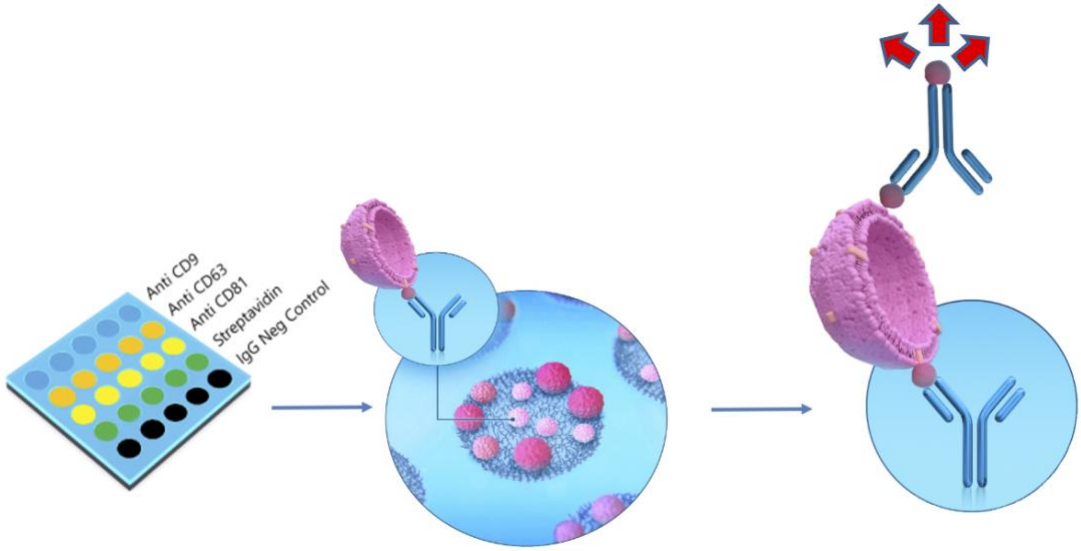



**Figure 10. Schematic representation of ExoView technology.**

The ExoView chip is coated with an antibody of interest. EVs that express corresponding antigen will bind to the antibody on the chip. Fluorochrome conjugated antibodies are then added to the chip to visualise colocalised multiple surface markers on a single EV. Image is taken from NanoView Biosciences website (https://www.nanoviewbio.com/).

## 2.9. Flow Cytometry Analysis

Samples were characterised using a BD LSRII flow cytometer (BD Biosciences, UK). Prior to MEDIUM/LARGE STB-EV FACS analysis, HUVEC cells were used for DPPIV and IR antibody titration. 2.5 x $10^5$ cells were incubated with 5 µL of Fc receptor for 10 minutes at 4ºC. Cell samples were stained with different concentrations of either anti-DPPIV-Alexa Flour 647 or recombinant engineered antibody (REA) anti-IR-APC or its corresponding isotype control. Samples were incubated in the dark for 30 minutes at RT, gently centrifuged and washed with filtered PBS. The volume was adjusted to 300 µL with PBS and 5,000 events were recorded per sample using BD LSRII.

MEDIUM/LARGE STB-EVs flow cytometry analyses

TruCount tubes, containing a known number of fluorescent beads suspended in 500 μL of filtered PBS, were used to establish the flow rate. The background event rate was set at <1000 events/min. MEDIUM/LARGE STB-EV samples from placenta perfusion or placenta explants (provided by Dr Wei Zhang) were diluted in filtered PBS to optimise an event rate of ~300 events/sec in a final volume of 300 μL. Prior to staining, samples were incubated with 10 μL of Fc receptor blocker (Miltenyi, UK) for 10 min at 4°C. Samples were then labelled with anti-PLAP-PE, Bio-maleimide-FITC (used as an STB-EV membrane marker (BODIPY FL N-(2-aminoethyl)-maleimide); Thermo Fisher, UK)) and anti-CD220-APC or anti-DPPIV-Alexa Fluor 647 for 15 min at RT. Isotype controls were matched to their respective antibodies according to the concentration, fluorochrome type, and heavy chain. Prior to data acquisition, final volumes were adjusted to 300 μL with PBS. 100,000 events were collected for each sample. EV gates were set at <1μm using fluorescent beads. The negative gates for staining were determined using isotype control tests and set at 1%. Both data analyses and figure generation were carried out using FlowJo version 10.1 (Tree Star Inc, USA).

Plasma sample flow cytometry analyses

PLAP and IR or DPPIV positive EVs were identified using a four-colour flow cytometry protocol, described previously (Inglis *et al.*, 2016), but with additional modifications to exclude contamination from other EV sources by defining a "dump channel" (Motta-Mejia *et al.*, 2017). The "dump channel" excluded the principal contaminants such as platelet EVs (using anti-CD-41a-PE-Cy7), erythrocyte EVs (using anti-CD235a-PE-Cy7) and EVs derived from all other sources except STB or erythrocytes (using anti-HLA Class I-PE-Cy7 and anti-HLA Class II-PE-Cy7). 100 μL of platelet-poor plasma was labelled with these antibodies, together with anti-PLAP-PE and anti-IR-Alex-Fluor 647 for 15 min at 4°C. Labelled plasma samples were

subsequently filtered using Ultrafree-MC/Durapore-PVDF (Millipore, UK) centrifugal filters (2 min, 800 xg). MEDIUM/LARGE STB-EVs were recovered from the top of the filter unit in 100 µL of filtered PBS, and stained with Bio-maleimide-FITC, which stains biological membranes. Volumes were then adjusted to 500 µL with filtered PBS, and each sample was analysed for 10 min by flow cytometry. Filtrate (negative for Bio-maleimide) was used to define control gates for Bio-maleimide and the 'dump channel' in order to separate the population that was positive for Bio-maleimide and negative for contaminates (**Figure *11***). Events that fell into this gate (i.e. biological membranes but not contaminants) were further analysed for PLAP and IR signal. To determine control gates for anti-IR-Alexa Fluor 647 and anti-PLAP-PE staining, samples were treated with detergent Nonidet P-40 (Sigma Aldrich, UK) to destroy the vesicle lipid membrane. The gates were set at 1% cut-off. Both data analyses and figure generation were carried out using a FlowJo version 10.1.

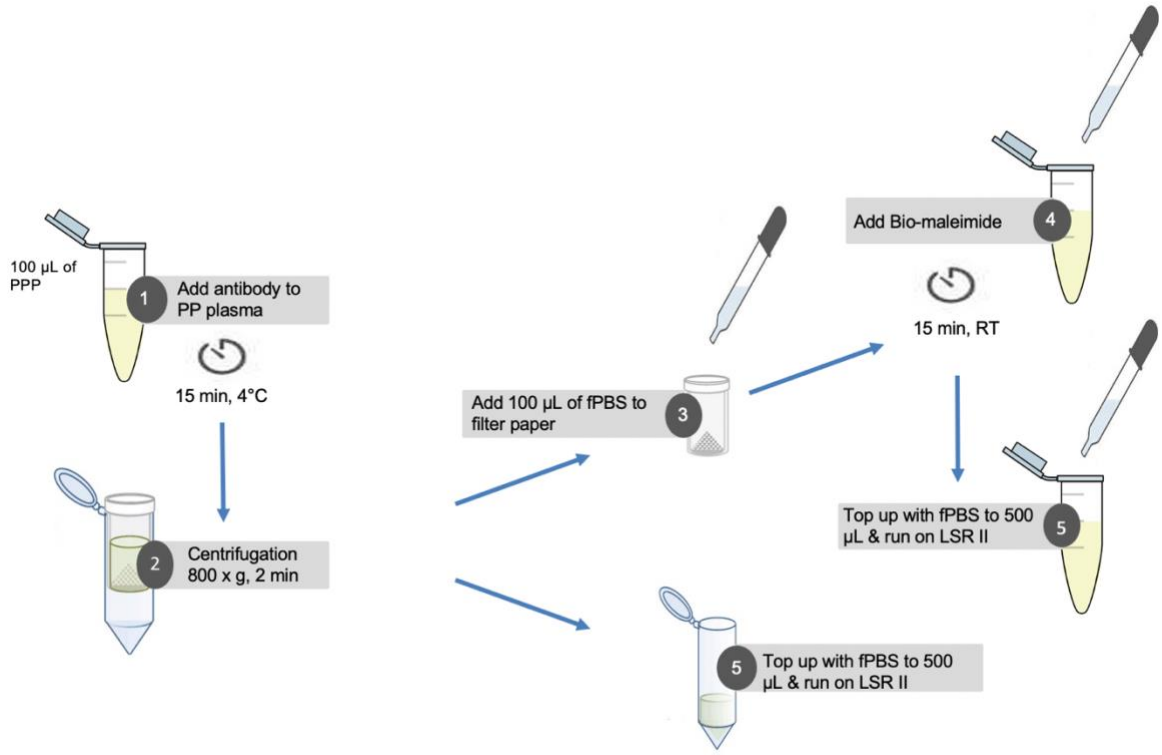



**Figure 11. Protocol for flow cytometry analysis of platelet-poor plasma (PPP) sample.**

Antibodies cocktail was added to 100 µL of PPP and incubated for 15 min at RT. Labelled plasma samples were then filtered using centrifugal filters (2 min, 800 x g). MEDIUM/LARGE

STB-EVs were recovered from the top of the filter unit in 100 µL of filtered PBS, and stained with Bio-maleimide-FITC. Volumes were then adjusted to 500 µL with filtered PBS, and each sample was analysed for 10 min by flow cytometry. Filtrate (negative for Bio-maleimide) was kept too, adjusted to 500 µL and used to define control gates for Bio-maleimide and the 'dump channel.

**Table 4. Antibodies used for flow cytometry.**

| Antibodies | Concentration | Antigen | Source |
|---|---|---|---|
| **Bio-maleimide (BODIFY FL N-(-2-aminoethyl)-maleimide** | 0.25µM | Thiol groups | Molecular probes |
| **Anti-PLAP-PE (NDOG2)** | 0.05µg/mL | PLAP | In-house antibody |
| **IgG1-PE (clone MOPC-21)** | 0.05µg/mL | Isotype control | Biolegend |
| **Anti-CD220-APC (clone REA260)** | 0.022 µg/mL | IR | Miltenyi Biotech |
| **REA-APC Ctrl** | 0.025µg/mL | Isotype control | Miltenyi Biotech |
| **Anti-CD26-APC (IgG2a, κ)** | 1:10 | DPPIV | BioLegend |
| **Isotype Ctrl Mouse IgG2a-APC** | 1:10 | Isotype Control | BioLegend |
| **Anti-CD41-PEvio770** | 0.33µg/mL | CD41 | Miltenyi Biotech |
| **Anti-CD235a/b-PEvio770** | 0.11µg/mL | CD235a/b | Miltenyi Biotech |
| **Anti-HLA Class I-PEvio770** | 2.2mg/mL | HLA Class I | Miltenyi Biotech |
| **Anti-HLA Class II-PEvio770** | 2.2mg/mL | HLA Class II | Miltenyi Biotech |

## 2.10. DPPIV enzyme activity assay

DPPIV enzyme activity of the STB-EVs was determined using a DPPIV-Glo Protease Assay (Promega, UK). The luminescent DPPIV-Glo Reagent was incubated at RT for 30 min with either clinical samples (STB-EVs isolated from perfused placentae from both GDM and normal pregnancy), Tris-BSA (blanks), or a purified DPPIV enzyme in Tris-BSA as standard (Recombinant human CD26 protein, Abcam, UK). Luminescence was measured using a FLUOstar Omega apparatus (BMG Labtech, UK).

For the DPPIV enzymatic inhibition studies, MEDIUM/LARGE STB-EVs and SMALL STB-EVs were pre-treated with Vildagliptin (DPPIV specific inhibitor) (Sigma Aldrich, Gillingham, UK) (0-100 nM) for 1 h, and DPPIV residual enzymatic activity was determined. STB-EV-bound DPPIV ability to break GLP-1 was measured using a GLP-1 active assay according to the manufacturer's instructions (Cisbio, France). MEDIUM/LARGE STB-EV and SMALL STB-EV pools of three GDM patients in series dilution were mixed with 1400 pg/mL of GLP-1 respectively, and incubated with anti-Active GLP-1-$Tb^{3+}$ Cryptate antibody and with anti-Active GLP-1-d2 antibody overnight at RT. Recombinant DPPIV (Recombinant human CD26 protein, Abcam, Cambridge, UK) was used as the positive control, and PBS was used as the negative control. Homogeneous Time Resolved Fluorescence (HTRF) measurement was performed using a CLARIOstar apparatus (BMG Labtech, UK).

## 2.11. Plasma insulin depletion by STB-EVs

Platelet-poor plasma (n=3) was collected from non-pregnant volunteers. 0, 10, 100, 200 and 500 µg/mL of MEDIUM/LARGE STB-EVs (n=3) were incubated with platelet-poor plasma for 30 min at RT. Plasma samples were then centrifuged at 30,000 x g at 4°C for 1 h to pellet the MEDIUM/LARGE STB-EV. The supernatant was collected and analysed using an Insulin

ELISA (DINS00, R&D Systems, UK) as defined by the manufacturer. Acknowledgment to Sylvia Shahjahan for performing the experiment.

## 2.12. Glucose uptake assay

C2C12 cells, passage 7 (provided by Dr Karl Morten, University of Oxford) were seeded at 50,000 cells per mL per well on a clear 12-well plate and grown to a confluence in DMEM (10% FBS). After medium removal, 1 mL of differentiation medium (DMEM with 2% horse serum) was added per well. The medium was changed daily for four days. Differentiated myotubes were then starved overnight in 1 mM glucose DMEM. The following day, 0.1, 1 and 10 nM insulin solutions (both glucose and serum free) were added to the cells for an hour rpior to glucose uptake measurment. Additionally, 150 µg/mL of MEDIUM/LARGE STB-EVs were preincubated with 1nM insulin for 30 min. Glucose uptake was initiated with 500 mL of 0.1 mM 2-deoxyglucose-6-phosphate in PBS and stopped with 250 mL of acidic detergent, which also lysed the cells. 75 mL of lysate was transferred to a 96-well plate and the assay (Glucose Uptake-Glo™ Assay, Promega, USA) was continued following the manufacturer's protocol (Valley *et al.*, 2016). The luminescence was measured using a CLARIOstar optical device (BMG Labtech, USA).

## 2.13. Mass spectrometry

Mass spectrometry analysis of STB-EVs obtained from placenta perfusion have been done in collaboration with the Target Discovery Institute (TDI), University of Oxford. After isolation and characterisation of STB-EVs, both MEDIUM/LARGE STB-EVs and SMALL STB-EVs from GDM (n=4 for both STB-EV subtypes) and normal (n=5 for both STB-EV subtypes) pregnancy were submitted to TDI.

Samples were thawed on ice and lysed in RIPA for 30 min (also on ice) followed by centrifugation at maximum speed. Clear supernatants were collected for each sample. Samples were then reduced with 5 mM dithiothreitol for 30 min, followed by alkylation with 20 mM iodoacetamide for another 30 min. Then, methanol-chloroform was used for precipitation. Pellets were resuspended in 1M (final concentration) urea and digested with approximately 0.85 μg trypsin at 37°C overnight. Digest samples were acidified to 1% formic acid and desalted on Sola Cartridges. Collected eluates were dried to completeness in a SpeedVac. Samples were resuspended in 2% acetonitrile/0.1% formic acid and diluted 1:20 prior to injection. Peptides were injected into a liquid chromatography-mass spectrometry system (LC-MS) comprised of a Dionex Ultimate 3000 Nano LC and a Thermo Q-Exactive mass spectrometer. Peptides were separated on a 50 cm long EasySpray column (ES803; Thermo Fisher, UK) with a 75 μm inner diameter and 60 minute gradient of 2% to 35% acetonitrile in 0.1% formic acid and 5% dimethyl sulfoxide (DMSO) at a flow rate of 250 nL/min.

MS1 spectra were acquired with a resolution of 70,000. The top 15 most abundant peaks were fragmented after isolation with a mass window of 1.6 Th at a resolution of 17,500.

Data analysis was done using Progenesis (Nonlinear/Waters) for quantification and Mascot for protein identification (against UPR_HomoSapiens).

Perseus (https://maxquant.net/perseus/) was used for subsequent analysis (Tyanova and Cox, 2018). Data was $\log_2$ transformed, filtered for valid values (70% valid values in at least one group), and normalised by median. Imputation was used to replace missing values from a normal distribution. Comparison analyses were done with two sample t-tests with permutation-based FDR correction $P<0.05$.

Functional enrichment analyses of differentially expressed proteins were conducted using g:Profiler (https://biit.cs.ut.ee/gprofiler) online software (Raudvere *et al.*, 2019). Proteins were validated using a cumulative hypergeometric test with g:SCS (Set Counts and Sizes) correction

method for multiple testing. Enriched terms from g:Profiler analysis were further summarised and filtered for redundant terms using REVIGO (http://revigo.irb.hr/) (Supek *et al.*, 2011). REVIGO's default settings were used for analysis.

## 2.14. Statistics

Apart from mass spectrometry data (see the paragraph above for a detailed description), results were statistically analysed using Prism 8.0 (GraphPad Software Inc, CA). Comparisons of means between two groups were tested using the independent two-sample Student's t-test, with statistical significance assigned when *$p<0.05$. Paired samples were compared with the Wilcoxon matched-pairs signed rank test. Unpaired samples were analysed using the Mann-Whitney test.

# 3. STB-EVs express active dipeptidyl peptidase IV (DPPIV); circulating levels are increased in GDM

## 3.1. Introduction

Dipeptidyl peptidase IV (DPPIV) is a transmembrane glycoprotein ubiquitously expressed by numerous tissues including the proximal tubule of the kidney, epithelial cells in the small intestine, the vascular endothelium, the liver, and the pancreas (Yazbeck, Howarth and Abbott, 2009; Deacon, 2019). DPPIV is composed of a short cytoplasmatic domain on N-terminus, a transmembrane portion, and a large extracellular domain on C-terminus, responsible for its enzymatic activity. In addition to membrane-bound DPPIV, its soluble form (sDPPIV) has been found in plasma and other biological fluids such as saliva and urine. It is believed sDPPIV originates from the cleavage of the extracellular portion of membrane-bound proteins, and therefore, maintains its catalytic activity (Ohnuma, Dang and Morimoto, 2008; Röhrborn, Eckel and Sell, 2014; Deacon, 2019). The physiological importance of the membrane-bound versus sDPPIV is yet to be established. Apart from the catalytic site, the extracellular domain consists of a cysteine rich region as well as a region rich in glycosylation sites, which are associated to DPPIV's non-enzymatic activity (e.g. interactions with adenosine deaminase or caveolin-1). DPPIV is also known as T-cells co-stimulatory antigen CD26 (Morimoto and Schlossman, 1998). Co-stimulatory molecules cannot directly activate T-cells, but instead will amplify the signal coming from other cell receptors. This function does not seem to be related to DPPIV's catalytic activity as cells lacking the entire catalytic domain were still able to stimulate activation of T-cells (Hühn *et al.*, 2000), and additionally, the use of DPPIV inhibitors did not affect the function (Vora *et al.*, 2009; Deacon, 2019).

DPPIV rapidly cleaves dipeptides with alanine or proline on the second position of their N-terminus, with its substrates including gastrointestinal hormones, neuropeptides, cytokines and chemokines. Notably, amongst these, it is responsible for breaking incretin hormones (e.g. Glucagon-like peptide 1 (GLP-1), Glucose-dependent insulinotropic polypeptide (GIP)), which are known to increase insulin secretion, regulating glucose homeostasis. Incretin

hormones are secreted from the intestinal mucosa after meal ingestion and account for 60% of postprandial insulin release (Lamers *et al.*, 2011). Plasma levels of GLP-1 increase rapidly after food consumption (within minutes): from 5-10 pmol/L in a fasting state to 15-50pmol/L after eating. However, DPPIV quickly decreases levels of GLP-1, resulting in only 10-20% of circulating GLP-1 being intact and biologically active (Holst, 2004; Drucker and Nauck, 2006). Intact GLP-1 activates GLP-1 receptors on pancreatic cells leading to an increase in cAMP and intercellular calcium, triggering insulin release. Additionally, GLP-1 also inhibits glucagon secretion and gastric emptying while stimulating β-cells proliferation and glucose disposal through neural mechanisms (Drucker and Nauck, 2006; Yabe and Seino, 2011) (Figure 11).

Marguet *et al.* were first to describe the critical role of DPPIV in regulating GLP-1 levels. In mice lacking DPPIV, improved glycaemic status was observed as well as reduced fat mass (Marguet *et al.*, 2000). Later, it has also been reported that DPPIV expression is increased in obese individuals' visceral fat (Lamers *et al.*, 2011). These studies encouraged the development of DPPIV inhibitors for the treatment of T2DM (gliptin class of drugs). An important step in gliptins' development was a proof that DPPIV is a key mediator of incretin hormone clearance as other clearance pathways did not compensate for its activity once it was blocked. Although DPPIV has a large number of substrates, inhibition of DPPIV did not lead to unwanted adverse effects. With these concerns allayed, sitagliptin became the first FDA approved DPPIV inhibitor in 2006. Currently, gliptins are well established as therapeutic agents for the treatment of T2DM, with at least 11 different inhibitors being licensed for use (Drucker and Nauck, 2006; Deacon and Lebovitz, 2016; Deacon, 2019). They inhibit more than 80% of DPPIV activity and maintain inhibition for 24 hours with once daily oral administration (Drucker and Nauck, 2006). DPPIV inhibitors are generally well tolerated with no gastrointestinal side effects and low risk of hypoglycaemia (Scheen, 2018). However, they have not yet been used for the treatment of GDM.

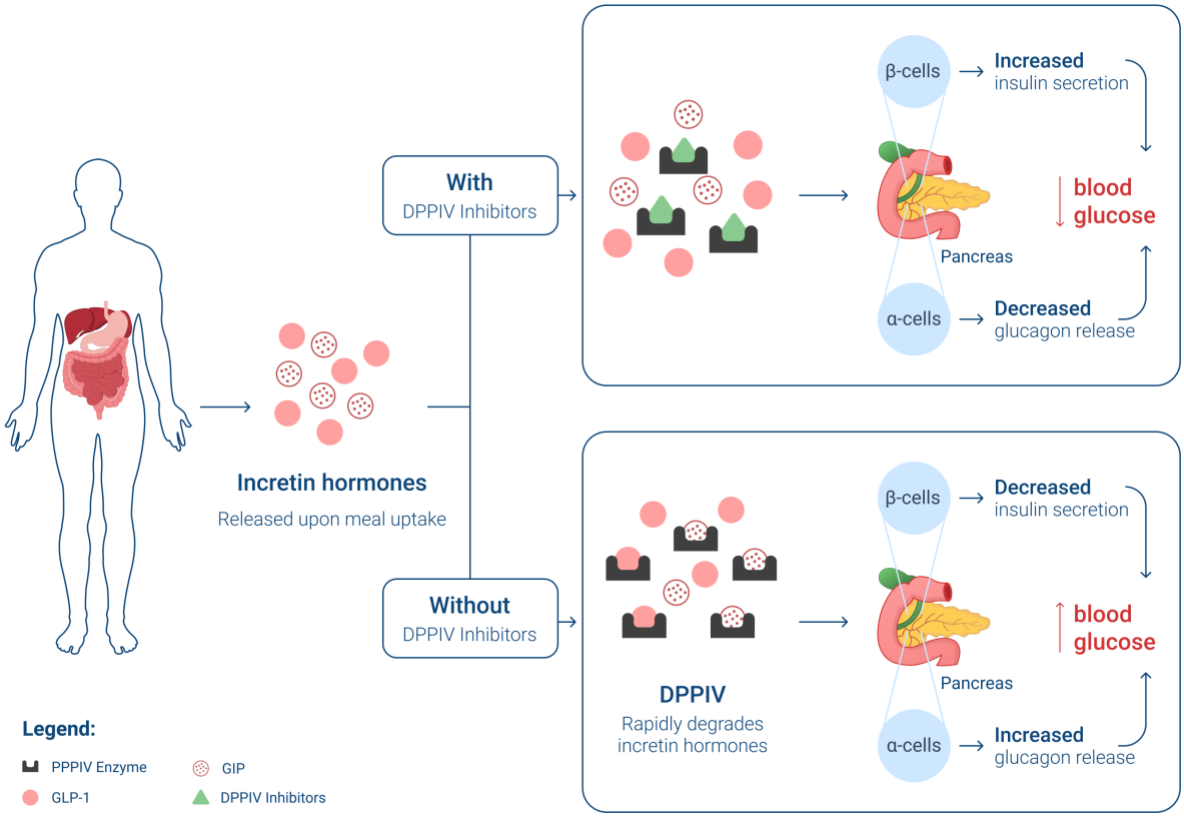



**Figure 12. Schematic representation of DPPIV role in glycaemic control.**

Upon food ingestion, the small intestine releases incretin hormones, stimulating pancreatic β-cells to secrete insulin and pancreatic α-cells to decrease glucagon release. Incretin action lowers plasma glucose levels. However, DPPIV rapidly cleaves dipeptides from the N-terminus of incretin hormones, inhibiting their activity and increasing glucose levels in the circulation.

It is also likely that DPPIV affects glycaemic control through mechanisms that do not involve incretin hormones. Some studies suggest that DPPIV might have a local effect on adipose tissue. Addition of recombinant protein DPPIV to primary human adipocytes, skeletal muscle and smooth muscle cells reduced their insulin sensitivity including decreased protein kinase B activity (Lamers *et al.*, 2011). This was followed with the observation that siRNA-mediated silencing of DPPIV in adipocytes led to improved insulin signalling response. Röhrborn *et al.* suggested that DPPIV might act as a negative regulator of insulin binding to insulin receptor similar to glycoprotein-1 or ectonucleotide pyrophosphatase/phosphodiesterase. Those

proteins interact with the extracellular domain of insulin receptor, negatively affecting the binding of insulin to it. When DPPIV inhibitors were used, in addition to short interfering RNA, the authors observed further enhancement of insulin receptor signalling, suggesting this mechanism is partially associated with DPPIV catalytic activity (Röhrborn *et al.*, 2016). It has also been suggested that DPPIV can interfere with insulin sensitivity through its binding of caveolin-1 (Ohnuma *et al.*, 2004), which interacts with the β-subunit of insulin receptor and is involved in insulin transduction pathways (Palacios-Ortega *et al.*, 2016). Taken together, these studies suggest that, besides its role in incretin breakdown, DPPIV can impact metabolic control through mechanisms independent of its catalytic activity.

Once it was known that DPPIV played a major role in the degradation of incretin hormones, several studies were conducted to investigate its levels in T2DM with contradictory findings. Some studies reported that DPPIV activity is lower in T2DM (Meneilly *et al.*, 2000; McKillop *et al.*, 2008), suggesting that this might be due to the compensatory role of DPPIV, as reduced incretin hormone clearance would lead to a higher secretion of insulin. However, several other reports showed that DPPIV activity is increased in T2DM, resulting in decreased insulin release and ultimately contributing to hyperglycaemia (Mannucci *et al.*, 2005; Fadini *et al.*, 2012).

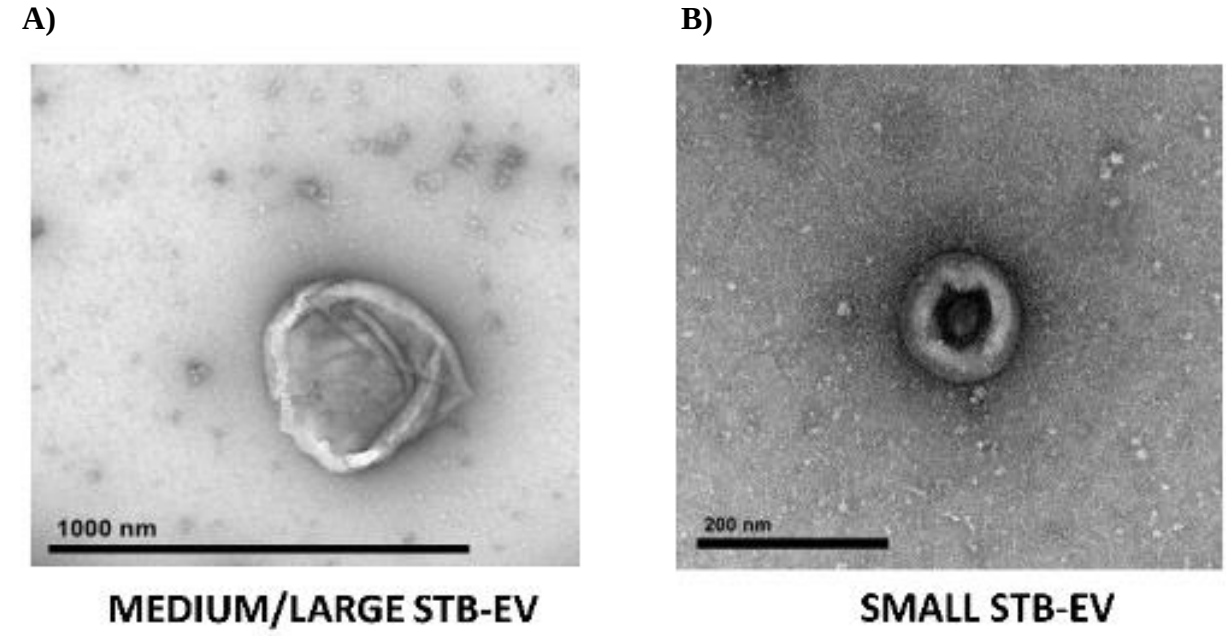
Increased levels of DPPIV have been reported in pregnancy compared to non-pregnant control (Zhao *et al.*, 2012). The authors compared sDPPIV from 80 normal pregnancies with those of 45 non-pregnant women and found significant increases in both early and late pregnancy. Another study showed increased DPPIV activity in preeclamptic placentae complicated with intrauterine growth restriction (Nishikawa *et al.*, 2005) and speculated on its role in the degradation of incretin hormones in the foeto-placental unit.

To the best of our knowledge, the potential role of STB-EV-bound DPPIV in GDM has not previously been investigated. Our hypothesis was that biologically active DPPIV is shed on STB-EVs and there might be increased circulating levels in GDM.

## 3.2. Results

### 3.2.1. Characterisation of STB-EVs

STB-EVs were collected after perfusion of placentae of control/normal pregnancies (described in *Materials and methods*). TEM analyses revealed particles with physical characteristics consistent with MEDIUM/LARGE STB-EVs and SMALL STB-EVs in pellets collected after 10K and 150K centrifugations of the perfusate, respectively (***Figure 13 A, B)***. Nanoparticle tracking analyses (NTA) confirmed the heterogeneous size of the MEDIUM/LARGE STB-EV population (approximately 0.2-1 μm) whilst the SMALL STB-EVs were more homogenous particles with a smaller size range (approximately 50-200 nm) (***Figure 13 C***).



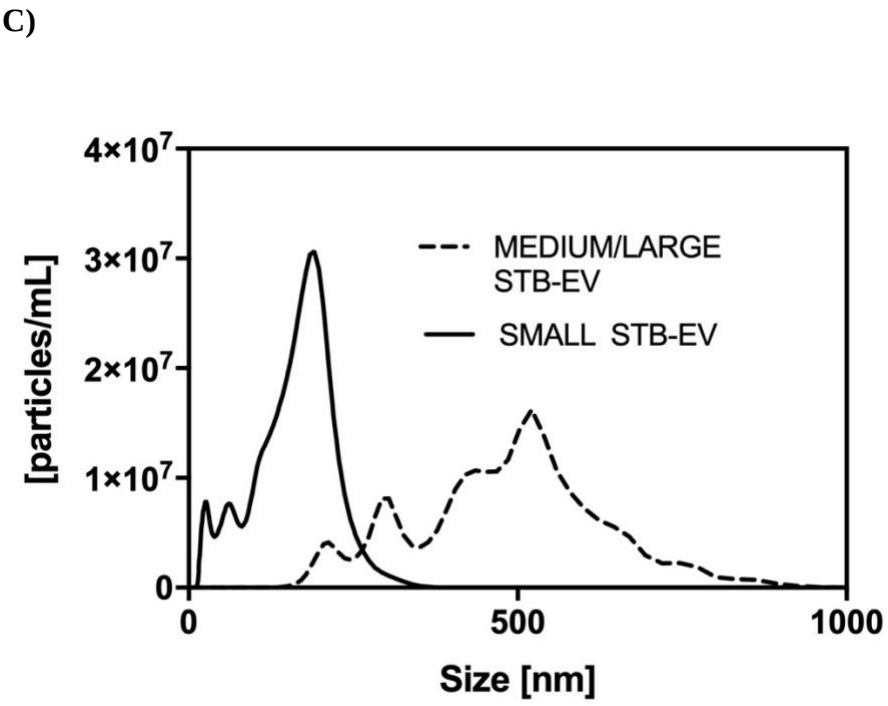




**Figure 13. Characterisation of MEDIUM/LARGE STB-EVs and SMALL STB-EVs by TEM and NTA.**

Transmission electronic microscopy (TEM) of **A),** MEDIUM/LARGE STB-EVs (the scale bar represents 1000 nm), and **B),** SMALL STB-EVs (the scale bars represent 200 nm) isolated from normal placentae. **C)** Representative Nanoparticle Tracking Analyses (NTA) size vs. distribution profiles of MEDIUM/LARGE STB-EVs and SMALL STB-EVs from normal pregnancies.

Expression of known exosomal markers Syntenin, Alix and CD9 were enriched in the SMALL STB-EVs fraction, with marginal expression of Syntenin and Alix in MEDIUM/LARGE STB-EVs (**Figure *14***). The syncytiotrophoblast-specific marker placental alkaline phosphatase (PLAP) was expressed in both MEDIUM/LARGE STB-EVs and SMALL STB-EVs, confirming the placental origin of these two particle populations (**Figure *14***). We have used this antibody in a number of publications after its specificity has been demonstrated (Sunderland, Redman and Stirrat, 1981; Knight *et al.*, 1998; Goswami *et al.*, 2006), but for clarity a blot that shows no reactivity with SMALL EVs isolated from breast cancer cells MDA-MB-231, human endothelial cells line EAHY923, human umbilical vein endothelial cells (HUVEC) or human embryonic kidney cells HEK293T, and no reactivity with liver hepatocellular cells (HEP G2), which express liver alkaline phosphatase (**Figure *15***).

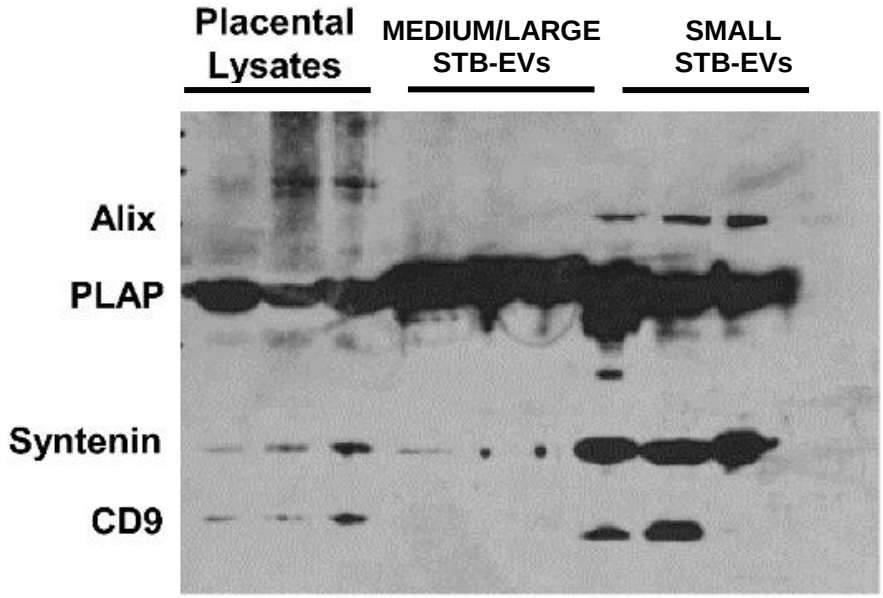



**Figure 14. Characterisation of normal pregnancy derived MEDIUM/LARGE STB-EVs and small extracellular vesicles SMALL STB-EVs by western blotting.**

Exosomal markers Alix, Syntenin and CD9 expression in whole placental lysates, MEDIUM/LARGE STB-EVs and SMALL STB-EVs isolated from control term placentae. PLAP expression confirmed syncytiotrophoblast origin. Blot is representative of n=4 experiments.

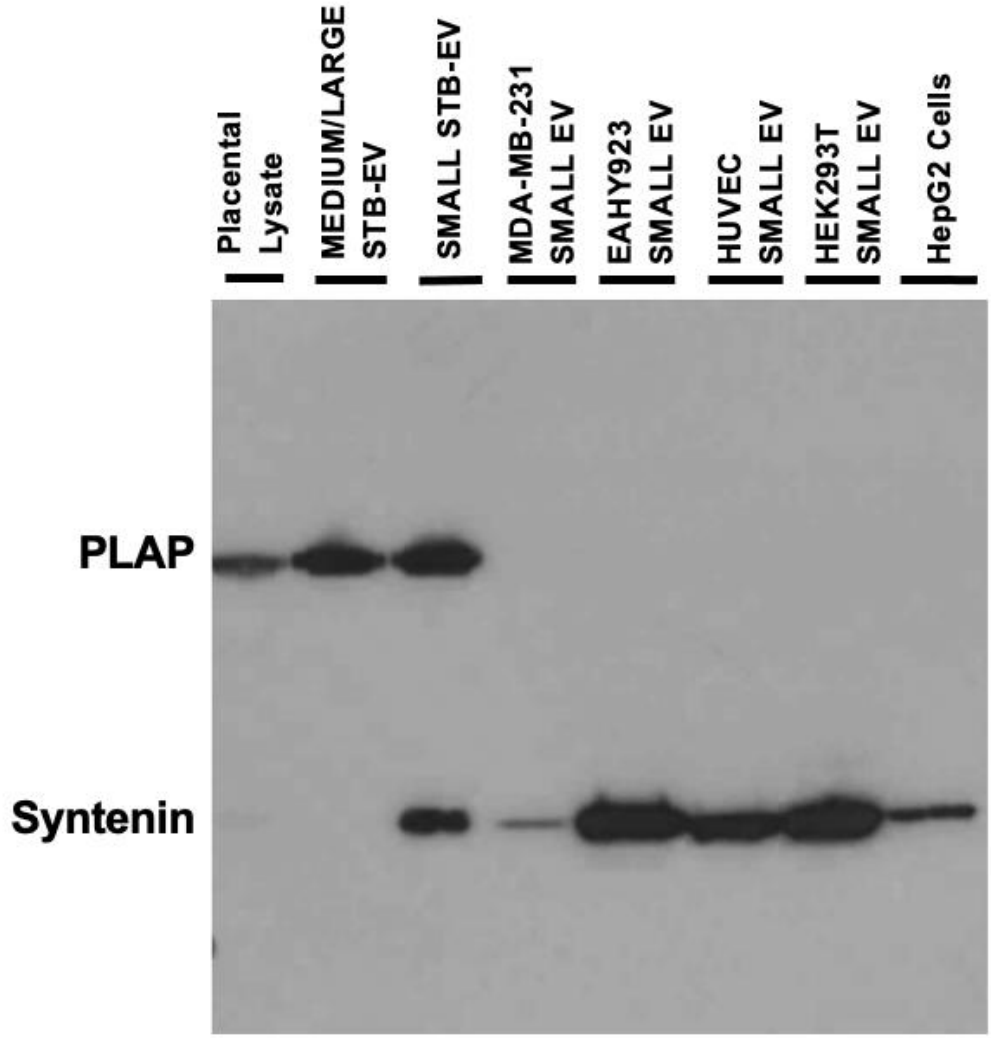


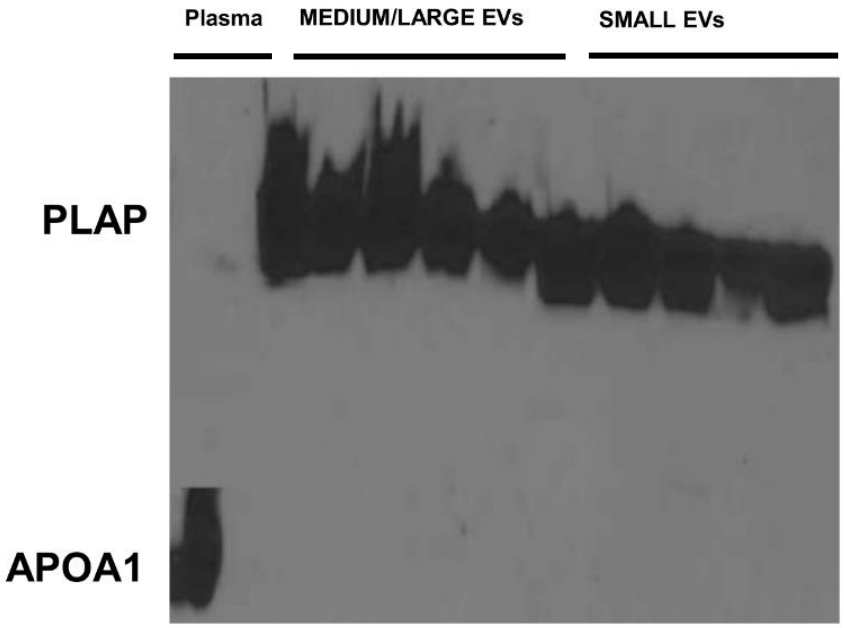

**Figure 15. Specificity of PLAP antibody confirmed by western blotting using SMALL EVs from different sources.**

PLAP antibody (NDOG2) showed no reactivity with SMALL EVs isolated from MDA-MB-231, EAHY923, HUVEC or HEK293T Cells, as well as no reactivity with HepG2 Cells. Whole placental lysate, MEDIUM/LARGE STB-EV and SMALL STB-EV isolated from control term placentae were used as a positive control for PLAP antibody. Syntenin, an exosomal marker, was expressed on SMALL EVs.

In line with new ISEV guidelines, negative controls Cytochrome C (CYC1) and apolipoprotein A1 (APOA1) were used to ascertain the purity of EV preparations. APOA1 is considered as the best negative marker to exclude the co-isolation of lipoproteins with EVs. Proteins associated with intracellular compartments of eukaryotic cells such as CYC1 are not enriched in small EVs, and therefore it is necessary to evaluate their presence in the preparation if

working with specific subtype of EVs (Théry *et al.*, 2018). Both MEDIUM/LARGE and SMALL STB-EVs have shown no expression of either protein (**Figure *16***).

**A)**




**B)**

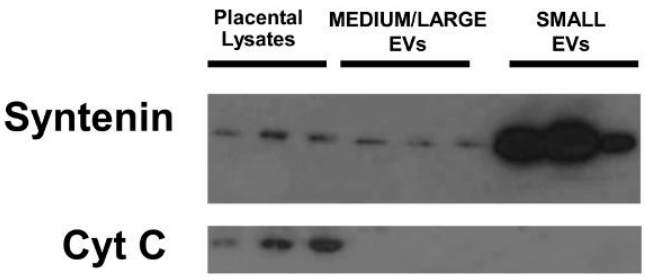



**Figure 16. Characterisation of normal pregnancy derived MEDIUM/LARGE STB-EVs and small extracellular vesicles SMALL STB-EVs by western blotting.**

Western blot showing that both MEDIUM/LARGE STB-EVs and SMALL STB-EVs do not express APOA1. A plasma sample from a non-pregnant woman was used as a positive control for APOA1 expression **(A).** Representative Western blot of Cytochrome C expression in whole placental lysates, MEDIUM/LARGE STB-EVs and SMALL STB-EVs isolated from control term placentae **(B).**

### 3.2.2. DPPIV is present in normal STB-EVs

Consistent with the literature, we detected DPPIV, a glycoprotein that rapidly cleaves and inhibits the incretin hormone GLP-1, in the whole placental tissue, with a signal localized in the syncytiotrophoblast layer (***Figure 17***), demonstrating that DPPIV was present at the site of STB-EVs production (Neudeck *et al.*, 1997; Kertesz, Linton and Redman, 2000).

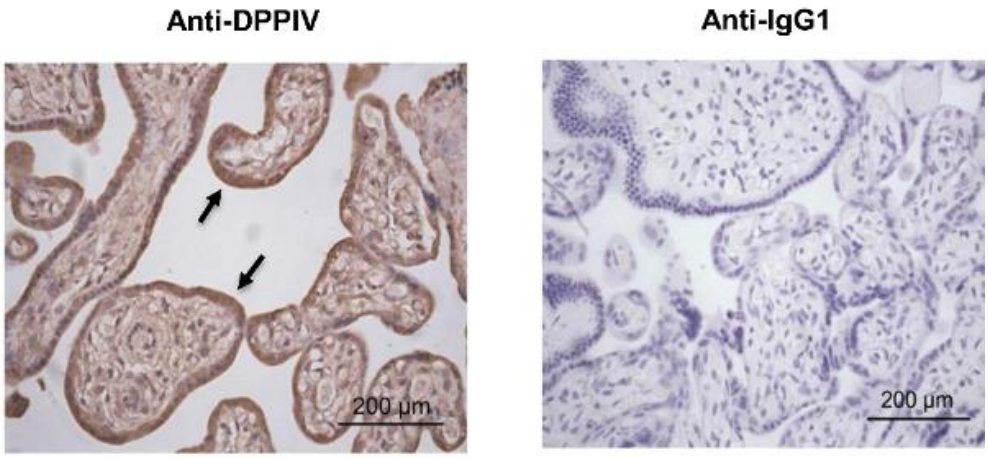



**Figure 17. Placental tissue express DPPIV.**

Control placental sections were subjected to immunohistochemical analysis for DPPIV expression **(left panel)**. DPPIV positivity is seen at the syncytiotrophoblast (indicated by the arrows). As negative controls, placental sections were incubated with anti-IgG1 antibody **(right panel)**. Images are representative of n=3 separate experiments. Scale bar set at 200 µm.

Our previous mass spectrometric analyses suggested the presence of DPPIV in MEDIUM/LARGE STB-EVs isolated using mechanically disruption of STB microvillous membranes (Kertesz, Linton and Redman, 2000). We now confirmed DPPIV protein expression in both MEDIUM/LARGE STB-EVs and SMALL STB-EVs of normal pregnancies (**Figure *18*** - upper band) obtained from placenta perfusion using western blotting.

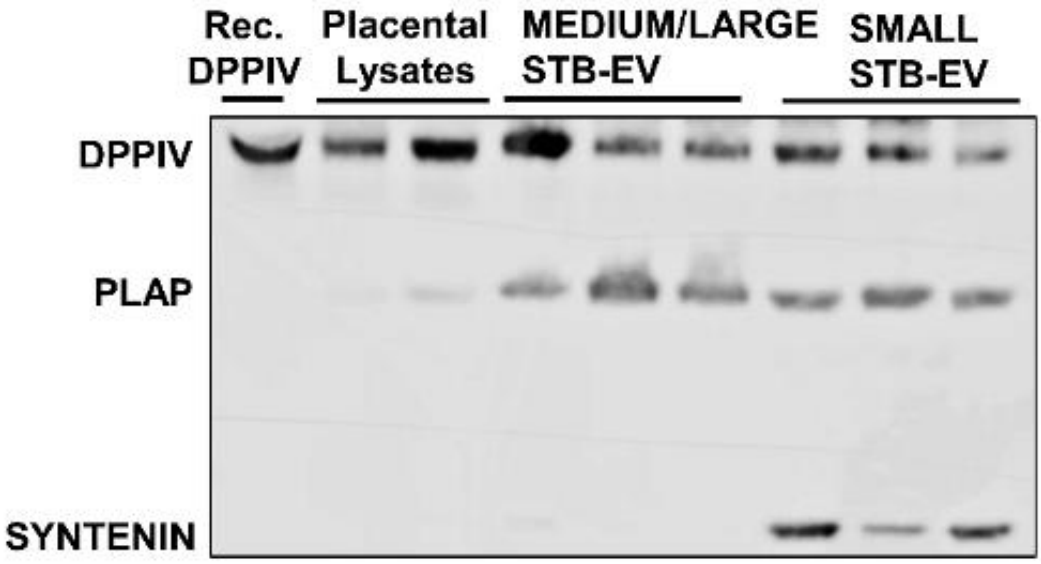



**Figure 18. Representative Western blot of DPPIV protein expression in whole placental lysates, MEDIUM/LARGE STB-EVs and SMALL STB-EVs isolated from control term placentae.**

Recombinant human DPPIV protein (Rec. DPPIV) was used as positive control. PLAP expression confirmed STB origin; expression of exosomal marker Syntenin was enriched in SMALL STB-EVs. Blots are representative of n=3 separate experiments.

### 3.2.3. DPPIV is co-expressed with PLAP on STB-EVs

Flow cytometry analysis was performed on MEDIUM/LARGE STB-EVs isolated with 10K centrifugation of maternal perfusate (representative data shown in ***Figure 19***). We first established an EV positive gate (***Figure 19A***) using fluorescent microspheres of 1μm. Events that fell into this gate were subjected to further analysis. Bio-maleimide (which stains biological membranes via cysteine residues and thiol groups) positive gate was defined by fluorescence minus one (FMO) (**Figure *19B***). PLAP FMO & isotype control and DPPIV FMO & isotype control were used to draw 1% cut-off gates for PLAP positive events (**Figure *19C***) and DPPIV positive events (**Figure *19D***), respectively. In **Figure *19E***, the significant co-expression of PLAP and DPPIV is demonstrated in quadrant 2 (Q2). We noted PLAP positive and DPPIV negative events in quadrant 3 (Q3) as well as a very small (0.22%) population of DPPIV positive PLAP negative events in quadrant 1 (Q1).

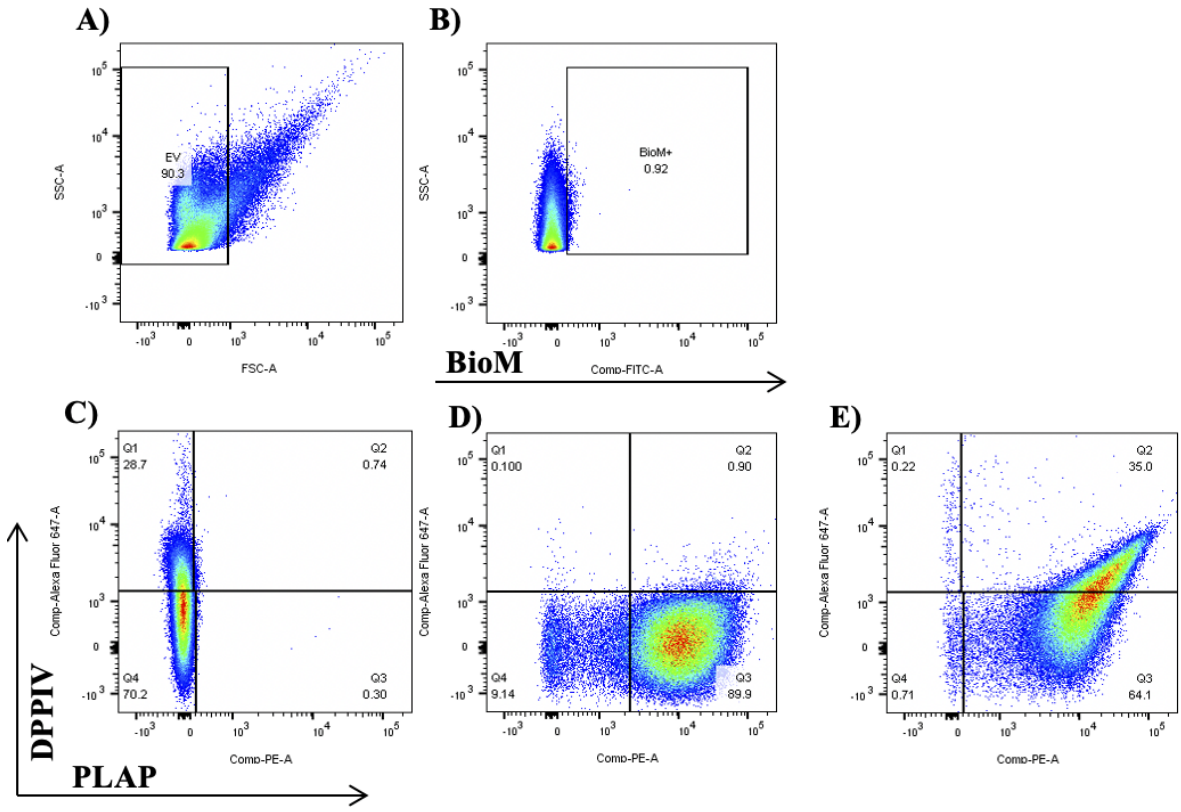



**Figure 19. Representative image of flow cytometry analysis of MEDIUM/LARGE STB-EV derived from placental perfusion.**

Dot plot is showing **(A)** forward scatter (FSC) versus side scatter (SSC) analysis of MEDIUM/LARGE STB-EVs (n=3). Fluorescent microspheres of 1 µm (Polysciences Inc., Warrington, PA) were used to establish a gate <1 µm. Events that fell into this gate were subject to further analysis. **(B)** Bio-maleimide (BioM) fluorochrome minus one (FMO) was used to draw 1% cut off gate for BioM positive events. **(C)** PLAP FMO was used to draw 1% cut off gate for PLAP positive events. **(D)** DPPIV FMO was used to draw 1% cut off gate for DPPIV positive events. **(E)** The co-expression of PLAP-PE and DPPIV-Alexa Fluor 647 on MEDIUM/LARGE STB-EVs (Quadrant 2).

Three separate analyses are shown in **Table *5***. More than half of MEDIUM/LARGE STB-EVs (56.5 ± 4.6%) were solely PLAP positive. Importantly, 42 ± 4.5% of the MEDIUM/LARGE STB-EVs were both PLAP and DPPIV positive, suggesting that a large proportion of MEDIUM/LARGE STB-EVs express both PLAP and DPPIV in control pregnancies.

**Table 5. Percentage of DPPIV expression on MEDIUM/LARGE STB-EV assessed by flow cytometry.**

| Sample | $PLAP^{+/}DPPIV^{+}$ (%) | $PLAP^{+}$ (%) |
|---|---|---|
| **1** | 40.6 | 57.1 |
| **2** | 50.3 | 48.2 |
| **3** | 35.0 | 64.1 |
| **Mean** | 42.0 | 56.5 |
| **SEM** | 4.5 | 4.6 |

In addition, total MEDIUM/LARGE STB-EVs were incubated with either anti-DPPIV or anti-PLAP coated magnetic beads and pulled out using a magnet. Particle numbers in the DPPIV or PLAP depleted supernatants were determined by NTA. **Figure *20A, B*** revealed that PLAP depletion decreased particle numbers by 60.61 ± 19.31%; and DPPIV depletion decreased particle numbers by 35.74 ± 18.65%, essentially confirming the FACS analyses. Control experiments using IgG1 or IgG2a-coupled magnetic beads did not alter MEDIUM/LARGE STB-EVs numbers (**Figure *20C***).

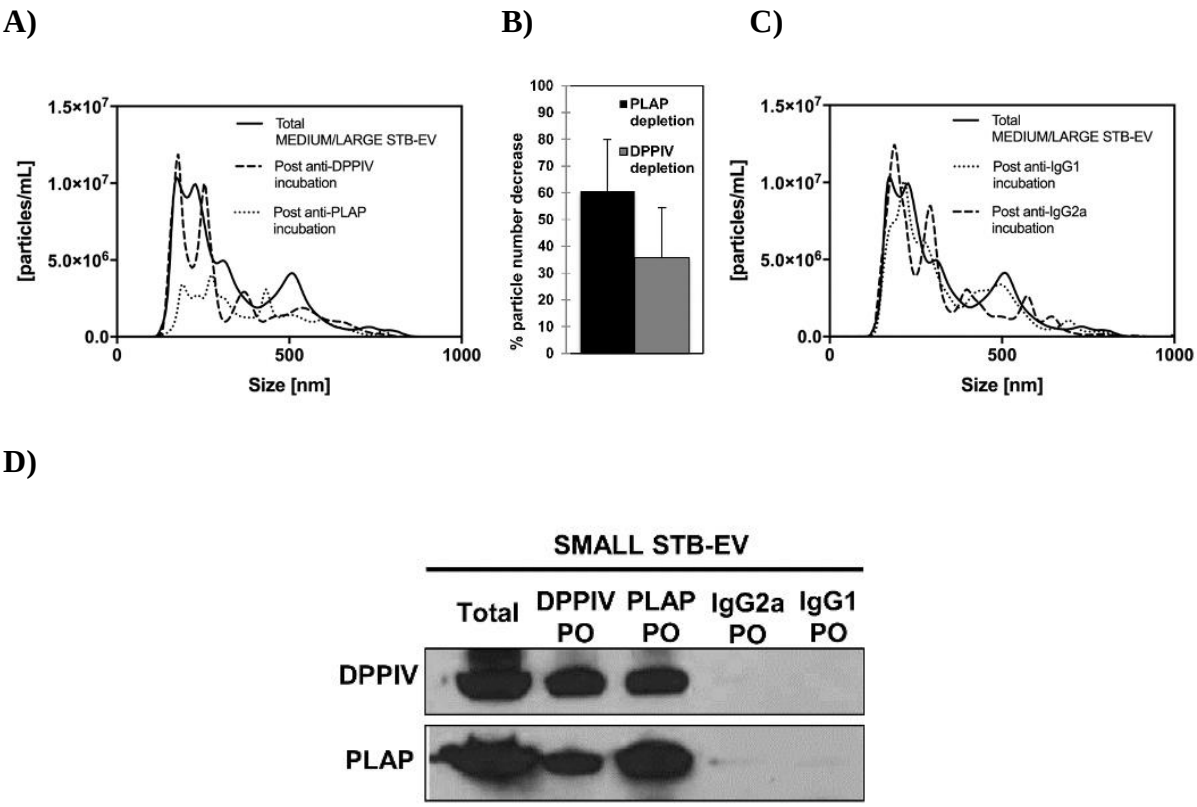



**Figure 20. DPPIV and PLAP co-expression in MEDIUM/LARGE STB-EVs.**

**(A)** Representative NTA size distribution profile of total MEDIUM/LARGE STB-EVs, MEDIUM/LARGE STB-EVs population depleted of MEDIUM/LARGE STB-EVs expressing DPPIV and MEDIUM/LARGE STB-EVs expressing PLAP. **(B)** Percentage of particle number after PLAP or DPPIV depletion. **(C)** Representative NTA size distribution profile of total MEDIUM/LARGE STB-EVs, MEDIUM/LARGE STB-EVs population depleted of MEDIUM/LARGE STB-EVs expressing IgG2a and MEDIUM/LARGE STB-EVs population depleted of MEDIUM/LARGE STB-EVs expressing IgG1. Graphs are representative of n=3 experiments. **(D)** DPPIV and PLAP protein expression in total MEDIUM/LARGE STB-EVs (Total), in MEDIUM/LARGE STB-EVs population pulled out with anti-DPPIV magnetic beads (DPPIV PO), in MEDIUM/LARGE STB-EVs population pulled out with anti-PLAP magnetic beads (PLAP PO), in MEDIUM/LARGE STB- EVs population pulled out IgG2a magnetic beads (IgG2a PO) and in MEDIUM/LARGE STB-EVs population pulled out with anti-IgG1 magnetic beads (IgG1 PO). Blot is representative of n=3 experiments.

DPPIV or PLAP pull-out fractions were analysed by immunoblotting to assess co-expression of DPPIV and PLAP protein (**Figure *20D***). PLAP was found in the DPPIV pull-out fractions and conversely, DPPIV was found in PLAP pull-out fractions, confirming co-expression on both MEDIUM/LARGE STB-EVs population. When MEDIUM/LARGE STB-EVs were incubated with magnetic beads coated with PLAP, pull out showed a greater signal for DPPIV

compared with the pull from magnetic beads coated with DPPIV suggesting that some DPPIV is intra-vesicular.

Lastly, essentially similar data were obtained for SMALL STB-EVs. SMALL STB-EVs could not be analysed by flow cytometry, as their size is below the limit of detection. Therefore, particle numbers in the DPPIV or PLAP depleted SMALL STB-EVs supernatants were determined by NTA. PLAP depletion decreased particle numbers by 36.45 ± 23.01% and DPPIV depletion decreased particle numbers by 18.94 ± 12.42% (***Figure 21A, B***). Control experiments did not alter SMALL STB-EV numbers (**Figure *20C***). Additionally, we confirmed that DPPIV and PLAP proteins were also found in the same population of SMALL STB-EVs (**Figure *21D***).

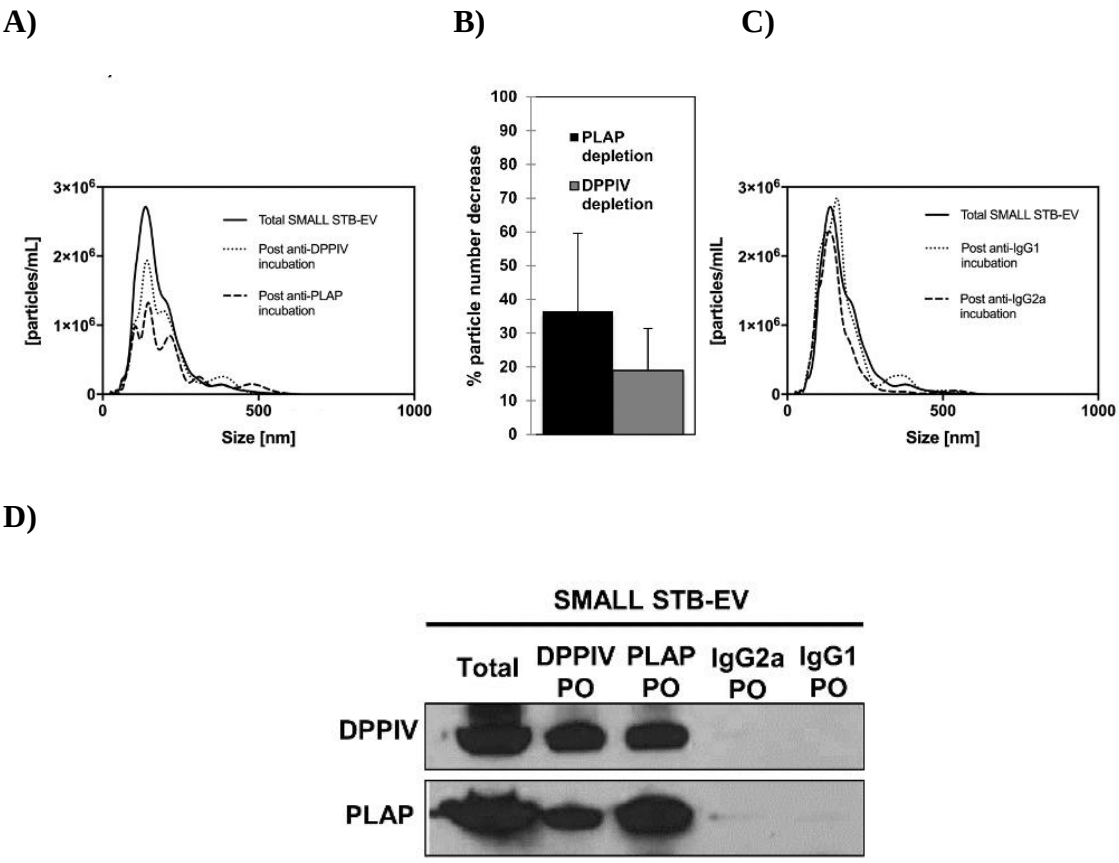


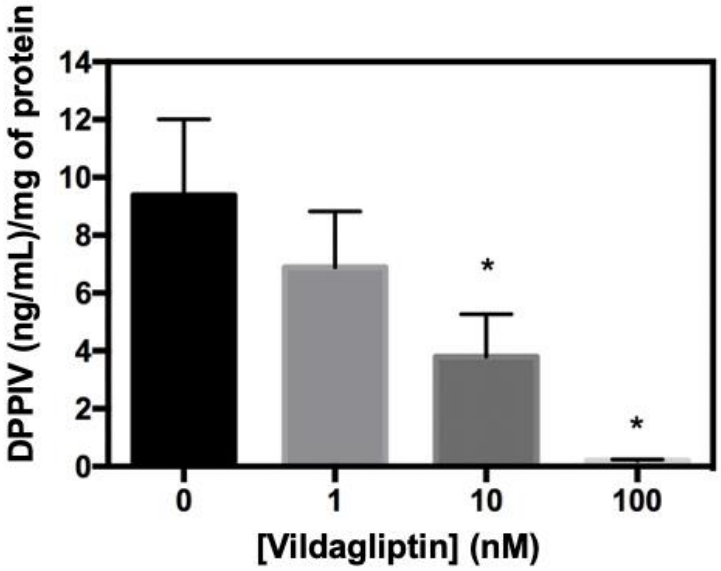

**Figure 21. DPPIV and PLAP co-expression in SMALL STB-EVs.**

**(A)** Representative Nanoparticle Tracking Analysis (NTA) size distribution profile of total SMALL STB-EVs, SMALL STB-EVs population depleted of SMALL STB-EVs expressing DPPIV and SMALL STB-EVs expressing PLAP. **(B)** Percentage of particle number after PLAP or DPPIV depletion. **(C)** NTA size distribution profile of total SMALL STB-EVs, SMALL STB-EVs population depleted of SMALL STB-EVs expressing IgG2a and SMALL STB-EVs population depleted of SMALL STB-EVs expressing IgG1. Graphs are representative of n=3 experiments. **(D)** DPPIV and PLAP protein expression in total SMALL STB-EVs (Total), in SMALL STB-EVs population pulled out with anti-DPPIV magnetic beads (DPPIV PO), in SMALL STB-EVs population pulled out with anti-PLAP (PLAP PO), in SMALL STB-EVs population pulled out with anti-IgG2a magnetic beads (IgG2a PO) and in SMALL STB-EVs population pulled out with anti-IgG1 magnetic beads (IgG1 PO). Blot is representative of n=3 experiments .

### 3.2.4. DPPIV present in STB-EVs displays enzymatic activity

Surface bound DPPIV activity was next determined in MEDIUM/LARGE STB-EVs and SMALL STB-EVs of control pregnancies. Basal DPPIV activity was similar in MEDIUM/LARGE STB-EVs and SMALL STB-EVs (**Figure *22***). Importantly, incubation with the DPPIV specific inhibitor vildagliptin inhibited DPPIV activity in both MEDIUM/LARGE STB-EVs and SMALL STB-EVs in a dose-dependent manner, demonstrating that placental EVs expressed functional DPPIV.

**A)**




**B)**

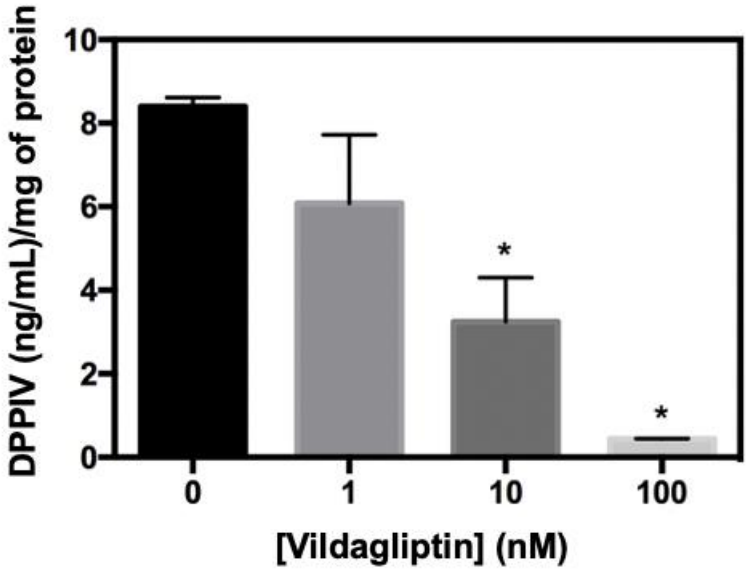
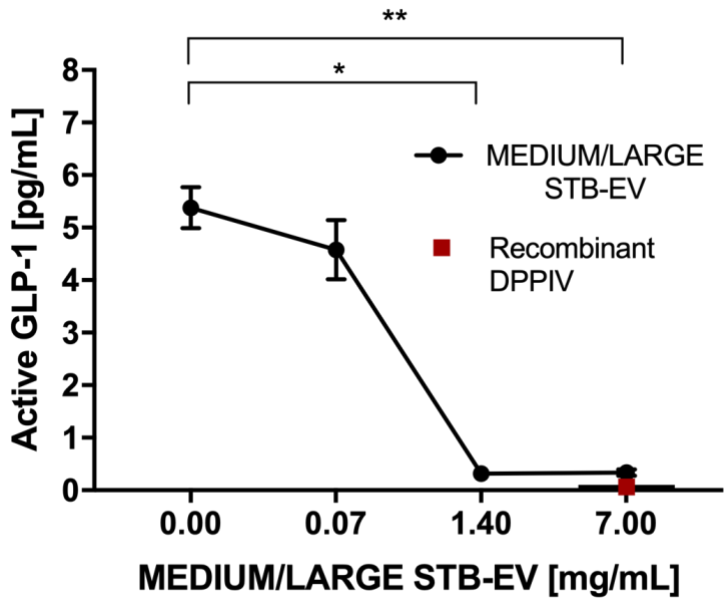



**Figure 22. DPPIV in MEDIUM/LARGE STB-EVs and SMALL STB-EVs is enzymatically functional.**

MEDIUM/LARGE STB-EVs **(A)** and SMALL STB-EVs **(B)** from control women were incubated with 0, 1, 10 or 100 nM Vildagliptin (inhibitor of DPPIV) and DPPIV activity was measured. Percentage of Residual DPPIV activity was calculated in MEDIUM/LARGE STB-EVs **(A)** and SMALL STB-EVs **(B)**. Graphs are representative of n=3 experiments performed independently in duplicates (*$p$< 0.05).

Furthermore, we demonstrated that functional DPPIV present on STB-EVs and SMALL STB-EVs can degrade active GLP-1. Figure 10 shows that increasing concentrations of MEDIUM/LARGE STB-EVs (**Figure *23A***) and SMALL STB-EVs (**Figure *23B***) resulted in a dose dependent decrease of active GLP-1.

**A)**




**B)**

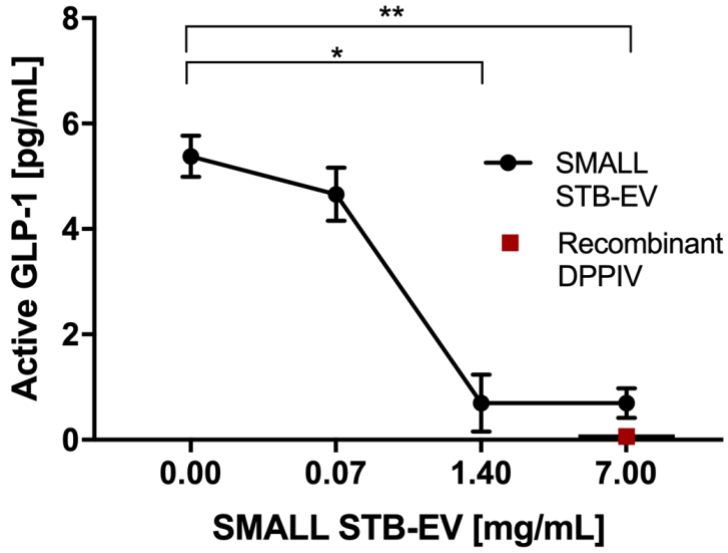



**Figure 23. STB-EV-bound DPPIV can degrade active GLP-1.**

MEDIUM/LARGE STB-EVs **(A)** and SMALL STB-EVs **(B)** pools from 3 GDM women were diluted to 7, 1.4 or 0.07 mg/ml and incubated with 1400 pg/ml of standard GLP-1. Graphs show levels of active GLP-1 measured after the incubation with MEDIUM/LARGE STB-EVs or SMALL STB-EVs. Recombinant DPPIV was used as positive control. Graphs are representative of n=3 experiments performed independently in duplicates (*$p$< 0.05; **p<0.001).

### 3.2.5. DPPIV expressing STB-EVs in the maternal circulation

The concentration of DPPIV positive STB-EVs in uterine vein (which drains the utero-placental unit) was compared to peripheral venous blood in the same women (n=5) in order to confirm its release from the placenta. Briefly, during routine caesarean section, blood samples were collected from the uterine vein (after reflection of the bladder and before uterine incision and prior to delivery of the fetus) in order to obtain blood as soon as it left the uteroplacental unit. Concomitantly blood was also taken from the left ante-cubital fossa (peripheral vein) from the same patient. Both samples were tested for presence of placental EVs expressing both DPPIV and PLAP by flow cytometry. As expected, concentrations of single PLAP positive STB-EVs were higher in uterine (25210 ± 4842.20 events/ml) than peripheral (6810 ± 1677.94 events/ml) venous plasma of these pregnant women (**Figure *24***).

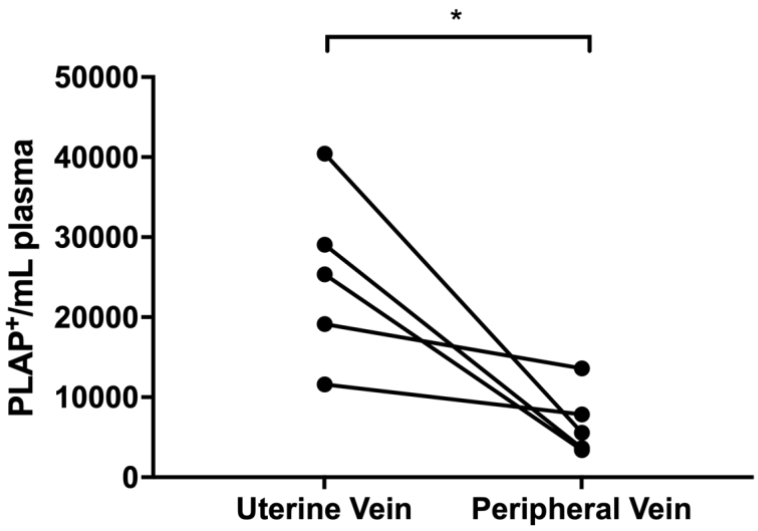



**Figure 24. PLAP expressing STB-EVs are present in the circulation and are higher in the uterine vein.**

Paired plasma samples were collected from the uterine and the peripheral vein of pregnant women. Individual PLAP positive event numbers from matched peripheral and uterine vein plasma samples (n=5 women; *p<0.05).

Importantly, a similar gradient of PLAP and DPPIV, double positivity was observed between uterine (2340 ±538.38 events/ml) and peripheral (760 ± 197.69 events/ml) blood confirming

placental origin of these double positive EVs. This gradient was present in all samples. Representative flow cytometry dot plot is presented on **Figure *25***.

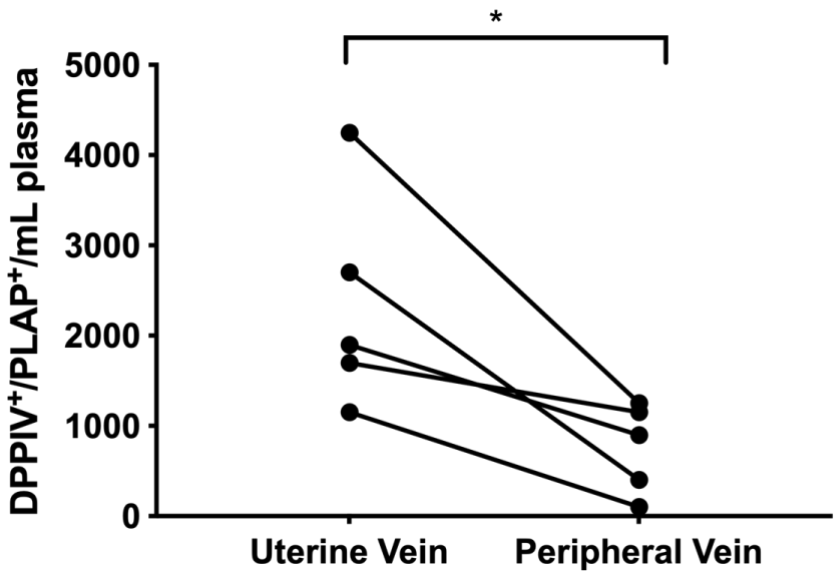



**Figure 25. DPPIV expressing STB-EVs are present in the circulation and are placentally derived.**

Paired plasma samples were collected from the uterine and the peripheral vein of pregnant women. Individual PLAP/DPPIV double positive event numbers from matched peripheral and uterine vein plasma samples (n=5 women; *$p<0.05$).

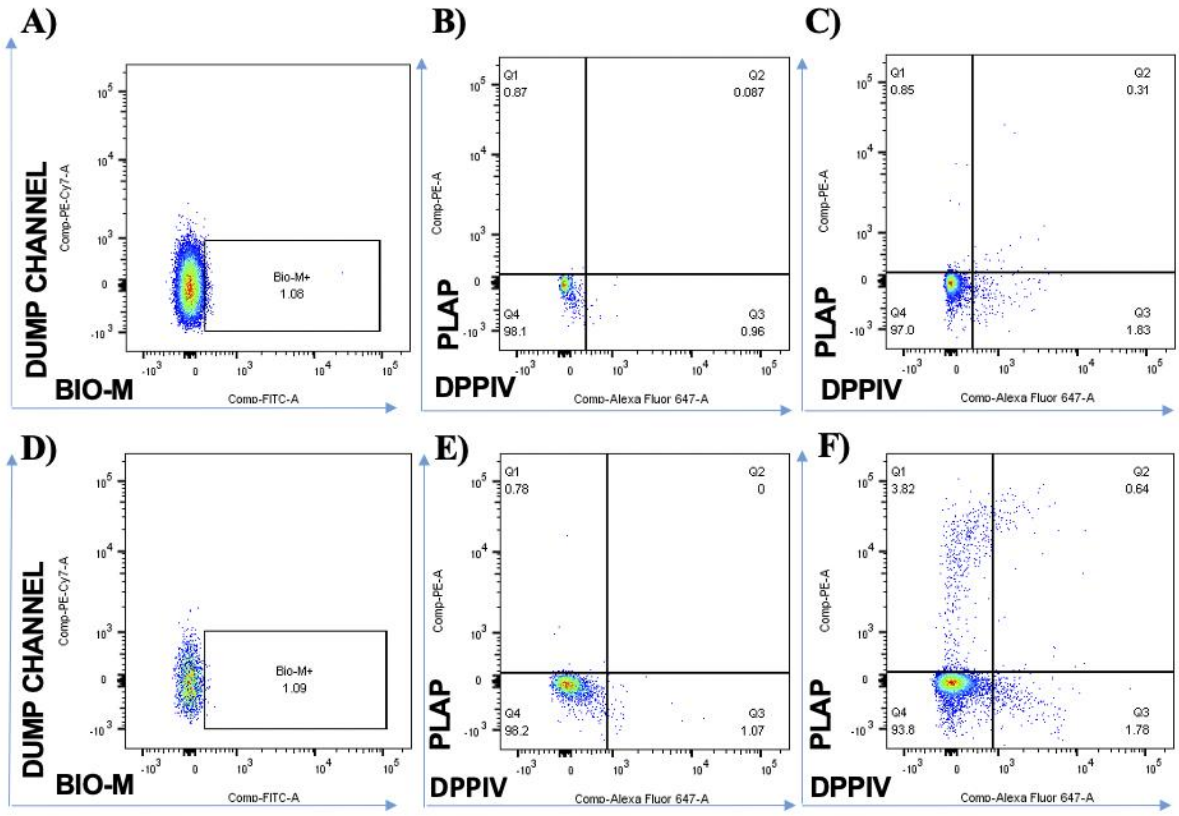



**Figure 26. Representative flow cytometry analysis of platelet-poor plasma (PPP) from peripheral and uterine vein.**

MEDIUM/LARGE STB-EVs were recovered from the top of the filter unit in 100 µl of filtered PBS and stained with Bio-maleimide-FITC.
The top panel **(A, B, C)** shows flow cytometry analysis of PPP plasma obtained from peripheral vein, while bottom panel shows analysis of uterine vein **(D, E, F)**.
**A & D)** Filtrate was used to determine Bio-maleimide positive and the contaminating markers ('Dump channel') negative gate. 'Dump Channel' gate was draw at 1% cut off using Dump channel-PeCy7 vs. Bio-maleimide-FITC dot plot. 'Dump Channel' includes contaminant markers such as CD231a/b, CD41, HLA-ABC and HLA Class II; all conjugated with PeCy7 labelling.
**B & E)** In order to draw 1% cut off gates for anti-DPPIV-Alexa Fluor 647 and anti-PLAP-PE staining, samples were treated with detergent (NP-40) prior to events acquisition.
**C & F)** 'Dump Channel' negative and Bio-maleimide positive population was analysed for PLAP and DPPIV double positivity.

### 3.2.6. DPPIV activity is increased in STB-EVs of GDM pregnancies

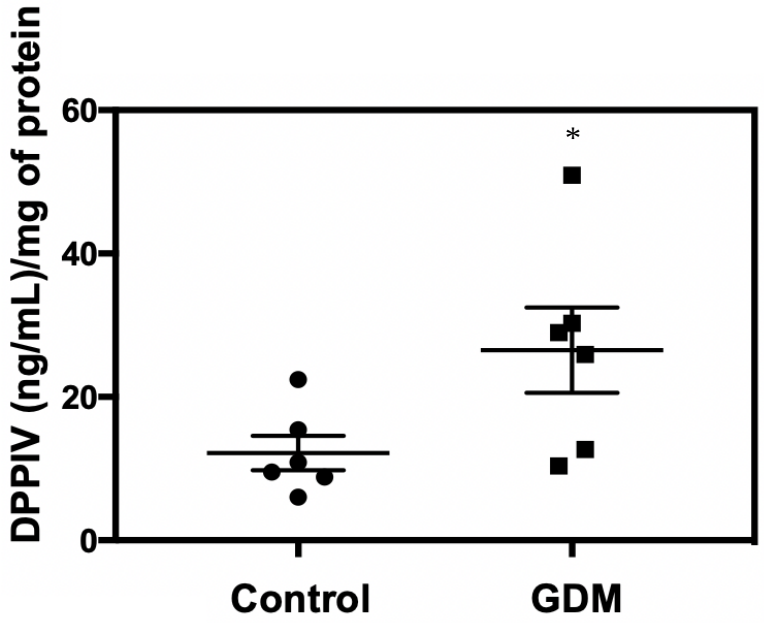
We compared DPPIV activity in placental EVs isolated from normal and GDM perfused placentae (n=6 for both). The clinical characteristics of the patients from whom STB-EVs were analysed are described in **Table *6***. MEDIUM/LARGE STB-EVs from GDM placentae showed significant 2-fold increase in DPPIV activity compared to MEDIUM/LARGE STB-EVs from controls (Figure 26A). This increased DPPIV activity was also seen in SMALL STB-EVs from GDM placentae and was 5-fold higher than that found in controls **Figure *27***.

**Table 6. Patient characteristics.**

Data is presented as mean ± SEM. Range is also included. Significant difference shown as * if $p<0.05$.

| | Normal pregnancy (n=14) | | GDM pregnancy (n=14) | |
|---|---|---|---|---|
| | **Plasma STB-EV (n=8)** | **Placental perfusion STB-EV (n=6)** | **Plasma STB-EV (n=8)** | **Placental perfusion STB-EV (n=6)** |
| **Age, year** | 37.8 ± 2.4 (24 - 45) | 35.3 ± 2.4 (28 - 43) | 37.4 ± 2.3 (33 - 42) | 29.8 ± 3.2 (22 - 39) |
| **Gestation age, weeks** | 39.3 ± 2.9 (38.3 – 41) | 39 ± 0.8 (38.6 – 39.4) | 39.5 ± 1.5 (39.1 – 40.6) | 38.7 ± 2.4 (37.3 – 39.4) |
| **Body mass index, kg/m2** | 26.7 ± 1.5* (22 – 34.5) | 30.2 ± 3.2* (25 – 43) | 36.4 ± 1.7 (31 - 44) | 34.3 ± 3.0 (26 - 45) |
| **Newborn weight, g** | 3656.3 ± 219.3 (2890 - 4550) | 3630.8 ± 172.7 (2890 - 4550) | 3864.3 ± 231.4 (2790 – 4500) | 3994.2 ± 261.2 (2790 – 4500) |
| **Max. systolic pressure, mmHg** | 129.6 ± 2.8 (119 - 140) | 133.8 ± 3.2 (120 - 140) | 135 ± 4.8 (120 - 151) | 139.8 ± 6.4 (127 - 170) |
| **Max. diastolic pressure, mmHg** | 77.4 ± 3.3 (68 - 95) | 86.5 ± 4.5 (72 - 100) | 84.4 ± 3.8 (74 - 100) | 85.3 ± 1.7 (79 - 90) |
| **GDM treatment** | - | - | Diet: 2<br>Metf: 4<br>Ins + Metf: 2 | Diet: 2<br>Metf: 2<br>Ins: 1<br>Ins + Metf: 1 |

**A)**




**B)**

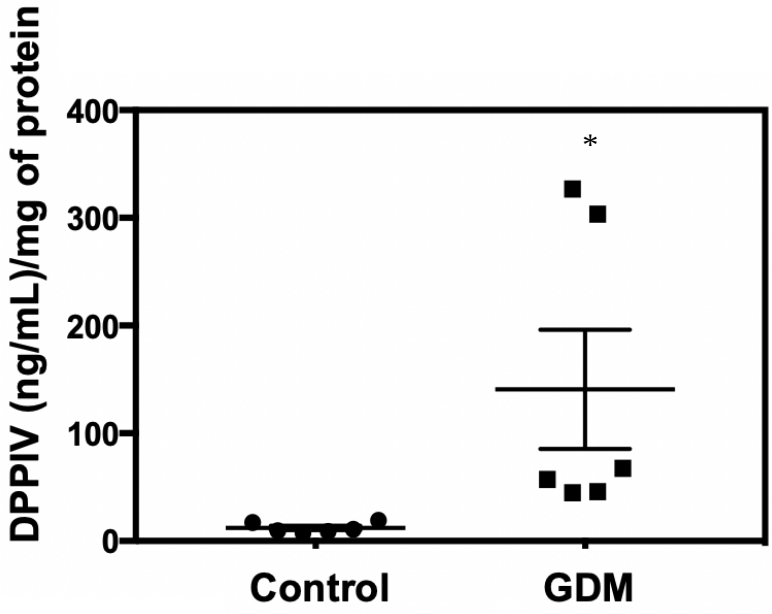



**Figure 27. DPPIV activity is increased in STB-EVs of GDM pregnancies.**

DPPIV concentration in MEDIUM/LARGE STB-EVs from GDM versus control isolated from placental perfusions (n=6 for both groups; *$p$<0.05). **(A)** DPPIV concentration in SMALL STB-EVs from GDM versus control isolated from placental perfusions (n=6 for both groups; *$p$<0.05). **(B)**

### 3.2.7. STB-EV bound DPPIV expression is increased in GDM peripheral plasma

Lastly, we investigated whether there were differences in STB-EVs expressing DPPIV in the plasma of women with GDM. Double positive PLAP and DPPIV STB-EV levels in peripheral blood were 8.58-fold increased in women with GDM, compared to control women (**Figure *28***). Patient characteristics are presented in **Table *6***.

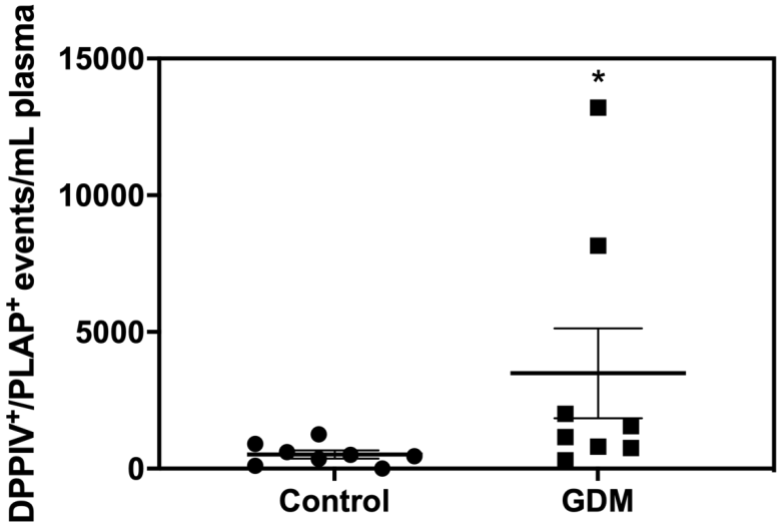



**Figure 28. Placenta-derived DPPIV expression is increased in GDM peripheral plasma.**

Peripheral gestation matched plasma samples were collected from GDM (n=8) and Control (n=8) pregnant women. DPPIV and PLAP double positive events in 1 ml of plasma were identified by flow cytometry. *p<0.05.

## 3.3. Discussion

Here, we investigated 1) the presence and bioactivity of the well-established regulator of insulin secretion DPPIV in syncytiotrophoblast-derived extracellular vesicles during pregnancy; and 2) whether DPPIV concentration and/or activity was changed in pregnancies complicated with GDM.

We found that the normal human placenta releases STB-EVs that carry biologically active DPPIV. This DPPIV was shown to have intrinsic enzymatic activity and was also shown to degrade active GLP-1. We further showed that GDM pregnancies are associated with a >8-fold increase in DPPIV-positive STB-EVs concentration in maternal plasma, compared to normal pregnancies. Increased DPPIV biological activity was also demonstrated in both MEDIUM/LARGE STB-EVs and SMALL STB-EV from GDM placentae, compared to controls.

EVs are now understood to play important roles in mediating intercellular communication as well as regulating biological signalling in target cells (Redman *et al.*, 2012; Tannetta, Collett, *et al.*, 2017). The concentrations of STB-EVs released by the placenta increases during normal pregnancy (Goswami *et al.*, 2006; Sarker *et al.*, 2014), which correlates with the physiological establishment of insulin resistance in normal pregnancies. In addition, the number of SMALL STB-EVs present in maternal plasma is reported to be significantly increased in pregnancies complicated with GDM (Salomon *et al.*, 2016). Consistent with the hyperglycaemia observed in GDM, glucose concentrations have been shown to increase exosome release from trophoblast cells *in vitro* (Rice *et al.*, 2015). We focused on possible changes in molecules known to impact insulin sensitivity or secretion, both of which are altered in pregnancies complicated with GDM.

In 2000, Kertesz *et al.* performed a mass spectrometric analysis of mechanically isolated MEDIUM/LARGE STB-EVs in attempt to identify complexes that might inhibit proliferation

of endothelial cells (Kertesz, Linton and Redman, 2000). One of the molecules identified was Dipeptidyl Peptidase-4 (DPPIV). We now demonstrate that not only is DPPIV expressed in STB-EVs, with increased concentration in GDM pregnancies, but also that DPPIV is biologically active and can be inhibited using a specific inhibitor. This differs from Liu *et al.*(Liu *et al.*, 2016) who reported no difference in DPPIV concentration between normal and GDM pregnancies. However, whilst Liu *et al.* measured the enzymatic activity of soluble DPPIV, we directly measured DPPIV activity bound to STB-EVs, which might explain the divergence. Another possible explanation is that they used serum for analysis in their study, which is not the most suitable medium for EV analysis (Witwer *et al.*, 2013). Conversely, Jayabalan *et al.* analysed plasma exosomes from normal and GDM women at diagnosis and showed that the overall DPPIV exosome levels were downregulated (Jayabalan *et al.*, 2019), but this analysis did not target placental extracellular vesicles specifically nor did it analyse medium/large EVs.

DPPIV plays a major role in glucose metabolism by regulating the secretion of insulin. In particular, DPPIV rapidly degrades GLP-1 (a member of the incretin family), consequently decreasing glucose-dependent insulin secretion (Drucker and Nauck, 2006). Decreased insulin secretion is also noted in GDM pregnancies (Homko *et al.*, 2001). Reduced GLP-1 concentration after meal uptake was described by Bonde *et al.* in both normal and GDM pregnancies, but with significantly higher decreases seen in GDM pregnancies (Bonde *et al.*, 2013). Supporting this, we have shown that STB-EVs can decrease active GLP-1. We also showed that DPPIV activity, although present in both normal and GDM pregnancies, was increased in GDM pregnancies. This might provide a possible explanation for the aforementioned decline of GLP-1 observed in GDM. Additionally, the reported greater numbers of SMALL STB-EVs in GDM could also contribute to increased breakdown of GLP-1 in GDM pregnancies. Interestingly, GLP-1 function rapidly returns to normal in both GDM

and normal pregnancies after delivery (Bonde *et al.,* 2013), showing that the effect is remarkably transient. Our finding is consistent with the hypothesis that STB-EVs could reduce incretin bioavailability during gestation by delivering active membrane-bound DPPIV, which decreases postpartum as the release of STB-EVs declines following placental delivery (Reddy *et al.,* 2008).

EV-bound DPPIV is not without precedence in diabetes research. Increased levels have been observed on urinary vesicles secreted by tubular epithelial cells from diabetic kidney disease (DKD) suggesting that these vesicles have the potential to be used as an early biomarker for DKD (Sun *et al.*, 2012).

Whilst increased DPPIV in STB-EVs of GDM pregnancies might impact insulin sensitivity via the regulation of GLP-1, other mechanisms could also be considered. For example, a recent randomised and double-blind trial included 206 women (102 in treatment group and 104 in placebo group) and demonstrated that the DPPIV inhibitor sitagliptin attenuated insulin resistance and improved overall glycaemic control in women with GDM by a purported reduction in RBP4 (Retinol Binding Protein 4) levels (Sun *et al.*, 2017). However, DPPIV levels were not determined in this study. Authors did not include any report of potential side effects associated with the use of gliptins so this remains to be investigated.

Finally, DPPIV is a multifunctional protein implicated in the regulation of chemokine and cytokine activities. GDM is also associated with an imbalance between circulating pro- and anti-inflammatory cytokines. Isolated SMALL STB-EV from GDM pregnancies increase cytokine release from endothelial cells to a greater extent than those of control pregnancies (Elfeky *et al.*, 2017). Therefore, it is possible that increased DPPIV activity in GDM pregnancies might also affect the release or the activity of circulating of pro- or anti-inflammatory factors, which have been implicated in the dysregulation of insulin signalling and the establishment of insulin resistance. Further work to dissect this is required.

Limitations of these experiments include, the number of patients we have analysed is small, but the isolation and characterisation of these STB-EVs is time intensive and complex. The data presented here is obtained from term pregnancies and it would be important to investigate the levels of STB-EVs-DPPIV earlier in pregnancy, since the presence of STB-EV-DPPIV might allow earlier diagnosis if the elevation seen in GDM occurs earlier in pregnancy. A larger study might allow us to understand the contribution of maternal characteristics (e.g obesity, ethnicity) to the circulating DPPIV levels and thus allow stratification of severity.

## 3.4. Summary

We have demonstrated that syncytiotrophoblast derived extracellular vesicles express DPPIV which is not only active but also present in higher quantities in the maternal circulation of GDM patients. This raises the possibility of their use as a potential diagnostic tool. A larger study would be required to further validate this approach as a potential means of early GDM screening/diagnosis. Additionally, we showed STB-EV-bound DPPIV can be inhibited by gliptin class drugs, which suggests the possibility of their use in the management of GDM. The results presented in this chapter were published in *The Journal of Extracellular Vesicles*, with me as the lead author (Kandzija *et al.*, 2019). The discovery of DPPIV on STB-EV was intellectually protected by Oxford University Innovations with me as a named inventor (international application number: PCT/G8201 8/051 500). Finally, we were awarded a Mathematical & Life Sciences Translational Fund grant to support the continuation of the project (see 6. *Thesis Summary and Future Work*).

# 4. STB-EVs express functional insulin receptor (IR) capable of binding insulin; circulating levels are increased in GDM

## 4.1. Introduction

Plasma glucose levels are tightly controlled and maintained between 4 and 7 mM in healthy individuals. One of the critical regulators of plasma glucose levels is insulin, the most potent anabolic hormone described to date. Insulin is involved in the synthesis and storage of carbohydrates, lipids and proteins (De Meyts, 2016). In 1949, Levine *et al.* observed that insulin plays an important role in hexose transport across the cell membrane. In their landmark paper, they injected non-metabolisable galactose into control and treated groups of eviscerated, nephrectomised dogs, with the treated group receiving insulin. They found that the galactose blood levels were significantly lower when accompanied by insulin. The authors proposed that "insulin acts upon the cell membranes of certain tissues (skeletal muscle, etc.) in such a manner that the transfer of hexoses (and perhaps other substances) from the extracellular fluid into the cell is facilitated" (Levine *et al.*, 1949). Despite these observations, the mechanism behind this concept remained unknown until decades later when it was shown that insulin is acting on a specific cell membrane receptor (insulin receptor, hereafter, IR) to promote glucose uptake by adipose tissue (Freychet, Roth and Neville, 1971) via the translocation of intracellular glucose transporters to cell membranes (Cushman and Wardzala, 1980; Suzuki and Kono, 1980).

Another milestone study in understanding the concept of insulin's regulation of glucose homeostasis was published by Rosen's group in 1982. They demonstrated that a tyrosine kinase activity was involved in the action of the IR (Petruzzelli *et al.*, 1982). This was followed by the work of Kasuga *et al.*, who suggested IR itself has a tyrosine kinase activity. The group immunoprecipitated IR and showed it becomes phosphorylated as a result of insulin binding to it (Kasuga *et al.*, 1982). The hypothesis was finally confirmed in 1985 by Ebina *et al.* and Ullrich *et al.* respectively through the identification of its complete amino acid sequence (Ebina *et al.*, 1985; Ullrich *et al.*, 1985). Both groups showed that IR is indeed a tyrosine kinase receptor and is therefore able to undergo autophosphorylation. Generally, the phosphorylation

is achieved by transfer of γ-phosphate from ATP to a specific amino-acid. In eukaryotes these are usually Serine, Tyrosine or Threonine, on a protein substrate, and, in a case of autophosphorylation, the receptor itself is a protein substrate (Ubersax and Ferrell, 2007; De Meyts, 2016).

IR is a transmembrane protein consisting of two extracellular α-subunits linked via disulphide bond to two transmembrane β-subunits, which have the tyrosine kinase activity in their intracellular portion (Häring, 1991; De Meyts, 2015). Insulin binding to IR through α-subunit leads to autophosphorylation of β-subunit, which activates a cascade of diverse signalling pathways responsible for the regulation of many different processes in a cell (i.e. vesicle trafficking, gene expression, glucose metabolism etc.). One of the principal actions insulin regulates via binding to IR is the translocation of glucose transporter-4 (GLUT-4) intracellular vesicles to the cell membrane, allowing glucose uptake by insulin sensitive tissue ***(Figure 29)***. IR autophosphorylation leads to the phosphorylation of docking proteins, including insulin receptor substrate-1 (IRS-1). Activated IRS-1 interacts with phosphatidylinositol 3-kinase (PI3K), which in turn catalyses the conversion of phosphatidylinositol-4,5-bisphosphate into phosphatidylinositol-3,4,5-trisphosphate (PIP3). PIP3 then activates phosphatidylinositol dependent kinase-1 (PDK1) leading to the activation of several other kinases, including protein kinase B (PKB, also known as AKT). PKB phosphorylates and inactivates AS160 and the RAL–GAP complex. Both AS160 and RAL-GAP complex belong to GTPase-activating proteins that stimulate the translocation of GLUT-4 intracellular vesicles (called GSV) to the cell surface (Leto and Saltiel, 2012).

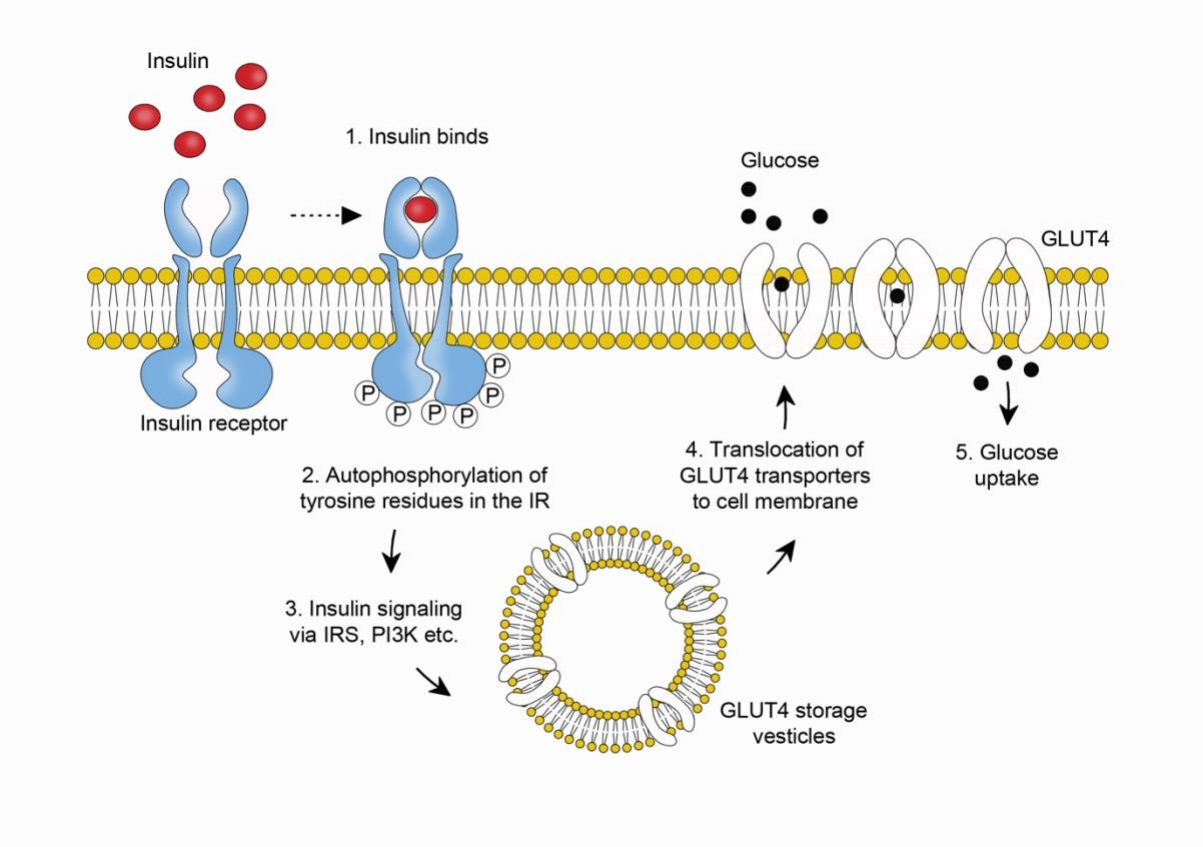



**Figure 29. Schematic representation of insulin stimulated glucose transport across a cell membrane.**

In insulin sensitive tissue, insulin binding to IR's α-domain will lead to the autophosphorylation of IR's intracellular portion, which in turn will stimulate signal transduction. The molecules that participate in this cascade include insulin receptor substrate-1 (IRS-1), phosphatidylinositol 3-kinases (PI3K), phosphatidylinositol-3,4,5-trisphosphate (PIP3), 3-phosphoinositide-dependent protein kinase-1 (PDK1), protein kinase B (PKB), etc. This results in the translocation of intracellular vesicles called GSV to the plasma membrane, allowing carrier-mediated diffusion of glucose across the cell membrane. Once insulin action ceases, the GLUT4 will be recycled back into intracellular GSV.

GLUT4 belongs to glucose transporter isoforms (GLUTs) and is stored in GSVs of adipose tissue, skeletal and cardiac muscle. GLUT4 facilitates glucose uptake across the cell membrane through passive diffusion (ATP-independent transport) in response to insulin and other stimuli (such as exercise). To prevent hypoglycaemia between the meals, only 5% of total GLUT4 is found on the surface of the cell membrane in the unstimulated state. The inability of GLUT4 to translocate to the cell membrane upon insulin simulation can lead to complications including as insulin resistance and T2DM (Leto and Saltiel, 2012).

IR has two isoforms, IR-A and IR-B, with IR-B containing an additional 12 amino acids on the C-terminus of its α-subunit. It is believed that isoform A has a stronger metabolic effect and is primarily expressed in the foetus whilst isoform B is a dominant form of IR in adult life (Haeusler, McGraw and Accili, 2018). In addition to insulin, IR can also bind insulin-like growth factors (IGF-I and IGF-II). Even though both isoforms bind insulin with similar affinity, IR-A has 100 times higher affinity for binding IGF-II compared to isoform B (Belfiore *et al.*, 2009; Siddle, 2011).

In 1972, Gavin *et al.* isolated soluble IR from cultured lymphocytes and demonstrated that it maintained its insulin binding affinity (Gavin, Buell and Roth, 1972). Later, circulating IR has been found in human plasma, again with the capacity to bind insulin (Pezzino *et al.*, 1992). It is believed that circulating IR originates from the proteolytic cleavage of the membrane bound form (Yuasa *et al.*, 2014). In 2003, Kanezaki *et al.* injected the α-subunit of human IR to mice and observed elevated plasma glucose levels within 30 minutes. This suggested soluble IR binds circulating insulin, reducing its ability to act as a blood glucose-lowering agent (Kanezaki *et al.*, 2003a). Subsequently, the same group measured soluble IR in humans, and showed that IR α-subunit, together with a portion of β-subunit, can be found in human plasma and is increased in hyperglycaemia (The Soluble Insulin Receptor Study Group, 2007). Furthermore, they showed plasma levels of soluble IR positively correlates with insulin resistance in patients with T2DM (Yuasa *et al.*, 2016).

Insulin resistance – the inability of insulin sensitive tissue to mount a glucose-lowering effect as a response to insulin stimuli – is associated with T2DM and atherosclerosis (Hall, Yu and Choi, 2020). As discussed in this thesis' introduction, it is also a normal feature of pregnancy. The natural response to the increased insulin resistance of pregnancy is to increase circulating insulin levels and thus normal pregnancy is both hyperinsulinaemic and euglycaemic. An

inability to overcome pregnancy induced insulin resistance by increasing maternal insulin release leads to complications such as GDM.

In pregnancy, it is already well established that the placenta can release molecules that act as decoy receptors, such as sFlt-1 in preeclampsia (Krysiak *et al.*, 2005). We thus hypothesised that a similar mechanism might explain the shortage of insulin seen in GDM pregnancies and, importantly, explain the rapid reversal seen post-partum.

We performed mass spectrometric analysis of STB-EV isolated from *ex vivo* normal placenta perfusion (Tannetta *et al.* unpublished data) and interrogated it for potential molecules that might alter insulin availability. One of the molecules we identified was the IR.

In this chapter, we study the expression of IR on STB-EVs and their role as decoy receptors capable of sequestering maternal insulin and reducing its biological effects.

## 4.2. Results

### 4.2.1. IR is present on STB-EVs

Immunohistochemistry confirmed that IR is expressed on placental tissue with strong signal in the syncytiotrophoblast layer. Control did not show staining (**Figure *30***).

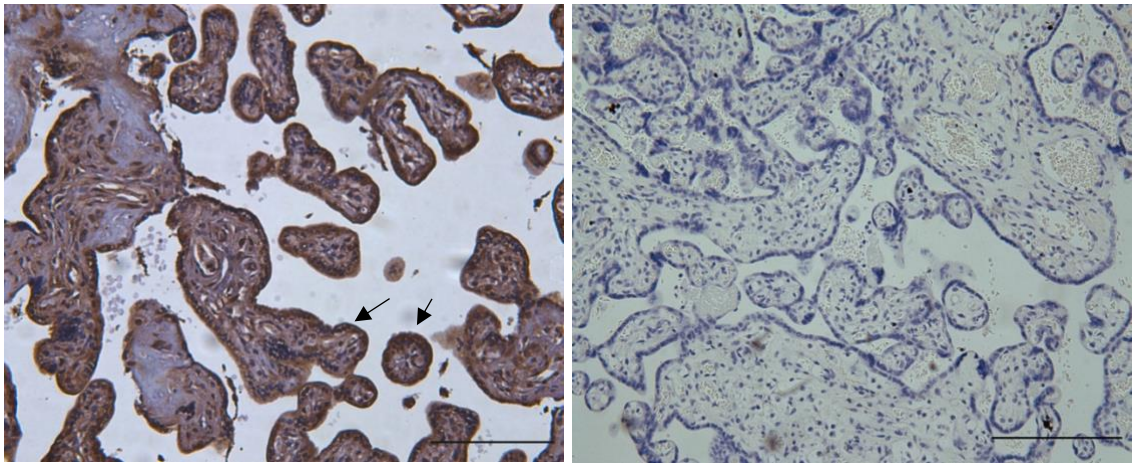


**Figure 30. IR is expressed on placental tissue.**

Immunohistochemical analysis of IR expression on placental tissue (**left panel**). Control placental sections showed enriched IR expression at the syncytiotrophoblast layer (arrow). Placental sections were also incubated with anti-IgG1 antibody as negative control (**right panel**). Images are representative of n=3 separate experiments. Scale bar set at 200 μm.

We then confirmed IR protein expression in both MEDIUM/LARGE STB-EVs and SMALL STB-EVs of normal pregnancies obtained from *ex vivo* placenta perfusion using western blotting. Placental lysate, MEDIUM/LARGE and SMALL STB-EVs were also positive for PLAP. HUVEC cells were used as positive control for IR expression (**Figure *31***).

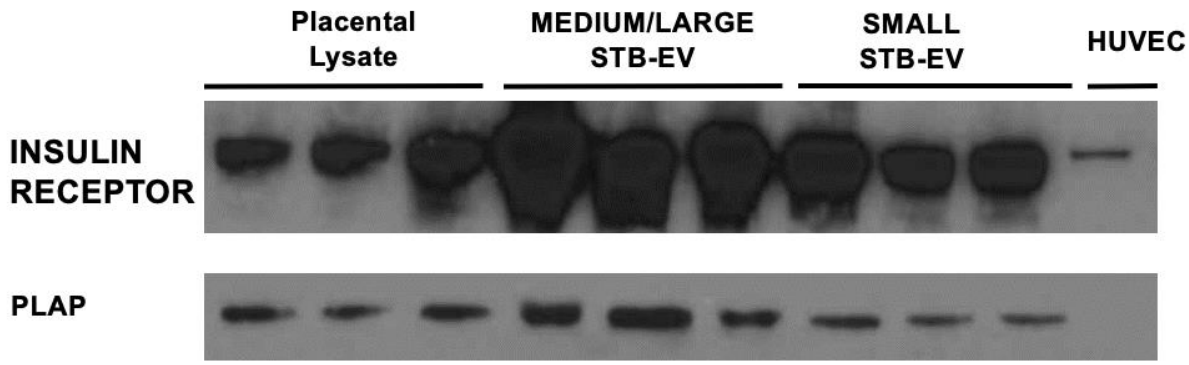


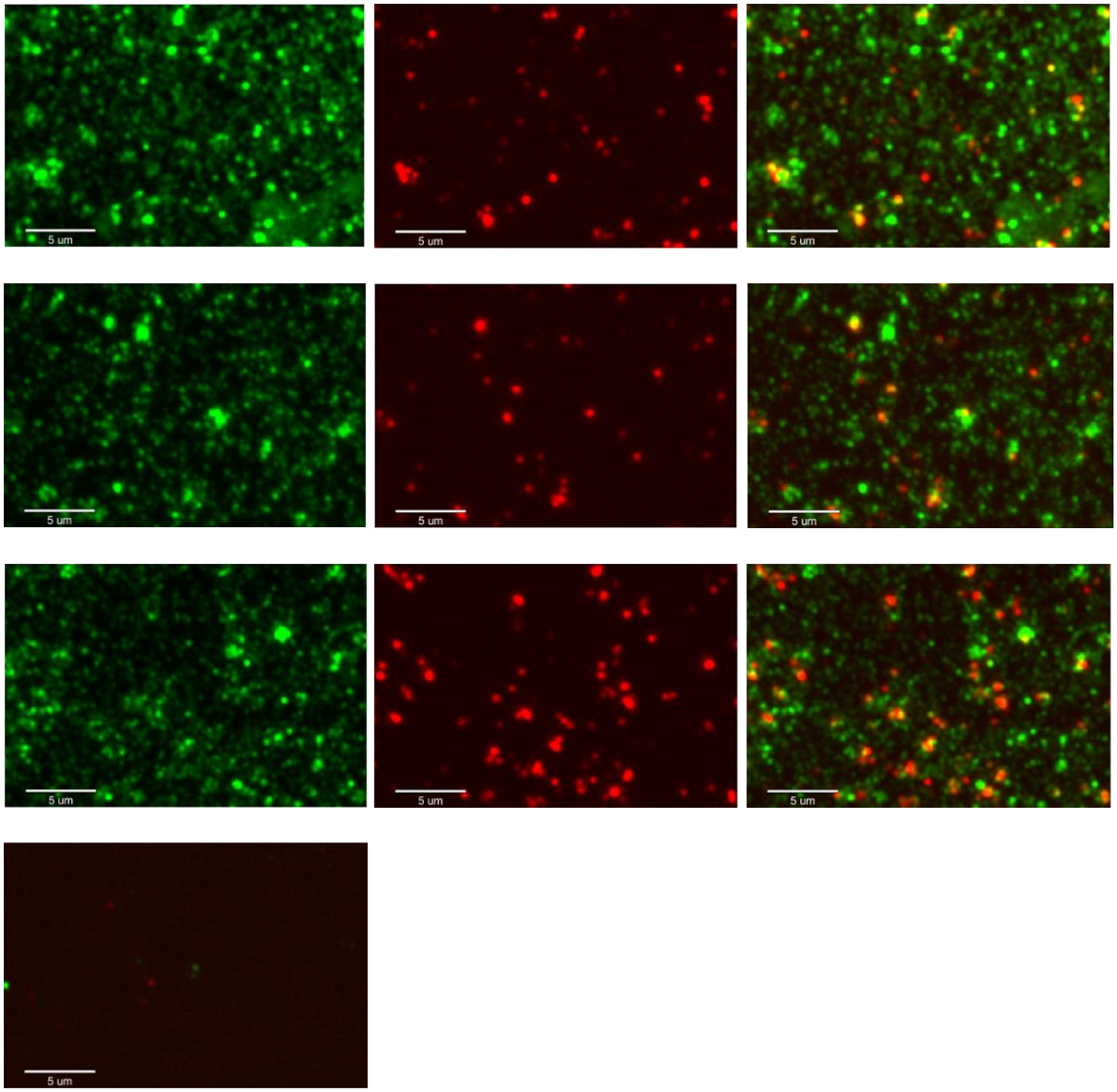

**Figure 31. IR and PLAP expression on placental tissue and STB-EVs.**

Representative Western blot (n=3) of IR protein expression in whole placental lysates, MEDIUM/LARGE STB-EVs and SMALL STB-EVs isolated from control term placentae. Human umbilical vein endothelial cells (HUVEC) were used as positive control for IR. PLAP expression confirmed syncytiotrophoblast origin. Blots are representative of n=3 separate experiments.

### 4.2.2. IR is co-expressed with PLAP on STB-EVs

In order to investigate the co-expression of IR and PLAP on MEDIUM/LARGE STB-EVs we used the ExoView platform from NanoView Biosciences. The instrument can provide quantification of EVs based on immunofluorescence. This technology can also determine co-localization of two antigens on a single particle. STB-EVs isolated from placenta perfusion were incubated on the chip previously coated with PLAP capture antibody. After sample incubation, the chip was washed three times with PBS and stained with Anti-IR/Alexa 647 and Anti-PLAP/Alexa 555. ExoView analysis revealed that there is a population of MEDIUM/LARGE STB-EVs that are both IR and PLAP positive. 17.6 ± 3.2% of particles that were captured by PLAP showed IR positivity, suggesting that in a significant proportion of MEDIUM/LARGE STB-EVs PLAP and IR are co-expressed (**Figure *32***).

**A)**


5 um

**B)**

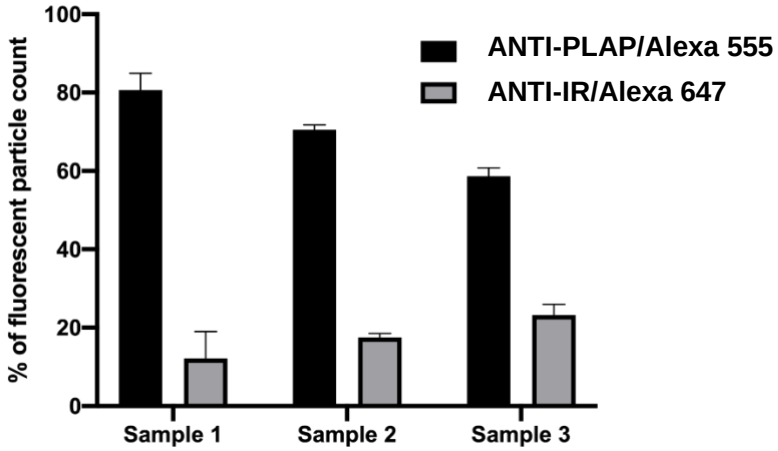

% of fluorescent particle count
100
80
60
40
20
0
Sample 1
Sample 2
Sample 3
ANTI-PLAP/Alexa 555
ANTI-IR/Alexa 647

**Figure 32. ExoView images of MEDIUM/LARGE STB-EVs showing co-expression of IR and PLAP.**

**(A)** Vesicles were captured by anti-PLAP antibody and detected using fluorescently conjugated anti-PLAP (green) and anti-IR antibodies (red). Merged images indicate co-expression of PLAP and IR on the same particle. In the bottom panel anti-PLAP capture antibody was replaced with IgG1 isotype control antibody. Images show n=3 different biological samples (one sample per row). **(B)** Bar graph showing percentage of fluorescent particles stained with fluorescently conjugated anti-PLAP and anti-IR respectively for n=3 different biological samples. Data presented as mean ± SEM.

In addition, we validated ExoView data using performing flow cytometry on three different biological samples. MEDIUM/LARGE STB-EVs from placental explants were stained for PLAP and IR (**Figure *33***) and these data confirmed a population of double positive events 21.4 ± 5.4% (**Table *7***), which correlated with the findings from the ExoView platform.

**Table 7. Percentage of IR expression on MEDIUM/LARGE STB-EV assessed by flow cytometry.**

| Sample | $PLAP^+/IR^+$ (%) | $PLAP^+/IR^-$ (%) |
|---|---|---|
| **1** | 17.6 | 80.3 |
| **2** | 32.0 | 60.3 |
| **3** | 14.5 | 71.9 |
| **Mean** | **21.4** | **70.8** |
| **SEM** | **5.4** | **5.8** |

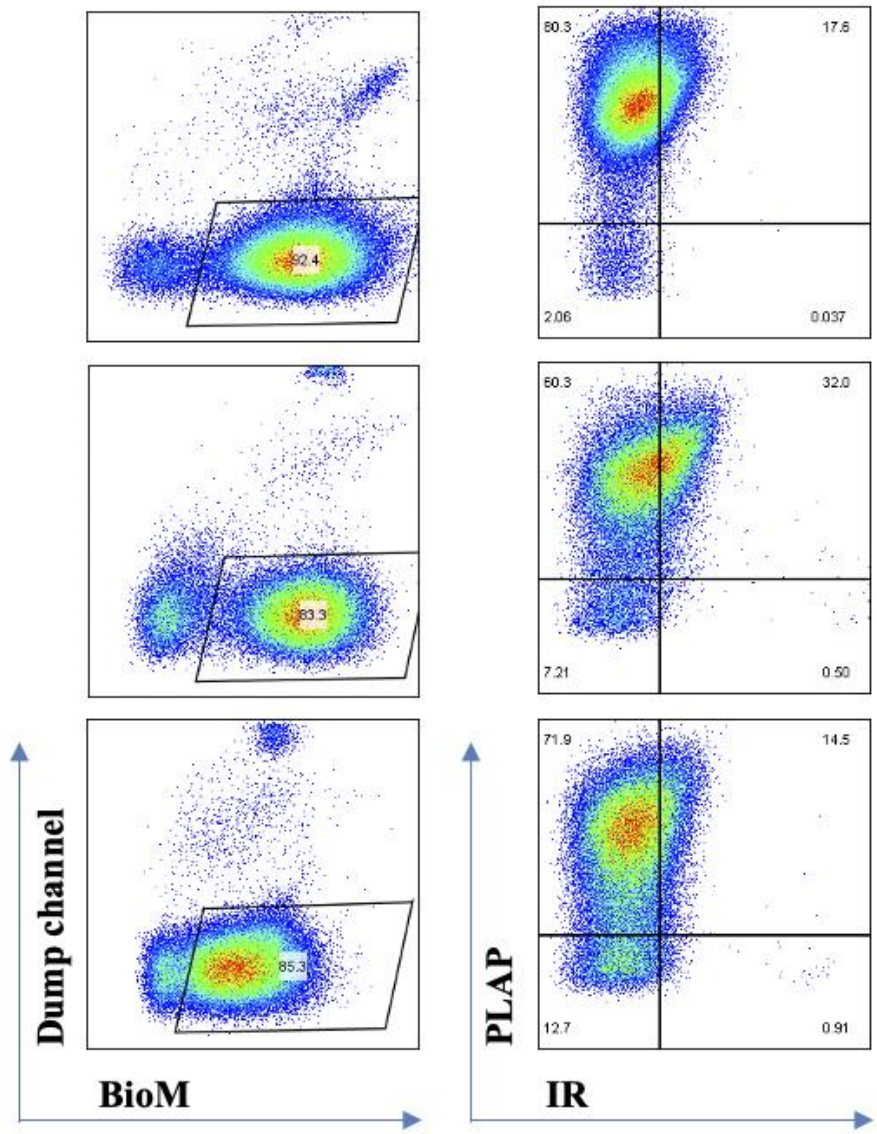


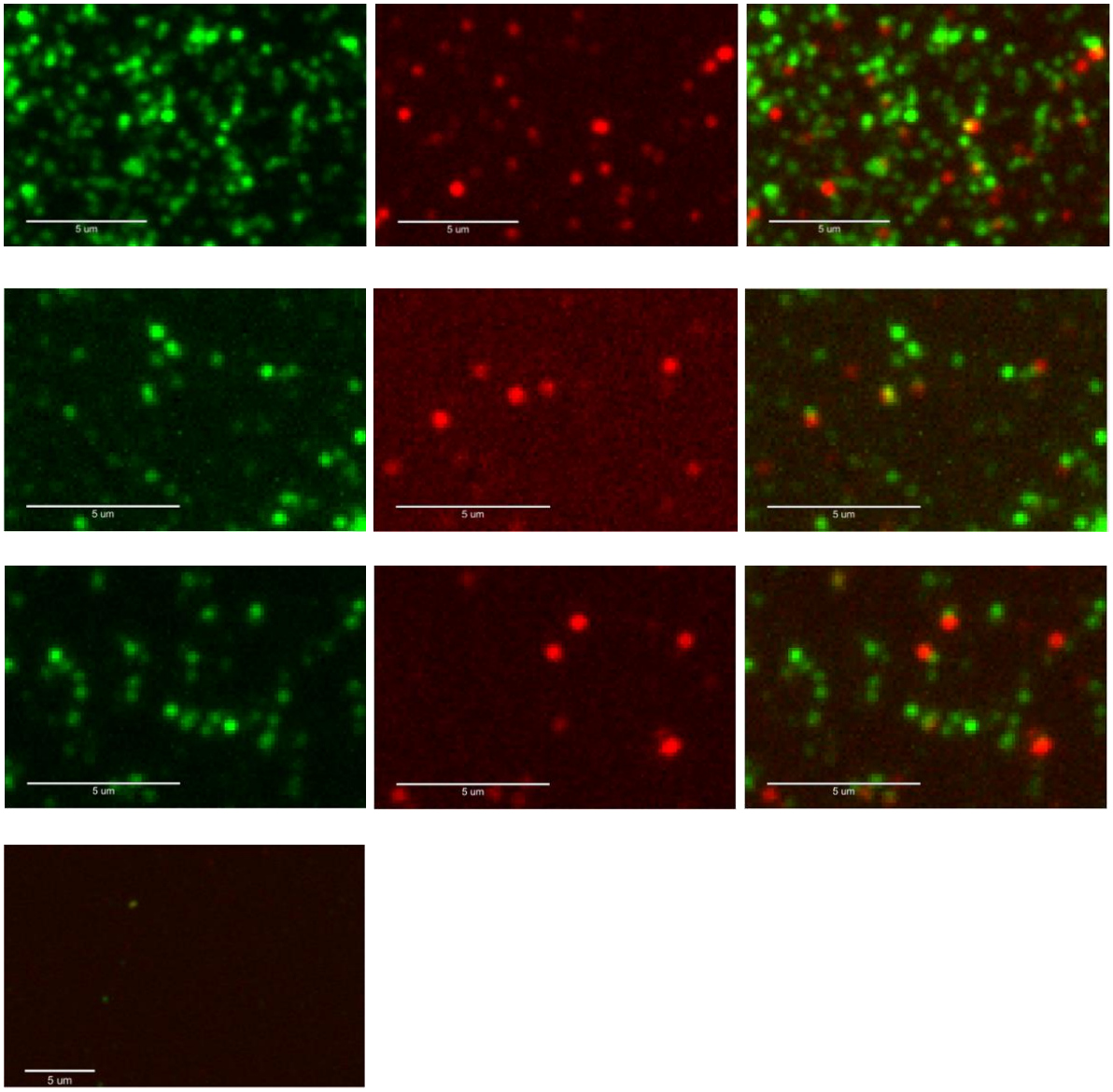

**Figure 33. Flow cytometry analysis of PLAP and IR co-expression on MEDIUM/LARGE STB-EVs.**

Representative image of flow cytometry analysis of IR expression on MEDIUM/LARGE STB-EV (n=3) derived from placental explants. MEDIUM/LARGE STB-EVs were stained with anti-IR-APC, anti-PLAP-PE, 'dump channel'- PeCy7 antibodies and bio-maleimide-FITC. 'Dump channel' negative and bio-maleimide positive events were investigated for $IR^+/PLAP^+$.

We also performed a similar analysis on the SMALL STB-EVs. Again, the chip was coated with anti-PLAP capture antibody. Afterwards, fluorescently labelled antibodies against PLAP and IR were added. The co-localisation of both antibodies on SMALL STB-EVs is showed on **Figure *34***. 2164.7 ± 680.3 of particles were captured by anti-PLAP antibody. Due to the older

version of ExoView software, it was not possible to convert these values into a percentage of population that is IR positive like it was done for MEDIUM/LARGE STB-EVs. However, the data clearly demonstrated that in SMALL STB-EVs PLAP and IR are co-expressed too.

**A)**


5 um

**B)**

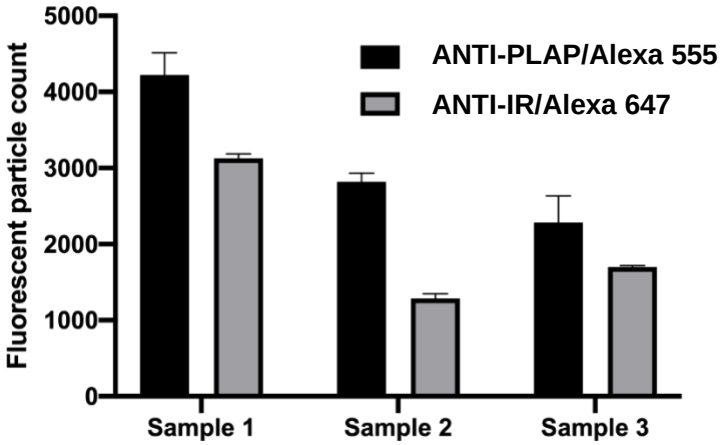

Fluorescent particle count
5000
4000
3000
2000
1000
0
ANTI-PLAP/Alexa 555
ANTI-IR/Alexa 647
Sample 1
Sample 2
Sample 3

**Figure 34. ExoView analysis of PLAP and IR co-expression on SMALL STB-EVs.**

**(A)** Representative ExoView images of SMALL STB-EVs captured by anti-PLAP antibody and detected using fluorescently conjugated anti-PLAP (green) and anti-IR antibodies (red). Merged images indicate co-expression of PLAP and IR on the same particle. In the bottom panel anti-PLAP capture antibody was replaced with IgG control. Images of n=3 different biological samples (one sample per row). **(B)** Bar graph showing number of fluorescent particles stained with fluorescently conjugated anti-PLAP and anti-IR respectively for n=3 different biological samples. Data presented as mean ± SEM.

Since standard flow cytometry is unable to resolve SMALL STB-EVs, we, therefore, confirmed the aforementioned findings using magnetic immunodepletion. Briefly, SMALL STB-EVs were incubated with magnetic beads coated with either PLAP or IR. These beads were magnetically separated, and the attached vesicles subjected to western blotting. PLAP pull-out vesicles were positive for both PLAP and IR. Conversely, IR pull-out vesicles were positive for both IR and PLAP confirming that these proteins were on the same vesicles (**Figure *35***).

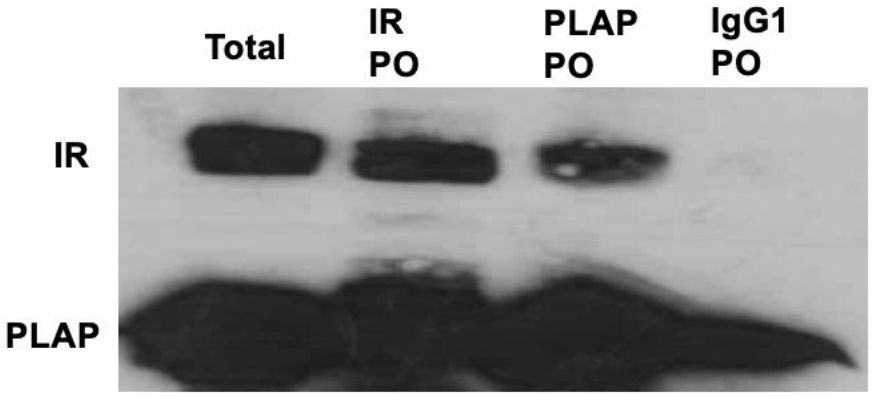


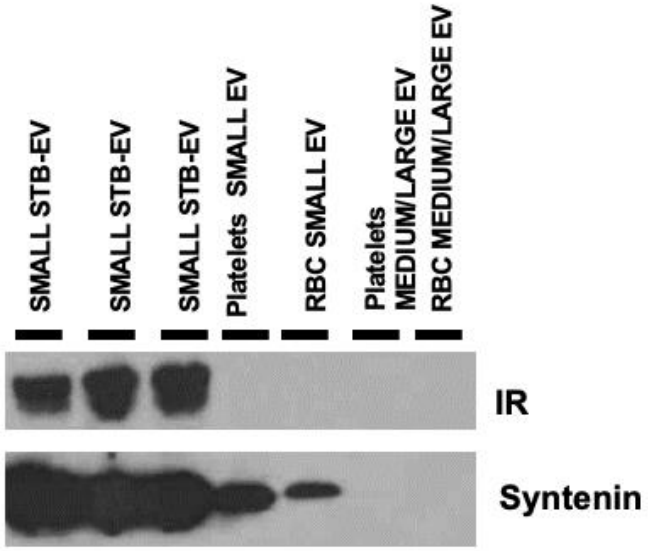

**Figure 35. Magnetic beads immunodepletion analysis of IR and PLAP co-expression on SMALL EVs.**

IR and PLAP protein expression in total SMALL STB-EVs (Total), in SMALL STB-EVs population pulled out with anti-IR magnetic beads (IR PO), in SMALL STB-EVs population pulled out with anti-PLAP magnetic beads (PLAP PO) and in SMALL STB-EVs population pulled out with anti-IgG1 magnetic beads (IgG1 PO). Blot is representative of n=3 experiments.

### 4.2.3. IR expressed on EVs in unique to placental vesicles

In order to understand if IR positive vesicles were a unique feature of placenta, we analysed SMALL EVs isolated from different sources using western blotting (**Figure *36***). In contrast to the STB-EVs, platelets and RBC derived MEDIUM/LARGE and SMALL EVs did not show IR expression. We additionally examined SMALL EVs from HUVEC, HEK293T (kidney), MDA-MB-231 (breast adenocarcinoma), EAHY923 (endothelial) cells, which were all negative for IR expression. HepG2 cells were used as a positive control for IR expression.

**A)**




**B)**

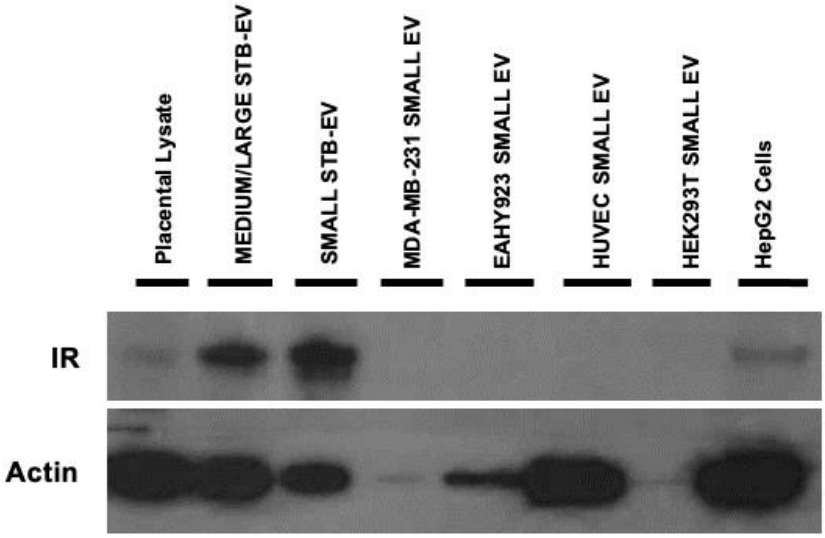



**Figure 36. Western blot analysis of IR expression on SMALL EVs from different sources.**

IR was expressed in SMALL EVs isolated from placenta (STB-EV), but not in MEDIUM/LARGE AND SMALL EVs derived from platelets and red blood cells. Syntenin, marker of exosomal origin, was enriched in SMALL EVs. **(A)** Additionally, SMALL EVs isolated from HUVEC, HEK293T (kidney), MDA-MB-231 (breast adenocarcinoma), EAHY923 (endothelial) cells did not express IR. HepG2 cells were used as positive control for IR. **(B)** Blots are representative of n=3 separate experiments.

### 4.2.4. IR expressed on STB-EVs binds insulin

To investigate the potential functional role of IR on STB-EV, we assessed STB-EV mediated depletion of insulin from plasma (**Figure *37***). We used plasma samples from non-pregnant volunteers (n=3) and incubated them with different concentrations of STB-EVs (0-500 µg/mL). After incubation, STB-EV were removed from the sample by ultracentrifugation and insulin levels were measured by ELISA analysis. Addition of differing concentrations of STB-EVs to non-pregnancy plasma revealed a dose dependent decrease of free insulin suggesting that IR positive STB-EVs are functionally active and have a high affinity for insulin binding. The highest concentration of STB-EVs (500 µg/mL) was able to deplete 53.07 ± 3.73% of insulin.

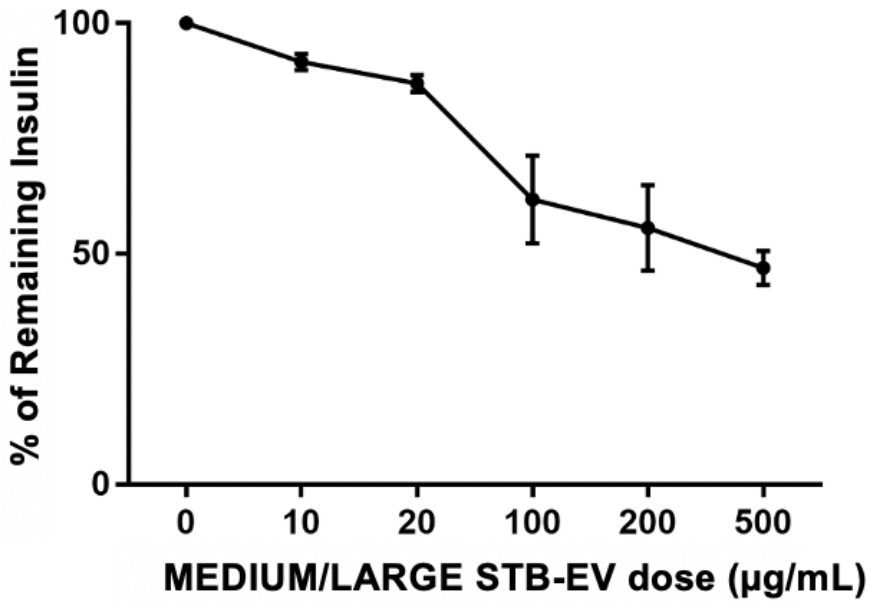



**Figure 37. STB-EV mediated depletion of insulin from plasma.**

Platelet poor plasma samples from non-pregnant volunteers (n=3) were incubated with different concentrations (0, 10, 20, 100, 200 and 500 µg/mL) of STB-EVs (n=3) prior to insulin ELISA analysis.

### 4.2.5. STB-EV reduced cellular glucose uptake

We next aimed to assess the ability for STB-EV-bound IR to act as a decoy receptor for insulin by analysing cellular glucose uptake. The assay measures glucose uptake in response to insulin.

The data showed that pre-incubation of the STB-EVs with the insulin reduced the bioavailability of free insulin leading to a reduction of cellular glucose uptake. In a pilot experiment, differentiated C2C12 cells were treated with different concentrations of insulin in order to determine the appropriate concentration of insulin for the future experiment (**Figure *38***). C2C12 myotubes that were treated with 1 nM insulin solution preincubated with 150 µg/mL MEDIUM/LARGE STB-EVs from normal pregnancy showed 1.86-fold reduction in glucose uptake compared to insulin stimulation in the absence of STB-EVs. We also confirmed this attenuation by looking at the phosphorylation of glycogen synthase kinase 3 beta (GSK-3β) – part of the insulin signalling pathway – in adipose cells. There was a reduction in GSK-3β phosphorylation when dose-dependent STB-EVs were added (Shahjahan, unpublished data), again suggesting a decrease in free insulin bioavailability.

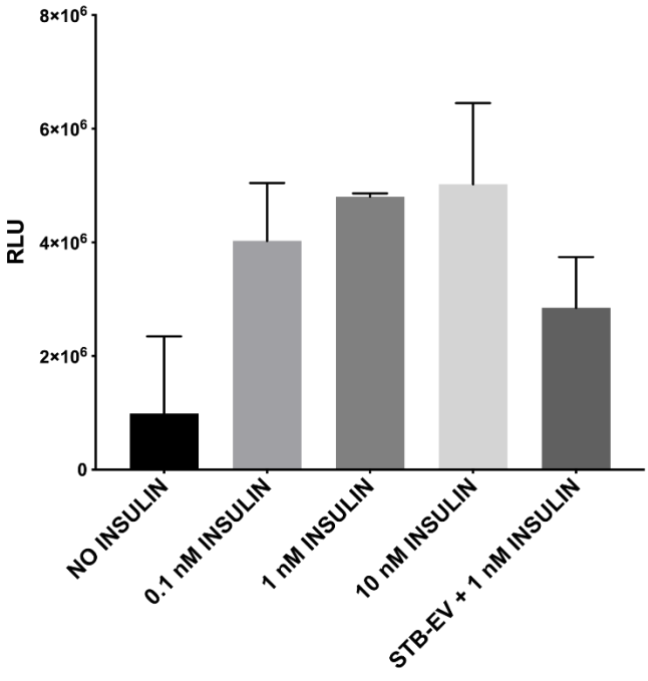



**Figure 38. Pilot experiment showing C2C12 glucose uptake in the presence of STB-EVs.**

Differentiated C2C12 myoblast were treated with different concentrations of insulin (0.1, 1 and 10 nM) prior to glucose uptake measurements. Additionally, 1 nM insulin was preincubated with 150 µg/mL MEDIUM/LARGE STB-EVs and reduced glucose uptake was observed. Measurement of the luminescence is expressed as relative light units (RLU). Data are presented as mean ± SEM (n = 2).

*Due to the Covid-19 pandemic and closure of our laboratory, I was not able to repeat the experiment by addition of different concentrations of STB-EVs. Furthermore, the goal was to investigate the specificity of this effect with the use of the insulin receptor specific antagonist S96. We hypothesised that adding S96 to the STB-EVs prior to their incubation with insulin would lead to abrogation of aforementioned effect.*

### 4.2.6. IR expressing STB-EVs in the maternal circulation

To confirm that trophoblast derived IR positive vesicles were being released into the circulation, we analysed both uterine vein (which drains the utero-placental unit, and therefore, approximates the total release of STB-EVs before their dilution in the peripheral blood) and peripheral vein blood from the same patients (n=6) using four-colour flow cytometry. As expected, the comparison showed higher levels of placental derived EVs in uterine than peripheral plasma (measured by PLAP positive events per mL of plasma) (**Figure *39***).

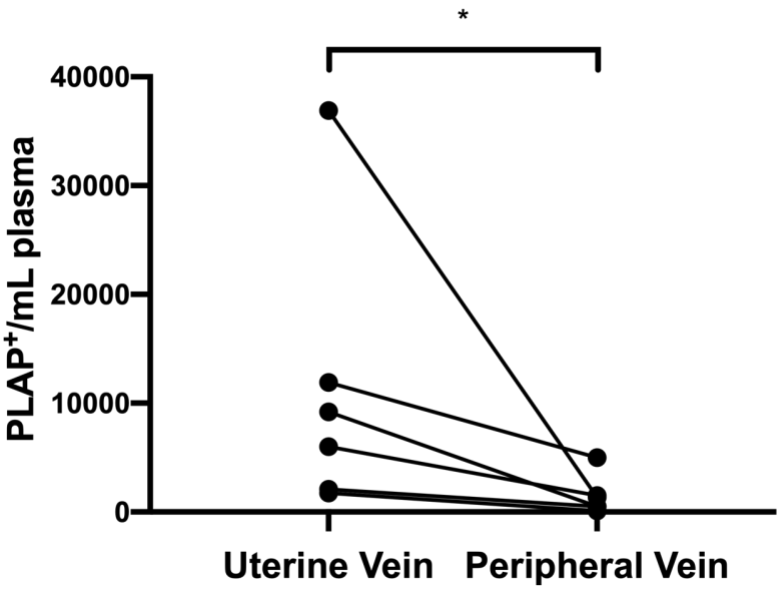



**Figure 39. PLAP-bound STB-EVs are present in the circulation of pregnant women and are higher in the uterine vein.**

Paired plasma samples were collected from the uterine and the peripheral vein at the term and analysed with flow cytometry. Presented are individual PLAP positive event numbers from matched uterine and peripheral vein plasma samples (n=6 women; Wilcoxon test *$p<0.05$). The statistical significance between the groups was observed even in the absence of the outlier sample that showed $PLAP^+$/mL of plasma in uterine vein higher than 30000.

We also observed that MEDIUM/LARGE STB-EVs carrying IR are present in significantly higher amount in the uterine vein ((1433.33 ±840.04 $PLAP^+/IR^+$ events per mL of plasma) compared with matched peripheral vein plasma (226.67 ± 135.89 $PLAP^+/IR^+$ events/mL of plasma) ($p<0.05$), confirming the placenta as a source of circulating levels of IR positive STB-EV during pregnancy (**Figure *40***).

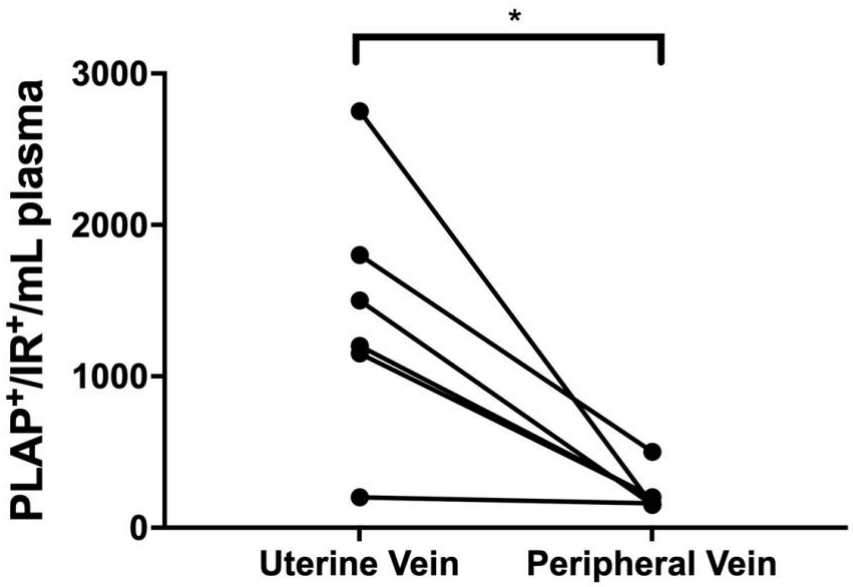



**Figure 40. PLAP/IR are present in the circulation of pregnant women and are higher in the uterine vein.**

Paired plasma samples were collected from the uterine and the peripheral vein at the term and analysed using flow cytometry. Presented are individual PLAP/IR double positive event numbers from matched peripheral and uterine vein plasma samples (n=6 women; Wilcoxon test *$p<0.05$).

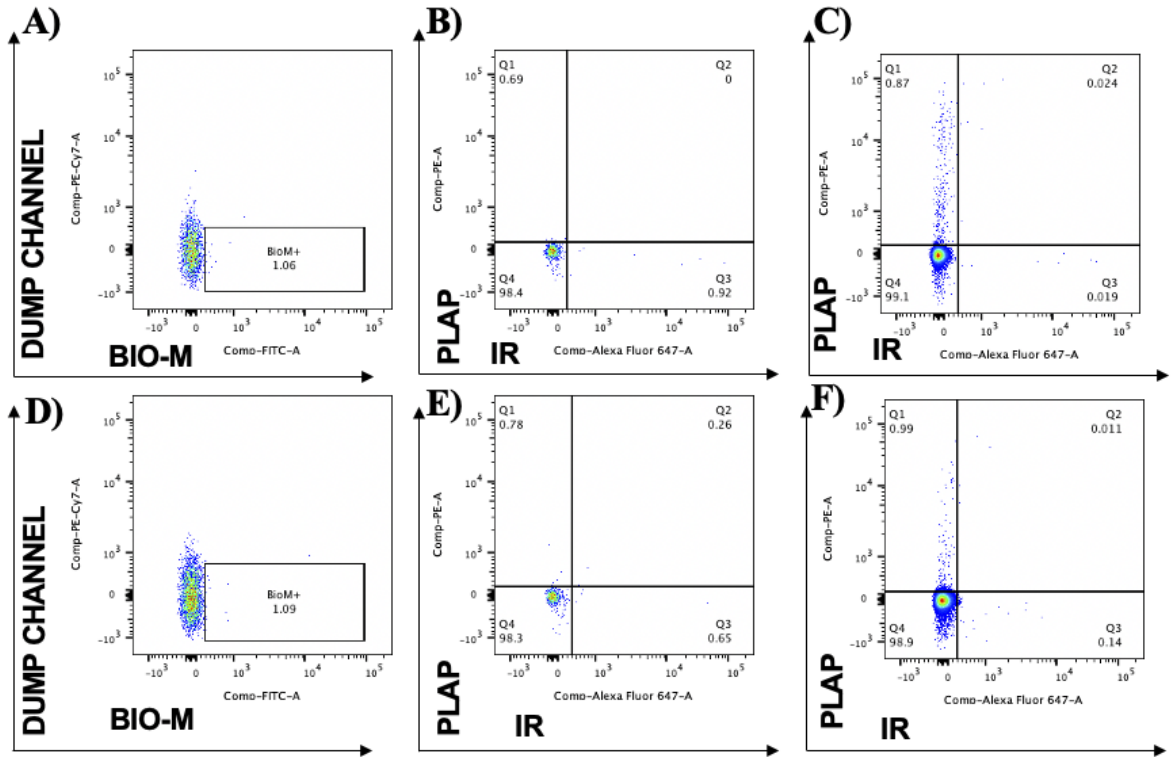



**Figure 41. Representative flow cytometry analysis of platelet-poor plasma (PPP) from peripheral and uterine vein.**

MEDIUM/LARGE STB-EVs were recovered from the top of the filter unit in 100 µL of filtered PBS and stained with bio-maleimide-FITC.
The top panel **(A, B, C)** shows flow cytometry analysis of PPP plasma obtained from uterine vein, while bottom panel shows analysis of peripheral vein **(D, E, F)**.
**A & D)** Filtrate was used to determine bio-maleimide positive and the contaminating markers ('Dump channel') negative gate. 'Dump channel' gate was draw at 1% cut off using dump channel-PeCy7 vs. bio-maleimide-FITC dot plot. 'Dump channel' includes contaminant markers such as CD231a/b, CD41, HLA-ABC and HLA Class II; all conjugated with PeCy7 labelling.
**B & E)** In order to draw 1% cut off gates for anti-IR-APC and anti-PLAP-PE staining, samples were treated with detergent (NP-40) prior to events acquisition.
**C & F)** 'Dump channel' negative and bio-maleimide positive population was analysed for PLAP and IR double positivity.

### 4.2.7. Circulating STB-EV bound IR in normal and GDM pregnancies

We next assessed the levels of circulating IR positive MEDIUM/LARGE STB-EVs in normal and GDM pregnancies at the term using flow cytometry. Significantly higher levels of STB-EVs expressing IR were observed in GDM pregnancies (3.24-fold increase) compared to

normal pregnancies (p=0.0051) (**Figure *42***), suggesting a potential diagnostic or pathological role. Patient characteristics are presented in **Table 8**.

**Table 8. Patient characteristics.**

Data is presented as mean ± SEM. Range is also included. Significant difference shown as * if $p<0.05$.

| | **GDM (n=8)** | **Normal pregnancy (n=7)** |
|---|---|---|
| **Age, year** | 34.9 ± 2.4 (21 - 40) | 36.1 ± 2.4 (24 - 42) |
| **Gestation age, weeks** | 39.4 ± 1.0 (38.3 – 41.0) | 39.0 ± 4.5 (36.0 – 40.6) |
| **Body mass index, kg/m2** | 35.6 ± 1.9* (28 – 44) | 25.7 ± 1.9 (20.5 – 34.5) |
| **Newborn weight, g** | 3610.6 ± 257.7 (2790 - 4500) | 3541.4 ± 254.0 (2890 – 4550) |
| **Max. systolic pressure, mmHg** | 129.3 ± 5.2 (105 - 150) | 128.3 ± 2.8 (119 - 140) |
| **Max. diastolic pressure, mmHg** | 82.5 ± 3.8 (74 - 100) | 74.7 ± 2.5 (68 - 84) |
| **GDM treatment** | Metf: 3<br>Ins + Metf: 2<br>Diet: 3 | - |

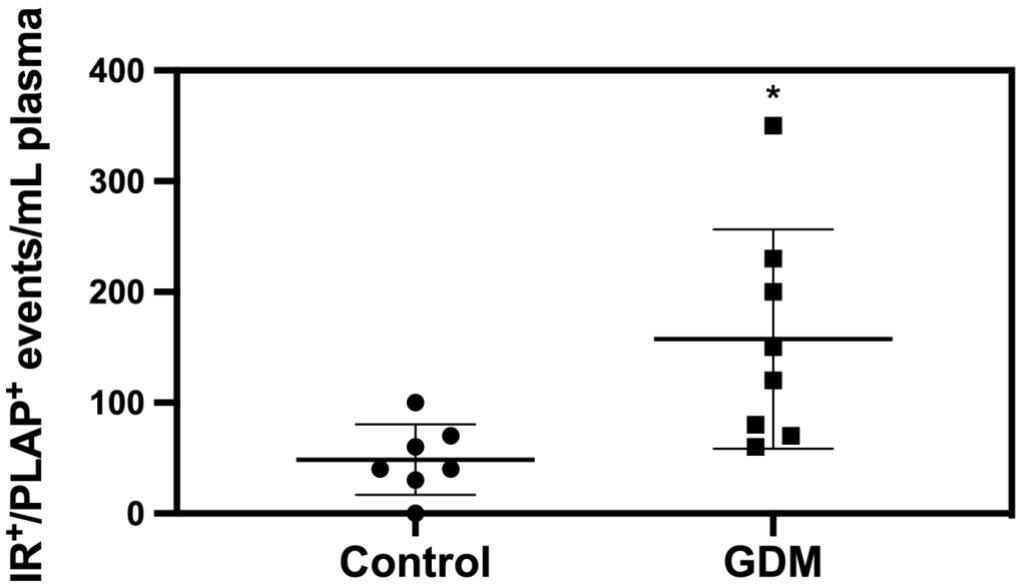


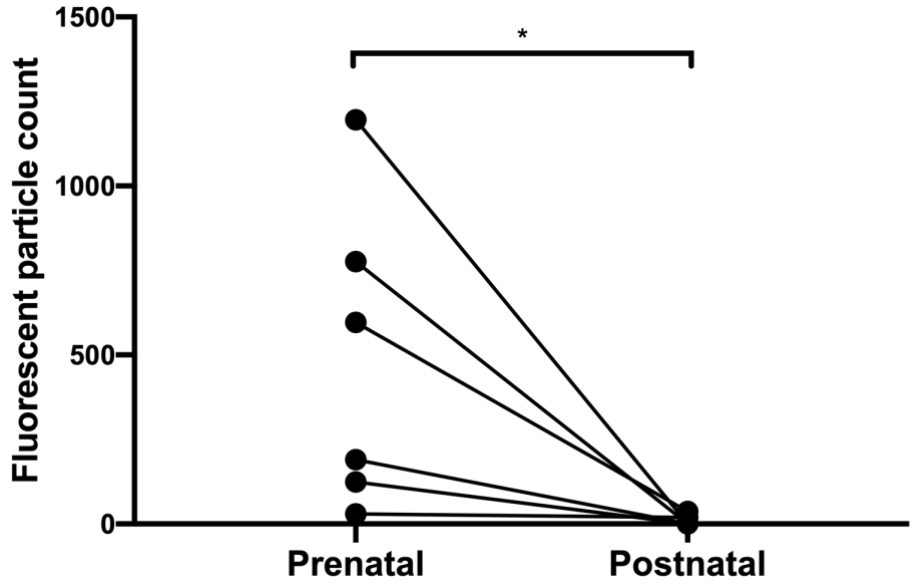

**Figure 42. Placenta-derived IR expression is increased in GDM peripheral plasma.**

Peripheral gestation matched plasma samples were collected from GDM (n=8) and Control (n=7) pregnant women. IR and PLAP double positive events in 1 ml of plasma were identified by flow cytometry. *p<0.05.

### 4.2.8. Postnatal reduction of STB-EVs

We sought to identify reduction in placenta-derived vesicles in the post-partum period. Samples were taken from women undergoing elective caesarean section and subsequently on day 1 post-delivery. Plasma samples were purified using qEV coloumn (70 nm) to remove contaminants smaller than 70 nm (i.e. soluble proteins). We then used the ExoView platform to quantify PLAP positive vesicles at these time points (n=6) and showed significant reductions in placenta-derived vesicles in all samples 24 hours after the delivery (**Figure *43***). ExoView chip was coated with either anti-PLAP or anti-CD81 antibody, and anti-PLAP/Alexa555 was used for a fluorescent staining. With anti-PLAP used as a capture antibody, we observed 98.09% reduction in fluorescent particle count in postnatal samples while when chips were coated with CD-81, a removal of 93.24% of particles has been observed postpartum.

**A)**




**B)**

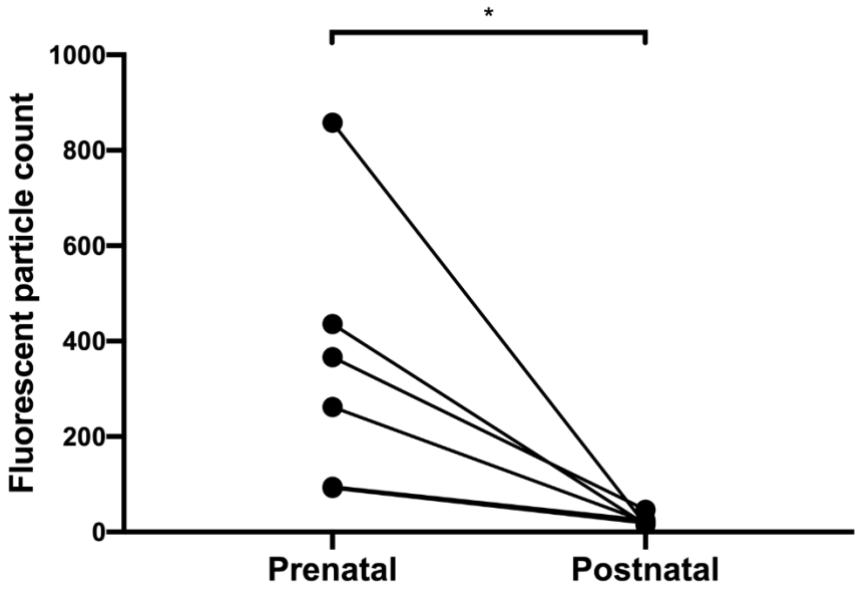



**Figure 43. Postnatal reduction of STB-EVs.**

Paired plasma samples were collected prior to caesarean section (Prenatal) and 24 hours after the delivery (Postnatal) and subjected to ExoView Analysis. Samples were purified using qEV (70 nm) and incubated on the chips coated with anti-PLAP **(A)** and anti-CD81 **(B)**. After incubation samples were immunolabeled with anti-PLAP/Alexa555. Reduction of STB-EVs was observed in all samples (n=6). Each sample had its corresponding IgG1 coated chip used as a control, which was later subtracted from the fluorescent particle count.

## 4.3. Discussion

The findings discussed in this chapter conclusively demonstrate that placenta-derived vesicles carry IR capable of sequestering insulin in a dose dependent manner, and that IR positive STB-EVs are increased in maternal plasma from GDM patients. These findings could help explain the mechanism behind the hyperinsulinemia with hyperglycaemia that occurs in GDM pregnancy.

Firstly, it was demonstrated that IR is expressed in term placenta tissue where it is enriched at the syncytiotrophoblast brush border (the layer in direct contact with maternal blood). This confirms previous findings (Whitsett and Lessard, 1978) of expression, but contradicts reports that IR expression is predominantly enriched at the syncytiotrophoblast in the first trimester before being more prominent in foetal vessels at term (Desoye *et al.*, 1997). The latest report published on the topic corroborates our results showing a high expression of IR in the maternal-facing microvillous plasma membrane (James-Allan *et al.*, 2019).

Next, it was shown that both MEDIUM/LARGE and SMALL STB-EVs (isolated by placenta perfusion) expressed IR. To confirm IR was indeed expressed on placental vesicles (and not a contaminant), we demonstrated IR and PLAP are co-expressed on the same vesicle using confirmatory experimental approaches. Flow cytometry and the ExoView platform showed co-localisation in MEDIUM/LARGE STB-EVs, while the ExoView platform and immunoprecipitation using magnetic beads demonstrated the same in SMALL STB-EVs. These varying approaches were used because SMALL STB-EVs cannot be visualised by standard flow cytometry techniques due to their size.

Shedding of soluble IR has been reported from various cultured cells (Berhanu and Olefsky, 1982; Papa *et al.*, 1993), subsequently leading to its investigation in circulation. Kanezaki *et al.* demonstrated that the administration of purified human IR α subunit into a mouse led to an increase in its blood glucose levels (Kanezaki *et al.*, 2003b). The same group showed that an

increase in soluble IRα ectodomain was observed in human plasma samples derived from both T2DM and T1DM patients and confirmed soluble IRα is capable of depleting insulin from the circulation. The observed positive correlation between soluble IR ectodomain and blood glucose implied that soluble IR has a potential to be used as a glycaemic biomarker (The Soluble Insulin Receptor Study Group, 2007). Association of soluble IR and insulin resistance has not been investigated solely in T2DM and T1DM. Increased levels of soluble IR were also reported in HIV-associated neurocognitive disorders with soluble IR acting as a decoy receptor significantly associated with insulin resistance (Gerena *et al.*, 2015). All these studies show changes in circulating IR levels could contribute to insulin resistance in various diseases - an observation further supported by the data discussed in this chapter.

Uniquely, while several reports have found soluble IR in plasma, this study appears to be the first to report IR on EVs. Furthermore, it seems that this feature is unique to placental EVs. We confirmed that IR is not present on a range of other extracellular vesicles (from kidney, breast cancer and endothelial cell lines). We also showed that platelet and red blood cell vesicles (isolated from non-pregnant patients) did not express IR. While the release of soluble IR ectodomain from HepG2 cells has been attributed to calpain (Yuasa *et al.*, 2016), protein that is also involved in the release of EV (Yuana, Sturk and Nieuwland, 2013), the mechanism of STB-EV-bound IR release remains to be explained.

Having shown IR was expressed on STB-EV, we then showed that it was functional; the addition of increasing concentrations of vesicles was able to dose dependently decrease free insulin from plasma. This decoy mechanism is not without precedent in placental physiology and pathophysiology. In preeclampsia, excess sFlt1 is released into the circulation and acts as a decoy receptor for VEGF and PLGF contributing to the endothelial dysfunction seen in that disease.

Given STB-EVs' ability to bind insulin, we propose STB-EV-bound IR may serve as decoy receptors responsible for neutralising insulin, thus limiting insulin availability and signalling. This is supported by the preliminary data showing that treating C2C12 myotubes with insulin pre-incubated with STB-EVs was able to reduce the cellular glucose uptake. Due to the closure of our laboratory because of the COVID-19 pandemic, this experiment was not able to be conducted with the addition of the irreversible IR antagonist S96 as planned. The intension was to test the specificity of this observation being attributable to IR by investigating if the abrogation of reduced cellular glucose would be observed after STB-EV's pre-treatment with an IR antagonist. Contrary to our findings, Nair et al. showed exosomes from normal pregnancy increased glucose uptake and cell migration of both primary human skeletal muscle myoblasts (HSMM) and T2DM-HSMM, while exosomes isolated from a GDM reduced cellular glucose uptake and migration (Nair *et al.*, 2018). In their later work, however, they reported the decrease in phosphorylation of IRS-1 and Akt in the presence of insulin in the skeletal muscle of mouse treated with SMALL EV from both normal and GDM pregnancy (James-Allan *et al.*, 2020); a finding at odds with their previous report.

To translate our *in vitro* findings into an *in vivo* situation, we then analysed the blood from pregnant women with flow cytometry. FACS analysis of blood from paired uterine veins (UV, which drains the uterus) and peripheral veins (PV) revealed higher IR/PLAP double positive events in the UV vs the PV confirming not only that the placenta is the source of STB-EVs carrying IR, but also that these EVs can be found in the maternal circulation.

This work suggests that circulating STB-EV-bound IR competes with IR expressed on cells for circulating insulin. We speculate that in normal pregnancy this is a potential mechanism for STB-EVs to promote the growth of the foetus. In the first six weeks, well-described features of a normal pregnancy are increased insulin sensitivity and lower plasma lipid levels. During this time STB-EVs have not been detected in maternal blood. By 10 weeks of gestation, a shift

towards increased insulin resistance begins leading to higher levels of fatty acids and phospholipids that continue to raise as pregnancy progresses (Armistead *et al.*, 2020). These changes correlate with the secretion of STB-EVs, as it is believed that their release starts at six weeks of pregnancy and increases throughout gestation. Recently, it has been shown that the injection of SMALL EVs isolated from healthy pregnancies promotes insulin resistance in the skeletal mussels of non-pregnant mice implicating EV's involvement in the maternal physiological adaptations to a normal gestation (James-Allan *et al.*, 2020). Our data corroborates this premise and provides some insights into a mechanism that might be involved. We therefore propose that, sequestration of insulin through STB-EV-bound IR could contribute to a relative insulin resistance that occurs in normal pregnancy in order to secure the growth and development of the foetus. This is further supported by our unpublished ELISA data showing that at term, IR has a higher expression in STB-EVs compared to placental tissue implying that the placenta is indeed increasing IR circulating levels in late pregnancy.

Increased $IR^+/PLAP^+$ double positive events were detected in the peripheral plasma of GDM patients compared to normal pregnancy (a 3.24-fold increase). Considering increased secretion of STB-EVs in pregnancies complicated with GDM (Salomon *et al.*, 2016), it might be the case that we observe the exacerbation of the aforementioned effect, which in turn contributes to the relative insulin deficiency described in this disease. Further work is required to compare the quantity of IR on a single STB-EV particle isolated from normal and GDM pregnancy as higher expression levels on STB-EVs from GDM might additionally contribute to the depletion of insulin.

Finally, we used ExoView technology to determine IR levels on the day of delivery and 24 hours post-natal. We observed 98.09% lower PLAP levels in peripheral plasma samples 24 hours after delivery. These results are in line with a study by Knight et al. that demonstrated that STB-EVs are not detectable 48 hours post-partum (Knight *et al.*, 1998). This prompt

postnatal decline in PLAP ties well with the observed rapid improvement in insulin sensitivity observed shortly after delivery (Ryan, Sullivan and Skyler, 1985). Recent work by Waters *et al.* investigated the association between rapid post-natal improvement in insulin sensitivity and maternal weight, lipids, adipokines or cytokines with no correlation being found. The authors concluded that other factors released by the placenta should be considered to elucidate the mechanism behind the alterations in insulin sensitivity during gestation (Waters *et al.*, 2020).

The limitation of this study is a relatively small sample size but, as stated previously, *ex vivo* placenta perfusion is resource intensive technique. We attempted to measure the expression of placentally derived IR in plasma using ELISA but were unable to conduct the experiment successfully because of the detection limits of the assay. Due to the time constrains and limited access to the laboratory during 2020, this work remains to be performed. Furthermore, in future, it will be important to investigate the role and levels of STB-EV-bound IR earlier in pregnancy. We have applied for a grant that would allow us to address these limitations with further study.

## 4.4. Summary

In summary, we demonstrated that placenta-derived EVs express functional insulin receptor capable of binding circulating insulin. This might contribute to the insulin resistance seen during gestation.

Furthermore, we observed increased levels of placenta-derived IR in GDM patients suggesting that the exacerbation of this sequestering mechanism might further the relative insulin insufficiency seen in GDM. We confirmed a rapid decline in STB-EV levels 24 hours postnatal, which corelates with prompt the improvement in insulin resistance observed clinically. This work suggests that STB-EV-bound IR might play a role in the pathogenesis of GDM and proposes their potential as biomarkers for the disease. Further work is needed to study the regulation of their release as well as their contributions to complicated pregnancies.

This work has been intellectually protected by Oxford University Innovations with me as a named inventor (international application number: PCT/G8201 8/051 500). We were also successfully selected for ‘Collaborations to Catalyse Translation’ funding to continue this project further.

# 5. Characterisation of the protein cargo of STB-EVs from normal and GDM pregnancy using mass spectrometry

## 5.1. Introduction

Studying the cargo of STB-EVs provides crucial evidence for understanding their diverse physiological and pathological roles throughout gestation. Since STB-EVs carry various proteins and RNA, attempts to decode their cargo have been done using both proteomic and transcriptomic methods.

Mass spectrometry has been used for EV analysis since around the turn of the millennium. Early studies were performed by first separating EV using gel electrophoresis in order to obtain the major bands, which were then further analysed by mass spectrometry. This approach yielded good results in identifying highly abundant proteins (such as annexins and tetraspanins), but was not effective enough for lower abundance proteins. With subsequent advances in proteomics methods, in particular with the development of high-throughput proteomics, this obstacle has been overcome and more proteins have been identified (Choi *et al.*, 2015). As a result, it has become clear that EV cargo-sorting is a control process, and not based purely on the abundance of a certain protein. Proteomic analysis of EVs from numerous cell sources have suggested that common vesicular proteins (tetraspanins, integrins, annexin, HSPs etc.) are associated with EV biogenesis, cargo-sorting and trafficking. Cell-specific vesicular proteins are linked with EV's cell-type associated pathophysiological roles and, as such, may serve as the biomarkers for the disease (Choi *et al.*, 2013).

The first proteomic analysis of STB-EV was performed in 2011 by Atay *et al*. using vesicles derived from Sw71 extravillious trophoblasts that displayed exosomal hallmarks, such as a cup-shaped morphology and the expression of known exosome molecules (CD81 and Alix) (Atay, Gercel-Taylor, Kesimer, *et al.*, 2011). They identified 282 proteins in Sw71 exosomes, of which 147 had not previously been described in exosomes derived from other sources. These included pregnancy zone protein (PZP) and alpha-fetoprotein (AFP) that were, therefore, thought to be potential markers of trophoblast-derived exosomes.

To understand the mechanism involved in the pathogenesis of gestational diseases such as preeclampsia (PE) and gestational diabetes mellitus (GDM), significant attention was focused on studies comparing the cargo of STB-EV from disease complicated pregnancy and normal healthy pregnancy. Baig *et al.* were the first to analyse STB-EV isolated from placental explants of three preeclamptic and six normal pregnancies with mass spectrometry (Baig *et al.*, 2014). They identified over 400 proteins with 25 of them being differentially expressed in PE compared to healthy normal controls including integrins, annexins, histones and heat shock proteins. These findings simultaneously emphasised not only the potential of STB-EVs as diagnostic markers but also triggered wider interest in their functionality. Further work by Li *et al.* identified significantly more proteins (194) differently expressed in STB-EVs isolated from early-onset severe preeclampsia placental explants. In their study, 122 were up-regulated and 72 were down-regulated, with the analysis also identifying Siglec-6 as the most up-regulated protein in early-onset severe preeclampsia (Li *et al.*, 2015). Summary of various functions ascribed to STB-EV's cargo in normal and preeclamptic pregnancy is presented in **Figure *44***.

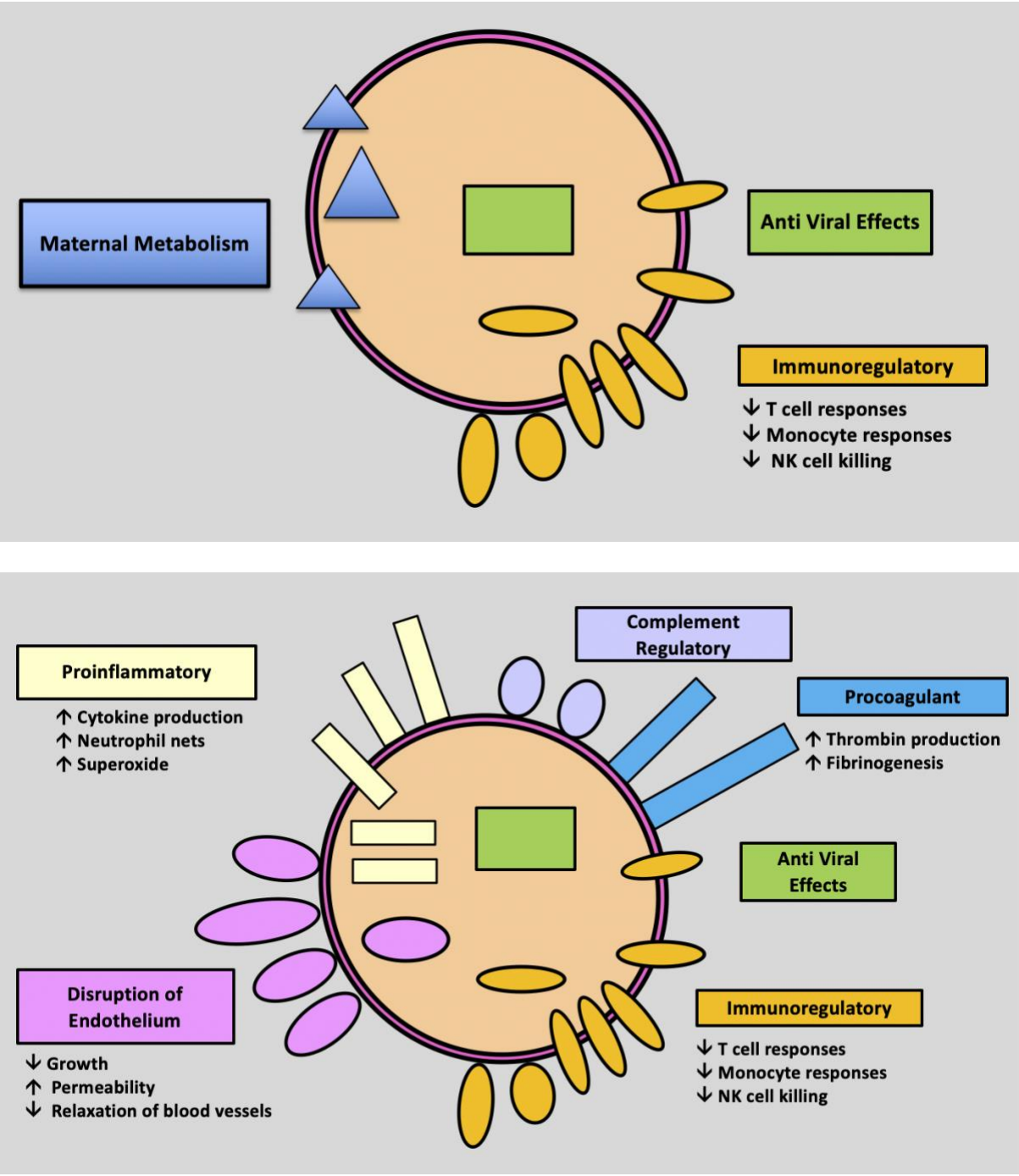



**Figure 44. Summary of various functions ascribed to STB-EV's cargo.**

Researchers have postulated several physiological and pathological functions of STB-EV in normal **(A)** and preeclamptic **(B)** pregnancy. In preeclampsia, STB-EVs have been associated with immunoregulatory molecules, proinflammatory factors, disruption of endothelium, complement regulatory molecules etc. Adapted from Tannetta, unpublished figures.

Protein cargo of macro-, micro-, and nano-vesicles from first trimester normal placenta explant cultures was demonstrated to be different between different vesicle fractions by Tong *et al*. Their work revealed that 1,125 proteins were shared among three EV fractions while 223 were

unique to each fraction. The presence of phagocytosis ‘eat me’ signals such as Annexin V and calreticulin were confirmed in all fractions, while anti-phagocytic ‘don’t eat me’ signals such as CD47 and CD31 were significantly lower in nano-vesicles compared to larger vesicles (Tong *et al.*, 2016). The study supports the hypothesis that each EV fraction has its own unique effects on different maternal cells.

Recently, the protein profile of placenta derived EVs in preterm birth has also been investigated, with 96 proteins differentially expressed in EVs isolated from preterm plasma. In placental SMALL EVs from preterm pregnancy, inflammatory pathways were significantly upregulated while coagulation and complement-activation associated proteins were downregulated in comparison to normal pregnancy. This work further supports the hypothesis that placental EVs allow for a real-time snapshot of the physiological state of the feto-maternal interface and as such could serve as biomarkers for gestational diseases (Menon *et al.*, 2020).

In GDM pregnancies, Jayabalan *et al* investigated proteomic cargo in SMALL EVs isolated from peripheral plasma samples of women undergoing OGTT. In total, 415 proteins were identified in their study, of which 78 were significantly and differentially expressed in SMALL EV isolated from GDM plasma. Significantly different proteins included spectrin alphaerythrocytic (SPTA)-1, CAMK2β, PAPP-A, Perilipin 4, fatty acid binding protein (FABP) 4, and hexokinase-3, all of which have been associated with insulin resistance previously (Jayabalan *et al.*, 2019). This study, however, did not investigate the protein cargo of placental vesicles specifically, instead using all EVs isolated from peripheral plasma samples. Evidence of different STB-EV proteomic cargo in GDM and normal pregnancy is encouraging as it confirms their diagnostic potential and provides better understanding of the pathogenesis of GDM.

RNA is another important component of STB-EV cargo, and both mRNA and microRNA have been confirmed within placental EVs. The first report of mRNA in STB-EVs was published by

Gupta *et al.* in 2004. Their study found corticotropin-releasing hormone (CRH) mRNA in vesicles isolated from villous explant culture, mechanical dissection and placental perfusion (Gupta *et al.*, 2004). The first discovery of microRNA happened some years later when Luo *et al*. identified pregnancy specific microRNAs in both whole placental tissue and human plasma samples (Luo *et al.*, 2009). They demonstrated that placenta specific microRNA is secreted via exosomes as well as confirmed its rapid decline in maternal plasma after delivery. That microRNA is packed in STB-EVs has been confirmed in several subsequent studies (Donker *et al.*, 2012; Ouyang *et al.*, 2014; Mouillet *et al.*, 2015; Escudero *et al.*, 2016).

Similar to proteomics research, changes in microRNA profile within STB-EVs have been observed in gestational disease, with special focus been given to preeclampsia. In 2014, Cronqvist *et al.* demonstrated that mir-517a, mir141 and mir-517b were downregulated in STB-EV from placentae supplemented with cell-free foetal haemoglobin used to mimic preeclampsia (Cronqvist et al., 2014). Salomon *et al*. analysed exosomal microRNA profiles from peripheral plasma samples and showed that miR-486-1-5p and miR-486-2-5p can be used to distinguish women with preeclampsia from those experiencing normal pregnancy, although it was not clear at which gestational age the samples were collected (Salomon *et al.*, 2017). Wei *et al.* used STB-EVs from placental culture of preeclamptic and normal placentae to show 16 differentially expressed microRNAs in preeclamptic samples (Wei et al., 2017).

In an effort to gain a fuller understanding of STB-EV cargo, we have recently sequenced short RNA isolated from STB-EVs after placenta perfusion and showed that most (>95%) belong to transfer RNA (tRNA) halves (Cooke *et al.*, 2019), suggesting that STB-EV derived RNA function might be more complex than initially thought.

In GDM specifically, Salomon *et al.* showed differential microRNA expression in exosomes isolated from placental explants in comparison to normal pregnancies. They identified 1065 microRNAs, of which nine were upregulated and 14 were downregulated in GDM SMALL

EVs secreted from chorionic villi. Five microRNAs (miRNAs hsa-miR-125a-3p, hsa-miR-99b-5p, hsa-miR-197-3p, hsa-miR-22-3p, and hsa-miR-224-5p) were found to vary in a consistent pattern between GDM and control placenta, STB-EV from placental explants, plasma STB-EVs and skeletal muscle. The study also found that SMALL EVs from GDM can interact with skeletal muscle cells and altered their migration and glucose uptake contributing to the insulin resistance observed in GDM (Nair *et al.*, 2018).

Taken together, these studies show changes in STB-EV cargo in gestational disease that might allow for the identification of novel disease-causing or disease-reporting targets. So far, most of STB-EVs research has been focused on preeclampsia, but in recent years it has become evident that STB-EV play an important role in other gestational complications as well. For these reasons, we decided to focus on identifying the protein cargo of placenta derived EVs from GDM pregnancy and compare it with STB-EVs derived from normal healthy pregnancy.

## 5.2. Results

### 5.2.1. Patient characteristics

The proteomic analysis described in this chapter included nine women in total (four GDM pregnancies; five normal pregnancies). Both MEDIUM/LARGE and SMALL STB-EVs were collected form *ex vivo* placenta perfusion after Caesarean section at 39–40 weeks of gestation. STB-EVs were isolated and characterised as described in the *Methods* chapter, prior to mass spectrometry analysis. Patient characteristics are presented in ***Table 9***. All GDM patients were under treatment for the disease (metformin and/or insulin). Women with multiple pregnancies as well as patients with pre-pregnancy diabetes, cardiovascular disease or preeclampsia were excluded from this study. There were no statistically significant differences in BMI, gestational age, or foetal birth weight between the two groups.

***Table 9. Patient characteristics.*** Data is presented as mean ± SEM. Range is also included.

| | **GDM (n=4)** | **Normal pregnancy (n=5)** |
|---|---|---|
| **Age, year** | 34.8 ± 3.9<br>(24 - 42) | 31 ± 1.2<br>(28 - 35) |
| **Gestation age, weeks** | 38.6 ± 1.0<br>(38.1 - 39.1) | 39.1 ± 0.3<br>(39.0 – 39.3) |
| **Body mass index, kg/m2** | 27.7 ± 1.5<br>(25 - 32) | 27.6 ± 1.4<br>(25 – 32) |
| **Newborn weight, g** | 3336.3 ± 386.2<br>(2840 - 4450) | 3379.0 ± 175.9<br>(2865 – 3890) |
| **Max. systolic pressure, mmHg** | 132.8 ± 6.1<br>(122 - 150) | 125.8 ± 4.3<br>(110 - 135) |
| **Max. diastolic pressure, mmHg** | 77.3 ± 5.7<br>(61 - 86) | 82.4 ± 1.2<br>(80 - 86) |
| **GDM treatment** | Metf: 2<br>Ins + Metf: 2 | - |

### 5.2.2. Proteomic characterisation of STB-EVs from GDM and normal pregnancy

Proteomic analysis of STB-EVs from normal and GDM pregnancy identified 1981 proteins in total. Filtering for valid values excluded seven proteins and 1974 proteins were used for the subsequent analysis. Prior to any statistical analysis, data was subjected to normalisation by median (**Figure *45***). Hierarchical clustering was used to observe the correlation between four groups. The strongest separation was observed between the two subtypes of EVs used in this study: MEDIUM/LARGE and SMALL STB-EVs in both GDM and normal pregnancy (**Figure *46***). This was further supported by multi-scatter plot analysis presented with their corresponding Pearson correlation factor (**Figure *47***). Finally, principal component analysis (PCA) was performed, confirming that EV proteins clustered based on their subtype (**Figure *48***). We also observed that MEDIUM/LARGE STB-EVs from GDM and normal pregnancy clustered separately, while this was not the case for SMALL STB-EVs. We then moved to establish the differences in the protein abundance between different subtypes of EVs from GDM and normal pregnancy respectively.

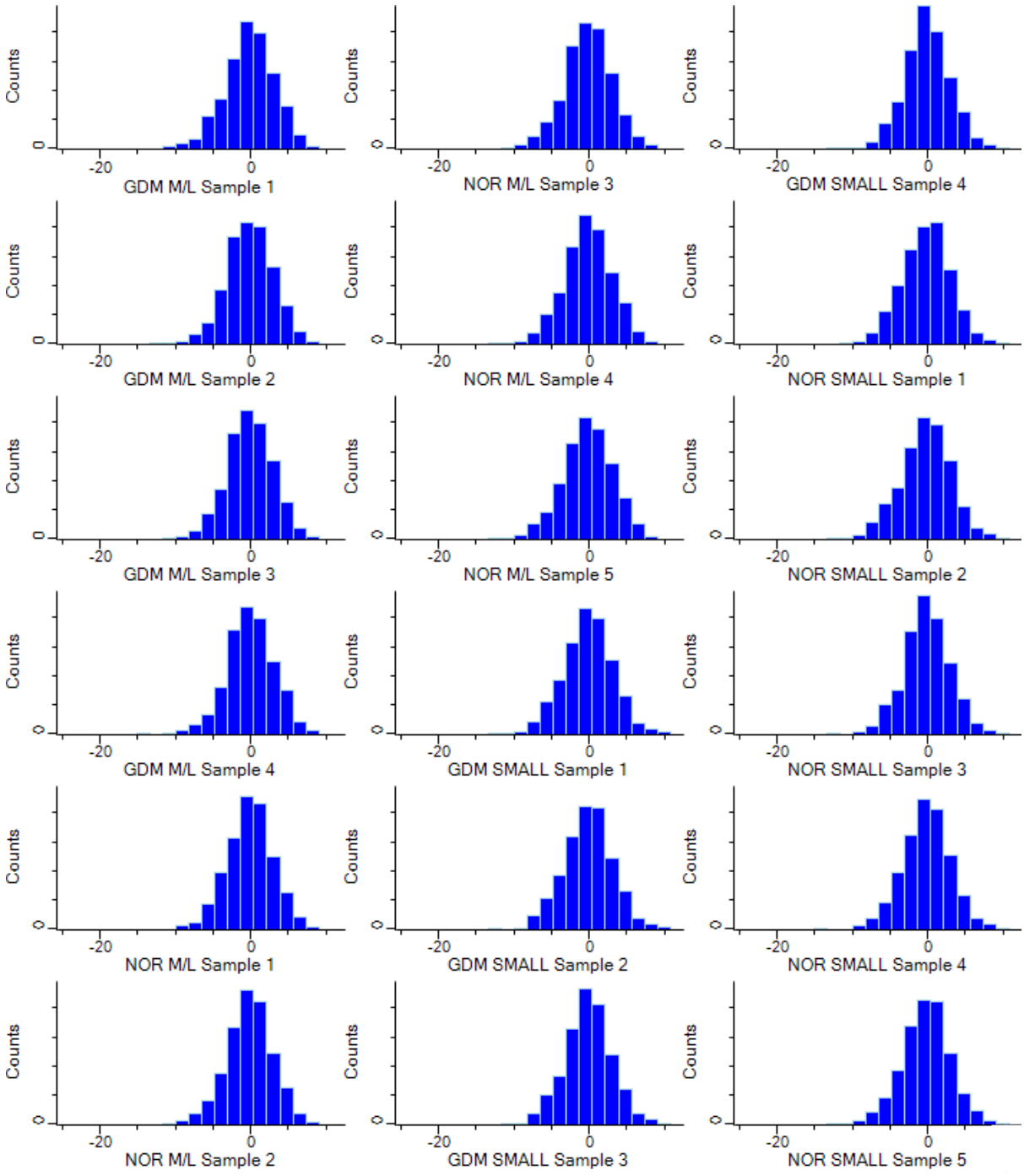



**Figure 45. Histograms of normalised protein abundance for all samples.**

Data are normally distributed after subtraction by median.

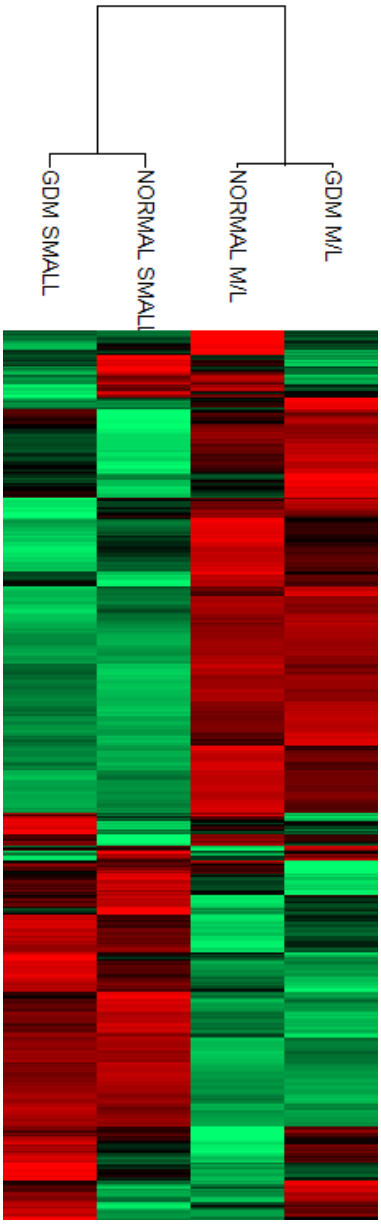



**Figure 46. Hierarchical clustering of MEDIUM/LARGE and SMALL STB-EVs from GDM and normal pregnancy.**

MEDIUM/LARGE STB-EVs from normal and GDM pregnancies clustered together. Similarly, SMALL STB-EVs from GDM and normal pregnancies have also clustered together.

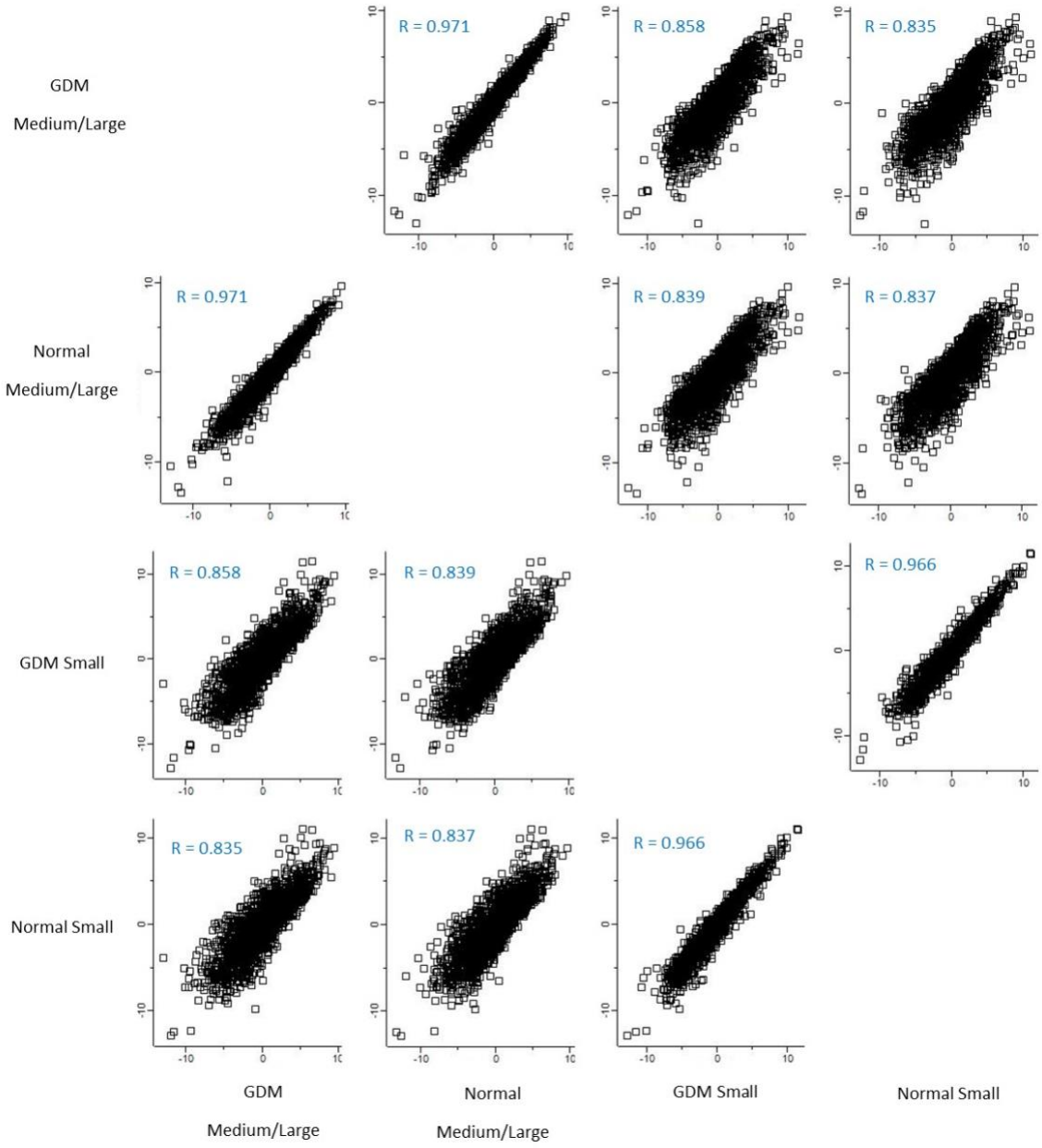



**Figure 47. Multi-scatter plot of MEDIUM/LARGE and SMALL STB-EVs isolated from GDM and normal pregnancies with the corresponding Pearson correlation factor (R).**

The strongest differences are observed between MEDIUM LARGE and SMALL STB-EVs from GDM (R=0.835) and MEDIUM LARGE and SMALL STB-EVs from normal pregnancy (R=0.837).

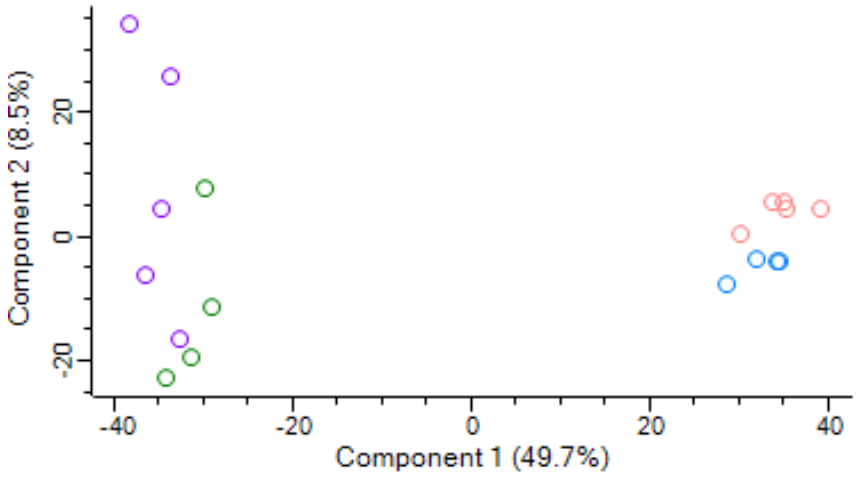


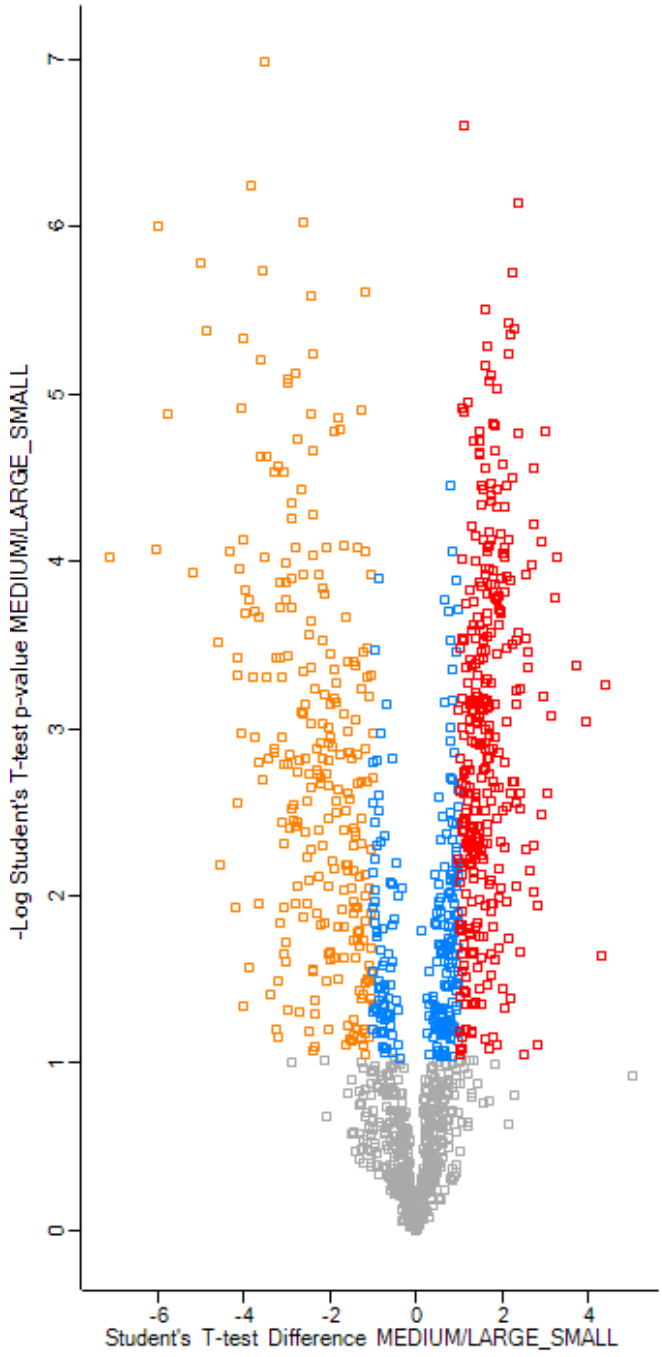

**Figure 48. Principal component analysis (PCA) for all samples.**

PCA showed the largest variance between two subtypes of STB-EVs. MEDIUM/LARGE STB-EVs from both GDM (blue dots) and normal pregnancies (pink dots) clustered separately from SMALL STB-EVs from GDM (green dots) and normal pregnancies (purple dots). PCA has also showed that within the same subtype of STB-EVs, samples from GDM and normal pregnancy were intermixed.

### 5.2.3. Differentially expressed proteins between MEDIUM/LARGE and SMALL STB-EVs

The comparative analysis between MEDIUM/LARGE and SMALL STB-EVs within GDM and normal pregnancies, respectively, demonstrated significantly different protein cargos between the two populations, suggesting that the biogenesis of these two types of EVs includes different cargo sorting mechanisms. In GDM, 856 proteins with unique peptides ≥2 were identified as being expressed differently (FDR adjusted p-value). 346 were upregulated ($log_2$ fold change ≥1), while 271 were downregulated ($log_2$ fold change ≤-1). In normal pregnancy, 815 proteins with unique peptides ≥2 were differentially expressed between MEDIUM/LARGE and SMALL STB-EVs. Again, differentially expressed proteins were then further filtered by their $log_2$ fold change (≤-1 or ≥1) to improve confidence in the data. In normal pregnancy samples, 394 proteins were upregulated in MEDIUM/LARGE STBE-EVs while 261 were downregulated (**Figure *49***).

**A)**


-Log Student's T-test p-value MEDIUM/LARGE_SMALL
0
1
2
3
4
5
6
7
-6
-4
-2
0
2
4
Student's T-test Difference MEDIUM/LARGE_SMALL

**B)**

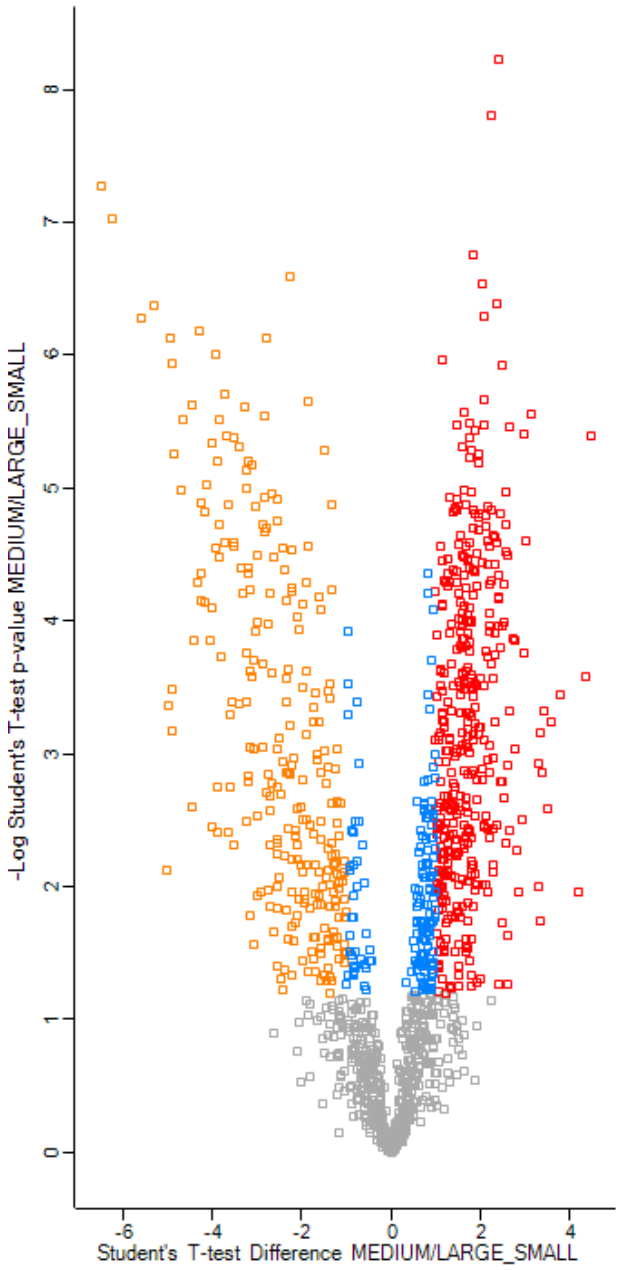



**Figure 49. Comparison of protein profile between MEDIUM/LARGE and SMALL STB-EVs.**

The above Volcano plots show differentially expressed proteins for MEDIUM/LARGE and SMALL STB-EVs isolated from GDM **(A)** and normal pregnancies **(B)**. Protein abundance has been analysed with student t-test, and differentially expressed proteins (FDR adjusted p-value=<0.05) with $log_2$ fold change ≤-1 or ≥1 are presented in yellow (downregulated) and red (upregulated). Differentially expressed proteins without $log_2$ fold change ≤-1 or ≥1 are presented in blue. Differentially expressed proteins that did not reach statistical significance are presented by grey squares.

Functional enrichment analysis of differentially expressed proteins was investigated using g:Profiler. Data sources included in g:Profiler analysis were Gene Ontology (GO) Metabolic Function (MF), GO Biological Processes (BP), GO Cell Components (CC) and Reactome datasets (***Figure 50***).

Differentially expressed proteins between two subtypes of STB-EVs in GDM showed 80 significantly enriched terms in GO:MF, with the most significant terms being cell adhesion molecule binding (GO:0050839), cadherin binding (GO:0045296) and protein-containing complex binding (GO:0044877). In GO:BF, 552 terms were significantly enriched including vesicle mediated transport (GO:0016192), transport (GO:0006810) and establishment of localisation (GO:0051234). GO:CC reported 163 categories to be enriched with extracellular exosomes (GO:0070062), extracellular organelle (GO:0043230) and extracellular vesicles (GO:1903561) being the top three. In the Reactome database, 225 terms were enriched, with the most significantly enriched terms including the innate immune system (REAC:R-HAS-168249), the immune system (REAC:R-HAS-168256) and the regulation of the expression of SLITs and ROBO (REAC:R-HAS-9010553) (**Table *10***).

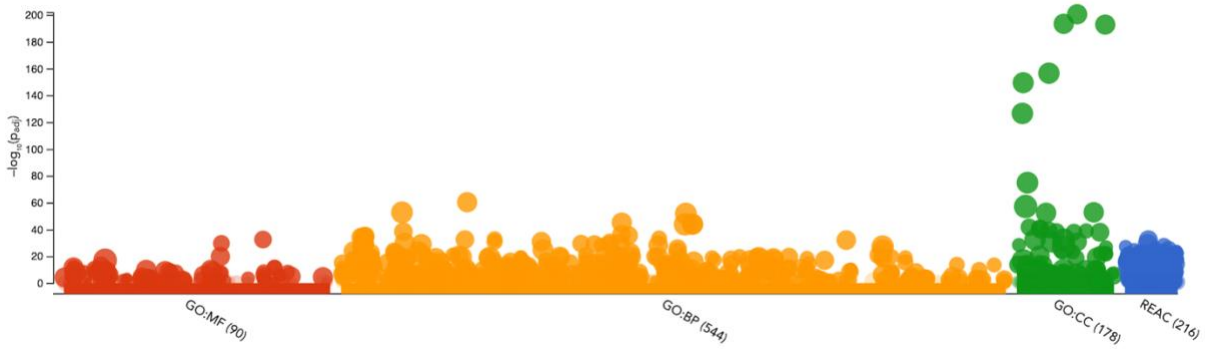



**Figure 50. Manhattan plot of functional enrichment analysis of differently expressed proteins between MEDIUM/LARGE and SMALL STB-EVs in GDM pregnancy.**

Differentially expressed proteins between two subtypes of STB-EV in GDM were subjected to g:Profiler analysis. The software used Gene Ontology (GO) Metabolic Function (MF), GO Biological Processes (BP), GO Cell Components (CC) and Reactome datasets for the analysis, with each dataset being colour coded. The above Manhattan plot shows that in GO:MF 90 terms were significantly enriched (dark red dots), in GO:BP 544 terms, (dark yellow dots) and in GO:CC 178 terms (dark green dots). 216 terms were significantly enriched in the Reactome data source. Each dot represents a single functional term and is size scaled according to the number of annotated genes in that term. The lighter coloured dots represent insignificant terms.

**Table 10. Functional enrichment analysis of differentially expressed proteins between MEDIUM/LARGE and SMALL STB-EVs in GDM.**

Top ten enriched terms from different data sources – GO:MO **(A)**, GO:BF **(B)**, GO:CC **(C)** and Reactome **(D)** – are presented together with the term ID and their adjusted p-value. Adjusted p-values are also presented by a colour gradient scheme: yellow shows insignificant findings while dark blue represents the most significant findings.

### A) Gene ontology: Molecular Function

| Term name | Term ID | $p_{adj}$ | $-\log_{10}(p_{adj})$ 0 ≤16 |
|---|---|---|---|
| cell adhesion molecule binding | GO:0050839 | $3.366\times10^{-33}$ | |
| cadherin binding | GO:0045296 | $2.758\times10^{-30}$ | |
| protein-containing complex binding | GO:0044877 | $1.649\times10^{-20}$ | |
| protein binding | GO:0005515 | $1.315\times10^{-17}$ | |
| structural molecule activity | GO:0005198 | $9.542\times10^{-14}$ | |
| translation initiation factor activity | GO:0003743 | $4.379\times10^{-13}$ | |
| RNA binding | GO:0003723 | $2.078\times10^{-12}$ | |
| peptidase regulator activity | GO:0061134 | $3.067\times10^{-12}$ | |
| endopeptidase regulator activity | GO:0061135 | $6.373\times10^{-12}$ | |
| translation factor activity, RNA binding | GO:0008135 | $3.317\times10^{-11}$ | |

### B) Gene ontology: Biological Function

| Term name | Term ID | $p_{adj}$ | $-\log_{10}(p_{adj})$ 0 ≤16 |
|---|---|---|---|
| vesicle-mediated transport | GO:0016192 | $5.086\times10^{-61}$ | |
| transport | GO:0006810 | $2.047\times10^{-53}$ | |
| establishment of localization | GO:0051234 | $1.305\times10^{-52}$ | |
| interspecies interaction between organisms | GO:0044419 | $7.649\times10^{-46}$ | |
| establishment of localization in cell | GO:0051649 | $1.204\times10^{-44}$ | |
| cellular localization | GO:0051641 | $1.465\times10^{-44}$ | |
| localization | GO:0051179 | $1.861\times10^{-44}$ | |
| exocytosis | GO:0006887 | $4.546\times10^{-39}$ | |
| symbiotic process | GO:0044403 | $5.286\times10^{-37}$ | |
| regulated exocytosis | GO:0045055 | $3.129\times10^{-36}$ | |

### C) Gene Ontology: Cellular Component

| Term name | Term ID | $p_{adj}$ | $-\log_{10}(p_{adj})$ 0 ≤16 |
|---|---|---|---|
| extracellular exosome | GO:0070062 | $3.400\times10^{-201}$ | |
| extracellular organelle | GO:0043230 | $4.072\times10^{-194}$ | |
| extracellular vesicle | GO:1903561 | $1.610\times10^{-193}$ | |
| vesicle | GO:0031982 | $3.245\times10^{-157}$ | |
| extracellular space | GO:0005615 | $4.170\times10^{-150}$ | |
| extracellular region | GO:0005576 | $2.897\times10^{-127}$ | |
| cytosol | GO:0005829 | $1.469\times10^{-75}$ | |
| cytoplasm | GO:0005737 | $8.029\times10^{-58}$ | |
| intracellular vesicle | GO:0097708 | $1.724\times10^{-53}$ | |
| cytoplasmic vesicle | GO:0031410 | $4.589\times10^{-53}$ | |

**D) Reactome**

| Term name | Term ID | $p_{adj}$ | $-\log_{10}(p_{adj})$ 0 ≤16 |
|---|---|---|---|
| Innate Immune System | REAC:R-HSA-168249 | $5.477\times10^{-33}$ | |
| Immune System | REAC:R-HSA-168256 | $1.249\times10^{-29}$ | |
| Regulation of expression of SLITs and ROBOs | REAC:R-HSA-9010553 | $1.456\times10^{-28}$ | |
| AUF1 (hnRNP D0) binds and destabilizes mRNA | REAC:R-HSA-450408 | $7.363\times10^{-28}$ | |
| Negative regulation of NOTCH4 signaling | REAC:R-HSA-9604323 | $8.043\times10^{-27}$ | |
| Signaling by ROBO receptors | REAC:R-HSA-376176 | $3.423\times10^{-26}$ | |
| NIK-->noncanonical NF-kB signaling | REAC:R-HSA-5676590 | $8.070\times10^{-26}$ | |
| Dectin-1 mediated noncanonical NF-kB signaling | REAC:R-HSA-5607761 | $1.898\times10^{-25}$ | |
| Regulation of activated PAK-2p34 by proteasome mediated degradation | REAC:R-HSA-211733 | $3.483\times10^{-25}$ | |
| FBXL7 down-regulates AURKA during mitotic entry and in early mitosis | REAC:R-HSA-8854050 | $1.427\times10^{-24}$ | |

Very similar results were obtained with differentially expressed proteins between MEDIUM/LARGE and SMALL STB-EVs from normal pregnancies (***Figure 51***). Functional enrichment analysis showed that GO:MF had 90 terms significantly enriched in normal pregnancy with the top three terms being cell adhesion molecule binding (GO:0050839), cadherin binding (GO:0045296) and protein-containing complex binding (GO:0044877). In GO:BF, 544 terms were significantly enriched including vesicle mediated transport (GO:0016192), transport (GO:0006810) and the establishment of localisation (GO:0051234). GO:CC reported 163 categories to be enriched with extracellular exosomes (GO:0070062), extracellular organelle (GO:0043230), and extracellular vesicles (GO: 0070062), being the top three. In the Reactome database, 225 terms were enriched, with the top three being the innate immune system (REAC:R-HAS-168249), the regulation of expression of SLITs and ROBO (REAC:R-HAS-9010553), and signalling by ROBO receptors (REAC:R-HAS-376176) as presented in **Table *11***.

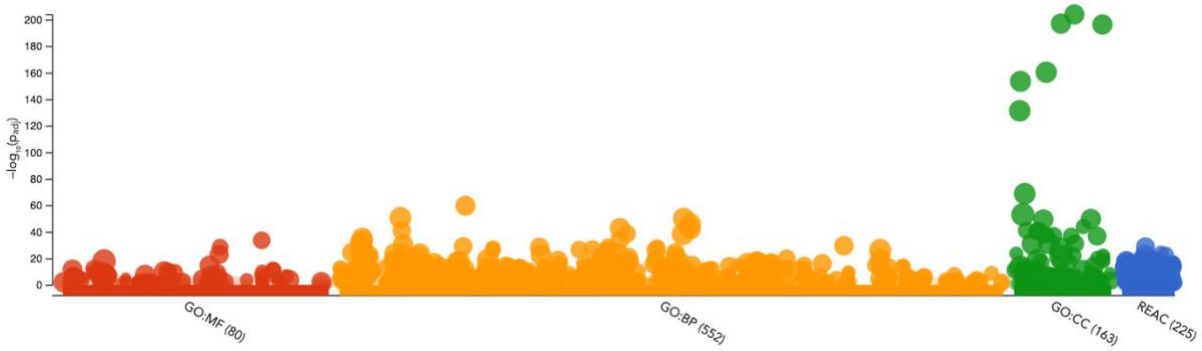



**Figure 51. Manhattan plot of functional enrichment analysis of differently expressed proteins between MEDIUM/LARGE and SMALL STB-EVs in normal pregnancy.**

Differentially expressed proteins were subjected to g:Profiler analysis. The software used Gene Ontology (GO) Metabolic Function (MF), GO Biological Processes (BP), GO Cell Components (CC) and Reactome datasets for the analysis, with each dataset being colour coded. The Manhattan plot showed that in GO:MF 80 terms were significantly enriched (dark red dots), in GO:BP 552 terms (dark yellow dots), and in GO:CC 163 terms (dark green dots). 225 terms were significantly enriched in the Reactome data source. Each dot represents a single functional term and is size scaled according to the number of annotated genes in that term. The lighter coloured dots represent insignificant terms.

**Table 11. Functional enrichment analysis of differentially expressed proteins between MEDIUM/LARGE and SMALL STB-EVs in normal pregnancy.**

Top ten enriched terms from different data sources – GO:MO **(A)**, GO:BF **(B)**, GO:CC **(C)** and Reactome **(D)** – are presented together with the term ID and their adjusted p-value. Adjusted p-values are also presented by a colour gradient scheme: yellow shows insignificant findings while dark blue represents the most significant findings.

### A) Gene ontology: Molecular Function

| Term name | Term ID | $p_{adj}$ | $-\log_{10}(p_{adj})$ (0 – ≤16) |
|---|---|---|---|
| cell adhesion molecule binding | GO:0050839 | $2.798\times10^{-34}$ | |
| cadherin binding | GO:0045296 | $4.034\times10^{-29}$ | |
| protein-containing complex binding | GO:0044877 | $1.327\times10^{-23}$ | |
| protein binding | GO:0005515 | $1.381\times10^{-18}$ | |
| identical protein binding | GO:0042802 | $2.696\times10^{-15}$ | |
| enzyme inhibitor activity | GO:0004857 | $3.967\times10^{-13}$ | |
| RNA binding | GO:0003723 | $3.075\times10^{-12}$ | |
| peptidase regulator activity | GO:0061134 | $3.441\times10^{-12}$ | |
| endopeptidase regulator activity | GO:0061135 | $8.954\times10^{-12}$ | |
| structural molecule activity | GO:0005198 | $1.898\times10^{-11}$ | |

### B) Gene ontology: Biological Function

| Term name | Term ID | $p_{adj}$ | $-\log_{10}(p_{adj})$ (0 – ≤16) |
|---|---|---|---|
| vesicle-mediated transport | GO:0016192 | $2.457\times10^{-60}$ | |
| transport | GO:0006810 | $3.186\times10^{-51}$ | |
| establishment of localization | GO:0051234 | $1.427\times10^{-50}$ | |
| establishment of localization in cell | GO:0051649 | $8.141\times10^{-47}$ | |
| interspecies interaction between organisms | GO:0044419 | $1.806\times10^{-43}$ | |
| cellular localization | GO:0051641 | $5.219\times10^{-43}$ | |
| exocytosis | GO:0006887 | $1.332\times10^{-41}$ | |
| regulated exocytosis | GO:0045055 | $3.302\times10^{-39}$ | |
| localization | GO:0051179 | $5.491\times10^{-39}$ | |
| immune system process | GO:0002376 | $5.900\times10^{-36}$ | |

### C) Gene Ontology: Cellular Component

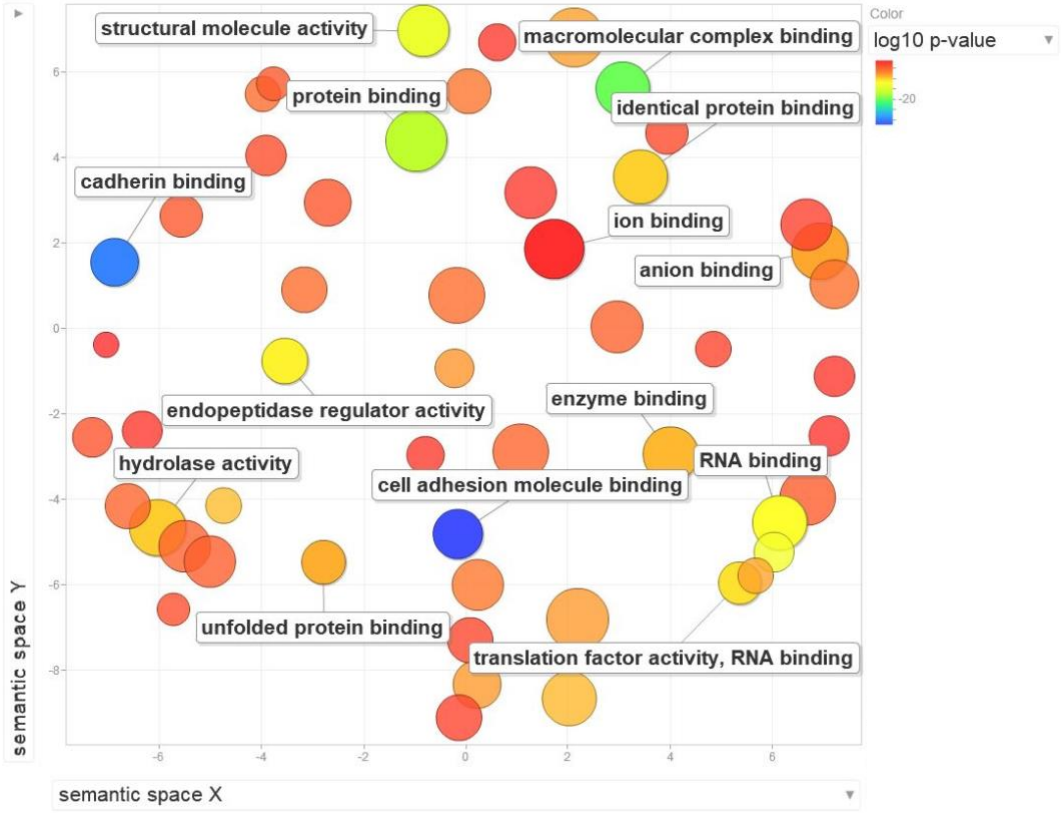
| Term name | Term ID | $p_{adj}$ | $-\log_{10}(p_{adj})$ (0 – ≤16) |
|---|---|---|---|
| extracellular exosome | GO:0070062 | $1.306\times10^{-204}$ | |
| extracellular organelle | GO:0043230 | $1.040\times10^{-197}$ | |
| extracellular vesicle | GO:1903561 | $4.450\times10^{-197}$ | |
| vesicle | GO:0031982 | $5.276\times10^{-161}$ | |
| extracellular space | GO:0005615 | $3.565\times10^{-154}$ | |
| extracellular region | GO:0005576 | $5.426\times10^{-132}$ | |
| cytosol | GO:0005829 | $1.825\times10^{-69}$ | |
| cytoplasm | GO:0005737 | $1.345\times10^{-53}$ | |
| intracellular vesicle | GO:0097708 | $2.191\times10^{-50}$ | |
| cytoplasmic vesicle | GO:0031410 | $5.899\times10^{-50}$ | |

**D) Reactome**

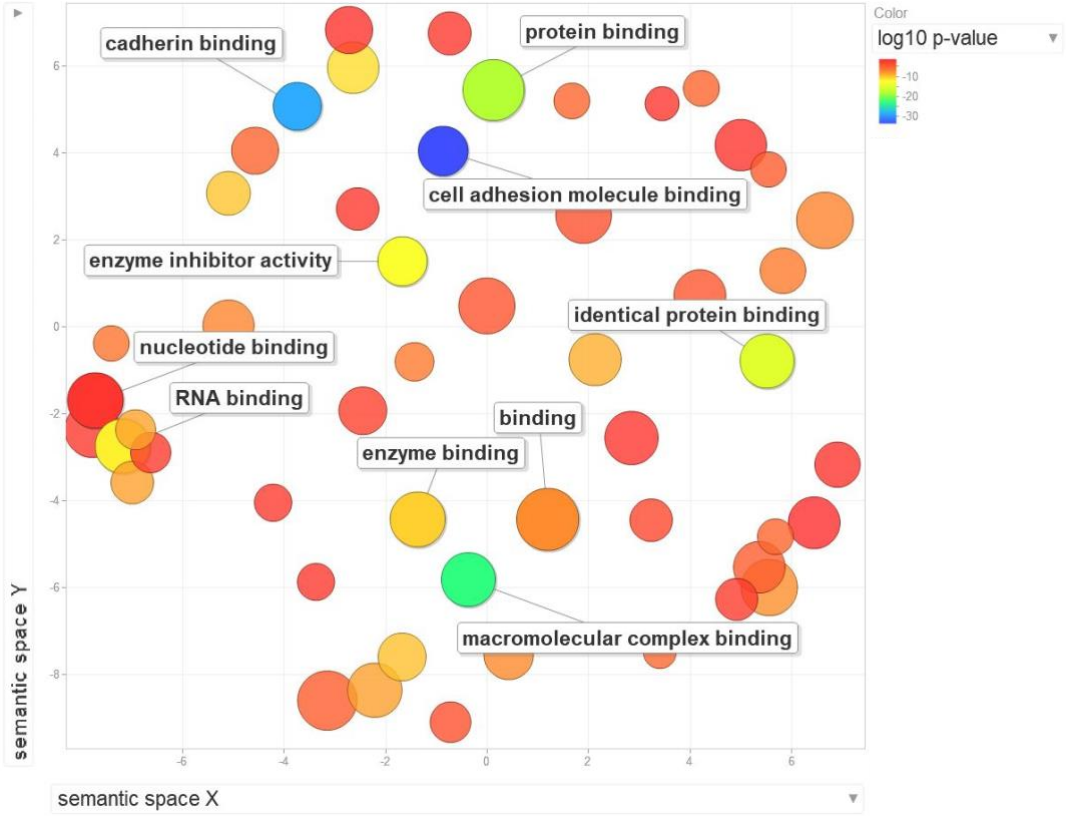
| Term name | Term ID | $p_{adj}$ | $-\log_{10}(p_{adj})$ 0 ≤16 |
|---|---|---|---|
| Innate Immune System | REAC:R-HSA-168249 | $2.144\times10^{-29}$ | |
| Regulation of expression of SLITs and ROBOs | REAC:R-HSA-9010553 | $2.555\times10^{-24}$ | |
| Signaling by ROBO receptors | REAC:R-HSA-376176 | $1.951\times10^{-23}$ | |
| Immune System | REAC:R-HSA-168256 | $3.501\times10^{-23}$ | |
| GTP hydrolysis and joining of the 60S ribosomal subunit | REAC:R-HSA-72706 | $2.910\times10^{-21}$ | |
| Eukaryotic Translation Initiation | REAC:R-HSA-72613 | $4.824\times10^{-20}$ | |
| Cap-dependent Translation Initiation | REAC:R-HSA-72737 | $4.824\times10^{-20}$ | |
| Neutrophil degranulation | REAC:R-HSA-6798695 | $5.867\times10^{-20}$ | |
| Axon guidance | REAC:R-HSA-422475 | $1.662\times10^{-19}$ | |
| L13a-mediated translational silencing of Ceruloplasmin expression | REAC:R-HSA-156827 | $1.907\times10^{-19}$ | |

Data obtained from g:Profiler were then subjected to REVIGO analysis to minimise redundancies and summarise significantly enriched GO terms. The results are presented on a scatter plot where semantically related GO terms are clustered together. In GDM, REVIGO analysis of enriched terms from the GO:MF dataset revealed that major clusters were cadherin binding, cell adhesion molecular binding and macromolecular complex binding (**Figure *52A***). Analysis of enriched terms from the GO:MF dataset in normal pregnancy, revealed the same main clusters: cadherin binding, cell adhesion molecular binding and macromolecular complex binding (**Figure *52B***). When REVIGO analysis were performed on enriched terms from GO:BP in GDM, some of the key identified clusters were associated with immune system, leukocyte mediated immunity and catabolism (**Figure *52C***). In GO:BF from normal pregnancy, REVIGO summary of enriched terms showed similar results: immune system, leukocyte mediated immunity and regulated exocytosis (**Figure *52D***).

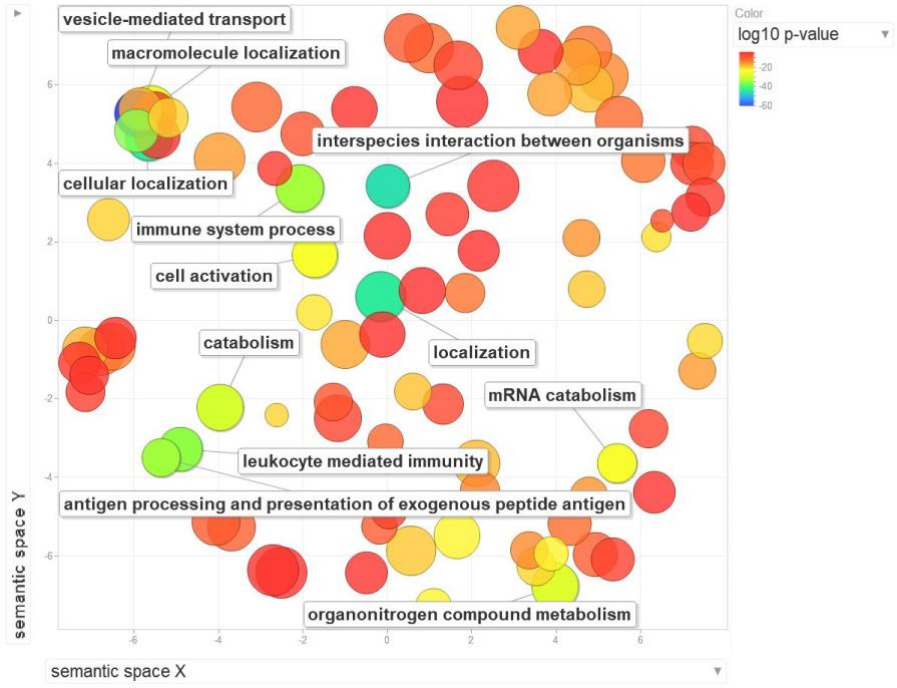
**A) GO:MF terms enriched in GDM**




**B) GO:MF terms enriched in normal pregnancy**



**C) GO: BP enriched terms in GDM**




**D) GO: BP enriched terms in normal pregnancy**

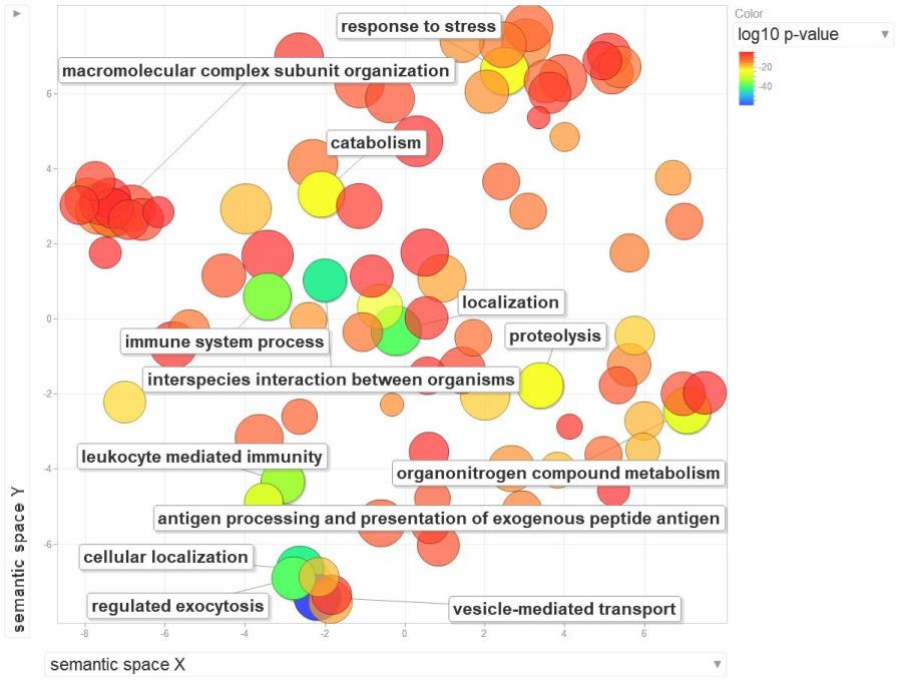



**Figure 52. GO enrich terms summarised by REVIGO.**

Concise presentation of GO:MF terms enriched in GDM **(A)** and normal pregnancy **(B)**. Summary of GO:BP enriched terms in GDM **(C)** and normal pregnancy **(D)**. Closeness on the scatter plot mirrors their closeness in the GO semantic similarity. The colour of the circle corresponds to the p-value obtained from the g:Profiler analysis while the size reflects the frequency of the GO term in the GOA database (larger circles are associated with more general terms).

### 5.2.4. Differentially expressed proteins in STB-EVs from GDM and NORMAL pregnancy

The comparative analysis of STB-EV cargos between GDM and NORMAL pregnancy have been conducted for both MEDIUM/LARGE and SMALL STB-EVs respectively. In MEDIUM/LARGE STB-EVs, the results showed that 56 proteins with unique peptides ≥2 were differently expressed (FDR adjusted p-value) between GDM and normal pregnancy. Differentially expressed proteins were then further filtered by their $\log_2$ fold change (≤-1 or ≥1) to help increase the confidence in the data. Among them, six proteins were upregulated (BANF1, CRYZL1, PSG3, ACPP, ANO10, ITIH2) in GDM while seven were downregulated (TREML2, EIF3M, GBP1, RANBP1, PTGES3, CARHSP1, OTUB1) (**Figure *53***). Surprisingly, in SMALL STB-EVs no proteins were identified to be significantly different between GDM and normal pregnancy (**Figure *54***). All differentially expressed proteins from MEDIUM/LARGE STB-EVs and their corresponding FDR adjusted p-value (q-value) are listed in **Table *12***.

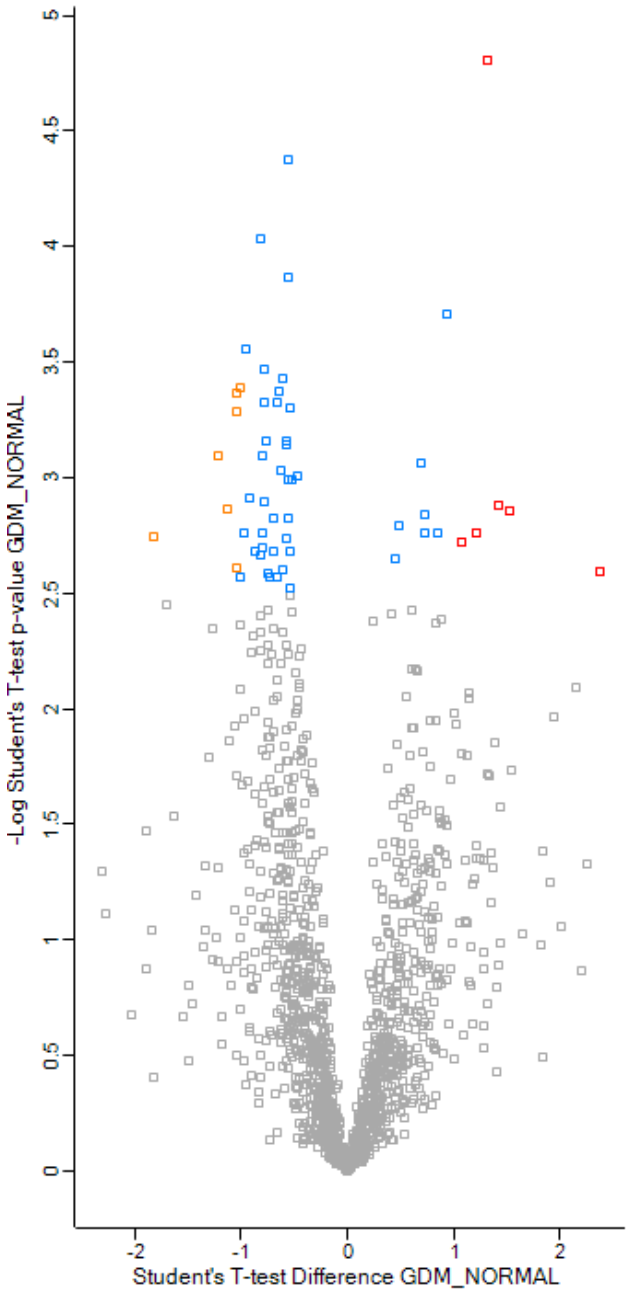



**Figure 53. Comparison of MEDIUM/LARGE STB-EV protein profile between GDM and normal pregnancy.**

The above Volcano plots shows differentially expressed proteins between GDM and normal pregnancy in MEDIUM/LARGE STB-EVs. Protein abundance has been analysed with student t-test, and differentially expressed proteins (FDR adjusted p-value=<0.05) with $\log_2$ fold change ≤-1 or ≥1 are presented in yellow (down regulated) and red (up regulated). Differentially expressed proteins (FDR adjusted p-value=<0.05) without $\log_2$ fold change ≤-1 or ≥1 are presented in blue. Differentially expressed proteins that did not reach statistical significance are presented by grey squares.

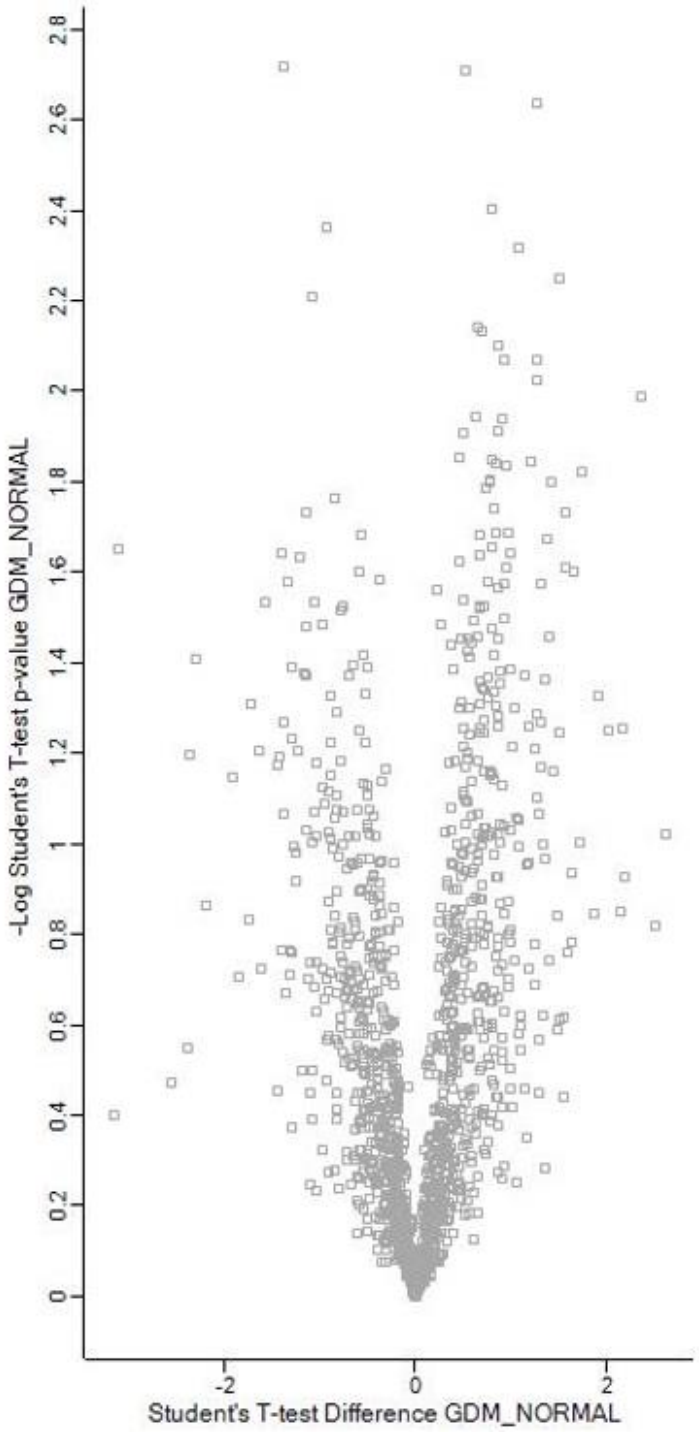



**Figure 54. Comparison of SMALL STB-EV protein profiles between GDM and normal pregnancy.**

Two samples t-test with FDR correction for multiple testing did not show any significantly differently expressed proteins between two groups. Differentially expressed proteins that did not reach statistical significance are presented by grey squares.

**Table 12. Differentially expressed proteins between MEDIUM/LARGE STB-EVs from GDM and normal pregnancy.** Up regulated proteins are indicated in red and down regulated in blue.

| Protein | q-value | p-value | Difference |
|---|---|---|---|
| **Barrier-to-autointegration factor** | 0.008 | 1.5867E-05 | 1.30996013 |
| **COP9 signalosome complex subunit 4** | 0.024 | 4.1937E-05 | -0.5596797 |
| **Calcium-regulated heat-stable protein 1 (Fragment)** | 0.02586667 | 0.00051904 | -1.0356117 |
| **GMP reductase** | 0.02707692 | 0.00047596 | -0.6525968 |
| **Cullin-5** | 0.02714286 | 0.00050147 | -0.5409105 |
| **Actin-related protein 2/3 complex subunit 3** | 0.02933333 | 0.00047484 | -0.7771788 |
| **Eukaryotic translation initiation factor 3 subunit M (Fragment)** | 0.03018182 | 0.00042916 | -1.0389393 |
| **Guanylate-binding protein 1** | 0.0314 | 0.00080078 | -1.2220971 |
| **UV excision repair protein RAD23 homolog B** | 0.03221053 | 0.00078986 | -0.7934964 |
| **Aldose reductase** | 0.03223529 | 0.00069685 | -0.5726541 |

| | | | |
|---|---|---|---|
| **Isoform 3 of Twinfilin-1** | 0.03288889 | 0.00071103 | -0.5767815 |
| **Isoform 3 of Reticulon-4** | 0.0332 | 0.00042166 | -0.6465006 |
| **UMP-CMP kinase** | 0.03425 | 0.00068068 | -0.7637424 |
| **Integrin beta-1** | 0.03657143 | 0.00086327 | 0.68686013 |
| **Prostaglandin E synthase 3** | 0.03688889 | 0.00040225 | -1.0072526 |
| **Elongin-B** | 0.03756522 | 0.00096094 | -0.4621809 |
| **T-complex protein 1 subunit delta** | 0.0376 | 0.00019572 | 0.93678346 |
| **Isoform 2 of Elongation factor 1-gamma** | 0.03776 | 0.0010248 | -0.5571422 |
| **Alpha-parvin** | 0.038 | 0.00101189 | -0.5276663 |
| **Isoform 2 of Kinesin light chain 2** | 0.03836364 | 0.00091909 | -0.6181082 |
| **Cell division control protein 42 homolog** | 0.039 | 0.00013928 | -0.560149 |
| **Tubulin-specific chaperone A** | 0.03991489 | 0.00213496 | -0.8182631 |

| | | | |
|---|---|---|---|
| **Isoform 1 of Deaminated glutathione amidase** | 0.04017391 | 0.00209093 | -0.8653197 |
| **Sorting nexin-9** | 0.0402 | 0.00177909 | 0.72804856 |
| **Eukaryotic translation initiation factor 2 subunit 3** | 0.04033333 | 0.00220814 | 0.45025353 |
| **NEDD8-activating enzyme E1 catalytic subunit** | 0.04063158 | 0.00174762 | -0.9790669 |
| **Trem-like transcript 2 protein** | 0.04102564 | 0.00177836 | -1.8172884 |
| **Quinone oxidoreductase-like protein 1** | 0.04104762 | 0.00191464 | 1.07774053 |
| **Activator of 90 kDa heat shock protein ATPase homolog 1** | 0.04106667 | 0.0020824 | -0.6881804 |
| **14-3-3 protein epsilon** | 0.04126829 | 0.0018585 | -0.5699852 |
| **Isoform 1B of Beta-arrestin-1** | 0.0415 | 0.00036855 | -0.6159174 |
| **Serine/threonine-protein phosphatase CPPED1** | 0.04152727 | 0.00269118 | -0.7273863 |
| **Pregnancy-specific beta-1-glycoprotein 3** | 0.04172973 | 0.00174198 | 1.2087852 |
| **Actin-related protein 2/3 complex subunit 2** | 0.042 | 0.00207294 | -0.5355681 |

| | | | |
|---|---|---|---|
| **Isoform 2 of Prostatic acid phosphatase** | 0.04223077 | 0.00255752 | 2.38245492 |
| **Isoform 2 of Coronin-1C** | 0.0422963 | 0.00268045 | -0.6556026 |
| **Cullin-2** | 0.04242424 | 0.0014969 | -0.6892327 |
| **Immunity-related GTPase family Q protein** | 0.04266667 | 9.0978E-05 | -0.8085251 |
| **Keratin, type I cytoskeletal 18** | 0.04266667 | 0.00172857 | 0.84190021 |
| **Trophoblast glycoprotein** | 0.0427907 | 0.0020254 | -0.8009386 |
| **Spartin** | 0.04279245 | 0.00265268 | -0.9998695 |
| **Monocarboxylate transporter 4** | 0.042875 | 0.0014769 | -0.5568041 |
| **Isoform 2 of Ras-related protein Rab-4B** | 0.04290196 | 0.00254245 | -0.7388124 |
| **Isoform 2 of Receptor-type tyrosine-protein phosphatase alpha** | 0.04305882 | 0.0016122 | 0.48871684 |
| **Isoform 2 of Destrin** | 0.04333333 | 0.00027368 | -0.9514709 |
| **Isoform 2 of Serine/threonine-protein phosphatase 2A 56 kDa regulatory subunit epsilon isoform** | 0.04352 | 0.00248797 | -0.6112685 |

| | | | |
|---|---|---|---|
| **Myristoylated alanine-rich C-kinase substrate** | 0.04388571 | 0.00170482 | -0.8004272 |
| **Vesicular integral-membrane protein VIP36** | 0.04425806 | 0.00145655 | 0.73318152 |
| **Ran-specific GTPase-activating protein** | 0.04440816 | 0.00247769 | -1.0355191 |
| **Isoform 2 of Anoctamin-10** | 0.0448 | 0.0013966 | 1.51864133 |
| **Ubiquitin thioesterase** | 0.04482759 | 0.00136681 | -1.1312524 |
| **Pyruvate kinase PKM** | 0.04514286 | 0.00033608 | -0.7798404 |
| **Exportin-7** | 0.04533333 | 0.00127124 | -0.7891689 |
| **Isoform 2 of NEDD8-activating enzyme E1 regulatory subunit** | 0.04584615 | 0.00121286 | -0.9162508 |
| **Inter-alpha-trypsin inhibitor heavy chain H2** | 0.04642857 | 0.001324 | 1.41273007 |
| **Heat shock 70 kDa protein 1A** | 0.04807143 | 0.00300704 | -0.5472665 |

The functional annotation of differentially expressed proteins were assessed by g:Profiler analysis using Gene Ontology (GO) Metabolic Function (MF), GO Biological Processes (BP), GO Cell Components (CC) and Reactome datasets (**Figure *55***). GO:MF showed that 10 terms were significantly enriched with the top three terms being cadherin binding (GO:0045296),

cell adhesion molecule binding (GO:0050839), and ubiquitin protein ligase binding (GO:0031625). In GO:BF, 11 terms were significantly enriched including. GO:CC reported 15 categories to be enriched, with the top three being cytosol (GO:005829), focal adhesion (GO:0005925), and cell-substrate junction (GO:0030055). In the Reactome data source, only one term has been enriched (**Table *13***).

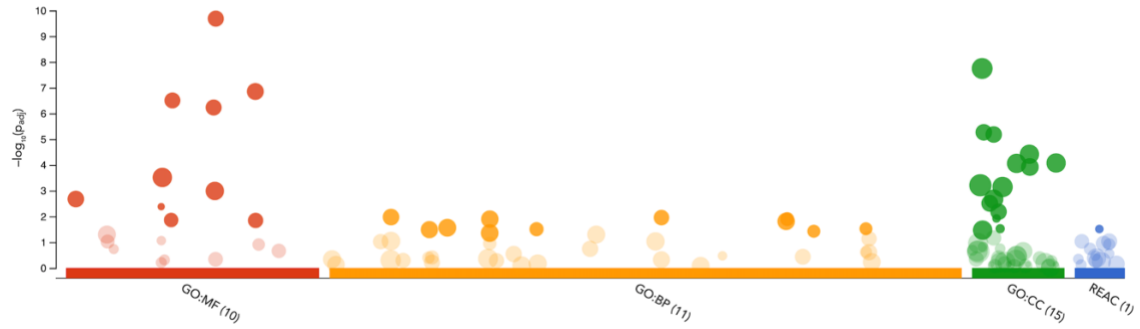



**Figure 55. Manhattan plot of Functional enrichment analysis of differently expressed proteins in GDM MEDIUM/LARGE STB-EVs.**

Differentially expressed proteins were subjected to g:Profiler analysis. The software used Gene Ontology (GO) Metabolic Function (MF), GO Biological Processes (BP), GO Cell Components (CC) and Reactome datasets for the analysis, with each dataset being colour coded. The above Manhattan plot shows that in GO:MF 10 terms were significantly enriched (dark red dots), in GO:BP 11 terms (dark yellow dots), and in GO:CC 15 terms (dark green dots). One term was significantly enriched in the Reactome data source. Each dot represents a single functional term and is size scaled according to the number of annotated genes in that term. The lighter coloured dots represent insignificant terms.

**Table 13. Functional enrichment analysis of differentially expressed proteins between GDM and normal pregnancy from MEDIUM/LARGE STB-EVs.**

Enriched terms from different data sources – GO:MO **(A)**, GO:BF **(B)**, GO:CC **(C)** and Reactome **(D)** – are presented together with their adjusted p-value.

## A) Gene ontology: Molecular Function

| Term name | Term ID | $p_{adj}$ | $-\log_{10}(p_{adj})$ |
|---|---|---|---|
| cadherin binding | GO:0045296 | $2.093\times10^{-10}$ | |
| cell adhesion molecule binding | GO:0050839 | $1.405\times10^{-7}$ | |
| ubiquitin protein ligase binding | GO:0031625 | $3.138\times10^{-7}$ | |
| ubiquitin-like protein ligase binding | GO:0044389 | $5.895\times10^{-7}$ | |
| enzyme binding | GO:0019899 | $3.065\times10^{-4}$ | |
| protein-containing complex binding | GO:0044877 | $1.023\times10^{-3}$ | |
| actin binding | GO:0003779 | $2.112\times10^{-3}$ | |
| NEDD8 activating enzyme activity | GO:0019781 | $4.177\times10^{-3}$ | |
| heat shock protein binding | GO:0031072 | $1.380\times10^{-2}$ | |
| actin filament binding | GO:0051015 | $1.437\times10^{-2}$ | |

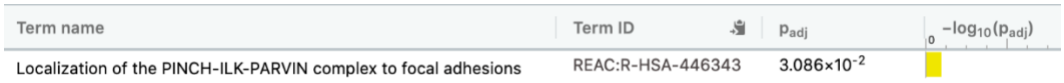
## B) Gene ontology: Biological Function

| Term name | Term ID | $p_{adj}$ | $-\log_{10}(p_{adj})$ |
|---|---|---|---|
| actin filament organization | GO:0007015 | $1.058\times10^{-2}$ | |
| positive regulation of cytoskeleton organization | GO:0051495 | $1.112\times10^{-2}$ | |
| lamellipodium organization | GO:0097581 | $1.271\times10^{-2}$ | |
| actin cytoskeleton organization | GO:0030036 | $1.275\times10^{-2}$ | |
| supramolecular fiber organization | GO:0097435 | $1.554\times10^{-2}$ | |
| viral process | GO:0016032 | $2.746\times10^{-2}$ | |
| regulation of lamellipodium organization | GO:1902743 | $3.004\times10^{-2}$ | |
| substrate adhesion-dependent cell spreading | GO:0034446 | $3.124\times10^{-2}$ | |
| positive regulation of organelle organization | GO:0010638 | $3.261\times10^{-2}$ | |
| regulation of substrate adhesion-dependent cell spread... | GO:1900024 | $3.776\times10^{-2}$ | |
| actin filament-based process | GO:0030029 | $4.416\times10^{-2}$ | |

## C) Gene Ontology: Cellular Component

| Term name | Term ID | $p_{adj}$ | $-\log_{10}(p_{adj})$ |
|---|---|---|---|
| cytosol | GO:0005829 | $1.802\times10^{-8}$ | |
| focal adhesion | GO:0005925 | $5.420\times10^{-6}$ | |
| cell-substrate junction | GO:0030055 | $6.582\times10^{-6}$ | |
| extracellular exosome | GO:0070062 | $3.839\times10^{-5}$ | |
| extracellular vesicle | GO:1903561 | $8.414\times10^{-5}$ | |
| extracellular organelle | GO:0043230 | $8.737\times10^{-5}$ | |
| anchoring junction | GO:0070161 | $1.199\times10^{-4}$ | |
| cytoplasm | GO:0005737 | $6.151\times10^{-4}$ | |
| vesicle | GO:0031982 | $7.204\times10^{-4}$ | |
| cell junction | GO:0030054 | $2.133\times10^{-3}$ | |
| actin cytoskeleton | GO:0015629 | $3.099\times10^{-3}$ | |
| cell leading edge | GO:0031252 | $6.582\times10^{-3}$ | |
| VCB complex | GO:0030891 | $1.202\times10^{-2}$ | |
| Cul5-RING ubiquitin ligase complex | GO:0031466 | $2.995\times10^{-2}$ | |
| cytoskeleton | GO:0005856 | $3.412\times10^{-2}$ | |

**D) Reactome**



| Term name | Term ID | $p_{adj}$ | $-\log_{10}(p_{adj})$ |
|---|---|---|---|
| Localization of the PINCH-ILK-PARVIN complex to focal adhesions | REAC:R-HSA-446343 | $3.086\times10^{-2}$ | 0 |

REVIGO online tool was used to summarise and visualise g:Profiler results. The data was presented on a scatter plot where semantically related GO terms are clustered together. Analysis of enriched terms from GO:MF dataset revealed three major clusters: cadherin binding, ubiquitin protein ligase binding and cell adhesion molecule binding (**Figure *56A***). The same type of analysis was performed to visualise g:Profiler data from GO:BF identifying positive regulation of cytoskeleton organization as a main cluster enriched in differentially expressed proteins between GDM and normal pregnancy in MEDIUM/LARGE STB-EVs (**Figure *56B***).

**A) GO: Molecular function**




**B) GO: Biological Processes**




**Figure 56. Summary of GO enriched terms between MEDIUM/LARGE STB-EVS from GDM and normal pregnancy.**

GO enriched terms obtained by g:Profiler analysis of differentially expressed proteins between GDM and normal pregnancy in MEDIUM/LARGE STB-EVS were summarised and visualised using REVIGO. Summary of GO enriched terms in MF **(A)** and BP **(B)**. Every rectangle represents a single cluster. The representatives are also linked to a 'superclusters' of roughly related terms indicated by the same colour. Size of the rectangles reflects the frequency of the GO term in the GOA database (larger rectangles are associated with more general terms).

## 5.3. Discussion

In this chapter, we characterised protein profile changes in STB-EVs isolated from GDM pregnancy in comparison to those isolated from normal pregnancy. We observed dramatic changes in the protein cargo of the two populations of isolated STB-EVs: MEDIUM/LARGE and SMALL STB-EVs. In the GDM group, 856 proteins were differentially expressed between MEDIUM/LARGE and SMALL STB-EVs, while in normal pregnancy 815 proteins were differentially expressed between the two populations of STB-EVs. Comparison analysis between GDM and normal pregnancies identified 56 proteins as differentially expressed in the MEDUIM/LARGE subtype, while in the SMALL STB-EVs no proteins reached statistical significance.

One of the biggest challenges in STB-EV research is the inability to isolate specific placental EVs. We are one of the few laboratories that perform *ex vivo* placenta perfusion, which allows for the specific isolation of placenta derived EVs (as discussed in the thesis' *Introduction*). To the best of our knowledge, this work presents the first comparison of STB-EVs' protein cargo from GDM and normal pregnancy, isolated using placenta perfusion. Furthermore, we isolated two populations of STB-EVs – MEDIUM/LARGE and SMALL STB-EVs – and described changes in the proteomic profile between them.

As discussed in the thesis' *Introduction*, the three major subtypes of EVs are: microvesicles (release by direct budding of cell membrane in response to stimuli; previously considered size range: 200-1000 nm ); exosomes (secreted by the fusion of MVB with cell membrane; size range: smaller than 200 nm); and apoptotic bodies (formed during the apoptosis; size range: above 1 μ). In recent years, it has become apparent that it is difficult to distinguish between these groups based on their size or conventional biomarker, as used to be the practise. In line with the latest ISEV guidelines, here two populations of STB-EVs were named MEDIUM/LARGE and SMALL STB-EVs as they were separated based on their size.

However, the data from this chapter shows their protein profiles provide an additional metric by which to clearly differentiate them.

In GDM, 271 proteins were downregulated and 346 were upregulated between two subtypes of STB-EVs (FDR adjusted p-value=<0.05, $\log_2$ fold change ≤-1 or ≥1). Very similar results were obtained from normal pregnancy, where 261 proteins were found to be downregulated while 394 were upregulated between MEDIUM/LARGE and SMALL STB-EVs, clearly showing their differing protein profiles.

Their different protein cargo might be associated with their different mode of biogenesis and it also suggests that the two subtypes of STB-EVs might have different functional effects. Functional enrichment analysis performed by g:Profiler (Raudvere *et al.*, 2019) were both filtered for redundant terms and summarised using REVIGO software (Supek *et al.*, 2011). GO enriched terms in biological processes showed that differentially expressed proteins between MEDIUM/LARGE and SMALL STB-EVs were associated with the immune system and leukocyte mediated immunity in both GDM and normal pregnancy. This is further supported by Reactome database analysis (Croft *et al.*, 2014), which revealed that the most significantly enriched term was associated with the innate immune system again in both GDM and normal pregnancy. This finding is in accordance with previous research that has described placentally derived microvesicles as immunostimulatory particles while exosomes were linked with immunosuppressive properties (Redman *et al.*, 2012). It has been believed that this might be particularly important in complicated pregnancies as discussed in more details below.

The main aim of this chapter was to compare the proteomic cargo of the same subtype of STB-EVs between GDM and normal pregnancy. In MEDIUM/LARGE STB-EVs, 56 proteins were statistically different, and among them 13 had a $\log_2$ fold change ≤-1 or ≥1. In SMALL STB-EVs, there were no statistically significant differentially expressed proteins between GDM and normal pregnancy. This data might support the hypothesis that SMALL STB-EVs (previously

classified as exosomes) that are continuously released from the placenta are predominantly expressed in normal pregnancy, while MEDIUM/LARGE STB-EVs (previously described as microvesicles) are produce as a result of inflammatory and oxidative stress stimuli to the STB. In PE, it has been suggested that inflammatory and oxidative stress prompt the shedding of microvesicles, subsequently shifting the balance towards this type of STB-EV, making them the most prominent subgroup over exosomes; the subgroup proposed to be most prominent in normal pregnancy (Redman *et al.*, 2012).

Summarised results from functional enrichment analysis of differentially expressed proteins in MEDIUM/LARGE STB-EVs from GDM and normal pregnancy found positive regulation of cytoskeleton organisation as the most significantly enriched biological process. Enriched cytoskeleton organisation has also been reported in other EVs confirming that vesicular proteins mainly originate from the plasma membrane, cytosol and internal vesicles, and as such are distinct from other intracellular compartments (i.e. endoplasmic reticulum, mitochondria etc) (Choi *et al.*, 2015).

Studying STB-EV cargo has multiple benefits. It provides insights into the pathophysiology of the gestational disease, and changes to EV protein signals in disease state could provide novel biomarker opportunities for the condition. This might be especially important in GDM considering the urgent need to improve GDM diagnostic tools. Among the 13 proteins that had adjusted p-value $<0.05$ and $\log_2$ fold change $\leq$-1 or $\geq$1, pregnancy specific glycoprotein-3 (PSG-3) emerged as a placenta specific protein. A Human Protein Atlas search for tissue expression (Pontén, Jirström and Uhlen, 2008), showed that PSG-3 is exclusively expressed by the placenta, suggesting it may have great biomarker potential. A literature search for PSG-3 revealed that increased levels of PSGs have been reported in preeclampsia, another gestational disease associated with increased insulin resistance (Bari *et al.*, 2016). Additionally, any differences that we observe in the protein expression level will be amplified in the plasma

considering increased placental exosome quantities seen in GDM pregnancy (Salomon et al., 2016).

As discussed above, comparison analysis of SMALL STB-EVs between GDM and normal pregnancy did not show statistically significant results, however, one protein still stood out. ADP-ribosyl-acceptor hydrolase (ARH3) has been identified with the most significant change (-2.6-fold) between the two conditions. ARH3 is responsible for degradation of Poly (ADP ribose) (PAR) (Mashimo, Kato and Moss, 2013; Fontana *et al.*, 2017), and interestingly, PAR accumulation has been associated with various diseases including diabetes mellitus (Curtin and Szabo, 2020). Even though ARH3 expression is ubiquitous in human tissues (Abplanalp *et al.*, 2017), it could still serve as a biomarker for GDM. This is because STB-EVs diagnostic potential is partially due to their expression of PLAP, which provides tissue specificity for these EVs. Therefore, combining PLAP as a biomarker of STB-EVs placental origin with the presence of a protein differentially expressed in GDM might provide a novel diagnostic tool for this disease.

*COVID-19 laboratory closure*

*An individual validation of differentially expressed proteins identified in this chapter is needed. My aim was to perform western blotting analysis of top three up- and downregulated proteins from this dataset, but the closure of our laboratory due to COVID-19 did not allow me to complete this work.*

## 5.4. Summary

This chapter shows the changes in the proteomic cargo of both MEDIUM/LARGE and SMALL STB-EVs in GDM pregnancy compared to normal healthy pregnancy. In MEDIUM/LARGE STB-EVs, 56 proteins were differently expressed. In SMALL STB-EVs, no proteins reached statistical difference. On the other hand, staggering differences were observed between MEDIUM/LARGE and SMALL STB-EVs indicating that the two subtypes of STB-EVs have a different proteomic cargo, which might be associated with divergent modes of action and lead to these two subtypes of EVs having different functional effects. Further studies are necessary to validate these results as well as to investigate the function of the differentially expressed proteins in GDM pregnancies. STB-EVs have great potential to allow a non-invasive, real-time snapshot of placenta health, providing both novel diagnostic and treatment opportunities for gestational diseases and enhancing our understanding of the mechanism involved in GDM's pathophysiology.

# 6. Thesis Summary and Future Work

It is increasingly apparent that the intrauterine environment plays a major role in shaping babies' long-term health, and pregnancy associated diseases have long-term impacts on mothers' health (foetal programming). Nowhere is this more clearly visible than in GDM. The offspring of mothers who suffer from GDM are up to six times more likely to develop T2DM compared to those born to healthy mothers; with the mothers' own chances of developing T2DM increasing between 40-70% within five years of delivery. GDM is therefore the most significant predictor of long-term T2DM in affected mothers.

GDM is diagnosed by either routine or targeted screening using an oral glucose tolerance test (OGTT). The OGTT is performed at 24-28 weeks gestation and consists of an assessment of fasting blood glucose followed by one- and two-hour blood glucose assessments after ingesting 75g of glucose. Considering that test has poor sensitivity, poor patient compliance, is time consuming and unreliable after 28 weeks, there is an unmet need for a better way to diagnose GDM.

The pathophysiology of the disease is mainly unknown, but previous research has observed that the placenta may play an important role in its development given its delivery results in the immediate reversal of diabetic symptoms. This thesis aimed to investigate the nature of the placenta's role in GDM, building upon the knowledge that the organ releases EVs into the maternal circulation from six weeks gestation until delivery. EVs' unique feature is that they carry a variety of ligands, including both proteins and RNA species. As such, EVs play an important role in cell-cell communication in both physiological and pathophysiological conditions and may provide novel biomarkers for the disease.

Recently, our laboratory performed a mass spectrometric analysis of STB-EVs isolated from normal and PE placenta (another gestational complication associated with insulin resistance). Bioinformatics analysis focused on factors impacting insulin bioavailability, a hallmark of pregnancy that is altered during the establishment of GDM. We identified two biologically

plausible biomarkers on STB-EVs (dipeptidyl peptidase 4 (DPPIV) and insulin receptor (IR)) that might play a role in GDM.

Firstly, we investigated STB-EV-bound DPPIV, an enzyme known to play a pathogenic role in T2DM by reducing insulin secretion, but that has not been previously associated with GDM. We have shown that the human placenta releases extracellular vesicles carrying DPPIV into the maternal circulation, which a) are biologically active, b) can be inhibited by commercially available DPPIV inhibitors, and c) are significantly increased in the circulation of women with GDM. DPPIV inhibitors (gliptins class of drugs) are currently used for the treatment of T2DM. This work has been published and intellectually protected by Oxford University Innovation. Our data suggested that using this class of drugs for the treatment of gestational diabetes may well have merit, and also raises the possibility of using DPPIV positive placental EVs as diagnostic markers for GDM. In order to address these two aims, we recently applied for, and were successfully awarded, funding from the University Translational Research Office to continue this work. The continuation of my DPhil project will allow us to translate our significant finding that STB-EV-bound DPPIV is elevated in the circulation of GDM women (described in *Chapter 3*) to a larger patient cohort. Furthermore, we joined forces with NanoView Biosciences to help achieve this aim using their proprietary technology. Our future goal is to validate the levels of STB-EV-bound DPPIV in plasma samples, both earlier in pregnancy and in a larger group of patients.

Secondly, this DPhil project demonstrated that IR, a transmembrane protein that plays a crucial role in maintaining normal blood glucose levels: 1) is expressed on STB-EVs, a feature that seems to be unique to the placental EVs; 2) may act as a "decoy" receptor capable of sequestering maternal insulin; and 3) is increased in maternal plasma from GDM patients. These results have also been intellectually protected by Oxford University Innovation. Together with the Shoklo Malaria Research Unit (SMRU) in Thailand, we successfully

obtained another grant to further investigate these important discoveries in a high GDM risk cohort from a low-resource setting. GDM affects more women in low- and middle-income countries where access to healthcare resources is limited. Additionally, women of South Asian background have a GDM prevalence 2.4-times higher than Caucasians. Therefore, we want to understand if the biomarkers are transferable across populations and in particular to "high-risk populations". Our future study will try to assess this by adjusting a sandwich ELISA to 'capture" PLAP positive EVs and then interrogate them with IR or DPPIV as a secondary probe. The main goals of this work will be to evaluate whether: 1) STB-bound IR/DPPIV levels could predict GDM earlier than the OGTT in pregnancy; and 2) if STB-EV-bound IR/DPPIV could be used to diagnose GDM in the 3rd trimester. Improving the accuracy of GDM diagnostic testing would allow us to identify affected mothers more effectively, leading to appropriate intervention, potentially reducing delayed diagnoses of GDM and its associated morbidities.

Finally, this thesis summarises the proteomic profile of STB-EVs in GDM pregnancy. This research goes beyond investigating the roles of DPPIV and IR in GDM development to include other factors present in STB-EVs that may also contribute to disease pathophysiology and/or provide novel biomarker targets for GDM. Future work will include the validation of mass spectrometry data using western blotting and ELISA techniques. Furthermore, as EVs are also known to carry nucleic acids, we intend to conduct RNA-sequencing analysis of STB-EVs' cargo. Our hypothesis is that studying the cargo of placental EVs will not only allow us to understand their role in the short-term insulin availability changes in GDM patients, but that it also might play a role in the disease's long-term consequences (i.e. the increased likelihood that affected mothers will later develop T2DM). When working to understand the long-term consequences of GDM, our analysis will focus on RNA. Transcriptomic results from this project will be integrated and compared by bioinformatic approaches with STB-EVs' mass

spectrometry dataset. Combining and utilising these two datasets will allow for the further elucidation GDM pathophysiology.

# Bibliography


- Abplanalp, J. *et al.* (2017) 'Proteomic analyses identify ARH3 as a serine mono-ADP-ribosylhydrolase', *Nature communications*, 8(1), p. 2055. doi: 10.1038/s41467-017-02253-1.
- American Diabetes Association (2004) 'Gestational diabetes mellitus.', *Diabetes care*, 27 Suppl 1(suppl 1), pp. S88-90. doi: 10.2337/diacare.27.2007.s88.
- Armistead, B. *et al.* (2020) 'Placental Regulation of Energy Homeostasis During Human Pregnancy', *Endocrinology*, 161(7). doi: 10.1210/endocr/bqaa076.
- Atay, S., Gercel-Taylor, C., Kesimer, M., *et al.* (2011) 'Morphologic and proteomic characterization of exosomes released by cultured extravillous trophoblast cells', *Experimental Cell Research*, 317(8), pp. 1192–1202. doi: 10.1016/j.yexcr.2011.01.014.
- Atay, S., Gercel-Taylor, C., Suttles, J., *et al.* (2011) 'Trophoblast-derived exosomes mediate monocyte recruitment and differentiation', *American Journal of Reproductive Immunology*, 65(1), pp. 65–77. doi: 10.1111/j.1600-0897.2010.00880.x.
- Baietti, M. F. *et al.* (2012) 'Syndecan-syntenin-ALIX regulates the biogenesis of exosomes', *Nature Cell Biology*. Nature Publishing Group, 14(7), pp. 677–685. doi: 10.1038/ncb2502.
- Baig, S. *et al.* (2014) 'Proteomic analysis of human placental syncytiotrophoblast microvesicles in preeclampsia', *Clinical Proteomics*, 11(1), pp. 1–8. doi: 10.1186/1559-0275-11-40.
- Balsells, M. *et al.* (2015) 'Glibenclamide, metformin, and insulin for the treatment of gestational diabetes: A systematic review and meta-analysis', *BMJ (Online)*, 350(January), pp. 1–12. doi: 10.1136/bmj.h102.
- Barbour, L. A. *et al.* (2007) 'Cellular mechanisms for insulin resistance in normal

pregnancy and gestational diabetes', *Diabetes Care*, 30(Supplement 2), pp. S112–S119. doi: 10.2337/dc07-s202.

- Bari, M. F. *et al.* (2016) 'Gestational diabetic transcriptomic profiling of microdissected human trophoblast', *Journal of Endocrinology*. Bristol, UK: Bioscientifica Ltd, 229(1), pp. 47–59. doi: 10.1530/JOE-15-0424.
- Belfiore, A. *et al.* (2009) 'Insulin Receptor Isoforms and Insulin Receptor/Insulin-Like Growth Factor Receptor Hybrids in Physiology and Disease', *Endocrine Reviews*, 30(6), pp. 586–623. doi: 10.1210/er.2008-0047.
- Bellamy, L. *et al.* (2009) 'Type 2 diabetes mellitus after gestational diabetes: a systematic review and meta-analysis', *The Lancet*. Elsevier Ltd, 373(9677), pp. 1773–1779. doi: 10.1016/S0140-6736(09)60731-5.
- Ben-Haroush, A., Yogev, Y. and Hod, M. (2004) 'Epidemiology of gestational diabetes mellitus and its association with Type 2 diabetes', *Diabetic Medicine*. John Wiley & Sons, Ltd, 21(2), pp. 103–113. doi: 10.1046/j.1464-5491.2003.00985.x.
- Berhanu, P. and Olefsky, J. M. (1982) 'Photoaffinity Labeling of Insulin Receptors in Viable Cultured Human Lymphocytes: Demonstration of Receptor Shedding and Degradation', *Diabetes*, 31(5), pp. 410 LP – 417. doi: 10.2337/diab.31.5.410.
- Boelens, M. C. *et al.* (2014) 'Article Exosome Transfer from Stromal to Breast Cancer Cells Regulates Therapy Resistance Pathways', *Cell*. Elsevier Inc., 159(3), pp. 499–513. doi: 10.1016/j.cell.2014.09.051.
- Bonde, L. *et al.* (2013) 'Reduced postprandial GLP-1 responses in women with gestational diabetes mellitus', *Diabetes, Obesity and Metabolism*, 15(8), pp. 713–720.
- Brill, A. *et al.* (2005) 'Platelet-derived microparticles induce angiogenesis and stimulate post-ischemic revascularization', *Cardiovascular Research*, 67(1), pp. 30–38. doi: 10.1016/j.cardiores.2005.04.007.

- Buchanan, T. a and Xiang, A. H. (2005) 'Gestational diabetes mellitus', *Journal of Clinical Investigation*, 115(3), pp. 485–491. doi: 10.1172/JCI200524531.The.
- Burkova, E. E. *et al.* (2018) 'Exosomes from human placenta purified by affinity chromatography on sepharose bearing immobilized antibodies against CD81 tetraspanin contain many peptides and small proteins', *IUBMB Life*, 70(11), pp. 1144–1155. doi: 10.1002/iub.1928.
- Burton, G. J. *et al.* (2014) 'Optimising sample collection for placental research', *Placenta*. Elsevier Ltd, 35(1), pp. 9–22. doi: 10.1016/j.placenta.2013.11.005.
- Burton, G. J. and Fowden, A. L. (2015) 'The placenta: A multifaceted, transient organ', *Philosophical Transactions of the Royal Society B: Biological Sciences*, 370(1663), pp. 1–8. doi: 10.1098/rstb.2014.0066.
- Burton, G. J., Fowden, A. L. and Thornburg, K. L. (2016) 'Placental origins of chronic disease', *Physiological Reviews*, 96(4), pp. 1509–1565. doi: 10.1152/physrev.00029.2015.
- Casey, B. M. *et al.* (1997) 'Pregnancy outcomes in women with gestational diabetes compared with the general obstetric population', *Obstetrics and Gynecology*, 90(6), pp. 869–873. doi: 10.1016/S0029-7844(97)00542-5.
- Catalano, P. M. *et al.* (1991) 'Longitudinal changes in insulin release and insulin resistance in nonobese pregnant women', *American Journal of Obstetrics and Gynecology*, 165(6, Part 1), pp. 1667–1672. doi: https://doi.org/10.1016/0002-9378(91)90012-G.
- Catalano, P. M. *et al.* (1999) 'Longitudinal changes in glucose metabolism during pregnancy in obese women with normal glucose tolerance and gestational diabetes mellitus', *American Journal of Obstetrics and Gynecology*, 180(4), pp. 903–916. doi: 10.1016/S0002-9378(99)70662-9.

- Catalano, P. M. *et al.* (2003) 'Metabolism Gestational Diabetes and Insulin Resistance : Role in Short- and long term implications for Mother and Fetus', *Journal of Nutrition*, 133(5), pp. 1674–1683.
- Chargaff, E. and West, R. (1946) 'The biological significance of the thromboplastic protein of blood', *Journal of Biological Chemistry*, 166(7), pp. 189–197.
- Choi, D.-S. *et al.* (2015) 'Proteomics of extracellular vesicles: Exosomes and ectosomes', *Mass Spectrometry Reviews*. John Wiley & Sons, Ltd, 34(4), pp. 474–490. doi: 10.1002/mas.21420.
- Choi, D. S. *et al.* (2013) 'Proteomics, transcriptomics and lipidomics of exosomes and ectosomes', *Proteomics*, 13(10–11), pp. 1554–1571. doi: 10.1002/pmic.201200329.
- Chu, S. Y. *et al.* (2007) 'Maternal Obesity and Risk of Gestational Diabetes Mellitus', *Diabetes*, 30(8), pp. 2070–2076. doi: 10.2337/dc06-2559a.
- Di Cianni, G. *et al.* (2003) 'Prevalence and risk factors for gestational diabetes assessed by universal screening', *Diabetes Research and Clinical Practice*. Elsevier Ireland Ltd, 62(2), pp. 131–137. doi: 10.1016/j.diabres.2003.07.004.
- Lo Cicero, A., Stahl, P. D. and Raposo, G. (2015) 'Extracellular vesicles shuffling intercellular messages: For good or for bad', *Current Opinion in Cell Biology*, 35, pp. 69–77. doi: 10.1016/j.ceb.2015.04.013.
- Cockell, A. P. *et al.* (1997) 'Human placental syncytiotrophoblast microvillous membranes impair maternal vascular endothelial function.', *British journal of obstetrics and gynaecology*, 104(2), pp. 235–40. doi: 10.1111/j.1471-0528.1997.tb11052.x.
- Cocucci, E., Racchetti, G. and Meldolesi, J. (2009) 'Shedding microvesicles: artefacts no more', *Trends in Cell Biology*, 19(2), pp. 43–51. doi: 10.1016/j.tcb.2008.11.003.
- Cooke, W. R. *et al.* (2019) 'Maternal circulating syncytiotrophoblast-derived

extracellular vesicles contain biologically active 5'-tRNA halves', *Biochemical and Biophysical Research Communications*, 518(1), pp. 107–113. doi: 10.1016/j.bbrc.2019.08.015.

- Croft, D. *et al.* (2014) 'The Reactome pathway knowledgebase', *Nucleic Acids Research*, 42(D1), pp. D472–D477. doi: 10.1093/nar/gkt1102.
- Curtin, N. J. and Szabo, C. (2020) 'Poly(ADP-ribose) polymerase inhibition: past, present and future', *Nature Reviews Drug Discovery*, 19(10), pp. 711–736. doi: 10.1038/s41573-020-0076-6.
- Cushman, S. W. and Wardzala, L. J. (1980) 'Potential mechanism of insulin action on glucose transport in the isolated rat adipose cell. Apparent translocation of intracellular transport systems to the plasma membrane', *Journal of Biological Chemistry*, 255(10), pp. 4758–4762.
- von Dadelszen, P., Hurst, G. and Redman, C. W. (1999) 'Supernatants from co-cultured endothelial cells and syncytiotrophoblast microvillous membranes activate peripheral blood leukocytes in vitro.', *Human reproduction (Oxford, England)*, 14(4), pp. 919–24. Available at: http://www.ncbi.nlm.nih.gov/pubmed/10221219.
- Deacon, C. (2019) 'Physiology and Pharmacology of DPP-4 in Glucose Homeostasis and the Treatment of Type 2 Diabetes', *Frontiers in Endocrinology*, 10, p. 80. doi: 10.3389/fendo.2019.00080.
- Deacon, C. F. and Lebovitz, H. E. (2016) 'Comparative review of dipeptidyl peptidase-4 inhibitors and sulphonylureas', *Diabetes, Obesity and Metabolism*, 18(4), pp. 333–347. doi: 10.1111/dom.12610.
- Desoye, G. *et al.* (1997) 'Location of insulin receptors in the placenta and its progenitor tissues', *Microscopy Research and Technique*. John Wiley & Sons, Ltd, 38(1-2), pp. 63–75. doi: 10.1002/(SICI)1097-0029(19970701/15)38:1/2<63::AID-

JEMT8>3.0.CO;2-V.

- Donker, R. B. *et al.* (2012) 'The expression profile of C19MC microRNAs in primary human trophoblast cells and exosomes.', *Molecular human reproduction*. Oxford University Press, 18(8), pp. 417–24. doi: 10.1093/molehr/gas013.
- Donovan, L. *et al.* (2013) 'Screening tests for gestational diabetes: A systematic review for the U.S. preventive services task force', *Annals of Internal Medicine*, 159(2), pp. 115–122. doi: 10.7326/0003-4819-159-2-201307160-00657.
- Dragovic, R. A. *et al.* (2015) 'Isolation of syncytiotrophoblast microvesicles and exosomes and their characterisation by multicolour flow cytometry and fluorescence Nanoparticle Tracking Analysis', *Methods*. Elsevier Inc., 87, pp. 64–74. doi: 10.1016/j.ymeth.2015.03.028.
- Drucker, D. J. and Nauck, M. A. (2006) 'The incretin system : glucagon-like peptide-1 receptor agonists and dipeptidyl peptidase-4 inhibitors in type 2 diabetes', *Lancet*, 368(9548), pp. 1696–705.
- Ebina, Y. *et al.* (1985) 'The human insulin receptor cDNA: The structural basis for hormone-activated transmembrane signalling', *Cell*, 40(4), pp. 747–758. doi: 10.1016/0092-8674(85)90334-4.
- Elfeky, O. *et al.* (2017) 'Influence of maternal BMI on the exosomal profile during gestation and their role on maternal systemic inflammation', *Placenta*, 50, pp. 60–69. doi: 10.1016/j.placenta.2016.12.020.
- Escudero, C. A. *et al.* (2016) 'Role of Extracellular Vesicles and microRNAs on Dysfunctional Angiogenesis during Preeclamptic Pregnancies', *Frontiers in Physiology*. Frontiers, 7, p. 98. doi: 10.3389/fphys.2016.00098.
- Fadini, G. P. *et al.* (2012) 'The increased dipeptidyl peptidase-4 activity is not counteracted by optimized glucose control in type 2 diabetes, but is lower in metformin-

treated patients', *Diabetes, Obesity and Metabolism*, 14(6), pp. 518–522. doi: 10.1111/j.1463-1326.2011.01550.x.

- Ferrara, A. (2007) 'Increasing Prevalence of Gestational Diabetes Mellitus', *Diabetes Care*, 30(Supplement 2), p. S141 LP-S146. doi: 10.2337/dc07-s206.
- Filipe, V., Hawe, A. and Jiskoot, W. (2010) 'Critical Evaluation of Nanoparticle Tracking Analysis (NTA) by NanoSight for the Measurement of Nanoparticles and Protein Aggregates', *Pharmaceutical Research*, 27(5), pp. 796–810. doi: 10.1007/s11095-010-0073-2.
- Fong, M. Y. *et al.* (2015) 'Breast-cancer-secreted miR-122 reprograms glucose metabolism in premetastatic niche to promote metastasis', *Nature cell biology*. 2015/01/26, 17(2), pp. 183–194. doi: 10.1038/ncb3094.
- Fontana, P. *et al.* (2017) 'Serine ADP-ribosylation reversal by the hydrolase ARH3', *eLife*, 6. doi: 10.7554/eLife.28533.
- Freychet, P., Roth, J. and Neville, D. M. (1971) 'Insulin receptors in the liver: specific binding of ( 125 I)insulin to the plasma membrane and its relation to insulin bioactivity.', *Proceedings of the National Academy of Sciences of the United States of America*, 68(8), pp. 1833–1837. doi: 10.1073/pnas.68.8.1833.
- Friedman, J. E. *et al.* (1999) 'Impaired glucose transport and insulin receptor tyrosine phosphorylation in skeletal muscle from obese women with gestational diabetes', *Diabetes*, 48(9), pp. 1807–1814. doi: 10.2337/diabetes.48.9.1807.
- Fuglsang, J. *et al.* (2003) 'Human Placental Growth Hormone, Insulin-Like Growth Factor I and -II, and Insulin Requirements during Pregnancy in Type 1 Diabetes', *The Journal of Clinical Endocrinology & Metabolism*, 88(9), pp. 4355–4361. doi: 10.1210/jc.2003-030726.
- Gavin, J. R., Buell, D. N. and Roth, J. (1972) 'Water-Soluble Insulin Receptors from

Human Lymphocytes', *Science*, 178(4057), pp. 168 LP – 169. doi: 10.1126/science.178.4057.168.

- Gerena, Y. *et al.* (2015) 'Soluble insulin receptor as a source of insulin resistance and cognitive impairment in HIV-seropositive women', *Journal of neurovirology*. 2015/01/21, 21(2), pp. 113–119. doi: 10.1007/s13365-014-0310-2.
- Germain, S. J. *et al.* (2007) 'Systemic Inflammatory Priming in Normal Pregnancy and Preeclampsia: The Role of Circulating Syncytiotrophoblast Microparticles', *The Journal of Immunology*, 178(9), pp. 5949–5956. doi: 10.4049/jimmunol.178.9.5949.
- Gill, M. *et al.* (2019) 'Placental syncytiotrophoblast-derived extracellular vesicles carry active NEP (Neprilysin) and are increased in preeclampsia', *Hypertension*, 73(5). doi: 10.1161/HYPERTENSIONAHA.119.12707.
- Goswami, D. *et al.* (2006) 'Excess syncytiotrophoblast microparticle shedding is a feature of early-onset pre-eclampsia, but not normotensive intrauterine growth restriction', *Placenta*. W.B. Saunders, 27(1), pp. 56–61. doi: 10.1016/J.PLACENTA.2004.11.007.
- Gould, S. J. and Raposo, G. (2013) 'As we wait: coping with an imperfect nomenclature for extracellular vesicles', *Journal of Extracellular Vesicles*. Taylor & Francis, 2(1), pp. 1–3. doi: 10.3402/jev.v2i0.20389.
- Griffiths, S. K. and Campbell, J. P. (2015) 'Placental structure, function and drug transfer', *Continuing Education in Anaesthesia, Critical Care and Pain*, 15(2), pp. 84–89. doi: 10.1093/bjaceaccp/mku013.
- Gupta, A. K. *et al.* (2004) 'Detection of Fetal DNA and RNA in Placenta-Derived Syncytiotrophoblast Microparticles Generated in Vitro', *Clinical Chemistry*, 50(11), pp. 2187–2190. doi: 10.1373/clinchem.2004.040196.
- Gupta, A. K., Holzgreve, W. and Hahn, S. (2008) 'Decrease in lipid levels of

syncytiotrophoblast micro-particles reduced their potential to inhibit endothelial cell proliferation', *Archives of Gynecology and Obstetrics*, 277(2), pp. 115–119. doi: 10.1007/s00404-007-0425-2.

- György, B. *et al.* (2011) 'Membrane vesicles, current state-of-the-art: Emerging role of extracellular vesicles', *Cellular and Molecular Life Sciences*, 68(16), pp. 2667–2688. doi: 10.1007/s00018-011-0689-3.
- Haeusler, R. A., McGraw, T. E. and Accili, D. (2018) 'Metabolic Signalling: Biochemical and cellular properties of insulin receptor signalling', *Nature Reviews Molecular Cell Biology*. Nature Publishing Group, 19(1), pp. 31–44. doi: 10.1038/nrm.2017.89.
- Hall, C., Yu, H. and Choi, E. (2020) 'Insulin receptor endocytosis in the pathophysiology of insulin resistance', *Experimental & Molecular Medicine*, 52(6), pp. 911–920. doi: 10.1038/s12276-020-0456-3.
- Häring, H. U. (1991) 'The insulin receptor: signalling mechanism and contribution to the pathogenesis of insulin resistance', *Diabetologia*, 34(12), pp. 848–861. doi: 10.1007/BF00400192.
- Holmgren, L. *et al.* (1999) 'Horizontal Transfer of DNA by the Uptake of Apoptotic Bodies', *Blood*, 93(11), pp. 3956–3963. doi: 10.1182/blood.V93.11.3956.
- Holst, J. J. (2004) 'On the physiology of GIP and GLP-1', *Hormone and Metabolic Research*, 36(11–12), pp. 747–754. doi: 10.1055/s-2004-826158.
- Homko, C. *et al.* (2001) 'Insulin Secretion during and after Pregnancy in Patients with Gestational Diabetes Mellitus [1]', *The Journal of Clinical Endocrinology & Metabolism*. Oxford University Press, 86(2), pp. 568–573. doi: 10.1210/jcem.86.2.7137.
- Hotamisligil, G. k. S. *et al.* (1996) 'IRS-1-Mediated Inhibition of Insulin Receptor Tyrosine Kinase Activity in TNF-alpha- and Obesity-Induced Insulin Resistance',

*Science*, 271(5249), pp. 665–670. doi: 10.1126/science.271.5249.665.

- Hotamisligil, G. S. *et al.* (1994) 'Tumor necrosis factor α inhibits signaling from the insulin receptor', *Proceedings of the National Academy of Sciences of the United States of America*, 91(11), pp. 4854–4858. doi: 10.1073/pnas.91.11.4854.
- Hühn, J. *et al.* (2000) 'Molecular analysis of CD26-mediated signal transduction in T cells', *Immunology Letters*, 72(2), pp. 127–132. doi: https://doi.org/10.1016/S0165-2478(00)00170-X.
- Hutson, J. R. *et al.* (2011) 'The Human Placental Perfusion Model: A Systematic Review and Development of a Model to Predict In Vivo Transfer of Therapeutic Drugs', *Clinical Pharmacology & Therapeutics*, 90(1), pp. 67–76. doi: doi:10.1038/clpt.2011.66.
- Inglis, H. C. *et al.* (2016) 'Techniques to improve detection and analysis of extracellular vesicles using flow cytometry', *Cytometry Part A*, 87(11), pp. 1052–1063. doi: 10.1002/cyto.a.22649.Techniques.
- James-Allan, L. B. *et al.* (2019) 'Insulin Stimulates GLUT4 Trafficking to the Syncytiotrophoblast Basal Plasma Membrane in the Human Placenta', *Journal of Clinical Endocrinology and Metabolism*, 104(9), pp. 4225–4238. doi: 10.1210/jc.2018-02778.
- James-Allan, L. B. *et al.* (2020) 'Regulation of glucose homeostasis by small extracellular vesicles in normal pregnancy and in gestational diabetes', *The FASEB Journal*. John Wiley & Sons, Ltd, 34(4), pp. 5724–5739. doi: 10.1096/fj.201902522RR.
- Jayabalan, N. *et al.* (2019) 'Quantitative Proteomics by SWATH-MS Suggest an Association Between Circulating Exosomes and Maternal Metabolic Changes in Gestational Diabetes Mellitus', *PROTEOMICS*. John Wiley & Sons, Ltd, 19(1–2), p.

1800164. doi: 10.1002/pmic.201800164.

- Jensen, D. M. *et al.* (2003) 'Proposed diagnostic thresholds for gestational diabetes mellitus according to a 75-g oral glucose tolerance test. Maternal and perinatal outcomes in 3260 Danish women', *Diabetic Medicine*, 20(1), pp. 51–57. doi: 10.1046/j.1464-5491.2003.00857.x.
- Jeppesen, D. K. *et al.* (2019) 'Reassessment of Exosome Composition', *Cell*. Elsevier Inc., 177(2), pp. 428-445.e18. doi: 10.1016/j.cell.2019.02.029.
- Kalra, H. *et al.* (2012) 'Vesiclepedia: A Compendium for Extracellular Vesicles with Continuous Community Annotation', *PLOS Biology*. Public Library of Science, 10(12), p. e1001450. Available at: https://doi.org/10.1371/journal.pbio.1001450.
- Kandzija, N. *et al.* (2019) 'Placental extracellular vesicles express active dipeptidyl peptidase IV; levels are increased in gestational diabetes mellitus', *Journal of Extracellular Vesicles*. Taylor & Francis, 8(1), pp. 1–13. doi: 10.1080/20013078.2019.1617000.
- Kanezaki, Y. *et al.* (2003a) 'Injection of the insulin receptor α subunit increases blood glucose levels in mice', *Biochemical and Biophysical Research Communications*, 309(3), pp. 572–577. doi: 10.1016/j.bbrc.2003.08.028.
- Kanezaki, Y. *et al.* (2003b) 'Injection of the insulin receptor α subunit increases blood glucose levels in mice', *Biochemical and Biophysical Research Communications*, 309(3), pp. 572–577. doi: https://doi.org/10.1016/j.bbrc.2003.08.028.
- Kasuga, M. *et al.* (1982) 'Insulin stimulates tyrosine phosphorylation of the insulin receptor in a cell-free system', *Nature*, 298(5875), pp. 667–669. doi: 10.1038/298667a0.
- Kerr, J. F. R., Wyllie, A. H. and Currie, A. R. (1972) 'Apoptosis: A Basic Biological Phenomenon with Wideranging Implications in Tissue Kinetics', *British Journal of*

*Cancer*, 26(4), pp. 239–257. doi: 10.1038/bjc.1972.33.

- Kertesz, Z., Linton, E. A. and Redman, C. W. G. (2000) 'Adhesion Molecules of Syncytiotrophoblast Microvillous Membranes Inhibit Proliferation of Human Umbilical Vein Endothelial Cells', *Placenta*. W.B. Saunders, 21(2–3), pp. 150–159. doi: 10.1053/PLAC.1999.0476.
- Kirwan, J. P. *et al.* (2002) 'TNF-alpha is a predictor of insulin resistance in human pregnancy', *Diabetes*, 51, pp. 2207–2213. doi: 10.1007/s00192-011-1606-x.
- Knight, M. *et al.* (1998) 'Shedding of syncytiotrophoblast microvilli into the maternal circulation in pre-eclamptic pregnancies', *Br J Obstet Gynaecol*, 105(6), pp. 632–40. Available at: https://doi.org/10.1111/j.1471-0528.1998.tb10178.x.
- Krysiak, O. *et al.* (2005) 'Soluble vascular endothelial growth factor receptor-1 (sFLT-1) mediates downregulation of FLT-1 and prevents activated neutrophils from women with preeclampsia from additional migration by VEGF', *Circulation Research*, 97(12), pp. 1253–1261. doi: 10.1161/01.RES.0000194324.29363.82.
- Lain, K. Y. and Catalano, P. M. (2007) 'Metabolic Changes in Pregnancy', *Clinical Obstetrics and Gynecology*, 50(4). Available at: https://journals.lww.com/clinicalobgyn/Fulltext/2007/12000/Metabolic_Changes_in_Pregnancy.12.aspx.
- Lamers, D. *et al.* (2011) 'Dipeptidyl peptidase 4 is a novel adipokine potentially linking obesity to the metabolic syndrome', *Diabetes*, 60(7), pp. 1917–1925. doi: 10.2337/db10-1707.
- Landon, M. B. *et al.* (2011) 'The relationship between maternal glycemia and perinatal outcome', *Obstetrics and Gynecology*, 117(2), pp. 218–224. doi: 10.1097/AOG.0b013e318203ebe0.
- Leto, D. and Saltiel, A. R. (2012) 'Regulation of glucose transport by insulin: Traffic

control of GLUT4', *Nature Reviews Molecular Cell Biology*. Nature Publishing Group, 13(6), pp. 383–396. doi: 10.1038/nrm3351.

- Levine, R. *et al.* (1949) 'The action of insulin on the distribution of galactose in eviscerated nephrectomized dogs', *Journal of Biological Chemistry*. American Society for Biochemistry and Molecular Biology, 179(2), pp. 985–986. Available at: http://www.jbc.org/cgi/content/short/179/2/985 (Accessed: 6 July 2020).
- Li, H. *et al.* (2015) 'Differential Proteomic Analysis of Syncytiotrophoblast Extracellular Vesicles from Early-Onset Severe Preeclampsia, using 8-Plex iTRAQ Labeling Coupled with 2D Nano LC-MS/MS.', *Cellular physiology and biochemistry : international journal of experimental cellular physiology, biochemistry, and pharmacology*. Karger Publishers, 36(3), pp. 1116–30. doi: 10.1159/000430283.
- Liu, B. *et al.* (2016) 'Association between maternal and umbilical cord serum dipeptidyl peptidase IV in pregnant women with and without gestational diabetes mellitus', *Journal of Obstetrics and Gynaecology Research*, 42(5), pp. 505–510. doi: 10.1111/jog.12931.
- Liu, J. *et al.* (2018) 'Gestational diabetes mellitus is associated with changes in the concentration and bioactivity of placental exosomes in the maternal circulation across gestation.', *European review for medical and pharmacological sciences*, 22 7, pp. 2036–2043.
- Lowe, W. L. *et al.* (2019) 'Hyperglycemia and Adverse Pregnancy Outcome Follow-up Study (HAPO FUS): Maternal Gestational Diabetes Mellitus and Childhood Glucose Metabolism', *Diabetes Care*, 42(3), pp. 372 LP – 380. doi: 10.2337/dc18-1646.
- Luo, S.-S. *et al.* (2009) 'Human Villous Trophoblasts Express and Secrete Placenta-Specific MicroRNAs into Maternal Circulation via Exosomes1', *Biology of*

*Reproduction*, 81(4), pp. 717–729. doi: 10.1095/biolreprod.108.075481.

- Mannucci, E. *et al.* (2005) 'Hyperglycaemia increases dipeptidyl peptidase IV activity in diabetes mellitus', *Diabetologia*, 48(6), pp. 1168–1172. doi: 10.1007/s00125-005-1749-8.
- Marguet, D. *et al.* (2000) 'Enhanced insulin secretion and improved glucose tolerance in mice lacking CD26', *Proceedings of the National Academy of Sciences of the United States of America*, 97(12), pp. 6874–6879. doi: 10.1073/pnas.120069197.
- Mashimo, M., Kato, J. and Moss, J. (2013) 'ADP-ribosyl-acceptor hydrolase 3 regulates poly (ADP-ribose) degradation and cell death during oxidative stress', *Proceedings of the National Academy of Sciences*, 110(47), pp. 18964 LP – 18969. doi: 10.1073/pnas.1312783110.
- Mathieu, M. *et al.* (2019) 'Specificities of secretion and uptake of exosomes and other extracellular vesicles for cell-to-cell communication', *Nature Cell Biology*, 21(1), pp. 9–17. doi: 10.1038/s41556-018-0250-9.
- McIntyre, H. D. *et al.* (2019) 'Gestational diabetes mellitus', *Nature Reviews Disease Primers*. Springer US, 5(1). doi: 10.1038/s41572-019-0098-8.
- McKillop, A. M. *et al.* (2008) 'Decreased dipeptidyl peptidase-IV activity and glucagon-like peptide-1(7-36)amide degradation in type 2 diabetic subjects', *Diabetes Research and Clinical Practice*, 79(1), pp. 79–85. doi: 10.1016/j.diabres.2007.08.001.
- Meneilly, G. S. *et al.* (2000) 'Effect of ageing and diabetes on glucose-dependent insulinotropic polypeptide and dipeptidyl peptidase IV responses to oral glucose', *Diabetic Medicine*, 17(5), pp. 346–350. doi: 10.1046/j.1464-5491.2000.00236.x.
- Menon, R. *et al.* (2020) 'Protein Profile Changes in Circulating Placental Extracellular Vesicles in Term and Preterm Births: A Longitudinal Study', *Endocrinology*, 161(4). doi: 10.1210/endocr/bqaa009.

- Metzger, B. E. *et al.* (2008) 'Hyperglycemia and adverse pregnancy outcomes', *New England Journal of Medicine*. Massachussetts Medical Society, 358(19), pp. 1991–2002. doi: 10.1056/NEJMoa0707943.
- Metzger, B. E. (2010) 'International Association of Diabetes and Pregnancy Study Groups recommendations on the diagnosis and classification of hyperglycemia in pregnancy', *Diabetes Care*, 33(3), pp. 676–682. doi: 10.2337/dc09-1848.
- De Meyts, P. (2015) 'Insulin/receptor binding: The last piece of the puzzle?: What recent progress on the structure of the insulin/ receptor complex tells us (or not) about negative cooperativity and activation P. D. Meyts', *BioEssays*, 37(4), pp. 389–397. doi: 10.1002/bies.201400190.
- De Meyts, P. (2016) 'The insulin receptor and its signal transduction network', in *Endotext [Internet]*. MDText. com, Inc.
- Morimoto, C. and Schlossman, S. F. (1998) 'The structure and function of CD26 in the T-cell immune response', *Immunological Reviews*, 161, pp. 55–70. doi: 10.1111/j.1600-065X.1998.tb01571.x.
- Motta-Mejia, C. *et al.* (2017) 'Placental Vesicles Carry Active Endothelial Nitric Oxide Synthase and Their Activity is Reduced in Preeclampsia', *Hypertension*, 70(2). doi: 10.1161/HYPERTENSIONAHA.117.09321.
- Mouillet, J.-F. *et al.* (2015) 'MicroRNAs in placental health and disease', *American Journal of Obstetrics and Gynecology*. Mosby, 213(4), pp. S163–S172. doi: 10.1016/J.AJOG.2015.05.057.
- Myllynen, P. *et al.* (2010) 'Preliminary interlaboratory comparison of the ex vivo dual human placental perfusion system', *Reproductive Toxicology*, 30(1), pp. 94–102. doi: https://doi.org/10.1016/j.reprotox.2010.04.006.
- Myren, M. *et al.* (2007) 'The human placenta - An alternative for studying foetal

exposure', *Toxicology in Vitro*, 21(7), pp. 1332–1340. doi: 10.1016/j.tiv.2007.05.011.

- Nair, S. *et al.* (2018) 'Human placental exosomes in gestational diabetes mellitus carry a specific set of miRNAs associated with skeletal muscle insulin sensitivity', *Clinical Science*, 132(22), pp. 2451–2467. doi: 10.1042/CS20180487.
- Neudeck, H. *et al.* (1997) 'Histochemical evaluation of placental dipeptidyl peptidase IV (CD26) in pre-eclampsia: Enzyme activity in villous trophoblast indicates an enhanced likelihood of gestational hypertensive disorders', *American Journal of Reproductive Immunology*, 37(6), pp. 449–458. doi: 10.1111/j.1600-0897.1997.tb00259.x.
- *NICE Guidelines. Diabetes in Pregnancy: Management from Preconception to the Postnatal Period* (2015) *NICE Guideline NG3*. Available at: https://www.nice.org.uk/guidance/ng3.
- Nishikawa, M. *et al.* (2005) 'Changes in Placental Dipeptidyl Peptidase IV in Preeclampsia with Intrauterine Growth Restriction', *Horm Metab Res*, 37(07), pp. 408–413. doi: 10.1055/s-2005-870229.
- O'Brien, M., Baczyk, D. and Kingdom, J. C. (2017) 'Endothelial Dysfunction in Severe Preeclampsia is Mediated by Soluble Factors, Rather than Extracellular Vesicles', *Scientific Reports*. Nature Publishing Group, 7(1), p. 5887. doi: 10.1038/s41598-017-06178-z.
- Ofei, F. *et al.* (1996) 'Effects of an Engineered Human Anti–TNF-α Antibody (CDP571) on Insulin Sensitivity and Glycemic Control in Patients With NIDDM', *Diabetes*, 45(7), pp. 881–885.
- Ogurtsova, K. *et al.* (2017) 'IDF Diabetes Atlas: Global estimates for the prevalence of diabetes for 2015 and 2040', *Diabetes Research and Clinical Practice*. Elsevier B.V., 128, pp. 40–50. doi: 10.1016/j.diabres.2017.03.024.

- Ohnuma, K. *et al.* (2004) 'CD26 up-regulates expression of CD86 on antigen-presenting cells by means of caveolin-1', *Proceedings of the National Academy of Sciences of the United States of America*, 101(39), pp. 14186–14191. doi: 10.1073/pnas.0405266101.
- Ohnuma, K., Dang, N. H. and Morimoto, C. (2008) 'Revisiting an old acquaintance: CD26 and its molecular mechanisms in T cell function', *Trends in Immunology*, 29(6), pp. 295–301. doi: 10.1016/j.it.2008.02.010.
- Ouyang, Y. *et al.* (2014) 'Review: placenta-specific microRNAs in exosomes - good things come in nano-packages.', *Placenta*. NIH Public Access, 35 Suppl, pp. S69-73. doi: 10.1016/j.placenta.2013.11.002.
- Palacios-Ortega, S. *et al.* (2016) 'Effects of high glucose on caveolin-1 and insulin signaling in 3T3-L1 adipocytes', *Adipocyte*. Taylor & Francis, 5(1), pp. 65–80. doi: 10.1080/21623945.2015.1122856.
- Pantham, P., Askelund, K. J. and Chamley, L. W. (2011) 'Trophoblast deportation part II: A review of the maternal consequences of trophoblast deportation', *Placenta*. Elsevier Ltd, 32(10), pp. 724–731. doi: 10.1016/j.placenta.2011.06.019.
- Pap, E. *et al.* (2008) 'T Lymphocytes are Targets for Platelet- and Trophoblast-Derived Microvesicles During Pregnancy', *Placenta*, 29(9), pp. 826–832. doi: https://doi.org/10.1016/j.placenta.2008.06.006.
- Papa, V. *et al.* (1993) 'An intact and functional soluble form of the insulin receptor is secreted by cultured cells', *Endocrinology*, 133(3), pp. 1369–1376. doi: 10.1210/endo.133.3.8396017.
- Petruzzelli, L. M. *et al.* (1982) 'Insulin activates a tyrosine-specific protein kinase in extracts of 3T3-L1 adipocytes and human placenta.', *Proceedings of the National Academy of Sciences of the United States of America*, 79(22), pp. 6792–6796. doi:

10.1073/pnas.79.22.6792.

- Pezzino, V. *et al.* (1992) 'Identification and initial characterization of insulin receptor-like immunoreactivity in human plasma', *The Journal of Clinical Endocrinology & Metabolism*, 74(5), pp. 1116–1121. doi: 10.1210/jcem.74.5.1314845.
- Pontén, F., Jirström, K. and Uhlen, M. (2008) 'The Human Protein Atlas—a tool for pathology', *The Journal of Pathology*, 216(4), pp. 387–393. doi: 10.1002/path.2440.
- Raposo, G. and Stoorvogel, W. (2013) 'Extracellular vesicles: Exosomes, microvesicles, and friends', *Journal of Cell Biology*, 200(4), pp. 373–383. doi: 10.1083/jcb.201211138.
- Raudvere, U. *et al.* (2019) 'g:Profiler: a web server for functional enrichment analysis and conversions of gene lists (2019 update)', *Nucleic Acids Research*, 47(W1), pp. W191–W198. doi: 10.1093/nar/gkz369.
- Reddy, A. *et al.* (2008) 'The Effect of Labour and Placental Separation on the Shedding of Syncytiotrophoblast Microparticles, Cell-free DNA and mRNA in Normal Pregnancy and Pre-eclampsia', *Placenta*. Elsevier Ltd, 29(11), pp. 942–949. doi: 10.1016/j.placenta.2008.08.018.
- Redman, C. W. G. *et al.* (2012) 'Review: Does size matter? Placental debris and the pathophysiology of pre-eclampsia', *Placenta*. Elsevier Ltd, 33(SUPPL.), pp. S48–S54. doi: 10.1016/j.placenta.2011.12.006.
- Revenfeld, A. L. S. *et al.* (2014) 'Diagnostic and prognostic potential of extracellular vesicles in peripheral blood', *Clinical Therapeutics*. Elsevier, 36(6), pp. 830–846. doi: 10.1016/j.clinthera.2014.05.008.
- Rice, G. E. *et al.* (2015) 'The effect of glucose on the release and bioactivity of exosomes from first trimester trophoblast cells', *Journal of Clinical Endocrinology and Metabolism*, 100(10), pp. E1280–E1288. doi: 10.1210/jc.2015-2270.

- Röhrborn, D. *et al.* (2016) ‘Reduced DPP4 activity improves insulin signaling in primary human adipocytes’, *Biochemical and Biophysical Research Communications*, 471(3), pp. 348–354. doi: 10.1016/j.bbrc.2016.02.019.
- Röhrborn, D., Eckel, J. and Sell, H. (2014) ‘Shedding of dipeptidyl peptidase 4 is mediated by metalloproteases and up-regulated by hypoxia in human adipocytes and smooth muscle cells’, *FEBS Letters*, 588(21), pp. 3870–3877. doi: 10.1016/j.febslet.2014.08.029.
- Ryan, E. A., Sullivan, M. J. and Skyler, J. S. (1985) ‘Insulin Action During Pregnancy: Studies with the Euglycemic Clamp Technique’, *Diabetes*, 34(4), pp. 380 LP – 389. doi: 10.2337/diab.34.4.380.
- Salomon, C. *et al.* (2016) ‘Gestational diabetes mellitus is associated with changes in the concentration and bioactivity of placenta-derived exosomes in maternal circulation across gestation’, *Diabetes*, 65(3), pp. 598–609. doi: 10.2337/db15-0966.
- Salomon, C. *et al.* (2017) ‘Placental Exosomes as Early Biomarker of Preeclampsia: Potential Role of Exosomal MicroRNAs Across Gestation’, *The Journal of Clinical Endocrinology & Metabolism*. Oxford University Press, 102(9), pp. 3182–3194. doi: 10.1210/jc.2017-00672.
- Sarker, S. *et al.* (2014) ‘Placenta-derived exosomes continuously increase in maternal circulation over the first trimester of pregnancy’, *Journal of Translational Medicine*, 12(1), p. 204. doi: 10.1186/1479-5876-12-204.
- Scheen, A. J. (2018) ‘The safety of gliptins : updated data in 2018’, *Expert Opinion on Drug Safety*. Taylor & Francis, 17(4), pp. 387–405. doi: 10.1080/14740338.2018.1444027.
- Scholtens, D. M. *et al.* (2019) ‘Hyperglycemia and adverse Pregnancy Outcome follow-up study (HAPO FUS): Maternal glycemia and childhood glucose metabolism’,

*Diabetes Care*, 42(3), pp. 381–392. doi: 10.2337/dc18-2021.

- Shomer, E. *et al.* (2013) 'Microvesicles of women with gestational hypertension and preeclampsia affect human trophoblast fate and endothelial function.', *Hypertension (Dallas, Tex. : 1979)*. American Heart Association, Inc., 62(5), pp. 893–8. doi: 10.1161/HYPERTENSIONAHA.113.01494.
- Siddle, K. (2011) 'Signalling by insulin and IGF receptors: Supporting acts and new players', *Journal of Molecular Endocrinology*, 47(1). doi: 10.1530/JME-11-0022.
- Simpson, R. A., Mayhew, T. M. and Barnes, P. R. (1992) 'From 13 weeks to term, the trophoblast of human placenta grows by the continuous recruitment of new proliferative units: A study of nuclear number using the disector', *Placenta*, 13(5), pp. 501–512. doi: 10.1016/0143-4004(92)90055-X.
- Smárason, A. K. *et al.* (1993) 'The effect of placental syncytiotrophoblast microvillous membranes from normal and pre-eclamptic women on the growth of endothelial cells in vitro.', *British journal of obstetrics and gynaecology*, 100(10), pp. 943–9. Available at: http://www.ncbi.nlm.nih.gov/pubmed/8217980 (Accessed: 14 March 2018).
- Stenqvist, A.-C. *et al.* (2013) 'Exosomes Secreted by Human Placenta Carry Functional Fas Ligand and TRAIL Molecules and Convey Apoptosis in Activated Immune Cells, Suggesting Exosome-Mediated Immune Privilege of the Fetus', *The Journal of Immunology*, 191(11), pp. 5515–5523. doi: 10.4049/jimmunol.1301885.
- Subramanian, S. L. *et al.* (2015) 'Integration of extracellular RNA profiling data using metadata, biomedical ontologies and Linked Data technologies', *Journal of Extracellular Vesicles*. Taylor & Francis, 4(1), p. 27497. doi: 10.3402/jev.v4.27497.
- Sun, A. L. *et al.* (2012) 'Dipeptidyl peptidase-IV is a potential molecular biomarker in diabetic kidney disease', *Diabetes and Vascular Disease Research*, 9(4), pp. 301–308. doi: 10.1177/1479164111434318.

- Sun, X. *et al.* (2017) 'Sitagliptin down-regulates retinol-binding protein 4 and reduces insulin resistance in gestational diabetes mellitus : a randomized and double-blind trial', *Metabolic Brain Disease*. Metabolic Brain Disease, 32(3), pp. 773–778. doi: 10.1007/s11011-017-9958-7.
- Sunderland, C. A., Redman, C. W. G. and Stirrat, G. M. (1981) 'Monoclonal antibodies to human syncytiotrophoblast', *Immunology*, 43(3), pp. 541–546.
- Supek, F. *et al.* (2011) 'REVIGO Summarizes and Visualizes Long Lists of Gene Ontology Terms', *PLOS ONE*. Public Library of Science, 6(7), pp. 1–9. doi: 10.1371/journal.pone.0021800.
- Suzuki, K. and Kono, T. (1980) 'Evidence that insulin causes translocation of glucose transport activity to the plasma membrane from an intracellular storage site', *Proceedings of the National Academy of Sciences of the United States of America*, 77(5 I), pp. 2542–2545. doi: 10.1073/pnas.77.5.2542.
- Tannetta, D., Collett, G., *et al.* (2017) 'Syncytiotrophoblast extracellular vesicles – Circulating biopsies reflecting placental health', *Placenta*. Elsevier Ltd, 52, pp. 134–138. doi: 10.1016/j.placenta.2016.11.008.
- Tannetta, D., Masliukaite, I., *et al.* (2017) 'Update of syncytiotrophoblast derived extracellular vesicles in normal pregnancy and preeclampsia', *Journal of Reproductive Immunology*. Elsevier Ireland Ltd, 119, pp. 98–106. doi: 10.1016/j.jri.2016.08.008.
- Tannetta, D. S. *et al.* (2013) 'Characterisation of Syncytiotrophoblast Vesicles in Normal Pregnancy and Pre-Eclampsia: Expression of Flt-1 and Endoglin', *PLoS ONE*. Edited by Y.-L. Wang, 8(2). doi: 10.1371/journal.pone.0056754.
- Taraboletti, G. *et al.* (2002) 'Shedding of the Matrix Metalloproteinases MMP-2 , MMP-9 , and MT1-MMP as Membrane Vesicle- Associated Components by Endothelial Cells', *The American Journal of Pathology*. American Society for

Investigative Pathology, 160(2), pp. 673–680. doi: 10.1016/S0002-9440(10)64887-0.

- The Soluble Insulin Receptor Study Group (2007) 'Soluble Insulin Receptor Ectodomain Is Elevated in the Plasma of Patients With Diabetes', *Diabetes*, 56(8), pp. 2028 LP – 2035. doi: 10.2337/db07-0394.
- Théry, C. *et al.* (2018) 'Minimal information for studies of extracellular vesicles 2018 (MISEV2018): a position statement of the International Society for Extracellular Vesicles and update of the MISEV2014 guidelines', *Journal of Extracellular Vesicles*. Taylor & Francis, 7(1), pp. 1–43. doi: 10.1080/20013078.2018.1535750.
- Thibault, G. *et al.* (1991) 'The inhibitory effect of human syncytiotrophoblast plasma membrane vesicles on in vitro lymphocyte proliferation is associated with reduced interleukin 2 receptor expression', *Cellular Immunology*, 138(1), pp. 165–174. doi: https://doi.org/10.1016/0008-8749(91)90141-W.
- Tong, M. *et al.* (2016) 'Proteomic characterization of macro-, micro- and nano-extracellular vesicles derived from the same first trimester placenta: relevance for feto-maternal communication', *Human Reproduction*. Oxford University Press, 31(4), pp. 687–699. doi: 10.1093/humrep/dew004.
- Tong, M. *et al.* (2017) 'In vivo targets of human placental micro-vesicles vary with exposure time and pregnancy.', *Reproduction (Cambridge, England)*. Society for Reproduction and Fertility, 153(6), pp. 835–845. doi: 10.1530/REP-16-0615.
- Tong, M., Abrahams, V. M. and Chamley, L. W. (2018) 'Immunological effects of placental extracellular vesicles', *Immunology & Cell Biology*, 96(7), pp. 714–722. doi: 10.1111/imcb.12049.
- Tyanova, S. and Cox, J. (2018) 'Perseus: A Bioinformatics Platform for Integrative Analysis of Proteomics Data in Cancer Research', in von Stechow, L. (ed.) *Cancer Systems Biology: Methods and Protocols*. New York, NY: Springer New York, pp.

133–148. doi: 10.1007/978-1-4939-7493-1_7.

- Ubersax, J. A. and Ferrell, J. E. (2007) 'Mechanisms of specificity in protein phosphorylation', *Nature Reviews Molecular Cell Biology*, 8(7), pp. 530–541. doi: 10.1038/nrm2203.
- Ullrich, A. *et al.* (1985) 'Human insulin receptor and its relationship to the tyrosine kinase family of oncogenes', *Nature*, 313(6005), pp. 756–761. doi: 10.1038/313756a0.
- Valadi, H. *et al.* (2007) 'Exosome-mediated transfer of mRNAs and microRNAs is a novel mechanism of genetic exchange between cells', *Nature Cell Biology*, 9(6), pp. 654–659. doi: 10.1038/ncb1596.
- Valkonen, S. *et al.* (2017) 'Biological reference materials for extracellular vesicle studies', *European Journal of Pharmaceutical Sciences*. The Authors, 98, pp. 4–16. doi: 10.1016/j.ejps.2016.09.008.
- Valley, M. P. *et al.* (2016) 'A bioluminescent assay for measuring glucose uptake', *Analytical Biochemistry*, 505, pp. 43–50. doi: https://doi.org/10.1016/j.ab.2016.04.010.
- Vora, K. A. *et al.* (2009) 'Genetic ablation or pharmacological blockade of dipeptidyl peptidase IV does not impact T cell-dependent immune responses', *BMC Immunology*, 10, pp. 1–11. doi: 10.1186/1471-2172-10-19.
- Waters, T. P. *et al.* (2020) 'Longitudinal changes in glucose metabolism in women with gestational diabetes, from late pregnancy to the postpartum period', *Diabetologia*, 63(2), pp. 385–394. doi: 10.1007/s00125-019-05051-0.
- Whitsett, J. A. and Lessard, J. L. (1978) 'Characteristics of the microvillus brush border of human placenta: Insulin receptor localization in brush border membranes', *Endocrinology*, 103(4), pp. 1458–1468. doi: 10.1210/endo-103-4-1458.
- Witwer, K. W. *et al.* (2013) 'Standardization of sample collection, isolation and analysis methods in extracellular vesicle research', *Journal of Extracellular Vesicles*,

2(1). doi: 10.3402/jev.v2i0.20360.

- Wolf, P. (1967) 'The Nature and Significance of Platelet Products in Human Plasma', *British Journal of Haematology*, 13(3), pp. 269–288. doi: doi:10.1111/j.1365-2141.1967.tb08741.x.
- Xu, R. *et al.* (2016) 'Extracellular vesicle isolation and characterization : toward clinical application', *Journal of Clinical Investigation*, 126(4), pp. 1152–1162. doi: 10.1172/JCI81129.It.
- Yabe, D. and Seino, Y. (2011) 'Two incretin hormones GLP-1 and GIP: Comparison of their actions in insulin secretion and β cell preservation', *Progress in Biophysics and Molecular Biology*. Elsevier Ltd, 107(2), pp. 248–256. doi: 10.1016/j.pbiomolbio.2011.07.010.
- Yáñez-Mó, M. *et al.* (2015) 'Biological properties of extracellular vesicles and their physiological functions', *Journal of Extracellular Vesicles*. Taylor & Francis, 4(1), p. 27066. doi: 10.3402/jev.v4.27066.
- Yang, C. *et al.* (2008) 'Lymphocytic microparticles inhibit angiogenesis by stimulating oxidative stress and negatively regulating VEGF-induced pathways', *American Journal of Physiology-Regulatory, Integrative and Comparative Physiology*, 294(2), pp. 467–476. doi: 10.1152/ajpregu.00432.2007.
- Yano, Y. *et al.* (1993) 'The effects of calpeptin (a calpain specific inhibitor) on agonist induced microparticle formation from the platelet plasma membrane', *Thrombosis Research*, 71(5), pp. 385–396. doi: 10.1016/0049-3848(93)90163-I.
- Yazbeck, R., Howarth, G. S. and Abbott, C. A. (2009) 'Dipeptidyl peptidase inhibitors, an emerging drug class for inflammatory disease?', *Trends in Pharmacological Sciences*, 30(11), pp. 600–607. doi: 10.1016/j.tips.2009.08.003.
- Yuana, Y., Sturk, A. and Nieuwland, R. (2013) 'Extracellular vesicles in physiological

and pathological conditions', *Blood Reviews*. Elsevier Ltd, 27(1), pp. 31–39. doi: 10.1016/j.blre.2012.12.002.

- Yuasa, T. *et al.* (2014) 'Development of in vitro model of insulin receptor cleavage induced by high glucose in HepG2 cells', *Biochemical and Biophysical Research Communications*. Elsevier Inc., 445(1), pp. 236–243. doi: 10.1016/j.bbrc.2014.01.187.
- Yuasa, T. *et al.* (2016) 'Sequential cleavage of insulin receptor by calpain 2 and γ-secretase impairs insulin signalling', *Diabetologia*, 59(12), pp. 2711–2721. doi: 10.1007/s00125-016-4102-5.
- Zhao, S. *et al.* (2012) 'Elevation of plasma soluble CD26 levels during pregnancy', *Journal of Obstetrics and Gynaecology Research*, 38(1), pp. 272–279. doi: 10.1111/j.1447-0756.2011.01638.x.
- Zhu, Y. and Zhang, C. (2016) 'Prevalence of Gestational Diabetes and Risk of Progression to Type 2 Diabetes: a Global Perspective', *Current Diabetes Reports*, 16(1), pp. 1–11. doi: 10.1007/s11892-015-0699-x.

# List of publications


Awoyemi, Toluwalase, Dionne Tannetta, Wei Zhang, **Neva Kandzija**, Carolina Motta-Mejia, Roman Fischer, Raphael Heilig, Sina Raiss, Christopher Redman, and Manu Vatish. 2020. "Glycosylated Siglec-6 Expression in Syncytiotrophoblast-Derived Extracellular Vesicles from Preeclampsia Placentas." *Biochemical and Biophysical Research Communications*. https://doi.org/https://doi.org/10.1016/j.bbrc.2020.09.081.

Cerdeira, A.S., **N. Kandzija**, P. Pargmae, M. Tome, W. Zhang, W.R. Cooke, S. Agrawal, T. James, C. Redman, and M. Vatish. 2020. "In Vivo Evidence of Significant Placental Growth Factor Release by Normal Pregnancy Placentas." *Scientific Reports* 10 (1). https://doi.org/10.1038/s41598-019-56906-w.

Cooke, W.R., A. Cribbs, W. Zhang, **N. Kandzija**, C. Motta-Mejia, E. Dombi, R. Ri, A.S. Cerdeira, C. Redman, and M. Vatish. 2019. "Maternal Circulating Syncytiotrophoblast-Derived Extracellular Vesicles Contain Biologically Active 5'-TRNA Halves." *Biochemical and Biophysical Research Communications* 518 (1). https://doi.org/10.1016/j.bbrc.2019.08.015.

Gill, M., C. Motta-Mejia, **N. Kandzija**, W. Cooke, W. Zhang, A.S. Cerdeira, C. Bastie, C. Redman, and M. Vatish. 2019. "Placental Syncytiotrophoblast-Derived Extracellular Vesicles Carry Active NEP (Neprilysin) and Are Increased in Preeclampsia." *Hypertension* 73 (5). https://doi.org/10.1161/HYPERTENSIONAHA.119.12707.

**Kandzija, Neva**, Wei Zhang, Carolina Motta-Mejia, Vuyane Mhlomi, Jennifer McGowan-Downey, Tim James, Ana Sofia Cerdeira, et al. 2019. "Placental Extracellular Vesicles Express Active Dipeptidyl Peptidase IV; Levels Are Increased in Gestational Diabetes Mellitus." *Journal of Extracellular Vesicles* 8 (1): 1–13. https://doi.org/10.1080/20013078.2019.1617000.

Motta-Mejia, C., **N. Kandzija**, W. Zhang, V. Mhlomi, A.S. Cerdeira, A. Burdujan, D. Tannetta, et al. 2017. "Placental Vesicles Carry Active Endothelial Nitric Oxide Synthase and Their Activity Is Reduced in Preeclampsia." *Hypertension* 70 (2). https://doi.org/10.1161/HYPERTENSIONAHA.117.09321.